UNIVERSIDADE TÉCNICA DE LISBOA
INSTITUTO SUPERIOR TÉCNICO

POLITECHNIKA WARSZAWSKA
WYDZIAŁ ELEKTRONIKI I TECHNIK INFORMACYJNYCH

MULTIUSER GEOMETRICALLY BASED CHANNEL MODEL

Rafał Zubala

Dissertation submitted for obtaining the degree of magister inżynier telekomunikacji (Master of Science in Telecommunication Engineering)

Supervisors: Doctor Luís Manuel de Jesus Sousa Correia, IST
Dr inż. Jerzy Kołakowski, PW

Jury

President: Doctor Maria Paula Queluz, IST
Members: Doctor Luís Manuel de Jesus Sousa Correia, IST
Doctor António Rodrigues, IST

September 2005

Dla moich kochanych rodziców.

Acknowledgements

In the first place I would like to thank Professor Luís M. Correia. I appreciate that he made my stay in Portugal possible and that he gave me the opportunity to write my master thesis at Instituto Superior Técnico. I thank him for the organisation of the work place, where I could focus on my thesis in comfortable conditions. I am thankful to Professor Luís M. Correia for his valuable time during our weekly meetings and for his flexibility, patient and help in solving the problems, as well as for his supervising methods. From the beginning of my work I have been seeing the goal, which gave me a motivation to the successive efforts. I am thankful to Professor Luís M. Correia for showing me the superb example of organization of work, which is valuable experience for me. I appreciate that he gave me the opportunity to participate in the GROW meetings, where I could take part in the interesting discussions. I thank him for his human personality and for the invitation to the Monsaraz party, where I had an opportunity to be in contact with the Portuguese culture.

I thank B. W. Martijn Kuipers for his involvement in my work and for his valuable hints and inestimable help. I would like to thank him for always finding time for me, for our weekly meetings, and for many hours of discussions when the problems occurred. I send my great thanks to Martijn Kuipers for his gigantic patient, for his incredible flexibility and for help in making corrections on my report. I am grateful to Martijn Kuipers for his sacrifice, for the fact that he could find a time during his vacations to help me in my thesis.

I would like to thank my supervisor in the Warsaw University of the Technology in the Department of the Electronic and Information Techniques, Dr inż. Jerzy Kołakowski. To make the master thesis in Portugal was his idea. This stay in Portugal was possible because of his involvement. I would like to thank Dr inż. Jerzy Kołakowski also for the wonderful cooperation that took place before coming to Portugal. During my studies, I had the opportunity to be involved in very interesting projects from different areas of telecommunications, which included software and hardware aspects connected with DSP and UWB system.

I send my thanks to the colleagues from GROW. In the meetings, I had the opportunity to enlarge my knowledge in many of domains. Also, I appreciate their efforts and the valuable

hints during the discussions after my presentations. It helped me to improve the quality of my performance.

I would like to thank Socrates-Erasmus coordinators in the Warsaw University of Technology, Dr inż. Tomasz Kosiło and Mgr. Bożena Snopińska. Thanks to their involvement and sacrifice, this scholarship was possible and took place. I also thank "Fundacja Rozwoju Radiokomunikacji I Technik Multimedialnych" for the financial support.

I thank the colleagues from my office: Sofia Correia and Gonçalo Martins. I would like to thank them for their help in the difficult beginnings in Portugal. I am grateful to them that they were my guides in the first moments in Portugal, and for their efforts in trying to find accommodation for me.

I send my acknowledgments to my parents and my family in Poland. In spite of the fact that I was a huge distance from Poland, from my home, I felt their presence and their care about me. I also thank all the hints that I received from them.

I am grateful to all my flatmates from the apartment. These months that I spent in Portugal in this house were the greatest in my student life. I appreciate them for the wonderful and nice atmosphere, which let me feel like in the real family home.

I also thank my friend Hubert Kokoszkiewicz with whom I shared the Socrates-Erasmus programme at IST. I would like to thank him for his support and help during the staying in Portugal.

Abstract

This study regards the development of the geometrically based channel model to simulate the interference caused by terminals in UMTS. The considered model consists of scatterers that are grouped in clusters, which are located on a 2D plane. The positions of the clusters are generated using the Gaussian distribution and are limited by the scenario dimensions. For the case of the pico- and macro-cells the positions of the clusters are bounded by a circle, whereas in the micro-cell an ellipse is taken.

Multiuser interference is considered in the "low level" approach. It means that both the desired power and the power of the interferences is estimated directly from the parameters obtained from the model. The modulation or multi access techniques are not taken into consideration in this dissertation. Every link between the receiver (Rx) and the transmitter (Tx) in the system is described by a separate region.

Multiuser propagation scenarios were generated using state of the art literature. These scenarios were enhanced to consider the up- and downlink cases. In the scenarios, only one base station was assumed. Before simulating these scenarios, an analysis of the parameters of the simulator was made. It was concluded that the time resolution of the detector in the Rx plays a very important role on the quality of the results.

The simulations in every type of scenario show that the distance between the Rx and the Txs plays the major role. This is the most important factor that decides about the quality of the link. Two types of the synchronisations were considered at the Txs and at the Rx, for which the distance influences in a different way the level of the interference. The results for the macro-cell show that the quality of this link is the poorest in compared to the other scenarios.

Keywords

Propagation channel, Wideband directional models, Multiuser Interferences, Simulation, UMTS

Streszczenie

Praca ta opracowuje model kanału radiowego, który mógłby posłużyć to wykonania symulacji interferencji pochodzących od wielu terminali w systemie UMTS. Rozważany model składa się z reflektorów, które są zgrupowane w kolekcje. Grupy te są rozmieszczone na płaszczyźnie 2D. Położenia tych grup są generowane za pomocą rozkładu Gaussa i są ograniczone przez wymiary poszczególnych scenariuszy. W przypadku pico-celi oraz macro-celi grupy są położone wewnątrz okręgów, w przypadku micro-celi wewnątrz elipsy.

W pracy tej, interferencje od wielu użytkowników są rozważane na „najniższym poziomie". Pożadana moc jak i moc interferencji są szacowane na podstawie parametrów bezpośrednio otrzymanych z zaimplementowanego modelu. Techniki modulacji czy wielodostępu nie są brane pod uwagę. Każde łącze pomiędzy nadajnikiem i odbiornikiem w systemie, jest opisane za pomocą odrębnego regionu.

W pracy tej, scenariusze opisujące środowiska złożone z wielu użytkowników zostały wygenerowane. Istniejące scenariusze musiały zostać poddane pewnym modyfikacjom by uwzględniały transmisje w górę i w dół. Zostało zrobione założenie, że w środowisko może istnieć tylko jedna stacja bazowa. Przed właściwymi symulacjami, badanie wpływu parametrów symulatora na otrzymywane wyniki zostało przeprowadzone. Parametrem, który w sposób istotny decyduje o jakości wyników, jest rozdzielczość w czasie odbiornika.

Wyniki symulacji dla każdego typu scenariusza pokazały, że parametrem, który w sposób istotny wpływa na jakość łącza jest odległość pomiędzy nadajnikami a odbiornikiem. Podczas symulacji były uwzględniane dwa typy synchronizacji, pierwszy dotyczył synchronizacji po stronie odbiornika, drugi synchronizacji po stronie nadajników. Jak pokazały wyniki, odległość dla tych dwóch typów synchronizacji, daje odmienne wnioski. Wyniki otrzymane z macro-celi były najgorsze, jakość łącza w tym scenariuszu jest zła w porównaniu z innymi scenariuszami.

Słowa kluczowe

Kanał propagacyjny, Model kierunkowy szerokopasmowy, Interferencje od wielu użytkowników, Symulacja, UMTS

Table of Contents

List of Figures

List of Tables

List of Acronyms

AoA	Angle of Arrival
AoD	Angle of Departure
BS	Base Station
CDMA	Code Division Multiple Access
CIR	Channel Impulse Response
COST	European CO-operation in the field of Scientific and Technical research
DECT	Digital Enhanced Cordless Telecommunications
DL	Downlink
DUM	Discrete Uniform Model
EMC	Electromagnetic Compatibility
FDD	Frequency Division Duplexing
FDMA	Frequency Division Multiple Access
FFT	Fast Fourier Transform
FLOWS	Flexible Convergence of Wireless Standards and Services
GBSB	Geometrically Based Single Bounce
GROW	A Group for Research On Wireless
GSM	Global System for Mobile Communications
GWSSUS	Gaussian Wide Sense Stationary Uncorrelated Scattering
IST	Instituto Superior Técnico
LoS	Line of Sight
MC	Multi Carrier
MIMO	Multiple Input Multiple Output

MT	Mobile Terminal
MU	Multiuser
MUI	Multiuser Interference
NLoS	Non Line of Sight
OVSF	Orthogonal Variable Spreading Factor
PDF	Probability Density Function
PDP	Power Delay Profile
QPSK	Quadrature Phase Shift Keying
RMS	Root Mean Square
Rx	Receiver
SIR	Signal to Interference
SINR	Signal to Interference plus Noise Ratio
SISO	Single Input Single Output
SU	Single User
TD-CDMA	Time Division – Code Division Multiple Access
TDD	Time Division Duplexing
TDMA	Time Division Multiple Access
ToA	Time of Arrival
Tx	Transmitter
UL	Uplink
UMTS	Universal Mobile Telecommunications System
USD	Uniform Sectored Distribution
UTRA	Universal Terrestrial Radio Access
W-CDMA	Wideband – Code Division Multiple Access

List of Symbols

$\overline{\alpha}$	Average orthogonality factor in the cell
α_n	Angular position of n^{th} element on the x-y plane
α_{SIR}	Orthogonality factor
β_{SIR}	Interference reduction factor
Γ	Complex reflection coefficient of a scatterer
$\overline{\eta_{DL}}$	Average load for the downlink
η_{DL}	Load for the downlink
η_{UL}	Load for the uplink
θ	Angle of departure
θ_{aa}	Angle of radiation pattern
λ	Wave length
λ_P	Parameter of Poisson distribution
μ_P	Mean value of power
μ_G	Mean value of Gaussian distribution
σ_τ	RMS time delay spread
σ_φ	RMS AoA spread
σ_θ	RMS AoD spread
σ_P	Standard deviation of power
$\bar{\tau}$	Mean Excess Delay
τ	Delay
$\overline{\tau^2}$	Mean Square Excess Delay
τ_k	k^{th} instant

τ_{max}	Maximum delay
φ	Angle of arrival
φ_0	Angle of arrival of the LoS component
φ_{aa}	Angle of radiation pattern
φ_{BW}	Range of change of φ
Φ_n	Phase of n^{th} in the antenna array
Φ_{Rx}	Phase of received multipath component
Φ_{sc}	Phase of the complex reflection coefficient of scatterer
Ψ	Phase coefficient of antenna array
ω_D	Angular velocity of scatterer
a	Radius of the circular antenna array
A	Amplitude of transmitted signal
AF	Antenna factor
A_{out}	Amplitude of received signal
B_C	Coherence Bandwidth
b_{ell}	Minor axis of ellipse
B_i	Bandwidth of data signal
B_{SS}	Bandwidth of signal after spreading
c	Speed of light
$conv$	Convolution
$corr$	Correlation between signals
$\boldsymbol{cov}$	Covariance matrix
$\mathbf{c}_{scr}$	Vector containing scrambling bits
d	Spacing between antennas in the antenna array
d_0	Distance between the MT and the BS

d_1	Distance between a receiving antenna and a scatterer.
d_2	Distance between a scatterer and a transmitting antenna
d_c	Cluster density
$\mathbf{d}_d$	Vector containing data bits
E_b	Energy per one bit
E_{Rx}	Amplitude of received multipath component
$\mathbf{F}$	Martix of interferences
f	Frequency
f_{ell}	Focal length of an ellipse
f_m	Maximum Doppler shift
G	Radiation pattern of an antenna array
G_0	Radiation pattern of a radiator
G_p	Processing gain
G_{Rx}	Radiation pattern of a receiving antenna
G_{Tx}	Radiation pattern of a transmitting antenna
H	The spectrum of the CIR
h_{eff}	Effective length of the receiving antenna
h_k	Amplitude of the channel impulse response
I	Power of interferences
i_{BS}	Inter- to intra-cell interferences ratio at the BS
I_{inter}	Power of the inter-cell interference
I_{intra}	Power of the intra-cell interference
i_{MT}	Inter- to intra-cell BS interferences ratio at the MT
I_n	Feeding amplitude of n^{th} antenna in the antenna array
k	Wave number

$\overline{L}_{pj}$	average attenuation between the BS and j^{th} user
N_0	Power of thermal noise
N_a	Number of antennas in an array
n_{BS}	Number of BSs
N_{cells}	Number of cells
N_{cl}	Number of clusters
N_{DL}	Number of connections per cell
N_{fft}	Number of samples in the spectrum
N_m	Number of multipath components
n_{MT}	Number of MTs
N_{Rx}	Noise level of the Rx
n_{Rx}	Number of Rxs
N_{sc}	Number of scatterers
$\overline{n_{sc}}$	Average number of scatterers per cluster
N_{sp}	Noise spectral density
N_{ter}	Number of terminals
n_{Tx}	Number of Txs
N_{UL}	Number of users per cell
N_{users}	Number of users
$\overline{P}$	Mean power gain
P_k	Power of the channel impulse response
P_{Rx}	Power of received signal
P_{Tx}	Power of the transmitter
$p_{\tau,\varphi}$	Probability density function
R	Radius of the circle where scatterers are deployed

R_A	Feedpoint impedance of an antenna
R_{bj}	Bit rate for j^{th} user
R_c	WCDMA chip rate
R_{max}	Maximum radius of a region
s_{dev}	Coordinates of the MT or the BS
$SINR$	Signal to Interference and Noise Ratio
SIR_{DL}	Signal to Interference Ratio for the downlink
SIR_{UL}	Signal to Interference Ratio for the uplink
T_b	Period of one bit
T_C	Coherence Time
v	Velocity
V	Voltage of the signal detected by the receiving antenna
$v_{i,b}$	Superposition of the steering vectors
v_j	Activity factor for the j^{th} user
V_r	Random variable with Gaussian distribution
w_{str}	Street width
$\mathbf{x}$	Vector containing transmitted signal
x_{Rx}	x-coordinate of a receiving antenna
x_{sc}	x-coordinate of a scatterer
x_{Tx}	x-coordinate of a transmitting antenna
$\boldsymbol{y}$	Vector containing received symbols
y_{Rx}	y-coordinate of a receiving antenna
y_{sc}	y-coordinate of a scatterer
y_{Tx}	y-coordinate of a transmitting antenna

List of Programmes

Dev C++, http://www.bloodshed.net

Matlab 7, http://www.mathworks.com

Microsoft Excel, http://www.microsoft.com

1 INTRODUCTION

This chapter gives a brief overview of this dissertation. This chapter is an introduction to the aspects that are considered in this work. The layout of the whole document is presented as well.

1.1 Motivation

The natural resources given to Mankind, which are available on Earth, are strictly bounded. Natural resources such as crude oil, coal or natural gas are running out. In a few decades, this lack of energy can be a huge problem, which touches especially the developed countries on the world. It is necessary to find alternative sources of energy or to find other resources in the surrounding universe. However, the last solution seems nowadays to be extremely unrealistic, and is only possible in science-fiction literature. On the other hand, the resources in the environment become very valuable. Engineers have to face the challenge, because their projects must work with the same or even higher efficiency, but with a lower cost. Lower cost means a lower energy consumption, and also that more consumers can share the same resource.

The above presented description about of the economy of projects and world resources problems is very suitable to characterise the problems of mobile communications. It is possible to use only a small fragment of the radio spectrum for commercial use. In many cases, the prospects of enlarging the bandwidth, which can be desired for mobile telephony, are not realistic. The range of frequencies that is useful for mobile phones is limited, inter alia by some physic rules describing the propagation of the signal. One can not also forget that virtually every data transmission, of course not for large distances, is going to be wireless. There are a lot of systems that transmit signals between terminals and work using very similar frequencies, which are located very close to each other. The radio frequency spectrum becomes saturated.

On the other hand, the demand on the mobile telephony services increases. The number of users of wireless telephones is growing, and at the same time the expectation of a higher speed of transmission is also increasing. These two tendencies are against each other, because the more users in the system the more transmitters (Txs) are transmitting at the same time. It is impossible to build a system, in which every user, every Tx, will be isolated from the environment and from other terminals. Unfortunately, when a device transmits power and even it does not matter if a wire is used or not, always some interaction with other different devices will appear. Of course, the problem is greater in the case of wireless transmissions. The energy is not focused on the specific medium, but it is spread over space. Every object, both inanimate and animate**,** will interact in some way with this energy. These problems are considered by the Electromagnetic Compatibility (EMC) science. The interaction between objects is larger when they work using the same signals, the same modulations, similar bandwidths, and they have

antennas to detect or to send energy. This description suits the situation where mobile telephones work close to each other, and communicate with the same or neighbouring base stations, being located in the same or in consecutive cells. The increasing number of terminals causes a grow of the disturbance of the signal from other users. Every additional active transmitter in the environment causes that in every link some level of unexpected power is added. On the other hand, to have a higher speed of transmission in the same bandwidth, it is necessary to have a larger ratio between the power of the desired signal and the powers of interference and noise. In case this ratio can not be kept in a satisfactory level, a correct transmission will not exist, and some errors during the detection of the signal will appear. As a result, the speed of the transmission will decrease, and in an extreme situation the link between receiver (Rx) and transmitter (Tx) will break. The conclusion is that it is necessary to have a good quality of the link to obtain a high transmission speed, and when the number of users increases, this condition must be realised.

Nevertheless, it is also possible to obtain a good speed of transmission, when the quality of the link is not that much satisfactory. One can use better and more efficient modulation techniques, as well as the more convenient multiple access techniques. By using these techniques one can make a characterisation of UMTS, which is a successor of GSM. This dissertation considers aspects connected to the influence on the quality of the link of terminals, their location in the cell and the shape of the deployment.

However to make possible the calculation of any parameters of the link, the first thing that must be done is the definition of the channel model, which enables the simulation of the way of signals propagate in the environment. The channel model has to satisfy many of conditions. The first, and the most important one, is that the results from the channel model in the statistical approach have to be in agreement with the results obtained from real measurement campaigns. It is important to define the level of compatibility which is expected. These results need to have a feature that after averaged over many measurements or many iterations of the simulation will be taken for comparison, mean values and standard deviations presenting the same tendency. It is not possible to obtain the same results, especially when a statistical model of the channel is used, but the results in the statistical domain need to be similar. Another aspect is the type of output parameters from the model. In 3G systems, channel models need to be considered in both time and space domains. It becomes important to consider and sort multipath components not only in time but also in angle. Intelligent antennas are used, thus, the direction of the arrival as

well as the departure one of the components will play an important role. A description of these aspects can be found in [MaCo04] and [LiRa99].

Propagation between the Tx and the Rx, especially in scenarios that contain a lot of objects with a dimension comparable or larger than the wave length, occurs in very complicated ways. This kind of situation is present in city scenarios, where the signal from the Tx reflects from the walls of buildings or disperses around their edges or the leaves from trees. In this case, it is expected that multipath components can appear around both the Tx and the Rx antennas. The channel model is defined by using the geometrical approach. One can imagine the plane containing some obstacles causing the reflection of the signal. This plane is not infinity in space, but has some dimensions that are determined by measurements campaigns. In this approach, a lot of assumptions are made. The most significant is that the propagation of all multipath components takes place in the same plane. This situation is realistic when the Rx and the Tx antennas are located in the same level over the ground, and when the distance between the two ends of the link is long enough. In this case, even when reflectors are located in different levels over the ground, the differences between the levels of the antennas and obstacles do not have a great influence on the accuracy of the results. Using this approach, the propagation of the signal can be easily described by a geometric way between the point that represents the Tx to the point that represents the Rx. When the path is direct, there is line of sight (LoS) component. In case the path is not a straight line, but passes through a reflector, it represents the non line of sight (NLoS) component. The number of multipath components is determined by the number of reflectors.

The model presented above is not accurate enough to describe the propagation of a signal. An improvement was implemented, proposed by the Group for Research On Wireless (GROW) from Instituto Superior Técnico (IST) [MaCo04]. It was noticed that multipath components arrive grouped in clusters, hence, instead of using a singular reflector, clusters of reflectors are used. This approach models also the dispersion of the signal.

The aim of this work is to simulate an environment with more than one user. In a system many, links exist between the Rxs and Txs. Every link can be described by a geometrical region, as mentioned earlier, and when terminals are located close enough, the regions which are related with them will have common elements. Of course, reflectors from the common elements are also common for the links. Propagation between the different terminals will consider partly the

same reflectors, therefore, the signals from the different links will be highly correlated with each other in some parts.

Multiuser aspects will be analysed in different scenarios, in micro-, macro- and pico-cells. In every scenario, a different users' layout will be defined. Terminals will be grouped in regular structures, and they will be positioned in random places as well. The quality of the links will be analysed for both the up- and downlink. Also aspects related with the different types of synchronisation of terminals will be investigated.

1.2 The dissertation outline

This dissertation is divided into some chapters. The work follows with Chapter 2, which contains the basic information about UMTS. The air interface and considerations about interferences and capacity are presented. Then a review of the channel models is made. Some models, in which the geometrical principles are used, are briefly described. The chapter is followed by a detailed description of the chosen model, Geometrically Based Single Bounce Channel Model (GBSBCM), and the scenarios in which this model is implemented. Simulations will be made in micro-, macro- and pico-cells. The most important features as well as the parameters of these scenarios are described there. The chapter finishes with general aspects of antenna arrays, as the simulator is able to use these antennas.

Chapter 3 contains the description of multiuser interferences, the main topic of this work. In the beginning, background knowledge on interference is presented. Two types of the models for interference are presented: Multi Access System and Interference Channel [Reza02]. These models describe multiuser interference in a general approach. Chapter 3 follows with the definition of multiuser interference in the form that is used in the simulations. Considerations are developed in the "lowest level", which means that is intended to obtain the output parameters in the form that is presented in Chapter 2. The next part of Chapter 3 contains the description of the two possible situations. The first one is connected with interferences, which sources are located within the same cell, i.e., intra-cell interferences. The second one considers the interferences from the different cells ,i.e., inter-cell interferences. Every type of interference is considered in the micro-, macro- and pico-cell scenarios. In the description of interferences there is also attached the "high level" approach. There is an explanation of the interference using the example of CDMA and TDMA multiple accesses techniques.

Chapter 4 contains the description of the developed simulator. This chapter is divided into two sections. Initially the basic simulator is presented, which calculates the channel model between a single Tx and the Rx antennas in three kinds of the scenarios. In this section a description of the input and output parameters is shown, as well as the algorithm. This section finishes with the explanation of the assessments that were carefully made to check the correctness of the program; the results were compared with others obtained from the other channel simulators, which were implemented using the same channel model. In the consecutive part of this chapter, one explains the enhanced version for different links. This section contains also the list of input and output parameters, the description of the algorithm, and finishes with the assessments.

Chapter 5 includes the results of the simulations. This chapter begins with the description of the scenarios that were taken for simulation. The ideas and basic parameters of these scenarios were taken from one of the Flexible Convergence of Wireless Standards and Services (FLOWS) project documents [VCGC03]. In this chapter, the cases of the up- and downlink scenarios in different types of cells are presented. The next part of Chapter 5 contains the results from the particular scenarios, and a discussion about the obtained results is presented.

In Chapter 6, the final conclusions of the work are drawn. This dissertation contains also Annexes, where one presents the calculations for the assessment and all results.

2 SYSTEM AND CHANNEL MODEL

In this chapter, some information related with radio interface of UMTS can be found. The system is also presented with reference to capacity and interferences. A review of radio channel models can be found in the chapter as well. The GBSB model is described in detail. In the end, some aspects related with linear and circular antenna arrays are presented.

2.1 UMTS – system aspects

2.1.1 Aspects of air interface

In Universal Mobile Telecommunications System (UMTS), one can distinguish two transmission modes between the Mobile Terminal (MT) and the Base Station (BS), which are related with the use of the frequency spectrum. Frequency bands are divided into complementary and non-complementary regions. Additionally, fragments of the spectrum are reserved for satellite communication, but this is out of interest for this work. The bandwidths for UMTS are shown in Figure 2.1.

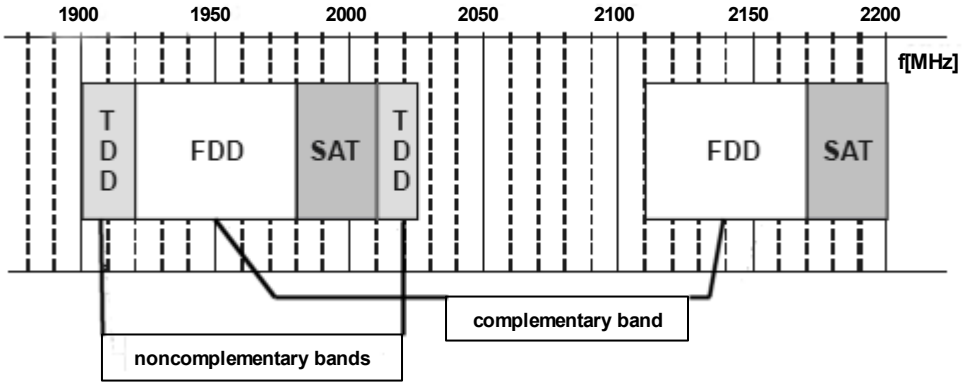

Figure 2.1 – UMTS bandwidth [KoCi04].

The non-complementary bandwidths are connected with Time Division Duplex (TDD), which are allocated at [1900-1920] MHz and [2010-2025] MHz. In these parts of the spectrum, Time Division-Code Division Multiple Access (TD-CDMA) is used [KoCi04].

TDD is a transmission method that uses only one frequency channel for transmitting and receiving, separating them by different time slots. This means that both the MT and the BS radiate power using the same frequency carrier, but in different periods of time.

In Figure 2.2 one can see time slots for three users. Users number 1 and number 2 use only one slot for the downlink (DL) and one slot for the uplink (UP), but user number 3 needs a bigger throughput for the download, therefore, the system allocates more time slots for the download.

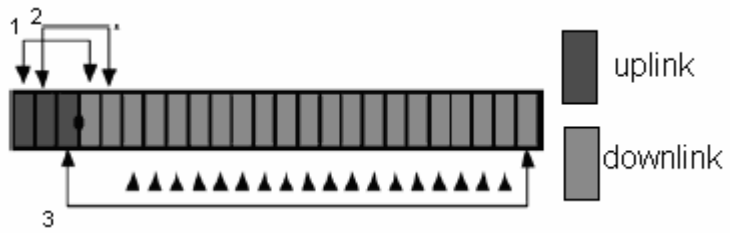

Figure 2.2 – Slots in TDD [KoCi04].

Generally speaking, there are the same propagation conditions in both directions. But it must be taken into consideration that the coherence time, the period that a radio channel can be treated like constant (later, it will be described more carefully), can be shorter than the time duplex interval, in which case the channel characteristics are dissimilar for the two directions of the radio link.

Frequency Division Duplex (FDD) is used in the complementary part of the bandwidth, which is allocated at [1920-1980] MHz (UL) and [2110, 2170] MHz (DL). Different from the method for TDD, Wideband-CDMA (W-CDMA) [KoCi04] is used. In FDD there are 12 radio channels, while in TDD there are 7.

The application of FDD means occupation of two identical bandwidths, which is very useful for voice transmission. For typical speech, both the UL and the DL are busy with the same ratio. In data or multimedia transmission, there exists a clear asymmetry in the UL and DL occupation. A link toward the subscriber can be used more intensive. Sometimes there is a tenfold difference in throughput of information. Concluding, TDD is best suitable for data and multimedia transmission, because in this technique link asymmetry is available. The number of time slots for the DL and UL depend on the need of the subscriber. System resources can be allocated in a dynamic way.

FDD is a transmission in which the two sides of the radio link use a different bandwidth to transmit. The distance in the radio spectrum between the MT and the BS is constant and equals 190 MHz for each cell. Due to this, there are different conditions for signal propagation for the DL and the UL. Thus, one must consider these links separately. Parameters for FDD and TDD are presented in Table 2.1.

There are three kinds of channels related with UMTS [KoCi04]:

- Physical channel – realise the transmission using the radio resources. They are defined by the radio channel (central frequency and bandwidth) and the scrambling codes.
- Transport channel – determine the way of the transmission:
  - Common – this type of channel is used to send information to all MTs within a cell.
  - Dedicated – carry information between the MT and the BS. It is possible to control the throughput and the power of the transmitter.
- Logical channel – determine the type of information.

Table 2.1 – Parameters of FDD and TDD in UMTS [KoCi04].

Duplex Method	FDD	TDD
Multi-access technique	FDMA, CDMA	TDMA, CDMA
Distance between adjacent channels [MHz]	5	5/1.6
Radio channel throughput [Mchip/s]	3.84	3.84/1.28
Spreading	4…512	1…16
Frame duration [ms]	10	
Amount time slots per frame	15	
Changing throughput to subscriber	Length of code	Amount of time slots and length of code
Protecting coding	Convolution codes and turbo-codes	
Interleave [ms]	10, 20, 40, 80	
Modulation	QPSK	
Detection in receiver	Coherent with pilot	Coherent with training sequence
Power control [Hz]	1500	100…800

2.1.2 Interference and capacity

A link from the MT to the BS determines the quality of the overall communication [KoCi04]. Power control of transmitters is a very important factor influencing the capacity of the entire system. In a system with code spreading, it is essential that the BS receives the signals from every user with the same power level.

According to [3GGP], the signal to interference and noise ratio for the UL and the DL are respectively given by:

$$SIR_{UL} = \frac{G_p P_{Rx}}{(I - \beta_{SIR}) I_{intra} + I_{inter} + N_0} \tag{2.1}$$

$$SIR_{DL} = \frac{G_P P_{Rx}}{\alpha_{SIR} I_{intra} + I_{inter} + N_0} \tag{2.2}$$

where:

- G_p: spreading gain - ratio bandwidth after spreading to bandwidth before spreading
- $P_{Rx[W]}$: power of the received signal
- $N_{0[W]}$: power of the thermal noise
- $I_{intra[W]}$: power of the interference generated inside the own cell
- $I_{inter[W]}$: power of the interference from other cells
- α_{SIR}: orthogonality factor
- β_{SIR}: interference reduction factor

The orthogonality factor α_{SIR} describes the influence of the multipath propagation on the characteristics of the DL for the radio interface (with code division). When α_{SIR} equals 0, it means perfect detection conditions and intra-cell interference does not exist. The opposite situation takes place when α_{SIR} equals 1.Typical values of orthogonality factor are [3GGP]:

- 0.4 for macro-cells
- 0.06 for micro-cells

The expression for the power of the interference from other cells, inter-cell interference, accumulates the influences of radio signal transmitted by users from adjacent cells. Additionally, another cellular operator can be a source of interference.

The capacity of a mobile cellular system determines the maximum number of users per cell. In UMTS, capacity is bounded mainly by the DL, because the transmit power of BS is limited. It is also related with aspects like spreading codes, user's behaviour (meaning, e.g., throughput or velocity of terminal) and many others. In UMTS, there are three main factors, which directly describe capacity:

- air interface traffic load
- the maximum BS transmission power
- number of OVSF codes

The influence of the number of OVSF codes on the overall system capacity is important in some situations, e.g., when almost all MTs are located near the BS and demand a low rate data transfer, see Table 2.2.

Table 2.2 – Maximum bit rate for Dedicated Physical Control Channel (DPCCH) [KoCi04].

Number of OVSF Codes	Bit rate for DPDCH [kbit/s]
256	15
128	30
64	60
32	120
16	240
8	480
4	960

The capacity of the system is also dependent on load factors, which define load both in the UL and the DL, respectively given by:

$$\eta_{\mathrm{UL}} = (1 + i_{BS}) \sum_{j=1}^{N_{UL}} \left(1 + \frac{\frac{R_c}{R_{bj}}}{\left(\frac{E_b}{N_{sp}} \right)_j \nu_j} \right)^{-1} \tag{2.3}$$

$$\eta_{\mathrm{DL}} = \left(\left(1 - \overline{\alpha} \right) + i_{MT} \right) \sum_{j=1}^{N_{DL}} \nu_j \frac{\left(\frac{E_b}{N_{sp}} \right)_j}{\frac{R_c}{R_{bj}}} \tag{2.4}$$

where:

- N_{UL}: number of users per cell
- N_{DL}: number of connections per cell = N_{UL} × (1 + soft handover overhead)
- ν_j: activity factor of user j at the physical layer, usually 0.67 for speech and 1 for data
- E_b: signal energy per bit
- N_{sp}: noise spectral density (including thermal noise and interference)
- R_c: WCDMA chip rate (3.84 Mchip/s)
- R_{bj}: bit rate of user j
- i_{BS}: inter-cell to intra-cell interferences ratio as seen by the BS receiver

- i_{MT}: inter-cell to intra-cell BS power received by the MT, typically 0.65 for macrocell and 0.2 for microcell
- $\overline{\alpha}$: average ortogonality factor in the cell, from range [0,1], typically values are 0.6 for vehicular and 0.9 for pedestrian [Reis04]

The capacity of the system is also bounded by the maximum power of the BS:

$$P_{\max} = \frac{N_0 R_c}{1-\overline{\eta_{\mathrm{DL}}}} \sum_{j=1}^{N_{UL}} \frac{\left(\frac{E_b}{N_0}\right)}{\frac{R_c}{R_{bj}}} \overline{L_{pj}} \tag{2.5}$$

where:

- $\overline{L_{pj}}$: average attenuation between the BS and user *j*
- $\overline{\eta_{DL\ [\mathrm{bit/s}]}}$: average throughput for downlink

One can see that the capacity increases with the processing gain or decreases with E_b/N_0. But a drop of E_b/N_0 is always related with a decrease of quality of service. Taking under consideration the fact that the specific profile of human conversation makes it possible to introduce an activity factor, applying this coefficient causes the capacity of the system to improve [KoCi04].

The dynamic exchange between the capacity and the quality exists in each code spreading system. When the number of users in the cell decreases, it causes E_b/N_0 to increase. Moreover, a lower number of subscribers in the cell causes a drop of power of the intra-interferences. This means an improve of quality makes it possible to transmit data with higher throughput. A similar relationship exists between capacity and coverage.

2.2 Channel models

2.2.1 General aspects

Considerations about the models of a radio channel and the aspects of propagation are very important to create a simulator of radio channel. The use of such a tool is necessary in conditions where it is impossible to do measurements, e.g., in an inaccessible terrain, where the

simulation is the sole way to achieve very valuable information about the profile of the radio channel. The results from simulations can be used in the design or to make improvements in the area of radio planning, sensible deployment of BSs, and many others. Only a well examined channel model provides the opportunity to make improvements. It is also possible to make estimations of the capacity and the coverage of the system, which is really important for operators.

Three kinds of propagations model can be distinguished:

- empirical (statistical) model
- deterministic model
- mixed, based on the empirical and deterministic model

Before discussing channel models, it is necessary to introduce the propagation aspects. There are three main mechanisms considered during the analysis of propagation [Kosi04]:

- reflection – takes place if the dimension of the obstruction is significantly bigger than the wave length.
- diffraction – appears when waves meet objects with sharp edges. The wave is bent by the edge of an obstruction.
- scattering – is present if the dimension of the obstruction is smaller than the wave length, e.g., plants, rain, rough surfaces.

The radio channel can be described using time dispersion parameters like [Kosi04]:

- Mean Excess Delay

$$\bar{\tau}_{[s]} = \frac{\sum_k h_k^2 \tau_k}{\sum_k h_k^2} = \frac{\sum_k P_k \tau_k}{\sum_k P_k} \tag{2.6}$$

- RMS Delay Spread

$$\sigma_{\tau[s]} = \sqrt{\overline{\tau^2} - \left(\bar{\tau}\right)^2} \tag{2.7}$$

where:

$$\overline{\tau^2}_{[s^2]} = \frac{\sum_k h_k^2 \tau_k^2}{\sum_k h_k^2} = \frac{\sum_k P_k \tau_k^2}{\sum_k P_k} \tag{2.8}$$

- $h_{k[V]}$: amplitude the Channel Impulse Response (CIR) at instant τ_k

- $P_{k[W]}$: a power of the CIR at instant τ_k

The radio channel can also be defined by a coherence bandwidth and a coherence time. The coherence bandwidth is a range of frequencies over which the radio channel is flat. It means that all spectral components pass the channel with the same gain and with a linear phase shift. The coherence bandwidth can be also defined in another way. It is possible to define the coherence bandwidth as the range of frequencies over which the frequency correlation is above 0.9, which gives [Kosi04]:

$$B_{C[Hz]} = \frac{1}{50\sigma_\tau} \tag{2.9}$$

In the typical mobile radio channel, the coherence bandwidth is significantly narrower than the frequency spacing in FDD. It means that the UL and the DL bandwidth should be considered separately [MaCo04].

The coherence bandwidth does not describe the varying nature of the channel caused by motion of a transmitter or a receiver, which is taken into consideration by the coherence time. The coherence time is the duration over which the CIR is essentially invariant, and it can be defined as [Kosi04]:

$$T_{C[s]} \propto \frac{1}{f_m} \tag{2.10}$$

where:

- $f_{m[Hz]}$: a maximum Doppler shift frequency:

$$f_m = \frac{v}{\lambda} \tag{2.11}$$

- $v_{[m/s]}$: velocity of the MT or the BS
- $\lambda_{[m]}$: wavelength

If a correlation above 0.5 is assumed, the coherence time has the following form:

$$T_{C[s]} = \frac{9}{16\pi f_m} \tag{2.12}$$

If the symbol period of the baseband signal is greater than the coherence time, the signal is changing during its transmission. The coherence time definition implies that two signals,

arriving with a time separation greater than the coherence time, are affected differently by the radio channel.

In most causes, especially when the velocity of the MT is low, the coherence time is longer than the time interval in TDD [MaCo04]. Thus, it is possible to use the same model for both ways of transmission.

2.2.2 Models

Empirical models are defined by statistical distributions, which are the result of the analysis of many measurement sessions. These models are very flexible and do not demand the tricky knowledge about an environment, but their accuracy is not very high.

In the deterministic models, the knowledge of the environments is needed. This approach uses a database of terrains and buildings within the desirable environment. Also electromagnetic techniques are exploited. Deterministic models estimate the propagation of radio waves analytically, relying on mathematical formulas. Two techniques are known: solving electromagnetic formulas, and ray tracing. The former is highly complicated, and the latter needs a huge computer power.

In a deterministic view, accuracy depends only on the accuracy of reproduction of the environment. So, it is possible to obtain an accurate channel model. But a disadvantage of this approach is that it demands huge amounts of geometry information about localisations of obstructions and a large computational effort.

Combined models, which mix the two models presented above, can achieve good accuracy, but do not demand such huge computational efforts, like the deterministic ones. These models are some kind of compromise between accuracy and complexity. As it is presented in [MaCo04], arriving signals can result from geometric contributors – just like in the deterministic model, but some properties of the contributors (e.g., localisation, physical characteristics) can be modelled statistically.

Some systems with omni-directional antennas working in a statistical model are described by a signal strength, a power delay profile (PDP), and a Doppler spectrum. An example of a model which has a path loss with distance as an output parameter is the COST 231 Okumura-Hata model [COST99]. Each environment specification is described by different equations. The model provides fast calculations and is not complex. But the calculation's precision is not very high, and depends on the structure of the terrain.

The Ikegami model is an example of a deterministic model [COST99]. The Ikegami model provides a deterministic prediction of field strength in some destinations points. To apply this method, a database including information about buildings, heights, shapes and localisations, is necessary. The model relies on ray tracing, and uses geometrical optics to model reflections of optical rays.

Space-time models provide spatial information and parameters like Angle of Arrival (AoA) and Time of Arrival (ToA), and are very important to analyze smart antennas and beamformers of space-time systems. In systems with multiple antennas, information about direction is very important and models that provide these types of data are required. Below, examples of the mentioned models are presented:

- Lee's Model
- Discrete Uniform Model
- Gaussian Wide Sense Stationary Uncorrelated Scattering Model
- Uniform Sectored Distribution Model
- Geometrically Based Single Bounce Channel Model

Lee's model was one of the first models, which considered spatial modelling [Lee73]. The Lee model assumes that reflection contributors are evenly deployed in a circle. At the centre of the circle is an MT, see Figure 2.3.

Scatters are distributed around the MT, and a receiver installed on the MT can only detect NLoS components. The drawn reflectors represent overall behaviour of blockers enclosed by the circle [Marq01].

Based on definitions of R and d_0 from Figure 2.3, one can derive a form describing the AoA (2.13) [Marq01].

$$\varphi_i = \frac{R}{d_0} sin\left(\frac{2\pi}{N_{sc}} i\right) \tag{2.13}$$

where:

- $i = 1,..., N_{sc}$
- N_{sc}: number of scatterers (all are uniformly distributed on circle)
- $d_{0[m]}$: distance between the MT and the BS
- $R_{[m]}$: radius of the circle, where the scatterers are deployed

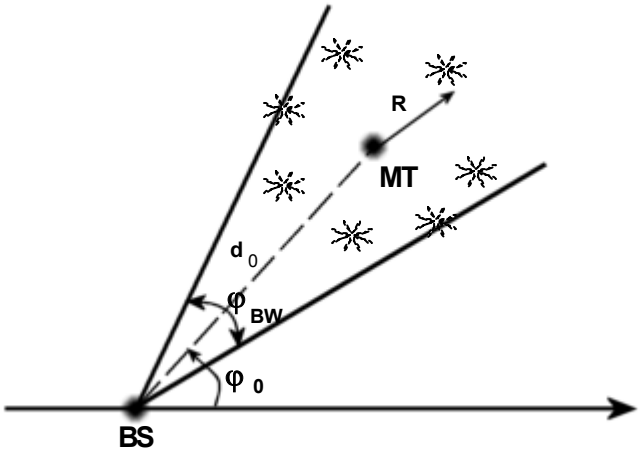

Figure 2.3 – Lee's model.

The signal correlations between two array elements, with assumptions that the complex magnitude has zero mean and unitary variance, has the form [Marq01]:

$$corr(d,\varphi_0) = \frac{1}{N}\sum_{i=0}^{N-1} exp\left[-j\frac{2\pi d}{\lambda} cos(\varphi_0 + \varphi_i)\right] \tag{2.14}$$

where:

- $d_{[m]}$: spacing between antennas in an antenna array

In its original form, this model was used to determine the correlation, but it was expanded to consider small-scale fading caused by the Doppler shift, by imposing an angular velocity on the ring of scatterers. The angular velocity of the scatterers, corresponding to the maximum Doppler shift, is equal to [ErCa98]:

$$\omega_D = \frac{V}{R} \tag{2.15}$$

where:

- $v_{[m/s]}$: velocity of the MT

In case of effective's scatterers on ellipse lines, the concentration of scatterers is focused on two areas: one finds them in ellipses connected with minimum delay, and with maximum delay. And in between them, the concentrations are low. This kind of distribution is called "U-shape".

The Discrete Uniform Model (DUM) is useful to predict the correlation function between any of two elements of an antenna array [ErCa98]. DUM is similar to the earlier presented Lee model. The model assumes N_{sc} uniformly distributed scatterers in space, within a narrow beamwidth, as shown in Figure 2.4. As one can see, the beamwitdh is centred relative to the LoS component.

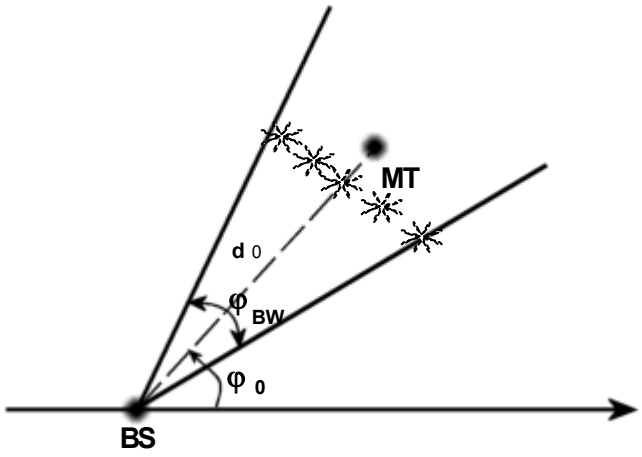

Figure 2.4 – Discrete Uniformly Distribution model.

The formula describing the AoA is given by [ErCa98]:

$$\varphi_i = \frac{1}{N-1}\varphi_{BW} i \tag{2.16}$$

where:

- $i = -\frac{N_{sc}-1}{2},\ldots,\frac{N_{sc}+1}{2}$

Correlation between two antenna elements can be described by:

$$corr(d,\varphi_0) = \frac{1}{N_{sc}} \sum_{i=-\frac{N_{sc}-1}{2}}^{\frac{N_{sc}+1}{2}} \exp\left[-j2\pi d \cdot \cos(\varphi_0 + \varphi_i)\right] \tag{2.17}$$

According to [ErCa98], the AoA distribution in the rural and suburban environments has a Gaussian continuous distribution, and the characteristic of the AoA in the urban environments tends to be discrete. Therefore, to describe the correlation function between two antenna arrays one should use the discrete version of the AoA distribution.

Using this model, it is possible to determine the array correlation matrix, but it does not enable to calculate such parameters like delay spread, and Doppler spread, which require simulations.

The Gaussian Wide Sense Stationary Uncorrelated Scattering (GWSSUS) model is an example of a statistical model. This model assumes that scatterers are grouped into clusters in space. The received signal is a result of scatterers, which are grouped in N_{cl} clusters [Marq01]. The difference between delays, which are correlated with particular contributors, is not larger than the period of the signal, so the channel can be considered as wideband. There is no correlation between clusters. It is possible to model a frequency-selective fading channel, by including multiple clusters. The vector of the received signal can be described as [ErCa98]:

$$y(t) = \sum_{i=1}^{N_{cl}} v_{i,b} conv(t - \tau_k) \tag{2.18}$$

where:

- N_{cl}: number of clusters
- *conv(t)*: the convolution of the modulation pulse shape with the receiver filter impulse response
- $v_{i,b}$: superposition of the steering vectors during the i^{th} data burst within the k^{th} cluster

$$v_{i,b} = \sum_{j=1}^{N_{sc,k}} E_{Rx\,i,j} e^{j\phi_{Rx\,i,j}} G_{Rx}\left(\varphi_{0,j} - \varphi_{i,j}\right) \tag{2.19}$$

- $N_{sc,k}$: number of scatterers within k^{th} cluster
- $E_{Rx\,i,j}$[V] amplitude of i^{th} component reflected from j^{th} cluster
- $\Phi_{Rx\,i,j}$[rad]: phase of i^{th} component reflected from j^{th} cluster
- $\varphi_{i,j}$[rad]:AoA of i^{th} component reflected from j^{th} cluster
- $\varphi_{0,j}$[rad]:mean value of AoA from j^{th} cluster
- $G_{Rx}(\varphi)$: array response vector in the direction of φ

In the case that every cluster consists of a sufficient large number of the scatterers $v_{i,b}$ can be assumed according to a Gaussian distribution. This model assumes that time delays τ_k can be

considered constant over several burst, phases $\Phi_{Rx\ i,j}$ vary more significantly, and vectors $v_{i,b}$ are zero mean complex Gaussian distributed wide sense stationary random processes (stationary during several data bursts in this case) [Marq01]. In case there is no LoS, the mean value will be zero due to the uniformly distributed phase form range [0,2π[. When LoS is present, the mean value corresponds to the array response vector [ErCa98]:

$$E\{v_{i,b}\} \propto G_{Rx}(\varphi_{0,j})$$

The expression for the covariance matrix for the j^{th} cluster has the form [Marq01]:

$$\mathbf{cov}_i = E\{v_{i,b} v_{i,b}{}^H\} = \sum_{j=1}^{N_{sc,k}} \left|E_{Rx,i,j}\right|^2 E\{G_{Rx}(\varphi_{0,i} - \varphi_{i,j}) G_{Rx}(\varphi_{0,i} - \varphi_{i,j})^H\} \tag{2.20}$$

The Gaussian Wide Sense Stationary Uncorrelated Scattering model provides a fairly general result for the form of the covariance matrix [ErCa98]. This model requires some additional information of the propagation environment, because it does not give any indication about the amount and localisation of scatterers.

The concept of Uniform Sectored Distribution Model (USD), based on [MaHu03], is presented in Figure 2.5. This model assumes that all scatterers are uniformly distributed within some region, which is bounded by some angular and radial range. Every scatterer has a coefficient, which magnitude and phase are selected random from the distribution of U[0,1] for magnitude, and of U[0,2π] for phase. When the number of scatterers reaches infinity, the received signal will be similar to Raleigh faded with uniform phase [MaHu03]. This model is convenient to consider aspects connected with the effects of angle spread on spatial diversity techniques [ErCa98].

In Geometrically Based Single Bounce (GBSB) [LiRa99] channel models, the ToA and the AoA are derived with reference to the position of the transmit antenna, the position of receive antenna and a distribution of scatterers. Trigonometric relations are used to determine the mentioned parameters, but the distribution of scatterers is drawn. Also the specification of scatterers is random, because the magnitude and the phase have random values. Every scatterer generates one multipath component, which arriving at the receiver has a unique magnitude and phase. Also the delay time is random. The scatterer has no dimension, and therefore the scatterers do not overshadow each other. So the GBSB Model is a combination of deterministic and statistical features.

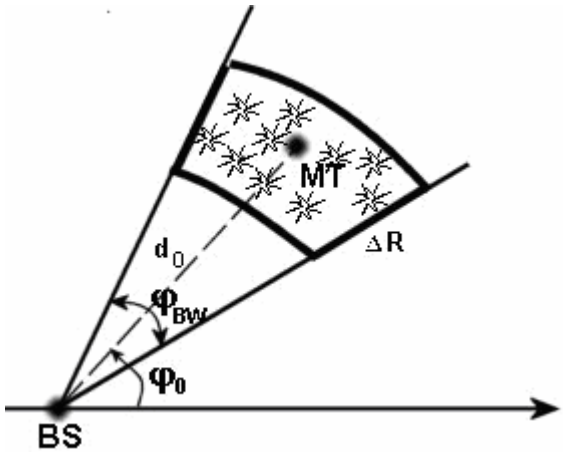

Figure 2.5 – USD model.

2.2.3 Scenarios

Usually three main typical scenarios are taken into account: a pico-, a micro- and a macro-cell. The location of the BS and the MT with reference to the deployment of scatterers is the main feature that distinguishes the scenarios [MaCo04]. The radius of the cell is also a factor which is helpful to sort the mentioned scenarios. According to the definition of Prasad [Pras98], the pico-cell has radius smaller than 200 m, the micro-cell has radius within [0.2, 1] km, and the macro-cell is larger than 1 km.

The area of the pico-cell is bounded by a circle, with the BS at its centre. The location of the MT is not defined, and depends on the actual position of the user. The LoS component exists in the considered scenario. A density of scatterers, Figure 2.6, is specific to each individual environment. The pico-cell is usually located inside buildings (e.g., hall of shopping centers). Dimensions of the place, where the pico-cell is established, mainly influences the radius of circle.

In micro-cells, the scattering takes place in the surroundings of both the BS and the MT, and also in the region between them [MaCo04]. The micro-cell scenario usually occurs when both the BS and the MT are located bellow rooftops, e.g., a street in the urban area. Scatterers are deployed, with the same density, around the BS, the MT, and in the zone between them.

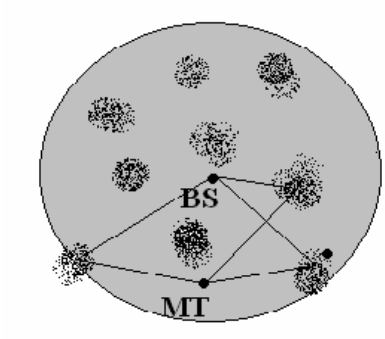

Figure 2.6 – Pico-cell scattering model.

When modelling a street-type environment the considered region should be bounded by the street width. The zone of multipath propagation has the shape of an ellipse, Figure 2.7, whose foci are the BS and the MT. The minor axis of the ellipse is determined by the width of the street.

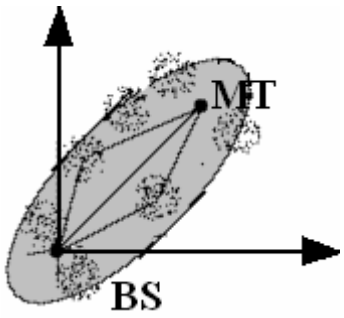

Figure 2.7 – Micro-cell scattering model.

Additionally, not only single bounces should be taken into account. Therefore, an effective street width is introduced, which is weighed by an effective street width ratio. Some parameters for the micro-cell model are presented in Table 2.3.

In the macro-cell scenario, the height of the BS antenna is larger than the height of the MT antenna, from which it follows that the scattering contributions are located in the area near to the location of the MT [MaCo04].

In the macro-cell case, the region of influence has the shape of circle, Figure 2.8. The scattering contributions in the vicinity of the BS will be disregarded.

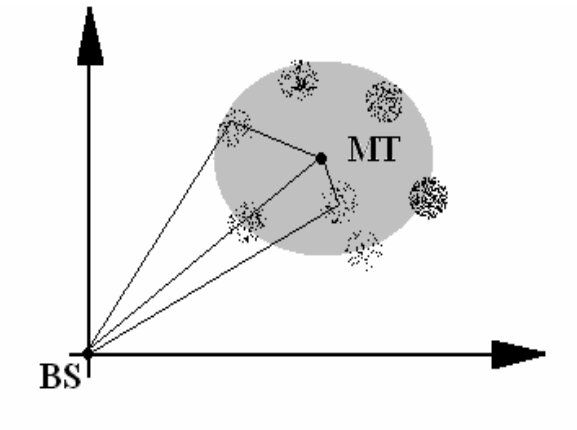

Figure 2.8 – Macro-cell scattering model.

The dimension of the circle is stipulated by a distribution of scatterers. The scatterers, placed on an external circle, produce the multipath components with the longest time delay. An assumption of a planar model is still correct, as long as the distance between the MT and the BS is large comparing to the difference between antenna heights.

Table 2.3 – Parameter list for the micro-, pico-, macro-cell model [MaCo04].

	Pico-cell	**Micro-cell**	**Macro-cell**
Region of influence:			
Region shape	Circle	Ellipse	Circle
Cluster distribution	Uniform within region		
Scattering circle radius	Measurement dependent		
Street width	Street dependent		
Effective street width ratio	Measurement dependent		
Cluster:			
Distribution of scatterers within clusters	Gaussian		
Cluster dimension (standard deviation)	Measurement dependent		
Cluster density	Measurement dependent		
Number scatterers per cluster	Poisson, Measurement dependent		
Average number scatterers per cluster	Measurement dependent		
Scatterers:			
Reflection coefficient magnitude distribution	Uniform [0, 1]		
Reflection coefficient phase distribution	Uniform [0, 2π[		
LoS path:	Yes	Yes	No

The next important difference between the macro- and the micro-cell is the fact that in the former there is no LoS component. The density of scattering contributors is essentially larger around the MT. So the LoS component is obstructed by the surrounding scatterers. Some parameters of the macro-cell scenario are presented in Table 2.3.

2.2.4 Geometrically Based Single Bounce Model

In the following part of this dissertation, the GBSB model [LiRa99] is presented in detail. This model is chosen to the implemented in a radio channel simulator.

In the GBSB model, the propagation environment is composed of scatterers, which are placed by statistical distributions, which are characteristic of specific conditions. More details about the deployment of scatterers can be taken from a description of the considered scenario, Table 2.3. Every scatterer is a source of one multipath component. A signal radiated from the transmitter and picked up at the receiver goes through the position of the corresponding scatterer, Figure 2.9. The scatterer is described by a random complex coefficient (2.21), which determines the influence on the multipath component. The magnitude of the coefficient, as well as the phase are random values,

$$\Gamma = |\Gamma| e^{j\Phi_{sc}} \tag{2.21}$$

where:

- $|\Gamma|$: the magnitude of the reflection coefficient, which has a uniform distribution in range [0,1]
- $\Phi_{sc\ [rad]}$: the phase of the reflection coefficient, which has a uniform distribution in range $[0,2\pi]$

After bouncing of the scatterer, the multipath component changes its magnitude and phase. The magnitude of the multipath is divided by the magnitude of the corresponding scatterer and the phase of the scatterer adds to the phase of the multipath component.

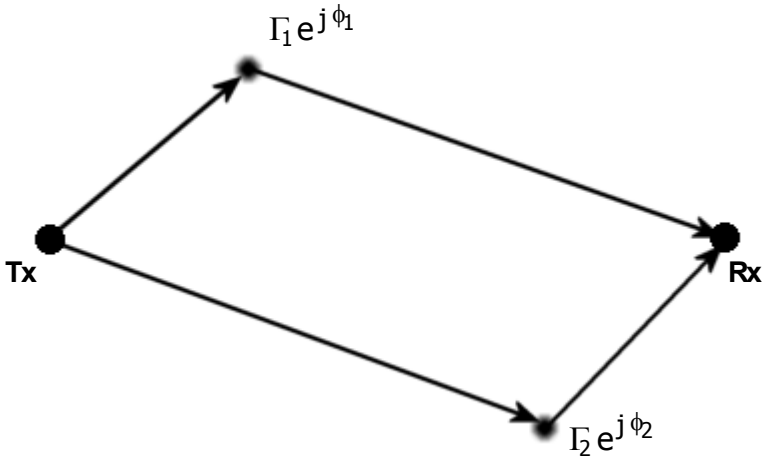

Figure 2.9 – Scatterers in the GBSB model.

During some research by Saleh and Valenzuela [SaVa87], [LKTB02], Vainikainen [AMSM02], and Bonek [MoBo99] a specific phenomenon was observed, i.e., the scatterers are grouped into clusters. In the area of a cluster there is dense deployment of reflectors. The time of arrival of the multipath component depends on the location and shape of the clusters. Looking at the number of groups of multipath, it is possible to approximate the number of clusters in the environment. The distribution of clusters is characteristic for a considered scenario, Table 2.3.

The phenomenon of grouping the scatterers into clusters is the main difference between the GBSB model [LiRa99] and IST-TUL model [Marq01]. The IST-TUL model was developed by the Group For Research On Wireless of the Instituto Superior Técnico.

The GBSB assumes that both the receiver (Rx) and the transmitter (Tx) are in the same plane that is parallel to the ground. Additionally, it is assumed, that all scatters are also located in this plane. Thus, it is natural that all multipath components also belong to this plane.

The model does not include rough surface scattering, diffraction, multiple bounce multipath and other mechanisms of propagation [LiRa99]. These assumptions make the analysis simpler, but the real zone of propagation is not modelled in a perfect way.

When both the Rx and Tx antenna are omni-directional, a complex envelope model for the multipath CIR is given by [LiRa99]:

$$\boldsymbol{h}(t) = \sum_{i=0}^{L-1} E_{Rx,i}\,\delta(t-\tau_i) = \sum_{i=0}^{L-1} \left|E_{Rx,i}\right| e^{j\Phi_{Rx,i}}\,\delta(t-\tau_i) \tag{2.22}$$

where:

- $\Phi_{Rx,i}$: phase of the i^{th} component
- τ_i: delay of the i^{th} component

It is possible to derive the probability density function based on geometrical consideration, for the case of elliptical deployment of the scatterers. This PDF has the form [Marq01]:

$$p_{\tau,\varphi}(\tau,\varphi)=\begin{cases}\dfrac{\left(d_0^{\,2}-\tau^2c^2\right)\left(d_0^{\,2}c+\tau^2c^3-2\tau c^2 d_0\cos(\varphi-\varphi_0)\right)}{\pi\tau_{\max}c\sqrt{\tau_{\max}^2c^2-d_0^{\,2}}\left(d_0\cos(\varphi-\varphi_0)-\tau c\right)^3}, & \dfrac{d_0}{c}<\tau\le\tau_{\max}\\ 0 & \text{,elsewhere}\end{cases} \tag{2.23}$$

where:

- τ_{max}: observation time window
- d_0, φ_0: geometry parameters defined on Figure 2.10

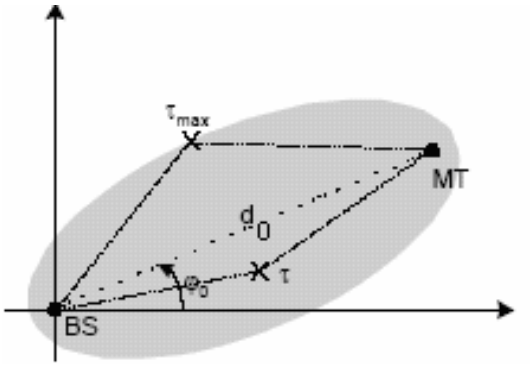

Figure 2.10 – Geometry for GBSBEM [Marq01].

To derive the joint density function for the AoA and the ToA, for the case of circular deployment of the scatterers, it is necessary to take advantage of the Jacobian Transformation, which makes it possible to achieve the PDF in an easy way. The resulting PDF is

$$p_{\tau,\varphi}(\tau,\varphi)=\frac{\left(d_0^{\,2}-\tau^2c^2\right)\left(d_0^{\,2}c+\tau^2c^3-2\tau c^2 d_0\cos(\varphi-\varphi_0)\right)}{4\pi R_{\max}^2\left(d_0\cos(\varphi-\varphi_0)-\tau c\right)^3} \tag{2.24}$$

where:

- R_{max}, φ_0: geometry parameter defined in Figure 2.11

The validity area for the BS and the MT cases are, respectively:

$$\frac{d_0^{\,2} - 2d_0\tau c\cos(\varphi-\varphi_0) + \tau^2 c^2}{\tau c - d_0\cos(\varphi-\varphi_0)} \le 2R_{\max} \wedge \tau > \frac{d_0}{c}$$

and (2.25)

$$\frac{d_0^{\,2} - \tau^2 c^2}{d_0\cos(\varphi-\varphi_0) - \tau c} \le 2R_{\max} \wedge \tau > \frac{d_0}{c}$$

Out of the validity area the PDF is equal to zero.

The presented model is based on geometrical assumptions, so all output parameters are calculated in a geometrical way. All variables, which are needed to obtain the parameters, are presented in Figure 2.12.

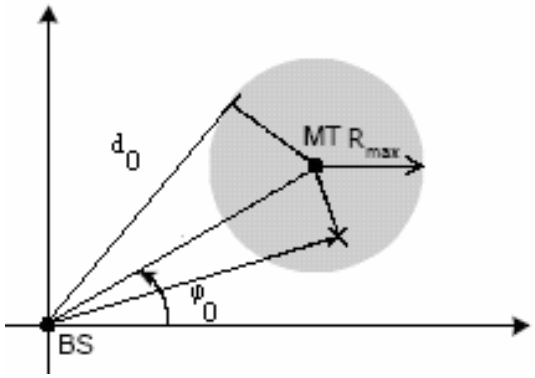

Figure 2.11 – Geometry for GBSBCM [Marq01].

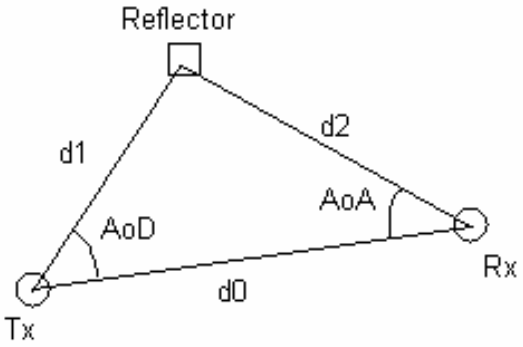

Figure 2.12 – Definition of some output parameters.

The AoA (φ) and AoD (θ) are obtained using the cosine formula:

$$\varphi_{[\deg]} = \arccos\left(\frac{d_0^2 + d_2^2 - d_1^2}{2d_0 d_2}\right) \quad (2.26)$$

$$\theta_{[\deg]} = \arccos\left(\frac{d_0^2 + d_1^2 - d_2^2}{2d_0 d_1}\right) \quad (2.27)$$

where distances d_0, d_1, d_2 are calculated from:

$$d_{0[m]} = \sqrt{(x_{Rx} - x_{Tx})^2 + (y_{Rx} - y_{Tx})^2} \tag{2.28}$$

$$d_{1[m]} = \sqrt{(x_{sc} - x_{Tx})^2 + (y_{sc} - y_{Tx})^2} \tag{2.29}$$

$$d_{2[m]} = \sqrt{(x_{Rx} - x_{sc})^2 + (y_{Rx} - y_{sc})^2} \tag{2.30}$$

where:

- (x_{Rx}, y_{Rx}): position of the Rx antenna
- (x_{Tx}, y_{Tx}) – position of the Tx antenna
- (x_{Ref}, y_{Ref}) – position of a reflector

The attenuation in free space and the reflection by scatterers must be taken into consideration to calculate the amplitude of a multipath component. The amplitude of the electric field detected at the Rx, is defined by:

$$E_{Rx[\mathrm{V/m}]} = \frac{\sqrt{30 \cdot P_{Tx} \cdot G_{Tx}(\theta)}}{d_1 + d_2} \cdot \Gamma \tag{2.31}$$

In case of the LoS component:

$$E_{Rx[\mathrm{V/m}]} = \frac{\sqrt{30 \cdot P_{Tx} \cdot G_{Tx}(0)}}{d_0} \tag{2.32}$$

where:

- $P_{Tx[\mathrm{W}]}$: the power of the Tx
- Γ: the reflection coefficient of the reflector
- G_{Tx}: radiation pattern of Tx antenna
- G_{Rx}: radiation pattern of Rx antenna

The signal detected by the antenna is described by equation [Orfa02]:

$$V = E_{Rx} \cdot h_{eff} \tag{2.33}$$

where:

- $h_{eff\,[\mathrm{m}]}$: effective lenght of antenna:

$$h_{eff} = \frac{\lambda}{\pi}\sqrt{\frac{R_A G_{Rx}(\varphi)}{120\pi}} \tag{2.34}$$

- $R_{A[\Omega]}$: feedpoint impedance of the antenna

Phase is another parameter obtained from simulation. The phase is related with the distance covered by the corresponding multipath component and complex reflection coefficient. The signal propagating from the Tx to the Rx covers the distance, which may not be equal to an integer multiple of the wave length. In case the signal reflects from a scatterer, an additional phase shift Φ_{sc} exists. An equation for the phase shift has the form:

$$\Phi_{Rx[^0]} = mod360\left(\left(\frac{d_1}{\lambda} - \left\lfloor \frac{d_1}{\lambda} \right\rfloor + \frac{d_2}{\lambda} - \left\lfloor \frac{d_2}{\lambda} \right\rfloor\right) \cdot 360 - \Phi_{sc}\right) \tag{2.35}$$

In case of the LoS component:

$$\Phi_{Rx[^0]} = \left(\frac{d_0}{\lambda} - \left\lfloor \frac{d_0}{\lambda} \right\rfloor\right) \cdot 360 \tag{2.36}$$

where:

- *mod360*(…): operation of modulo 360
- $\Phi_{sc[^0]}$: the reflector phase shift

The ToA describes the time delay of component, which is connected only with the distance of propagation:

$$\tau_{[s]} = \frac{d_1}{c} + \frac{d_2}{c} \tag{2.37}$$

and for the LoS component:

$$\tau_{[s]} = \frac{d_0}{c} \tag{2.38}$$

2.3 Antenna arrays – general aspects

In the channel simulator, both the Rx and the Tx can have singular radiators, multiple antennas, or antenna arrays. Some aspects connected with a linear and circular arrays, are presented in the next parts of the work.

There are two approaches for systems using several antennas; the antenna arrays and the multiple antennas are distinguished. The former takes into consideration the mutual coupling between the antennas, all antennas in the set influence one another, thus, all antennas can be treated like one abstract antenna with one radiation pattern. Looking at the transmit side of a

radio system it is worth noticing that each of the antennas transmits the same piece of information. The shape of the radiation pattern depends on some factors, the impact of each factor being described below. The latter approach does not consider the condition about the mutual coupling between antennas. Each of the antennas is treated separately, and the radiation pattern of the whole structure is the sum of radiation patterns of all antennas. In this case, the distance between antennas is larger, so they do not influence one another. In a real system, the small coupling between antennas exists, but in this work it will be neglected. This way of looking to a set of antennas is addressed for the MIMO system. So, each of the input antennas can transmit different information.

A uniform linear array consists of radiators, which are distributed uniformly along a line, with constant spacing *d*, Figure 2.13.

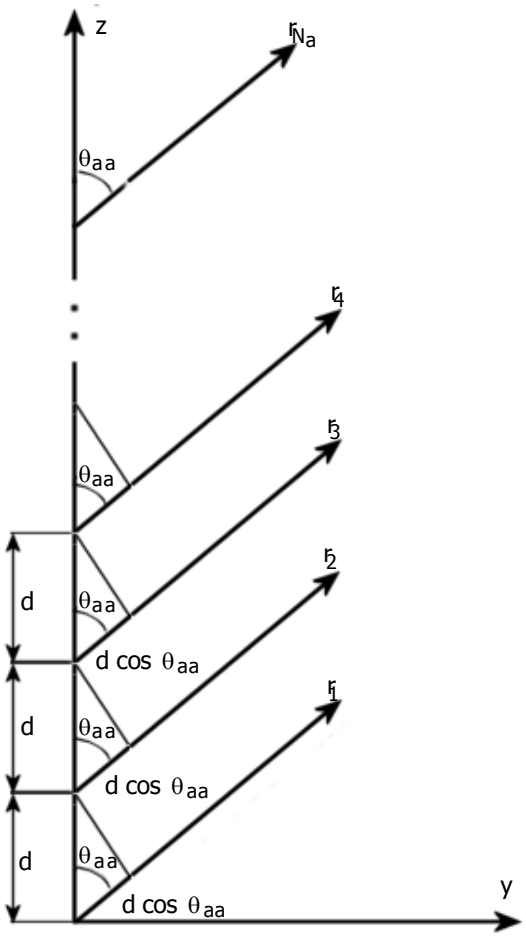

Figure 2.13 – Uniform linear array.

In the simplest array, all radiators are fed with the same amplitude and phase. The radiation pattern for the antenna array can be obtained as multiplication of a single antenna radiation

pattern and the Antenna Factor (AF). For the linear antenna array, the AF has the form of [VCGC03]:

$$AF = \sum_{n=1}^{N_a} e^{j\psi(n-1)} \tag{2.39}$$

where:

- N_a: number of antennas in array
- $\psi_{[rad]}$: phase coefficient given by:

$$\psi = kd\cos\theta + \psi_0 \tag{2.40}$$

- $\psi_{0[rad]}$: phase shift between radiators
- k: wave number

$$k = \frac{2\pi}{\lambda} \tag{2.41}$$

- d: spacing between antennas

The AF can be written in reduced form:

$$AF = \frac{\sin\left(\frac{N_a}{2}\psi\right)}{\sin\left(\frac{1}{2}\psi\right)} \tag{2.42}$$

The final radiation pattern for antenna array can be written as:

$$G(\theta_{aa}, \varphi_{aa}) = AF \cdot G_0(\theta_{aa}, \varphi_{aa}) \tag{2.43}$$

- $G_0(\theta_{aa},\varphi_{aa})$: radiation pattern of singular antenna

In a circular array, all radiators are distributed in the shape of a circle, Figure 2.14. The AF for the circular antenna array is of the form [VCGC03]:

$$AF(\theta_{aa}, \varphi_{aa}) = \sum_{n=1}^{N_a} I_n e^{j[ka\sin\theta\cos(\phi_{aa}-\alpha_n)+\Phi_n]} \tag{2.44}$$

where:

- $a_{[rad]}$: radius of circle
- I_n: feedings amplitude of n^{th} radiator – relative to the center of circle
- Φ_n: feedings phase of n^{th} radiator – relative to the center of circle
- $\alpha_n = 2\pi\frac{n}{N_a}$: the angular position of n^{th} element on the x-y plane

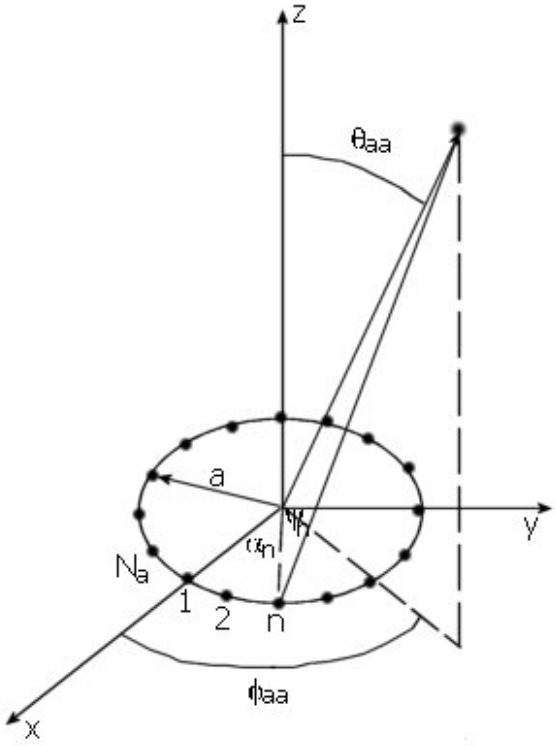

Figure 2.14 – Circular array [VCGC03].

3 MULTIUSER INTERFERENCE

This chapter contains the description of multiuser interferences. In the beginning, background knowledge on interferences is presented, followed by the definition of multiuser interferences in the form that is used in simulations. The next part of the chapter contains a description of the two possible situations: intra- and inter-cell interferences.

3.1 General aspects

In any mobile communications system, radio resources are strictly bounded. The main task of an operator is sharing these resources in an optimal way among subscribers. One must choose between quality and capacity. In the case of many users communicating in a cell, the level of interference will be considerable, and as a result, the quality of the links between particular users and the BS decreases. A larger number of users means a worse quality, a lower throughput and also less coverage, so a compromise is needed. There are two major factors that limit capacity and quality: multipath propagation and co-channel interference. The best parameter that describes the above mentioned aspects is the Signal to Noise plus Interference Ratio (SINR) [HoSz98]. The cellular operator should provide acceptable levels of SINR to every MT in the network, which can be achieved by controlling the power of the BS and the MTs, and also by limiting the number of active subscribers at the same time in a cell.

Multiuser interferences (MUI) are connected mainly to the uplink, because the BS detects the signals from many MTs at the same time. In CDMA, users share the same time interval and the same frequency band, as opposed to TDMA and FDMA. Users are separated by different spreading codes with a low cross-correlation between them. However, due to multipath propagation, orthogonality can not be maintained at the receiver and as a result, signals from other users interfere with each other. This aspect affects the sources not only inside the cell, but also outside it. CDMA techniques are used in both the TDD and the FDD modes, so MUI in UMTS can be based on code division access.

One can describe MUI in different views. One approach can be to consider the topology of the multiple access systems [Reza02]. In this case, some MTs are using the same radio resources to communicate with the BS that serves the cell, Figure 3.1. This approach is convenient to model the uplink, in cases where the BS detects the signals from all users in the cell. Signals from the MTs outside the cell are not considered here. The receiver in the BS detects and works only on the sum of signals from the users and thermal noise. This type of interference is called intra-cell interference.

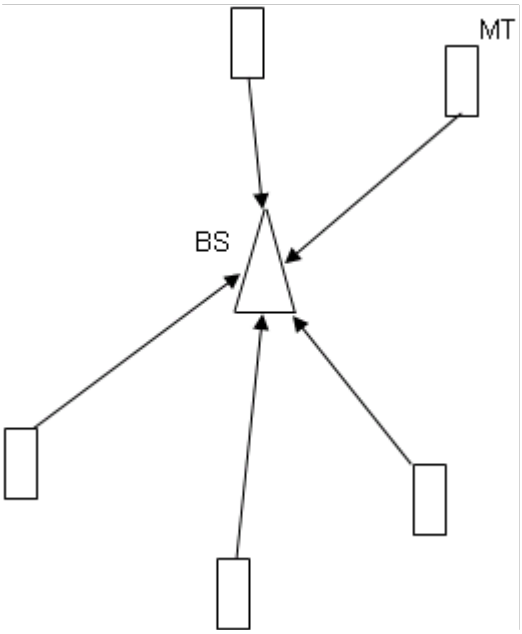

Figure 3.1 – Multi Access System [Reza02].

Another type of topology is the interference channel [Reza02]. In this approach, interference of users from other cells is taken into consideration. Any receiver in the system detects not only signals from the MTs of the home cell, but also from any other cell. The simplest model, which consists of two transmitters and receivers, is depicted in Figure 3.2 . This model is suitable to considerer the interference in multi-cell systems, where interference from other cells is noticeable. In comparison with the previous model, the channel is affected by non intended interference in addition to the channel's internal noise and multiple access interference. This type of interference is named as inter-cell interference.

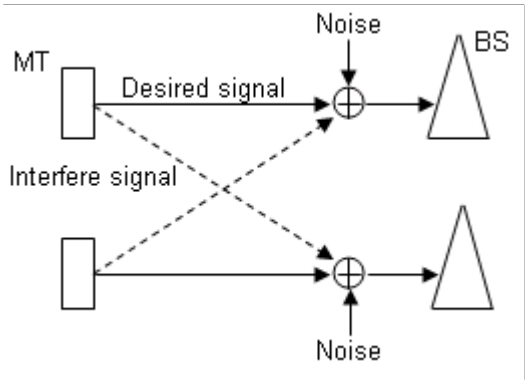

Figure 3.2 – Interference Channel [Reza02].

Considerations on MUI will be based on the GBSB model, which was described in Chapter 2. General problems connected with MUI are presented in Figure 3.3, which depicts two cells,

interfering with each other, with both inter- and intra-cell interferences. The BS from cell 2 can interfere both with the BS and the MTs from cell 1, the MTs can interfere with each other, within one and neighbour cells.

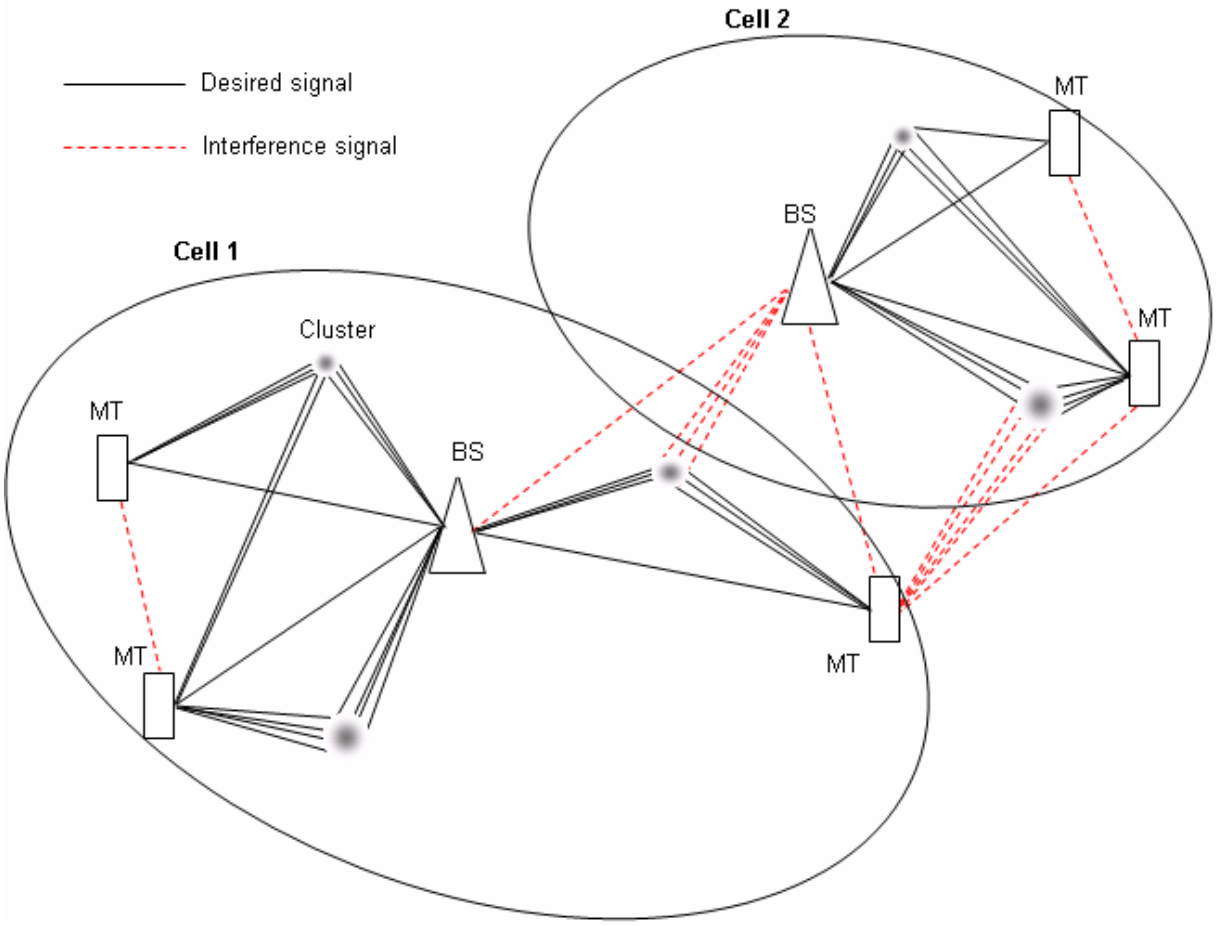

Figure 3.3 – MUI in the general approach.

All considerations about MUI are developed at "the lowest level", which means that it is intended to use the output parameters that were described in Chapter 2, from (2.26) to (2.38). Aspects connected with the interference, taking into account modulation, multiple access mode and others, can be developed after post processing these raw results. In this approach, the program will only simulate the propagation of the signal, which can reach the Rx in direct way (the LoS component) or indirect way, after reflection from scatterers (the NLoS component). In this way interfering signals are presented as a set of parameters, including angles, amplitude, power and phase. There is no difference, if this signal comes from the MT within the cell or the BS from another cell, because the parameters are exactly the same in both cases. This approach is very flexible, because it gives the advantage to simulate any radio system, and reduces the difficulty of the problem considerably.

In the subsequent part of this work, two cases of interference are presented. Every type of interference is decomposed into some scenarios, which are described in Chapter 2. Some general aspects, which are connected with MUI in the "higher level", including multiple-access, are be described.

3.2 Intra-cell interference

When considering intra-cell interference, users that are transmitting at the same time, disturb each other. During receiving and decoding of the signal from a particular user, the others are considered as sources of interference. The antenna at the BS is detecting all signals from users inside and even outside the cell.

The analysis about the multiuser channel in a micro-cell environment is based on the GBSB model. The propagation environment is modelled by an ellipse, which foci are the BS and the MT. Reflectors are uniformly distributed within the cell. Every user is related to a separate ellipse. There are as many ellipses as MTs active in the cell. In Figure 3.4 a cell with three MTs is presented. The cell is modelled as a family of ellipses, which have one common focus at the location of the BS. The dimensions of each ellipse are obtained separately, and are connected with the maximum path delay of the particular MT-BS link.

One can see that some ellipses have common areas, and it is natural that some reflectors can be related with more than one MT. In the presented case, one MT is considered as the desired user, and the others that are transmitting a signal at the same time are interferers.

A macro-cell is modelled in a similar way. The only difference is that the environment is modelled using the GBSB model, which was described in Chapter 2. All scatterers are located in circular areas around the MTs, and the BS is not surrounded by reflectors. Every user is related to a separated circle, and as in the previous case, there are as many circles as users that are transmitting at the same time, Figure 3.5. It is possible that some MTs have common reflectors.

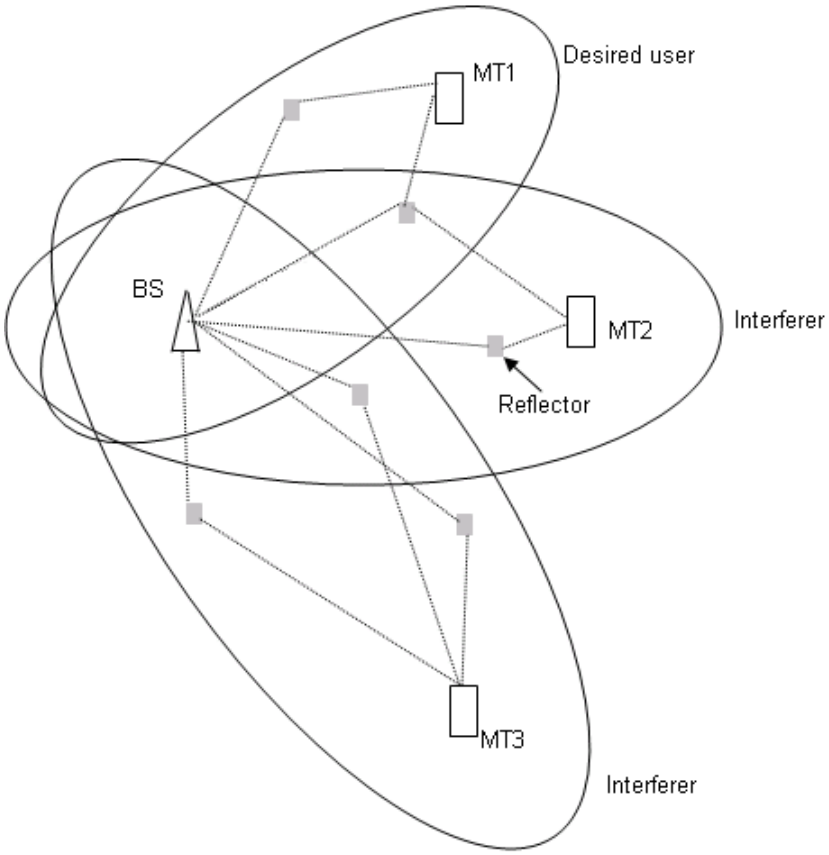

Figure 3.4 – Intra-cell interferences in a micro-cell environment.

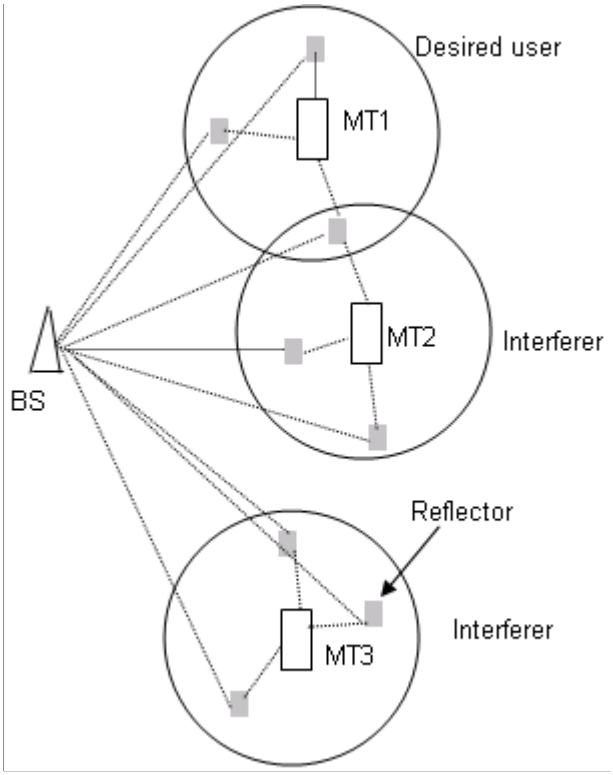

Figure 3.5 – Intra-cell interferences in a macro-cell environment.

Pico-cell environments can be modelled as a circular shape in which the BS is located at the centre; all the MTs are inside this region. In this case, only one region is considered for all users, as opposed to the micro- and macro-cell. The pico-cell environment is presented in Figure 3.6. The placement of reflectors depends mainly on the characteristics of the environment. In this case, the same scatterers reflect the signals from other links.

Scenarios, as presented above, will be more realistic, when clusters of reflectors are used instead of simple reflectors. This approach is based on the GBSB model extended by [Marq01]. Every cluster consists of many scatterers, which reflection coefficients are modelled separately. Both magnitude and phase of the coefficients are random variables. Signals, which come from the different MTs, propagate in different ways, thus correlation between them is not total. The correlation between paths is related with many aspects, e. g., the distance between users; in case when they are very close together correlation can be near to one.

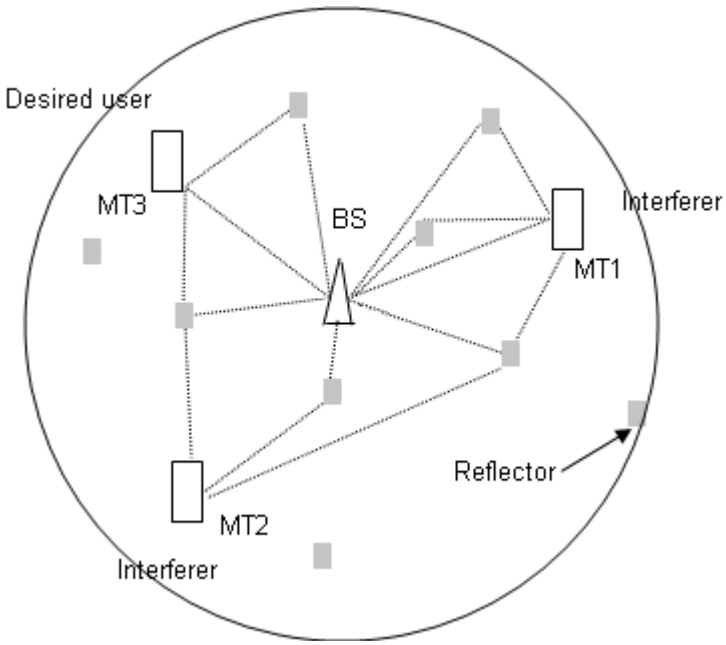

Figure 3.6 – Intra-cell interferences in pico-cell.

To describe interference in the "higher level" approach, CDMA is presented with more detailed, as the main multiple access mode in UMTS. In CDMA systems, users share the same bandwidth, but every user's signal is scrambled by a code sequence. Since the codes have a low cross-correlation, it is possible to distinguish the users apart at the BS. The signal, which is transmitted by a MT, can be formulated as [HoSz98]:

$$\mathbf{x}_i(t) = A_i \mathbf{d}_{d,i}(t)\mathbf{c}_{scr,i}(t) \tag{3.45}$$

where:

- A_i: amplitude of the signal of the i^{th} user
- $\mathbf{d}_{d,i}$(t): data signal of the i^{th} user
- $\mathbf{c}_{scr,i}$(t): scrambling sequence of the i^{th} user

In Figure 3.7, a simply scheme for the receiver in the BS is presented.

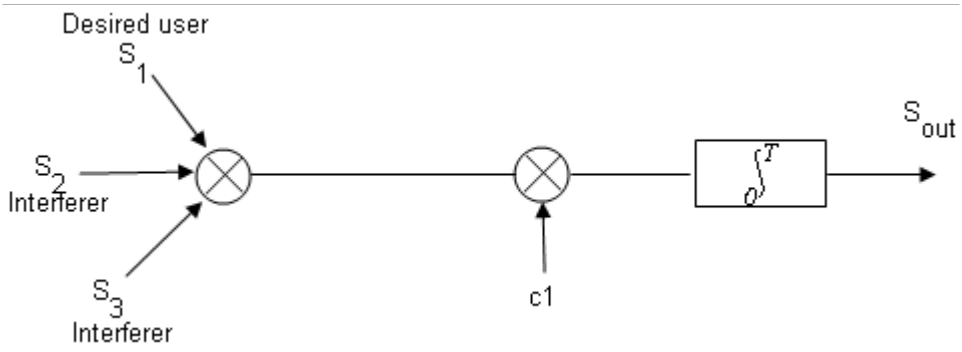

Figure 3.7 – Scheme of receiver in BS.

When the signal from user 1 (S_1) is the desired signal, the signals from users 2 and 3 are sources of disturbance at the receiver in the BS; the signal that was detected is descrambled by the code of user 1 and filtered. The outgoing signal, in case the channel model is ideal (no multipath propagation), can be written as [HoSz98]:

$$A_{out} = A_x \int_0^{T_b} \mathbf{d}_{d,x}(t)\mathbf{c}_{scr,x}(t)\mathbf{c}_{scr,x}(t)dt + \sum_{\substack{i=1 \\ i\neq x}}^{N_{users}} A_i \int_0^{T_b} \mathbf{d}_{d,i}(t)\mathbf{c}_{scr,i}(t)\mathbf{c}_{scr,x}(t)dt \tag{3.46}$$

where:

- $T_{b\,[s]}$: period of one data bit
- N_{users}: number of users
- index x is the desired user

This form can also be written also as a sum [HoSz98]:

$$A_{out} = A_x G_p + \sum_{\substack{i=1 \\ i\neq x}}^{N_{users}} A_i V_{r,i} \tag{3.47}$$

where:

- G_p: processing gain, ratio of bandwidth after spreading to bandwidth of data signal

- V_r: random variable with Gaussian distribution
- $A_x G_p$: desired signal, which should be detected
- $A_i V_{r,i}$: interference signal of user *i*

In Figure 3.8 the bandwidths before and after spreading (respectively B_i and B_{SS}) for only one user in the system are presented. In case of a multiuser system, Figure 3.9, every interfering user contributes to the power of interference, which is often assumed as additional Gaussian noise and causes a decrease in SINR [HoSz98]. This additional Gaussian noise is modelled by random variables $V_{r,1}$ and $V_{r,2}$.

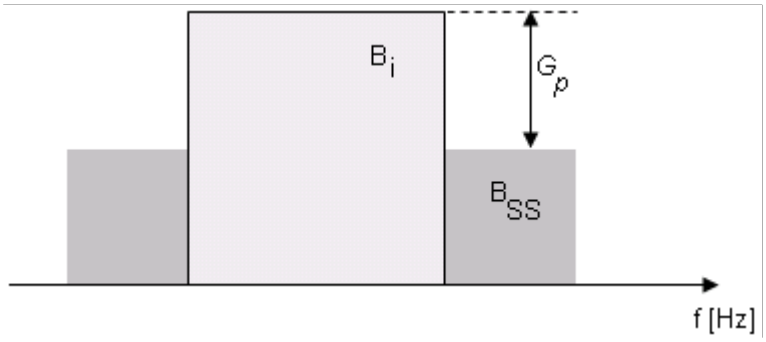

Figure 3.8 – Bandwidth of single user CDMA system.

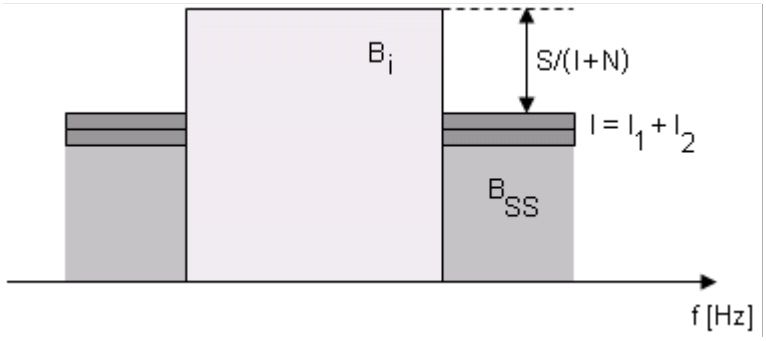

Figure 3.9 – Bandwidth of multiuser CDMA system.

The more users are active in a system, the stronger the signal of interference, and the SINR ratio decreases. Previous considerations were for the case, where there is an ideal radio link between the MT and the BS. In real environments, the signal is disturbed by many mechanisms, especially by multipath propagation, where signal components arrive at the BS via indirect paths. At the receiver, components arrive with different time delays, amplitudes, phases and angles, but the information that they carry is the same for all. These signals add at the receiver

in destructive or constructive ways; in the time domain, the signal is dispersed. Because of the multipath propagation, the signal that is detected at the Rx is distorted. As a result, the orthogonality between users is lost, and the influence of other users in the overall signal after descrambling is higher, and therefore the SINR ratio is lower.

When signals come from separate users, they are scrambled by different codes with low cross-correlation. After considering the fact that every signal is disturbed by a multipath channel, some bits of data can be detected with error. Received signals from other users are no longer orthogonal and the correlation function is not as low as before. As a result, signals from other users interfere with the desired signal.

In FDD, because of frequency duplexing between UL and DL, these channels do not interfere with each other. In UTRA-FDD, CDMA is used as multiple access technique, so interferences with UL and DL are described by interference in CDMA (both for intra- and inter-cell interferences). However in TDD, both the MT and the BS share the same bandwidth and the same frequency. During the normal operation of the system and with full synchronisation, interference does not exist. Different MTs are at different distances from the BS, and time synchronisation of the Tx and the Rx of particular users is very important. In case synchronisation is lost, interference appears, which is presented in Figure 3.10.

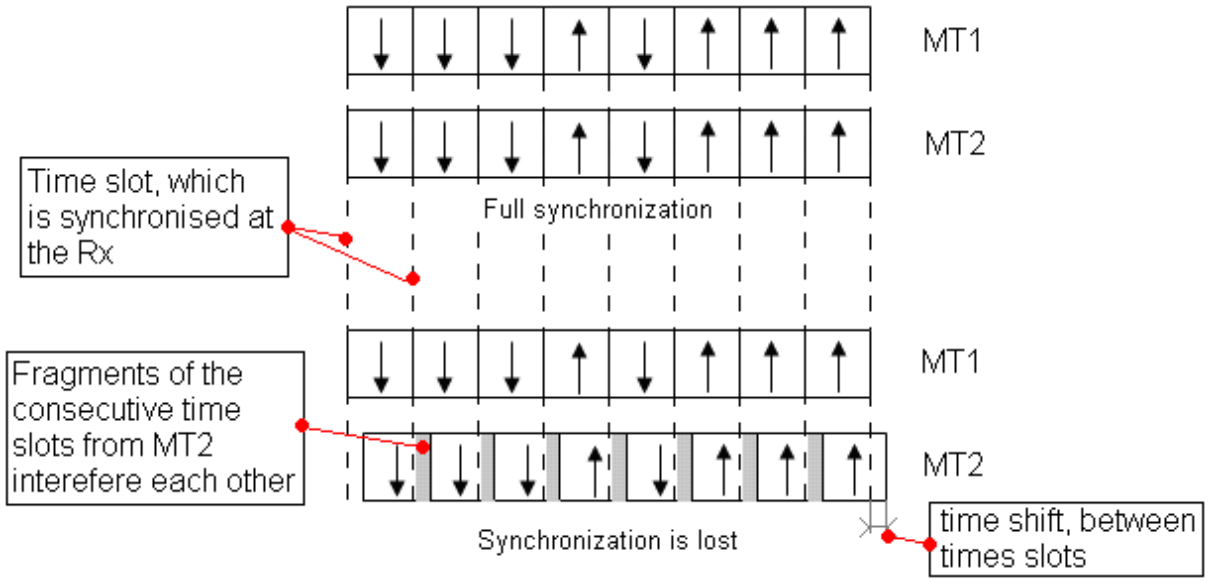

Figure 3.10 – Time slots in TDD.

When there is full synchronisation, exactly the same time slots scheme exists on the both sides of the link (Rx-Tx), and when the Tx transmits the Rx receives. However, in case

synchronisation is lost, the scheme of time slots is different at the Rx and the Tx. Between the time slots at the Rx and the Tx some time shift appears. During one time slot, the Rx detects a signal, which is partly from the desired slot and partly from the disturbing one. In Figure 3.10 an example when the synchronisation is distorted, is presented. In this example, two terminals MT1 and MT2, work with the same BS. The layout of the timeslots is depicted in this figure. MT1 and MT2 can be located at different distances from the BS, but given the synchronisation, the signals from the particular time slots arrive in the appropriate moments to the Rx. In Figure 3.10, one presents the situation when in the link between the BS and MT2 some error occurs, and the MT2 works with the time slots that are shifted by some time period. When MT2 works as the Tx, the data from the time slots arrives to the BS with a certain delay. This causes that the information can not be correctly detected. This signal disturbs both the link between the BS and the MT2 and the link between the BS and the MT1. The interferences appear also in the case when MT2 works as the Rx: the BS transmits the signal to MT2 in proper moments, but the receiving block in the MT2 tries to detect data in a different range of time.

3.3 Inter-cell interferences

Inter-cell interference is described by the interference channel model. The MT can detect signals not only from the BS of the cell in which it is active, but also from BSs in adjacent cells. Inter-cell interference is a relevant source of disturbance in case the MT is on the edge of the cell, and signals from adjacent BSs have comparable power levels. One can distinguish some types of interference, which are connected to different environments.

Inter-cell interference in micro-cell scenarios can be described by using a GBSB model, Figure 3.11. In this case, the concept of the model is similar to the case of intra-cell interference in micro-cells, but here the MT is common to some BSs. There are as many ellipses as BSs, which are the sources of interference. The BS is located at one of foci of each ellipse, and the other is the common place of the MT. Some ellipses have common regions, and every reflector that is bounded by this area reflects multipath components from or to another BS.

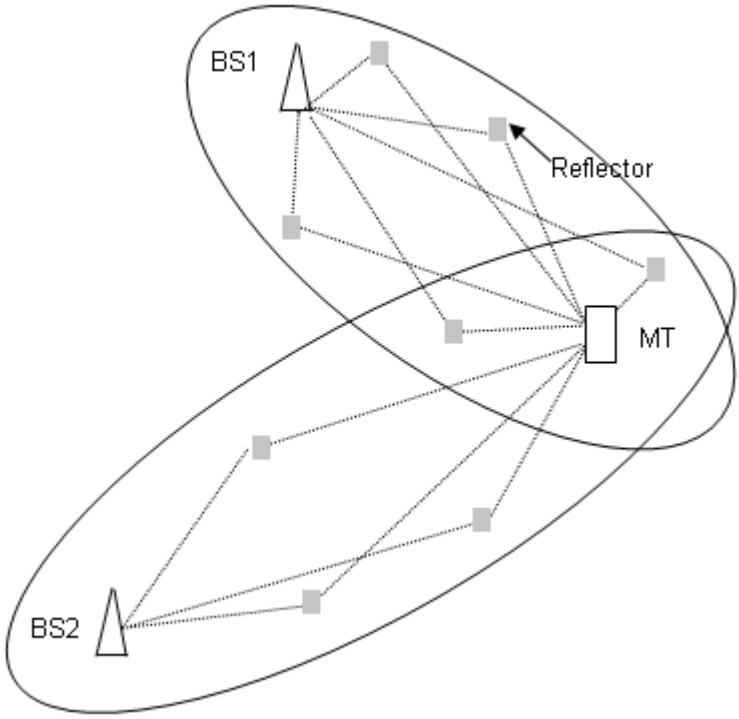

Figure 3.11 – Inter-cell interference in a micro-cell environment.

Inter-cell interference in macro-cell scenarios can be considered based on the GBSB model, Figure 3.12. The antennas of the BSs are located above rooftops and are not surrounded by reflectors. Each of the reflectors is located nearby the MT. In this case, as opposed to intra-cell interferences in macro-cells, there exists only one circle with its centre at the MT. In this situation, it is probable that reflectors bounce path components from more than one BS.

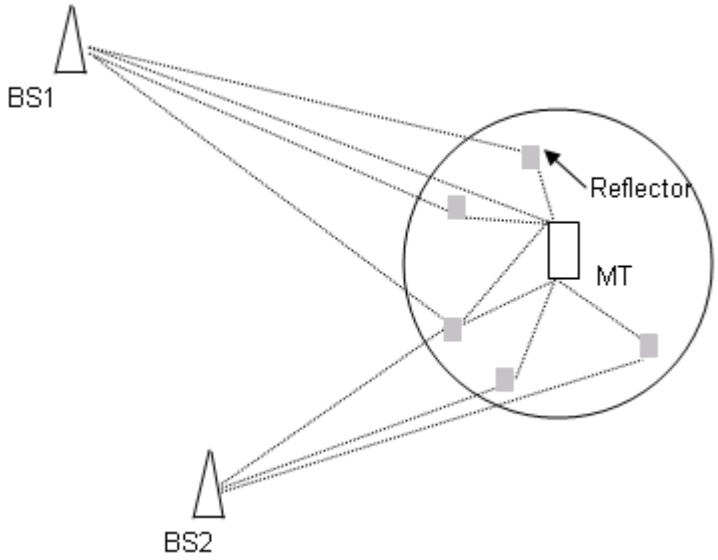

Figure 3.12 – Inter-cell interference in a macro-cell.

In the case of pico-cells, every region is correlated with one BS, which is in its centre. In inter-cell interference, the scenario can be modelled as a family of pico-cells regions, Figure 3.13.

There are as many regions as there are BSs in the system, which are sources of interference. Interference in this case is more probable when the MT is on the edge of the cell and the distance between MT and both BSs are similar.

As mentioned for the case of the intra-cell interference, also in this case propagation will be more realistic when instead of reflectors, clusters of scatterers will be used. Every cluster is composed of many reflectors, and this approach models situation, when signals arrive in clusters from particular directions, which are connected with particular objects.

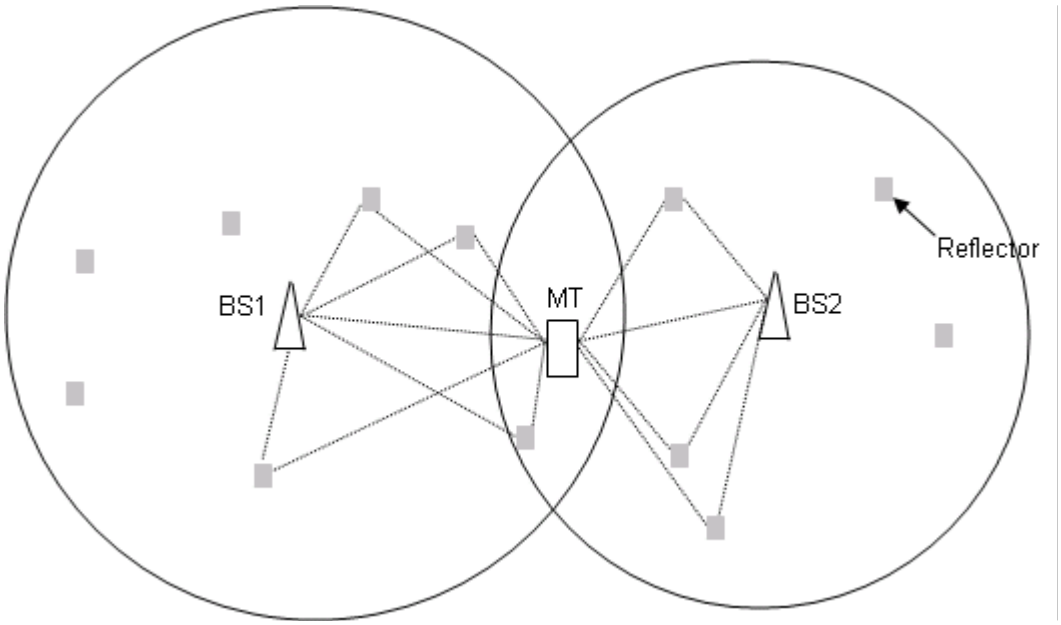

Figure 3.13 – Inter-cell interference in a pico-cell.

In CDMA systems, BSs in adjacent cells work in the same frequencies. Every BS uses another shift of the long code sequence to differentiate signals. CDMA is designed to mitigate the influence of interference, which is achieved by power control. The BS controls the powers of the MTs, which work within a cell, but interfering signals arrive also from the BSs from other cells. Hence, every BS influences the active MTs in the system somehow, Figure 3.14.

The levels of interference can be described by using the interference matrix. In the case of N_{cells} cells, the size of the matrix is $N_{cells} \times N_{cells}$ [AkPa04]:

$$\mathbf{F}[i,j] = \begin{bmatrix} I_{11} & I_{12} & \dots & I_{1N_{cells}} \\ I_{21} & I_{22} & \dots & I_{2N_{cells}} \\ \dots & \dots & \dots & \dots \\ I_{N_{cells}1} & I_{N_{cells}2} & \dots & I_{N_{cells}N_{cells}} \end{bmatrix} \tag{3.48}$$

where:

- $\mathbf{F}[i,j]$: is the power of interference, which is contributed by cell j to cell i

Signals from other cells are scrambled also by codes, and after decoding at the receiver, they amplify the level of interference. This is similar to the case of intra-cell interference. Signals from other BSs are distorted by multipath propagation, thus, the cross-correlation function among them is higher, and it causes an increase of the level of interference.

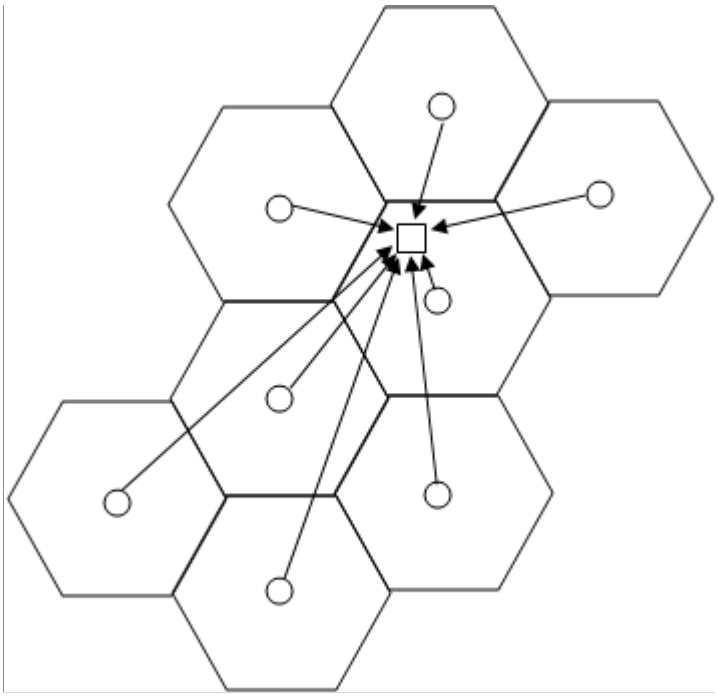

Figure 3.14 – Inter-cell interferences in CDMA.

TDD inter-cell interference is an important source of signal distortion. The same carrier is used for both UL and DL, so all MTs and all BSs can interfere with each other. The level of interference depends on the synchronisation frame and on the UL and DL asymmetry used in the particular cell. One of the cases of interference is the MT to MT interference [HHLT00]. This kind of interference takes place when MTs are in adjacent cells. In neighbour cells another frame scheme is used, and a different asymmetry between UL and DL exists. The example of this type of interference is presented in Figure 3.15. There are two consecutive cells where the

scheme of the frames is different: in cell 1 communicates MT1, and in cell 2 is MT2; when these terminals work in different modes, one of them being the Rx and the other being the Tx, the signal from MT2 is transmitted to BS2, but in case when the terminals are close enough to each other, the signal is also detected by MT1 causing the increase on the level of interference.

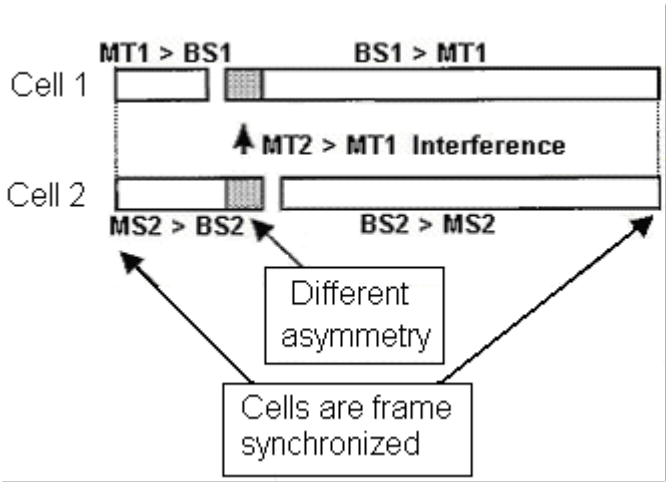

Figure 3.15 – Mobile-to-Mobile Interferences [HHLT00].

The other type of inter-cell interference is the BS to BS interference [HHLT00]. This type of interference exists between BSs that work in the same or adjacent frequency bands in adjacent cells. This interference depends on the path loss between the two BSs, and can occur both within one operator's bands and between different operator's BSs. BS to BS interference within one operator's band is depicted in Figure 3.16. This situation is very similar to MT to MT interference. Adjacent cells use a different scheme of time slots. BS2 can detect the signal, that is transmitted by all MTs within the cell and also the signal from BS1.

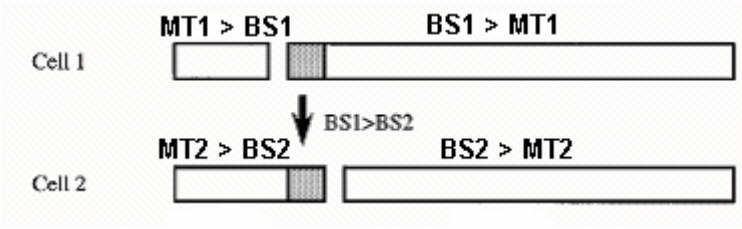

Figure 3.16 – Base Station-to-Base Station Interferences [HHLT00].

One can summarise the considerations on TDD interference [HoTo00]. To mitigate the effect of interference, it is required that each BS is frame synchronised, and it is recommended that BSs that belong to different operators, if they are close to each other, should also be frame

synchronised. In order to reduce the interference problems within the TDD band, dynamic channel allocation is needed. Interference can also occur between the lower TDD band and the FDD uplink band. If they occur, it is not feasible to reduce them by dynamic channel allocation, because FDD has continuous transmissions and reception. Coexistence of TDD and FDD can also cause a decrease on the FDD uplink coverage area and on TDD quality of service.

4 IMPLEMENTATION

Chapter 4 contains the description of the developed simulator. In the beginning, the basic simulator is presented, including input and output parameters, the algorithm and assessments. In the consecutive part of this chapter, one describes the enhanced version of the simulator to deal with multiuser interference.

4.1 General structure

In the MUI case, the simulator runs pre-defined links between the Rx and the Tx, Figure 4.1. There are n_{Tx} Tx users in one side of the radio link, and n_{Rx} Rx users on the other side. But before focusing on the aspects related to the specification of the MUI simulator, one must describe the way the simulator handles the Single User (SU) and the Single Input Single Output (SISO) cases. The radio channel simulator is a core, which simulates a link between two points, between the Tx and the Rx antennas. The global simulator, which considers more complex situations, like environments that contain many users or MIMO antennas, is just an extended versions of the radio channel simulator.

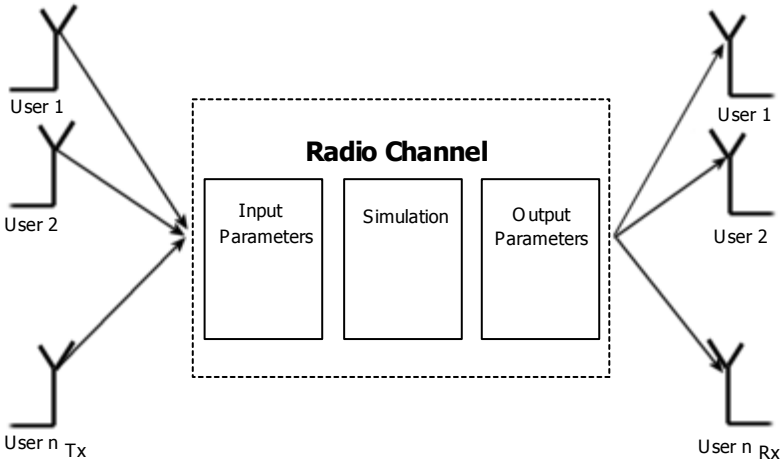

Figure 4.1 – The general structure of the simulator in the MUI case.

In order to describe the implementation of the simulator, its structure has been decomposed into a simple form, based on blocks, Figure 4.2. The *Input Parameters* block contains the input parameters of the simulator, which determine the way the program works, and allows different modes of the running it.

The *Simulation* block contains the heart of the program, emulating the behaviour of the radio channel. This part includes the realisation of the algorithm in the simulator. In this part of code the sequence of steps are made according to the mentioned algorithm. It is worth noting that calculations are made separately for the LoS component and NLoS components. In case of NLoS, the scatterer related with considered component influences the received signal from what follows the necessity of separation in the calculations. In the last block called *Output parameters,* the results are presented. Every mentioned part of the program will be described in more detail in this chapter.

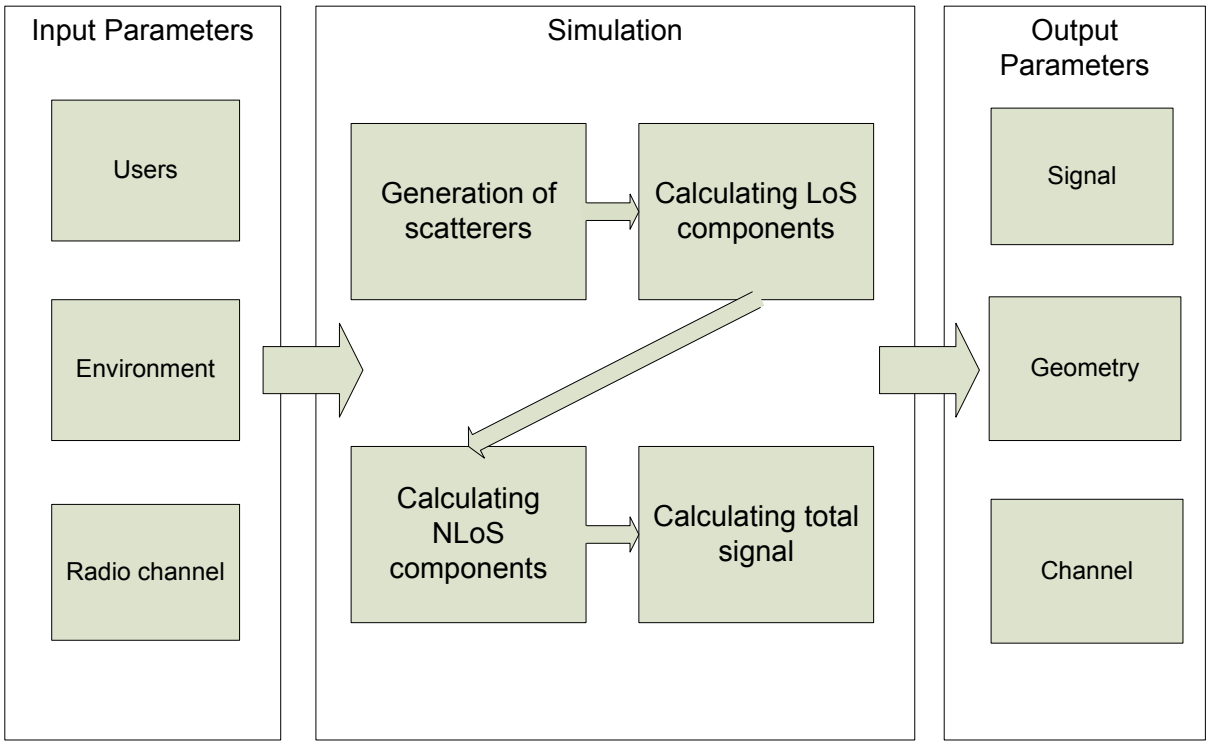

Figure 4.2 – Structure of the program.

4.2 Channel

4.2.1 Input parameters

Input parameters can be organised in three groups. In the first group, there are parameters that describe the location and properties of the MT and the BS. The next group determines propagation environment and the type of scenario, and the last one illustrates some radio properties of the system. The groups of the parameters are presented in Figure 4.2.

In the *User* group, parameters describe some aspects connected with the users in the system. The positions of the MT and the BS are described by coordinates as [*x*,*y*], which determines a position in the *x*-*y* plane. Locations are deployed only in the 2-D plane, which is agreement with the assumption of the used propagation models. For the transmitter, it is important to determine the level of transmitting power; the receiver is defined by the noise level. Signals with power below the sensitivity of the Rx are not considered. The BS and the MT have a separately defined radiation pattern of the antennas. Every antenna can be a single radiator or an antenna array. In case of the antenna array, the parameters to determine the group characteristic are presented below. It is assumed that the radiation pattern for a singular antenna is defined by the

radiation pattern for an omnidirectional antenna. Additionally, the radiation pattern of the antenna can be loaded from a file. So, a user of the simulator can define any radiation pattern, suitable for a considered application. The following parameters can be defined:

- $s_{dev[m,m]}$: position of the MT or the BS on the 2-D plane
- $P_{Tx[W]}$: transmit power of Tx
- $N_{Rx[W]}$: noise level of Rx

The antenna array can be described using the following parameters:

- N_a: number of antennas in the array
- $d_{[m]}$: spacing between antennas in case of linear array,
- $a_{[m]}$: radius of the circle in case of circular array
- $\Phi_{0[rad]}$: phase shift between consecutive radiators, it is assumed that all radiators are fed with the same amplitude (one feeding point)
- $\Phi_{n[rad]}$: phase feeding of n^{th} radiator (multiple feeding points)
- $I_{n[A]}$: amplitude of feeding of n radiator (multiple feeding points)

Antennas can have different names, which are helpful for sorting output files. The names of the output files consist of the names of the antennas between which radio links are established.

The Parameters from the *Environment* group, which describe a region of propagation, contain information on the scenario properties. The type of scenario is defined by choosing a pico-, micro- or macro-cell mode. The next parameter is the dimension of the scenario. For the micro-cell case, the scenario is defined by street width ratio, which describes an effective width of the region. The width of ellipse characteristic for micro-cell is multiplied by a constant factor. A pico- and macro-cell scenario is defined by the radius of an appropriate circle. The following parameters describe the distribution of reflectors within the region. The distribution of scatterers is determined by the cluster density, and an average number of scatterers. The cluster density is used to calculate the number of clusters in a region and the average number of scatterers is used to calculate a number of scatterers within a cluster. The radius of the cluster determines the size of the cluster because every cluster has the shape of a circle. The parameters from the Environment group are:

- $dim_{[m]}$: a dimension of a scenario
- $d_{c[1/m^2]}$: cluster density
- n_{sc} : average number of scatterers per cluster

The parameters from the *Radio channel* group define propagation conditions and the transmitted signal. The radio signal is described by the carrier frequency:

- $f_{[Hz]}$: frequency

Some parameters are present in a config file, but are not consider among input parameters, because they are not related with a single run of the simulator.

In Figure 4.2, the structure does not take into consideration the modes of the simulator and the number of simulation once the environment has been defined. The mode of work is important when the number of simulations is greater than 1, because some changes of the environment are made for each run of the simulator. The structure presented in the figure is only appropriate for one run of the simulator. The description of the modes is presented in the following part of the work.

Parameters related with visualisation are not considered in the figure, as well. The parameters like time resolution, angle resolution and time sectors are only necessary for the present application of the simulation, so that the mentioned parameters are not placed in the general structure of the program. The Matlab environment was used to present results in graphic way, but, the parameters can be used by different environment for visualisation.

4.2.2 Description of the simulator

The simulator consists of some main processing blocks. In the beginning, based on the input parameters, the positions of the clusters are set in a random way using the uniform distribution. Both coordinates *x* and *y* are drawn apart. In this way, clusters are placed evenly distributed on the area of region. The shape of the region depends on the researched scenario. In case of the micro-cell, clusters are placed inside the ellipse, but in case of the macro-cell or the pico-cell, the clusters must be deployed inside a circle. During the drawing of the coordinates of the clusters, the considered shape of the scenario is limited by an appropriate rectangle. After drawing the parameters *x* and *y* are inside of the rectangle but belonging to a zone of the scenario is not sure, Figure 4.3. If the coordinates are not inside the considered shape of the scenario (circle or ellipse), another position of the cluster is drawn and considered. The number

of clusters is defined by the dimension of the scenario and the cluster density related with the scenario. So, the number of clusters is fixed for every scenario.

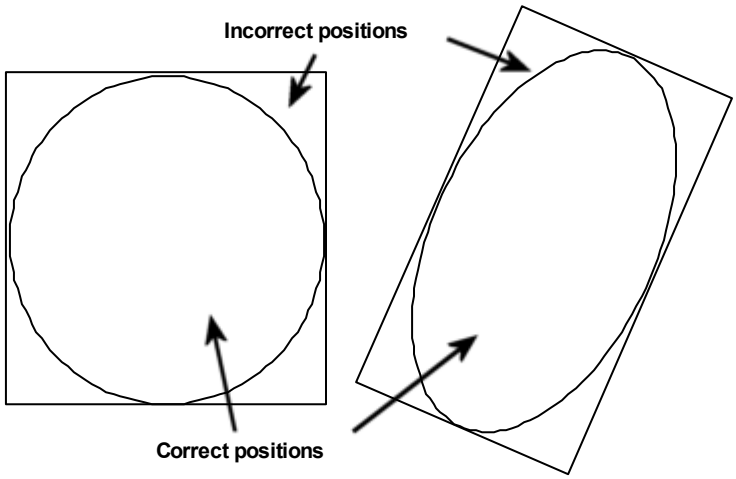

Figure 4.3 – Drawing of the positions of clusters.

In the next step, the simulator computes the location of the scatterers. Every scatterer belongs only to one cluster. The position of the considered scatterer is determined using the spherical coordinates. The distribution of the radius is determined by the Gaussian distribution. The mean value of the distribution is 0 and the standard deviation is determined by the radius of the cluster, but the angle is determined by the uniform distribution in the range [0, 2π]. Using the drawn angle and radius, the scatterer is deployed with reference to the centre of the cluster. Each cluster is defined by an average number of scatterers, so that in one scenario different clusters may have different numbers of scatterers. The number of scatterers related with one cluster is described by the Poisson distribution. The flow of information in the first block is depicted in Figure 4.4.

When the simulation environment is set, the calculations of the radio channel start. In the beginning, the LoS component is taken into account. The scheme of data processing is depicted in Figure 4.5. The power picked up at the receiver is calculated using the formulation for free space. So, only the positions of transmitter and receiver, transmitted power, and the radiation patterns must be known to estimate the received power. In some radio channel models, the path loss exponent is used. The path loss component is different for special terrain of propagation. In the simulator, the influence of the environment of the propagation is taken into consideration. The specific deployment of the scatterers for considering terrain makes the special shape of the final signal.

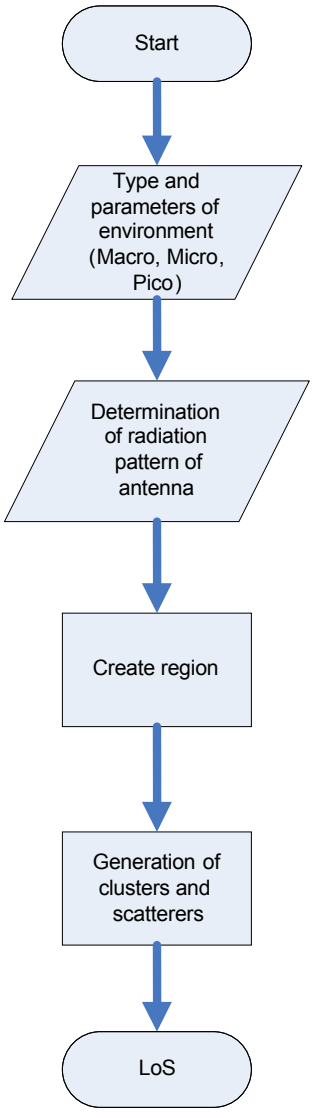

Figure 4.4 – Start of a simulation.

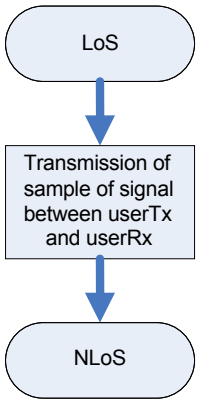

Figure 4.5 – Calculation of the LoS component.

After calculating the LoS component, the program goes on to the next part of the calculations, i.e., the NLoS components. An algorithm for this part of the program is presented in Figure 4.6.

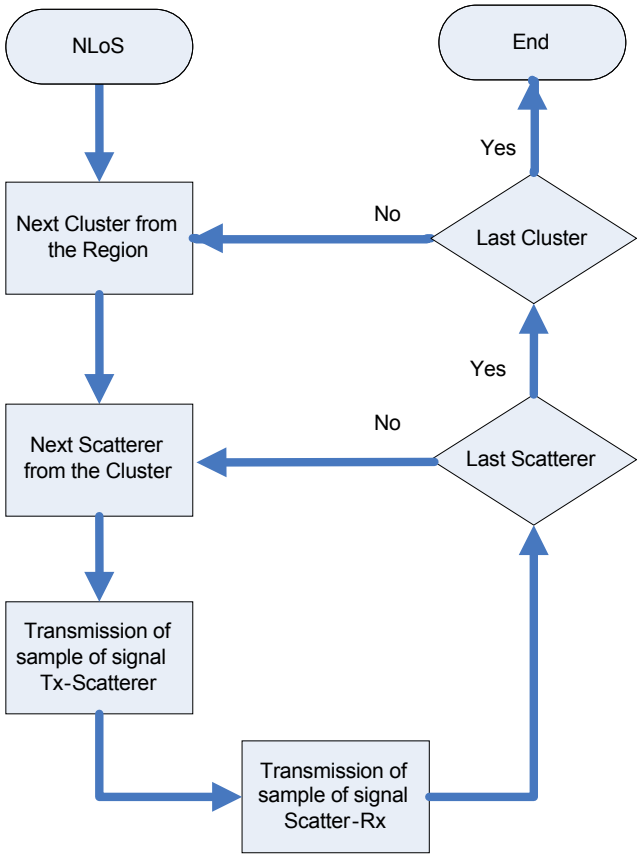

Figure 4.6 – Calculation of a NLoS component.

The simulation for the NLoS components is trickier, because all scatterers must be considered as check point for every ray in the considered environment. Every scatterer is a source of one multipath component picked up at the receiver. The calculations for the NLoS components can be simplified. Every NLoS link can be treated like two LoS links, the first link being between the transmitter and the considered scatterer and, the second being between the scatterer and the receiver. The power picked up at the scatterer in the first link is radiated to the second link, but before transmitting, the power must be reduced by the magnitude of the reflection coefficient. Also the phase of the signal must be changed with reference to the phase of the reflection coefficient. This approach is possible, because the scatterers do not overshadow one another. The mentioned assumption guarantees the existence of the directional path between the transmitter and any scatterer. The same situation is true for the link between any scatterer and the receiver.

4.2.3 Output parameters

Output parameters are grouped as shown in Figure 4.2. The parameters from the first group represent *Signal* parameters. Every multipath component is associated to a set of parameters, so, the number of sets of parameters is equal to the number of the scatterers, plus one in scenarios where LoS exists, e.g.; a micro- and a pico-cell, whereas for a macro-cell the number of sets is constrained by the number of scatterers. The LoS component is not related with any scatterer. The mentioned set of parameters is listed bellow and the particular parameters were described in Section 2.2.1:

- Angle of Arrival (AoA) – from (2.26)
- Angle of Departure (AoD) – from (2.27)
- Amplitude of ray – from (2.31) or (2.32)
- Phase of ray – from (2.35) or (2.36)
- Time of Arrival (ToA) – from (2.37) or (2.38)

The parameters are given by the simulator in output files. One output is related with a radio link between single input and output antennas. The output file consists of parameters generated by all scatterers in an environment. The size of the output file is connected with the richness of the scatterers in the environment; for more complicated ones, heavier files are produced.

It is possible to restore the possible positions of the scatterers, using the above parameters and the position of the BS and the MT. In the case of the micro-cell, one multipath component can be described by the ellipse; the position of the scatterer, with which this multipath component is connected, is located on the ellipse. For the pico- and the macro-cell scenarios, the appropriate circle estimates the possible localisation of the related scatterer.

The group *Geometry* parameters presents the real position of all scatterers in the considered environment. These parameters can be helpful to confirm the correct position, achieved using the *Signal* parameters. The positions are saved in the file, which name can be defined by the user of the simulator. The file can be used in a direct way to run the simulator with the environment defined, and one or more changes can be done to check on influence of a disturbance.

The results, which are obtained from the simulator, are more useful when they are averaged over many iterations. For each iteration, the simulator has to build a new scenario, which is changed with reference to a previous one. The simulator can be run in four modes, which define the way of changes the environment. The description of the modes is presented in Table 4.1.

Table 4.1 – Description of the simulator modes.

Mode	Description
0	For each run of the simulator, positions of clusters are kept in the same places. The only difference between the iterations is in a different reflection coefficient of scatterers. Output parameters from every iteration are generated.
1	The same changes are made as in mode 0, but for this mode, all results are averaged by the simulator, and only average results are generated as output parameters.
2	Positions of clusters remain the same, but scatterers within any cluster are independently generated for each run of the simulator. As a result, scatterers have different positions and reflection coefficients. The same as in the mode 0, all results from all iterations are written by the simulator.
3	Positions of terminals are kept in the same places. All clusters with scatterers are generated from the beginning for each iteration. Output parameters from all iterations are saved.

Like mentioned above, every multipath component, which propagates directly from the Tx to the Rx or through the reflector, is described by a set of parameters. But these sets of parameters are not enough to evaluate the model and to make any conclusions. Having appointed all signal parameters to all ray components, it is necessary to process them in a statistical way. The statistical processing is made outside the simulator; in this work, it was made in Matlab environment. The statistical parameters used are (parameters were described in Chapter 2):

- $\overline{\tau}$: mean delay
- σ_τ : delay spread
- σ_φ, σ_θ : angular spread of AoA and AoD
- $\overline{P}$: mean power gain
- standard deviations for all these parameters

The raw output parameters are in filtered and unfiltered form. There are some ways of filtering. One of them is refusing components, that have a level of amplitude below the sensitivity of Rx. Another kind of filtering is overriding rays, which have angles out of the range of antenna. Every parameter from the mentioned set can be filtered in an appropriate way.

4.2.4 Assessments

The simulator was carefully checked, and some assessments were made, see Annex A and Annex B. These tests were made to assure that the calculations and the generation of the environment is done in a correct way. These include the following aspects:

- The environment was generated with the Rx, the Tx and only one scatterer. Having knowledge about parameters of the scatterer, calculations of all output parameters were made, which are described in Section 2.2.3. Results obtained from the simulator were verified.
- The entire environment is generated using random number generators, so the correctness of these generators is very important for the simulator. The simulator uses three kinds of statistical distributions: Gaussian, Poisson and Uniform. Every generator produced 1 000 000 of the samples, and after that, the histograms were plotted, see Annex B. Obtained shapes of the histograms agree with theoretical expectations.
- The correctness of the deployment of clusters within a region, and scatterers within a cluster, was checked. Clusters should be distributed uniformly in the region, which was generated with a few clusters, and the mean values of *x*- and *y*-coordinates of all clusters were calculated. These mean values, were the same (with some marginal error) as the centre of the clusters.
- Scatterers within a cluster are distributed with the Gaussian distribution, but also in this case, the mean values of *x*- and *y*- coordinates should be the same as the centre of the cluster. Obtained results confirmed, that the scatterers are generated correctly. Scatterers also have to prove some symmetry in the cluster. The cluster was divided into two identical regions in a vertical (up- and down-sides) and a horizontal (left- and right-sides) orientation. In every quarter of the region, scatterers were counted – the results for both regions in each pair were the same (with some marginal error).
- It was also checked that the way of averaging the raw results in the time domain. Some multipath components with the determined amplitude, phase and delay were generated, and

after that they were processed by the averaging function. The obtained results agreed with the expectations.

- Some aspects related with a CIR were also checked. Every region has a finite dimension, so the maximum possible delay, which is obtained from the region, is strictly bounded and depends only on the dimension of the region. The three different scenarios were generated: micro-, macro-, and pico-cells, and for each of them, the maximum possible delay was calculated. After that, it was checked if there were any of the multipath components over exceeding these values.
- The correctness of the working of simulator in different modes was modes as well. The respective parameters of the scenario, connected with the different modes of the simulator, were checked for every iteration.
- The computational effort also was checked, and the conclusions are reported in Annex C.

4.3 Multi User Interference channel

4.3.1 Input parameters

In the MUI case, the inputs parameters extend the ones previously presented, the differences being in the definition of antennas and objects within the environment. Every user has only a single antenna (the antenna arrays are treated as one radiator). There are also some additional parameters, which describe the number of the users in the environment.

There are three groups of input parameters, Figure 4.2. In the *Users* group, parameters define the MUI case, containing the number of MTs and the number of BSs: n_{MT} and n_{BS}. Also here, for every user in the environment, the definition of the position using the parameter s_{dev} is done. As mentioned earlier, every user has only a single radiator, so parameters describing the antenna arrays, such the definition of the geometry and the feeding of the particulars radiators, are important to calculate the radiation pattern of the whole array.

The parameters from the other groups are taken without change for the case of MUI. The parameters from the *Environment* group contain the information about the scenario properties. In this group the type of the scenario is defined: pico-, micro- or macro-cell scenario. Every MT

can be located at a different distance from the BS and others MTs, so links MT-BS and MT-MT can be different in scenarios. In the *Environment* group is defined which links (MT-BS, MT-MT or BS-BS) have to be simulated by the program as well as the scenarios for these links.

The *Environment* group also defines the properties of clusters and scatterers. The number of clusters is described by the cluster density, and the number of scatterers by the average number of scatterers. In the MUI case, the regions connected with the different Rx-Tx links, can have common areas, thus, parameters describing clusters and scatterers these regions must be the same. In general, one can assume that every cluster and scatterer within the environment, is defined by using the same parameters.

The parameters from the *Radio* Channel group for the MUI case are taken without any change. One can assume that in every environment the propagation conditions are the same.

4.3.2 Description of the simulator

The simulator in case of the MUI works in a way similar, to the one presented in Section 4.2.2, but some blocks are not used and some are extended. The flow of information is depicted in Figure 4.7. Every link between users (between the Rx and the Tx) gets its own region, which contains clusters and scatterers. Clusters are placed using the uniform distribution and scatterers within the cluster according to the Gaussian distribution.

A presentation of the algorithm for the generation of clusters within particular regions is based on the scenario, which is described in Annex D. In the first step, the simulator checks if the regions defined by the user in a configuration file, have common areas. After that, a graph is generated, which nodes represent the particular regions. Between the particular nodes exists a link only in case the regions have a common area. The graph for the scenario case considered here is shown in Figure 4.8, the algorithm for the generation of clusters in different regions being depicted in Figure 4.9.

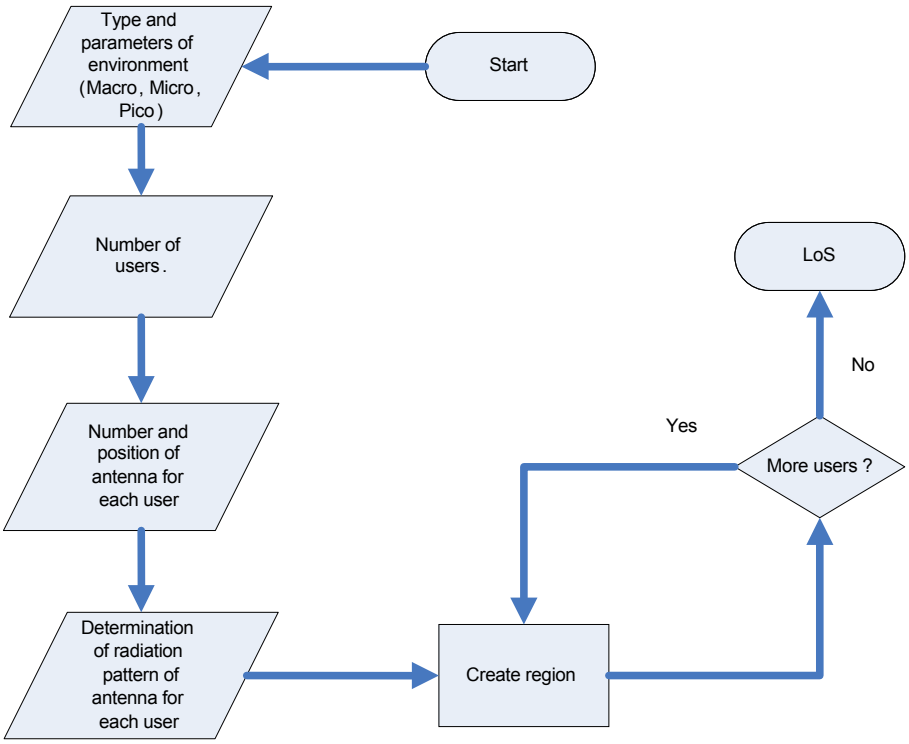

Figure 4.7 – Start of the simulation – MUI.

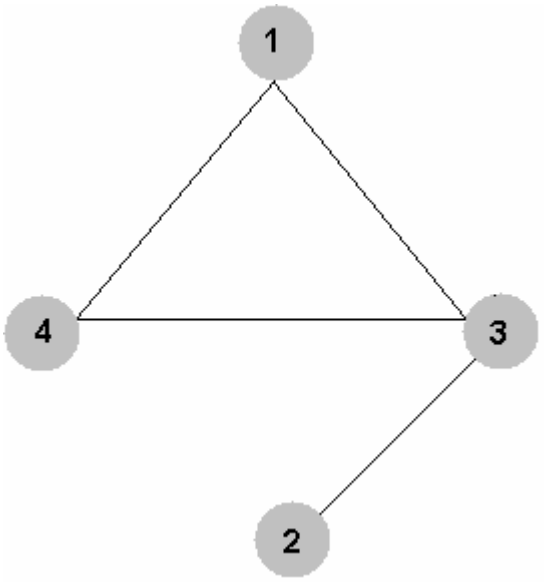

Figure 4.8 – The graph of regions for the test scenario.

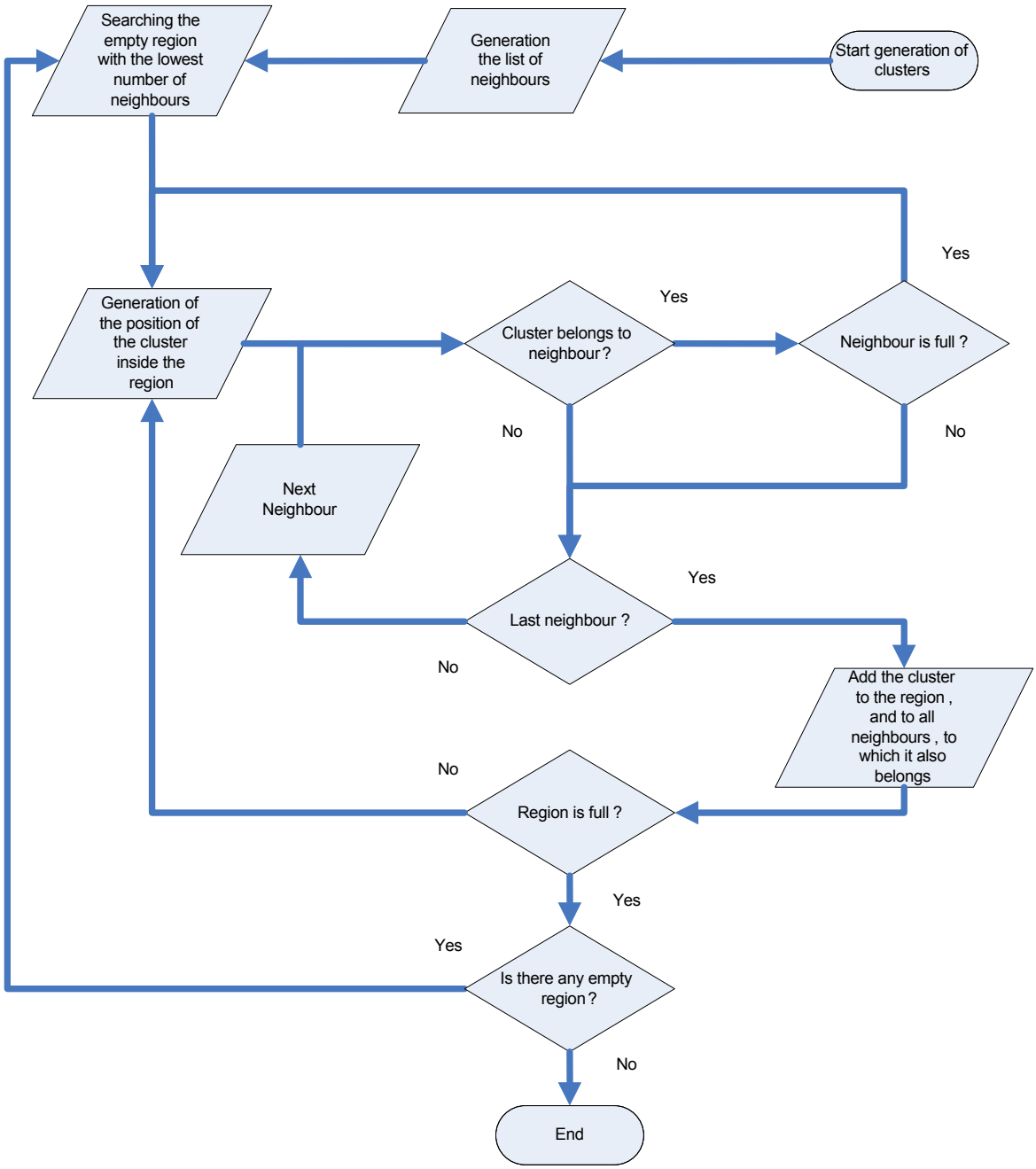

Figure 4.9 – The algorithm for the generation of clusters within different regions.

After the graph of the regions is generated, nodes are sorted from the lowest to the highest row. In case there are nodes in the same row, the first one to be taken is the one earlier defined in the configuration file. In case of the considered test scenario, the sequence is shown in Table 4.2.

Clusters are then generated in the regions, in the sequence presented in Table 4.2. During the generation of clusters for the channel simulator, it was checked only if the position of the cluster is located inside of the area. In the MUI simulator, it is also checked if the position of the cluster belongs to the other region.

Table 4.2 – Order of the regions after sorting.

Sequence	Region	Row of the node
1	Region 2	1
2	Region 1	2
3	Region 4	2
4	Region 3	3

Every region has the list of the neighbours regions defined, i.e. the list of the regions that have common areas with the desired one. For the considered example, the list of neighbours is presented in Table 4.3.

Table 4.3 – The list of the neighbours.

Desired region	Neighbour regions		
1	3	4	-
2	3	-	-
3	1	4	2
4	1	3	-

When the position of a cluster is obtained, in the next step the simulator checks if the cluster belongs to the particular neighbour regions. In case the cluster is also located in another region, it is checked if the region is not full, i.e. if it is possible to add this region the next cluster (every region has a number of clusters, which is obtained from the cluster density parameter). These conditions are checked for all regions from the list. The cluster is taken into account only in case it can be added to the common regions; in case the position of the cluster belongs to full regions, the cluster is rejected.

The generation of clusters starts with regions that do not have any common areas with other regions, or that have the lowest number of neighbours; it is finished when the region with the highest number of neighbours is achieved. This sequence of generation enables a uniform distribution of clusters in most of the regions. It is obvious that in the regions in which clusters are generated in the end, the uniform distribution can be not so accurate because in the areas

common to other regions, where clusters are already generated, the new one can not be added, since the regions are full.

In some cases, it can happen that the number of clusters is not achieved, this can takes place when a small region is located inside greater ones; the former has a large number of neighbours, and clusters within it are generated in the end. In this case, the whole area of this region belongs also to other regions, which have already clusters i.e., they are full, and new clusters can not be added. So, the small area can not have new clusters, and it has only the initial ones, which were generated earlier for the other common areas. This situation, and the solution of this problem, is presented in Annex D.

After setting the simulation environment, the program calculates the LoS component, Figure 4.10. In this case, antenna arrays are treated as one radiator, so parts of the code, related to the transmission between particular antennas in the array are not used; in Figure 4.10, these are shown with non-continuous lines. Aspects related to MIMO antenna arrays are described in [Koko05].

After the LoS component is obtained, the program calculates the NLoS ones, Figure 4.11. It starts with the location of the Tx and the Rx in the environment. After that, clusters that belong to the considered region of Rx and Tx are chosen. A signal is transmitted between the Rx and the Tx, through every scatterer from a cluster. In the MUI case, calculations are made between every Rx and every Tx from the defined regions. In a particular Rx-Tx link in the micro-cell scenario, there are as many components as there are scatterers in the region; however, in case of the pico- and macro-cell scenarios, an additional LoS is considered, thus, in these cases, the amount of the components is equal to the number of the scatterers plus one.

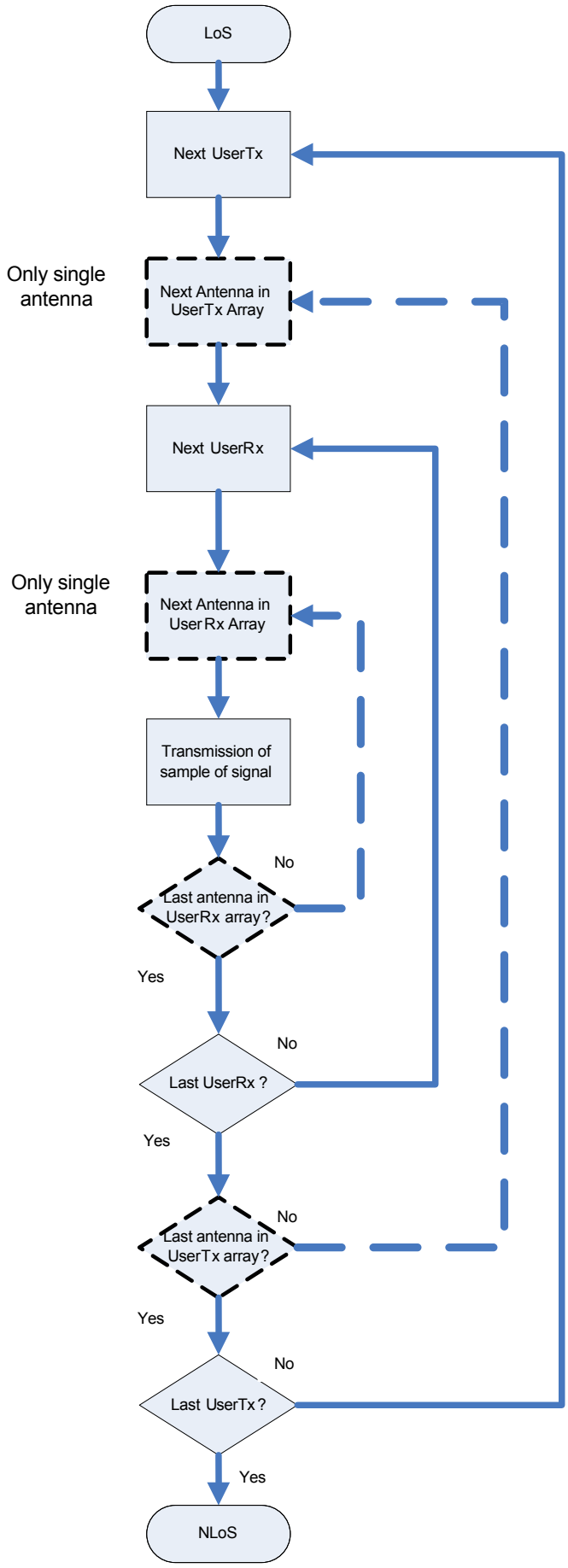

Figure 4.10 – Calculation of the LoS component in MUI.

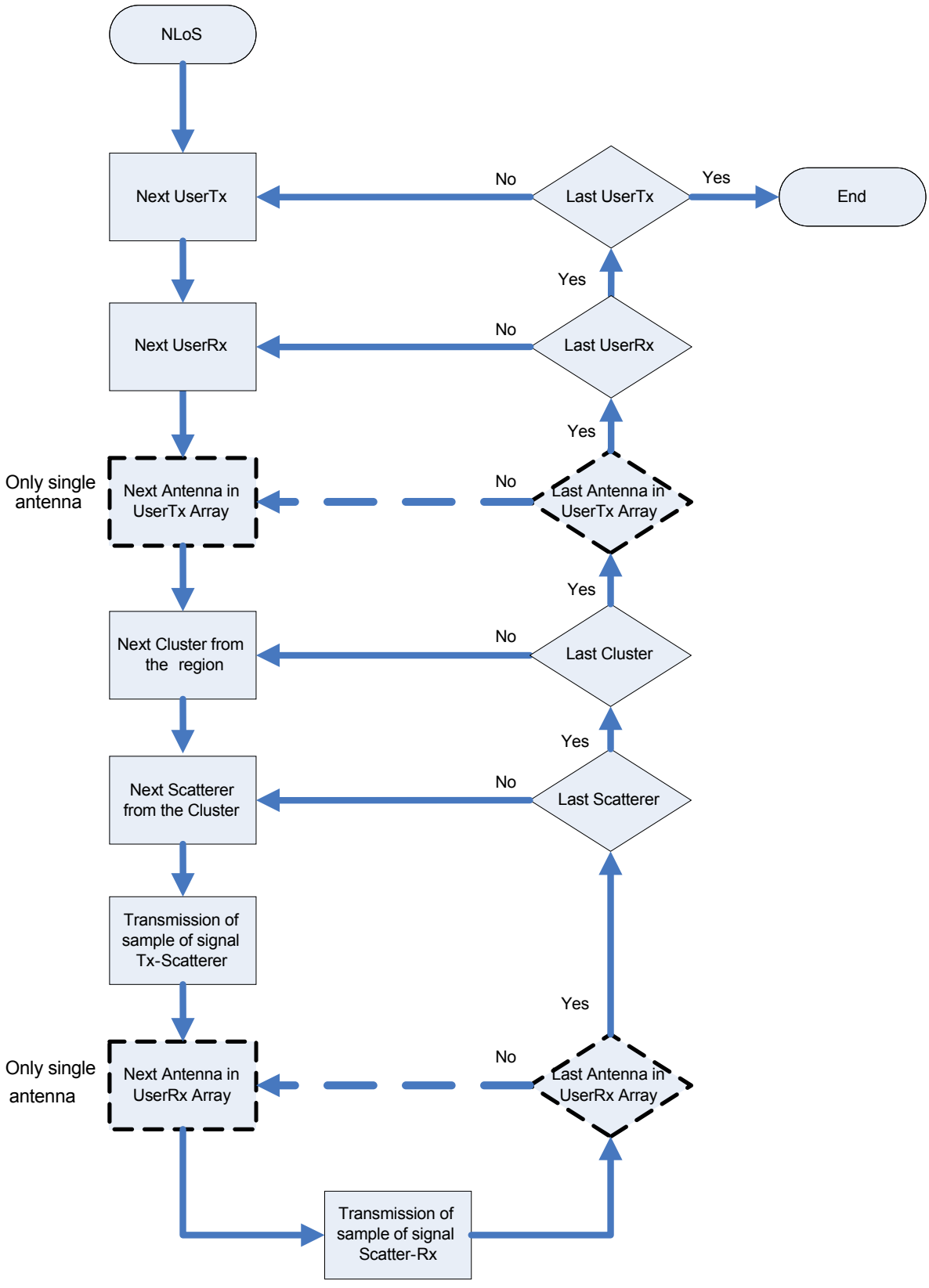

Figure 4.11 – Calculation of NLoS components in MUI.

4.3.3 Output parameters

The output parameters are the same as in the general case. The *Signal* group contains the raw results of the simulations for every link, parameters being the same like in Section 4.2.3:

- Angle of Arrival (AoA) $_{\text{link } n\text{-th}}$ – from (2.26)
- Angle of Departure (AoD) $_{\text{link } n\text{-th}}$ – from (2.27)
- Amplitude of ray $_{\text{link } n\text{-th}}$ – from (2.31) or (2.32)
- Power of ray $_{\text{link } n\text{-th}}$
- Phase of ray $_{\text{link } n\text{-th}}$ – from (2.35) or (2.36)
- Time of Arrival (ToA) $_{\text{link } n\text{-th}}$ – from (2.37) or (2.38)

The number of sets of raw parameters is equal to the number of links that are considered in the simulation multiplied by the sum of the number of scatterers from the region of the link and the LoS component, however only for the micro- and pico-cells; in the macro-cell, the LoS component does not exist. Every set of the raw parameters is written to a separate file, which has a name making possible to recognise the region and the number of the iteration of the simulator. It is worthwhile to mention that more complicated environment, having the large number of regions, is set, the more space of a disk is needed to write the data. This problem becomes more critical, when the large number of the iteration is set, because in the simulator modes 0,2 and 3, results from every iteration are written to a separate file.

These raw results for the particular links are then processed in Matlab. The statistical parameters, which describe the radio channel, are obtained from sets of raw parameters. In the MUI case, it is possible to calculate the radio channel impulse response for the particular links, and also to calculate the correlation between the links. The powers needed to calculate the SINRs, are obtained basing on the CIRs. The description of different ways of the calculations of the SINR can be found in Sections 5.2.3 and 5.2.4.

As presented in Section 4.2.3, the radio channel over the particular *n*-th link, can be described using the statistical parameters:

- $\bar{\tau}_{\text{ link n-}th}$: mean delay
- $\sigma_{\tau\ \text{link n-}th}$: delay spread
- $\sigma_{AoA\ \text{link n-}th}$, $\sigma_{AoD\ \text{link n-}th}$: angular spread of AoA and AoD

- $\overline{P}_{\text{link n-}th}$: mean power gain
- standard deviations for all these parameters

The group *Geometry* parameters presents the positions of all scatterers for every region in the environment. The positions are saved in the files, which names can be defined by the user of the simulator; every file name includes also the number of the region. The scatterers that are common for several regions are included in every file, which describes them.

4.3.4 Assessments

The MUI simulator works on the same principles of the channel model simulator. As a simplification, one can describe the MUI simulator as a channel model simulator that is run for every region. One can assume that the tests made for the channel model simulator confirm the correctness of the results.

But the assessments that were presented for the channel simulator must be extended. The most important difference between these two kinds of simulators is the generation of the regions between the Tx and Rx. In many cases, the regions describing the links have common areas, thus, the clusters that are located inside these regions are also common. These aspects were checked, and the description of the tests is presented in Annex D.

Another thing was checked related to the generation of clusters. Annex D contains the description of the situation when the intended amount of clusters in the region can not be achieved, which was also mentioned during the description of the MUI simulator. A solution is presented connected with the different types of declarations in the configuration file. But it is worthwhile to mention that during the final simulations, presented in Chapter 5, this problem did not appear; and it is connected with very specific, and in most cases non realistic, scenarios.

Some tests also were made to check if the clusters that are common to some regions are considered in all these regions for the calculations of the CIR. The total amount of multipath components has to be equal to the whole number of scatterers in the particular regions. Scenarios consisting of many regions, which overlap with each other, were generated; in all

cases, the clusters from the common regions were taken into consideration to the calculation of the CIR.

5 ANALYSIS OF RESULTS

Chapter 5 includes the results of the simulations. This chapter begins with the description of the scenarios, which were taken for simulation. In this chapter, the cases of the up- and downlink scenarios in different types of cells are presented. The next part of Chapter 5 contains the results from the particular scenarios and the discussion about the results.

5.1 The scenarios for the simulations

A review was made to find appropriate scenarios for the simulations of multiuser interferences. A project, Flexible Convergence of Wireless Standards and Services (FLOWS) was chosen, in which simulations based on the Geometrically Single Based Channel Model were described, all the scenarios being taken from [VCGC03].

5.1.1 The city street scenario

This scenario describes the busy environment of a city with many people working. In Figure 5.1, the city scenario is presented, where active MTs are located along the street.

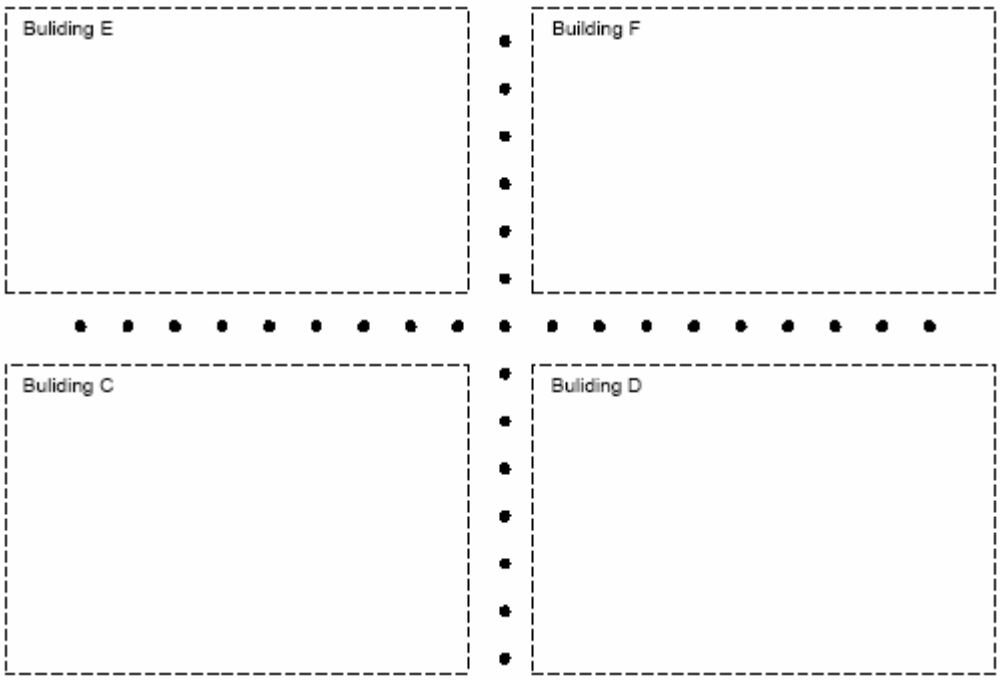

Figure 5.1 – The city scenario [VCGC03].

The distribution of users is strongly determined by the layout of streets and buildings. This scenario corresponds to the micro- and pico-cell cases, where users are positioned uniformly on the square grid. The city scenario is used to simulate the micro-cell situation (for the up- and downlinks) and the pico-cell situation (for the downlink). The areas are depicted in Figure 5.2. However, to consider a micro-cell scenario, it is important to provide an appropriate distance

between the transmitter and the receiver. The spacing should be more than 200 m (see Section 2.2.3), thus, the scenario was transformed so that it is according to the micro-cell principles. Instead of using the uniformly distribution of MTs along the whole street, users are grouped into clusters. Every group satisfies the condition of the 200 m distance. The layout of MTs, which has the shape of a straight line, was also changed. The assumption is that the distribution can have an arbitrary deployment.

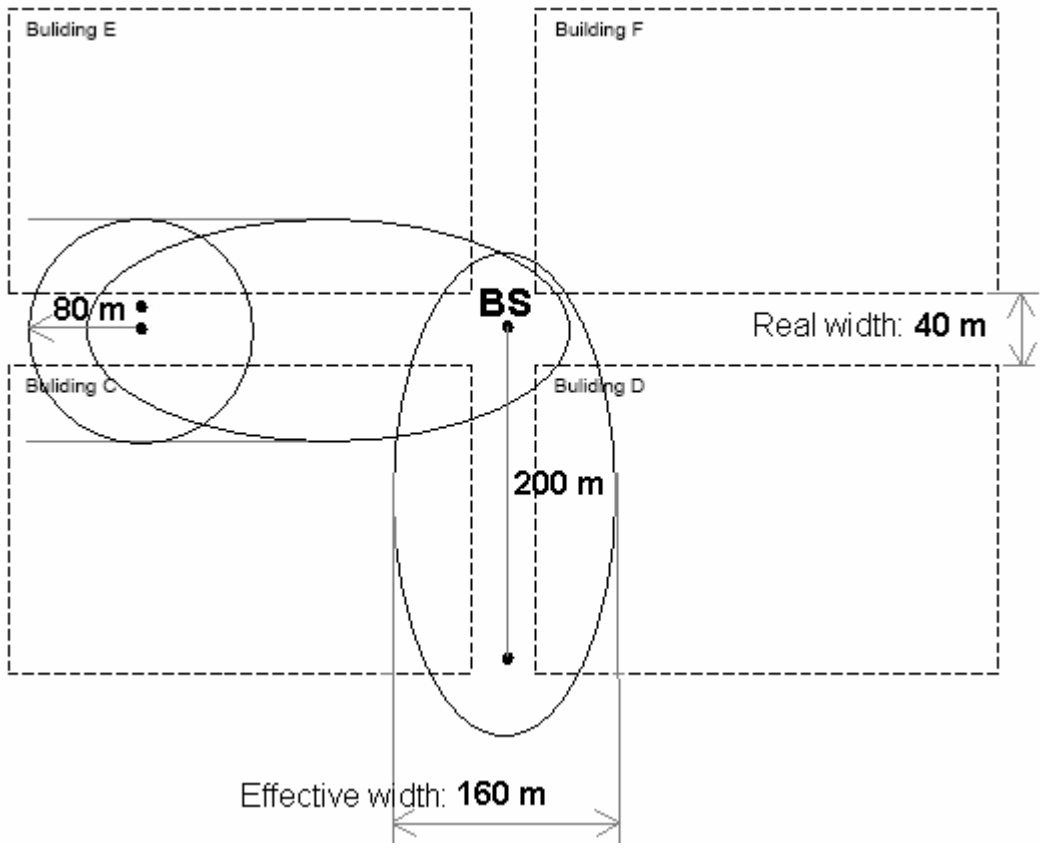

Figure 5.2 – The regions in the city street scenario.

This scenario describes the link between devices in the system, using an elliptical region with the scatterers. The parameters of the region were determined based on [VCGC03], Table 5.1.

The scenario was also enhanced to consider the downlink case. It is necessary to describe the links between the terminals, which are very close to each other (less than 200 m). In this situation, it is convenient to describe the region of scatterers by the circular pico-cell, with the MT at its centre.

Table 5.1 – Parameters for the city street scenario.

The minor axis of the ellipse [m]:	80
The major axis of the ellipse:	Depends on the distance between the MT and the BS
The radius of the circle (only for the downlink) [m]:	80
Cluster density [$1/m^2$]:	$3 \cdot 10^{-4}$
Average number of scatterers	20
Cluster radius [m]:	1
Carrier frequency [GHz]:	1.9525
Power of MTs [W]:	0.125
Power of the BS [W]:	0.125
Type of antennas (the MT and the BS):	Omni-directional
Noise level of the Rx [W]:	10^{-12} (-120 dB)
Orthogonality factor:	0.06

The cluster density was chosen to be $3 \cdot 10^{-4}$ m^{-2}. It means that the ellipse, which can be described by a minor axis of 80 m and a distance between foci equal to 200 m, has 10 clusters. In the case of the circle, which is used to describe the downlink, the amount of clusters is 6.

The uplink in the micro-cell uses the elliptical regions in the city street scenario, considering the worst case. The system consists of 8 active MTs, which are Txs at the same time. The only Rx in the system is the BS. The BS is located in the common place for both streets (in the middle of the crossroads). Active MTs are divided into 2 groups, each group covering a separate street. The considered streets are orthogonal to each other. It is assumed that the MTs from the separate groups can not see each other, because of the existing buildings in between; this assumption is important for the downlink. Every user (MT) has one ellipse associated to it, one of the focus being located in the BS and the other in the MT. The city street scenario is considered for different deployments of MTs; the MTs are located at a different distance to the BS and with different distances among each other. The group of users can be spread or can be put together. For all deployments, the BS is located in (0,0) (in the Cartesian coordinates).

All MTs transmit the signal at the same time. During the simulations the SINR ratio is calculated for every MT-BS uplink. At the same time, only one link is the desired one, the

remaining links being treated as a source of interference. There are 8 users in the city street scenario, thus, 8 SINRs are calculated.

The overview of the deployments in the city street scenario is presented in Table 5.2.

Table 5.2 – Overview of the deployments in the city street scenario.

No.	Figure (from Annex E)	Description
1	Figure E.1	There are two groups of active Tx users in the streets. Users from these groups are deployed uniformly. Every group has 4 users and users are located on the shape of the square, which is located 200 m away from the BS. The length of the side of the square is 20 m.
2	Figure E.2	This deployment is very similar to the previous one. Active users are divided into two groups with 4 users each. Users are also deployed on the shape of the square, but in this case, the length of the side of the square is 1 m. These groups are located almost in the centre of the previous squares. Distances between consecutive users are 20 times shorter than the previous ones corresponding to users together in a group.
3	Figure E.3	This deployment is a combination of the previous two. In the first street users are located on the shape of the large square, with a side of 20 m, but on the second one users are deployed on the small square, with a side of 1 m.
4	Figure E.4	This deployment is exactly the opposite to the previous one. Active users in the first street are located on the small square with a side of 1 m, while users in the second one, they are located on the shape of the square with the side of 20 m.
5	Figure E.5	This deployment is quite different. In this case, an asymmetry exists between the number of users from the different streets. In the first street there is only one user, but in the second one all other users are located. This group of users is situated 200 m away from the BS. All users are inside the square, which side is equal to 20 m.

Table 5.2 (contd.) – Overview of the deployments in the city street scenario.

6	Figure E.6	This deployment is a variation on the previous one. Here, there is also asymmetry between the number of users from the different streets, but in this case, the group of users is inside the square with a side of 2 m. The group is located 210 m away from the BS.
7	Figure E.7	This deployment considers also asymmetry between the number of users from the different streets. In the first street there are 5 users, while in the other 3 users exist. In this case users from the first street are located inside the square, with length a side of 20 m, but users from the second street are deployed on the straight line. The distance between users at the edges is 20 m. The first user is located 200 m away from the BS.
8	Figure E.8	This deployment is a variation of the previous one. Users in the second street are grouped in a region about 2 m long. This group is positioned about 210 m away from the BS.
9	Figure E.9	The groups of users from both streets have the same number of members. Both groups have the shape of a straight line, and the distance between users at the edges in both cases is the same, equal to 20 m.
10	Figure E.10	This case is quite different. Users are not deployed in groups, but rather located in the whole area. The distances between the users at the edges is over 150 m. Opposite to the other cases, symmetry does not exist of deployment. This deployment could be described as a random, but it is not completely the case. One can notice that the condition of 200 m spacing between the MT and the BS is not always satisfied. When the distance between the BS and the MT is short, instead of the micro-cell the pico-cell should be used, but in the simulations, only the micro-cell case is considered for the links. This approach enables to compare results from the different deployments of the city street scenario very easily, because in every case the same shapes are used. When the focal length approaches zero, the ellipse approaches the circle, thus, in some cases, this approach is not totally away from the pico-cell.

The downlink in the city street scenario is considered only in one street. Users, which are in the separate streets, can not see each other. In the deployments that are considered here, streets are orthogonal to each other, and users from separate groups are hidden behind the buildings. There is no LoS between users from separate groups. NLoS are not considered here, because the power associated to these rays is very low and probably below the sensitive level of the Rx.

An overview of the deployments in the city street scenario is presented in Table 5.3.

Table 5.3 – Overview of the deployments in the city street scenario.

No.	Figure (from Annex E)	Description
1	Figure E.24	This deployment takes the first street from the uplink in deployment 1. Users are spread over the large square region, and the desired user (MT1) is located in the farthest corner. The positions of the terminals are exactly the same as in the uplink case.
2	Figure E.25	In this case, the deployment of the MTs is based on deployment 2 of the uplink. Users are spread over the small square area, at a distance to the BS about 210 m. The desired user (MT1) is located in the farthest corner of the region.
3	Figure E.26	The positions of the MTs are the same as the uplink deployment 5. There is a group of 5 users, which are spread uniformly within the large square region. The desired user (MT2), which works as a receiver, is located in the middle of the group.
4	Figure E.27	The deployment of MTs in this case is a variation of the previous one. MTs are located in a small square region, which dimension is 20 times less than before. The positions of the MTs are based on the uplink deployment 6. The desired user (MT2) is located in the middle of the group.
5	Figure E.28	This deployment takes into account only 3 MTs. MTs are located on a straight line, just like uplink deployment 7. The desired user (MT7) is positioned in the centre of the group.
6	Figure E.29	This deployment considers also 3 MTs, but in this case the group of users is spread over the small region. The dimension of the region is about 1 m. The desired user (MT7) is located in the farthest corner.

The downlink is considered in the worst case, i.e., there is only one a desired a MT, the others MTs and BS work being transmitters. The investigation of MUI in the downlink is based on different deployments of the MT, with different distances between consecutive users.

In these deployments, there are two kinds of different links. There is the link between the BS and the desired MT, and the links between MTs. These two kinds of connections are different, however, they use almost the same scatterers. The link between the BS and the MT can be described in the same way as for case of the uplink. The region of the scatterers can be described by the ellipse, however, the connection between consecutive MTs should be done in a different way. Because the distance between terminals is not large, less than 200 m, the link should be described by a pico-cell. The minor axis of the ellipse is chosen to 80 m, thus, the same radius is chosen for the circle of the pico-cell. The scenario is a combination of one micro-cell and some pico-cells. Of course scatterers that are in the common area of these regions are also common when considering the propagation of the signal.

In Table 5.4 one presents which MTs work as Rx:

Table 5.4 – The desired MTs in the downlink deployments for the city street scenario.

Deployment	1	2	3	4	5	6
Desired MT user	1	1	2	2	7	7

In Annex F, example results obtained from this scenario are presented.

5.1.2 The highway scenario

The highway scenario describes the situation in a highway during a traffic jam, therefore, the speed of the particular vehicles is low or even equal to zero. This assumption is very important, because it enables to neglect the Doppler effect during simulations. This scenario was chosen because it is possible to simulate the macro-cell scenario for the up- and downlinks, and also the micro-cell for the downlink. These aspects are described in the following sections. The layout of the active MTs along the highway is presented in Figure 5.3.

This scenario considers the traffic jam only on one side of the.

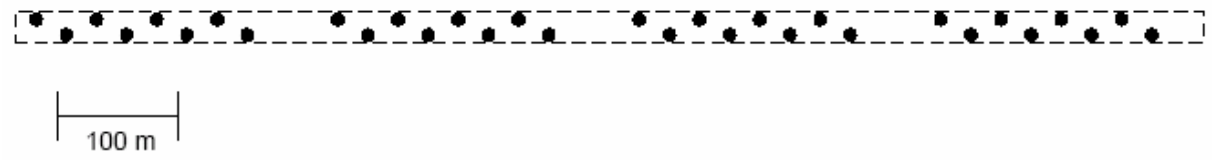

Figure 5.3 – The highway scenario [VCGC03].

The BS is located at a large distance from the terminals on the highway. To consider a macro-cell, this distance should be more than 1.5 km; in the simulations this distance was set to about 3 km. The region containing the scatterers has the shape of a circle centred at the MT. The radius of the circle was set to 200 m.

In the scenario presented in Figure 5.3, there are 32 active users. However, this amount seems to be too large, causing an unnecessary increase of complexity in the simulations. To reduce the number of users some modifications were made, namely considering a shorter length of the highway. The influence of the local density of active MTs is analysed as well as the spacing between active MTs from different groups.

The scenario was enhanced to consider links between two MTs, which will be useful for simulating the downlink approach. Every MT is surrounded by the circular area with scatterers. When two MTs are very close to each other, and the distance between them is much less than the radius of the region, the circular region can be kept, but when the distance increases, the shape of the region requires some modification. To simulate the link between two devices, which are almost in the same level over the ground and at a not so large distance from each other, the best is the micro-cell scenario, thus, in this case, these kinds of links are described by ellipses. The minor axis of each ellipse has a length of 200 m, like the radius of the circle in the macro-cell case. This length was chosen because when MTs are very close to each other, the shape of the ellipse is more similar to the circle; as it was said earlier, this circle should be the same as for case of the macro-cell. The regions are presented in Figure 5.4

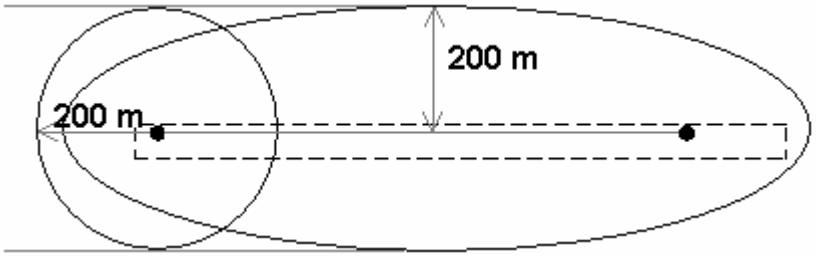

Figure 5.4 – The regions in the highway scenario.

In Table 5.5, the parameters used to simulate this scenario are presented. The values are based on [VCGC03].

Table 5.5 – Parameters for the highway scenario.

The minor axis of the ellipse (only for the downlink) [m]:	200
The major axis of the ellipse (only for the downlink):	Depends on the distance between MTs
The radius of the circle [m]:	200
Cluster density [$1/m^2$]:	$4 \cdot 10^{-5}$
Average number of scatterers	20
Cluster radius [m]:	1
Carrier frequency [GHz]:	1.9525
Power of MTs [W]:	0.125
Power of the BS [W]:	10
Type of antennas (the MT and the BS):	Omni-directional
Noise level of the Rx [W]:	10^{-12} (-120 dB)
Orthogonality factor:	0.4

The cluster density was defined as $4 \cdot 10^{-5}$ per 1 m^2; this means that the ellipse, which can be described by minor axis of 200 m and distance between focuses equal to 500 m, has 8 clusters. In the case of the circle, which is used to describe the downlink, the amount of the clusters is 5.

The uplink in the highway scenario is considered in the example of the circular regions in the traffic jam on the highway. In the deployments, MTs are distributed uniformly in a rectangular region, 9 active users being considered. These deployments assume that the BS is the only Rx in the system and that all MTs work as transmitters. The position of the BS and example positions of MTs are presented in Figure E.11.

In the macro-cell case, all scatterers are located in the circular area around the MT. In this scenario, there are as many circles as active users. When users are close to each other, circles related with them have large common parts, and the probability that clusters belong to the same regions is higher. During the investigations, these aspects are carefully checked.

An overview of the deployments in the city scenario is presented in Table 5.6:

Table 5.6 – Overview of the deployments in the highway scenario.

No.	Figure (from Annex E)	Description
1	Figure E.12	In this case, one considers a rectangle 4 m wide and long 300 m. Within this region, 9 active MTs are distributed uniformly. The distance between consecutive terminals is set to 30 m.
2	Figure E.13	This deployment is similar to the previous one, but users are twice closer. Here, it is more probable that the same cluster is shared by many of the users.
3	Figure E.14	In this deployment, one can distinguish two separate groups of active users: the first group has 5 members and the second one has 4. These two groups are located at a distance of 500 m from each other. The separation between consecutive users in the both groups is 30 m.
4	Figure E.15	In this deployment, users are also divided in two groups, and the distance between them is 500 m. The only difference to the previous case is that the separation between neighbouring users is twice less, i.e., 15 m.
5	Figure E.16	In this case users are divided in two groups as in the previous cases, but the separation is different for each group. Users from the first group are located at a distance of 30 m from each other but users from second group are separated by 15 m. Like before, groups are at a distance of 500 m from the each other.
6	Figure E.17	This deployment is exactly opposite to the previous one. Users are grouped in two collections, but the spacing between neighboring terminals is different. Users from the first group are at a distance of 15 m from each other, while in the second group the distance is 30 m.

The downlink in the highway scenario is considered in a similar way as in the city street scenario. One of the terminals is considered as a receiver and the rest as transmitters. At the same time, the BS works as a transmitter. Thus, in this case, there is only one receiver in the system, which is the worst one, since the level of the sum interferers is the highest.

In case of the downlink one considers the desired link between the BS and the MT, and the interferers' links between every other MT and the desired MT. The link from the BS to the desired MT is considered in the same way as in the case of the uplink. However the scatterers exist only around the MT in the circular region and the particular links between MTs can not be simulated in the same way. One can assume that the antennas of the MT are at the same level over the ground, and of course the distance between them is much shorter than between the BS and the MT. Thus, the most convenient way is to simulate this link as a micro-cell. MTs are located in the focuses of the particular ellipses, and all scatterers are located inside them. The radius of the circle is set to 200 m, therefore, the same dimension is set for the minor axis of the ellipse. The regions of scatterers of MTs that are close to each other become circles as in the case of the pico-cell, therefore there is a smooth transformation from a pico- to a micro-cell. Nevertheless scatterers that are connected with links of users located at a large distance between each other are positioned in the elliptical area.

To simulate downlink deployments, the same deployment of MTs were used, Figure E.30 to Figure E.35. Only one MT is the desired signal, Table 5.7.

Table 5.7 – Desired MTs in downlink deployments for the highway scenario.

Deployment	1	2	3	4	5	6
Desired MT user	1	1	1	1	1	1

In Annex F, example results obtained from this scenario are presented.

5.1.3 The Railway Station scenario

The railway station scenario is located on the train station of a small city. Using this scenario, it is possible to consider the pico- and micro-cells, both for the up- and downlinks. This scenario is used to simulate the pico-cell, and it was chosen because it gives the opportunity to make some scenarios that can consider complex situations combining the micro- and pico-cell scenarios. The original scenario consists of a train standing on the tracks, a platform and surrounding areas, with shops, waiting rooms, etc. In this work, only aspects connected to the pico-cell are used. Active users are located only in the surrounding areas, where they are

grouped in different ways, which can be describe as passengers in the waiting room, in the shop, etc. The whole scenario is presented in Figure 5.5.

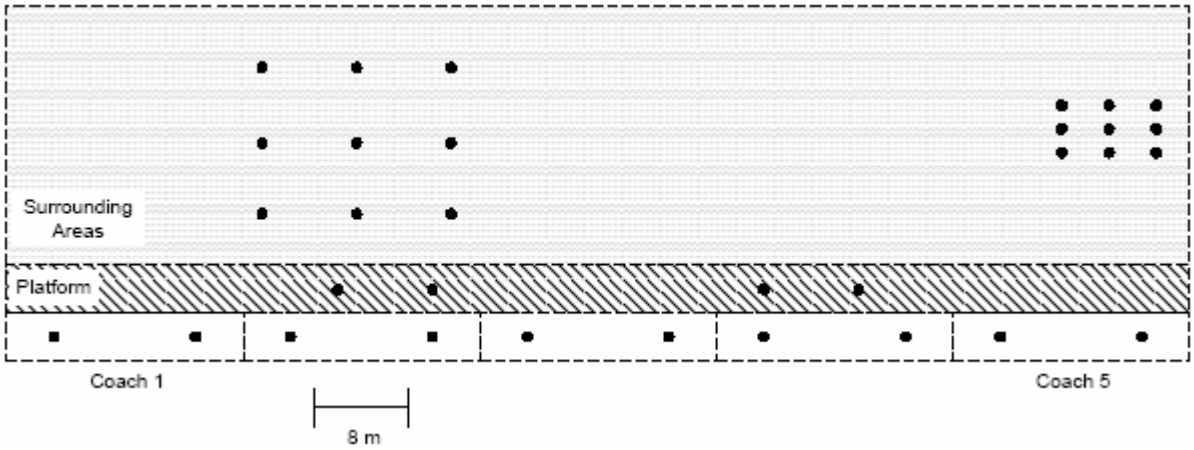

Figure 5.5 – The Station scenario [VCGC03].

To simulate the pico-cell with many users within the cell, only one region is enough defined by a circle centred at the BS. All MTs and scatterers are included inside it. In this case, there is no difference between the up- and downlinks. Always the same region is used and the circle has a radius of 50 m. The region is presented in Figure 5.6.

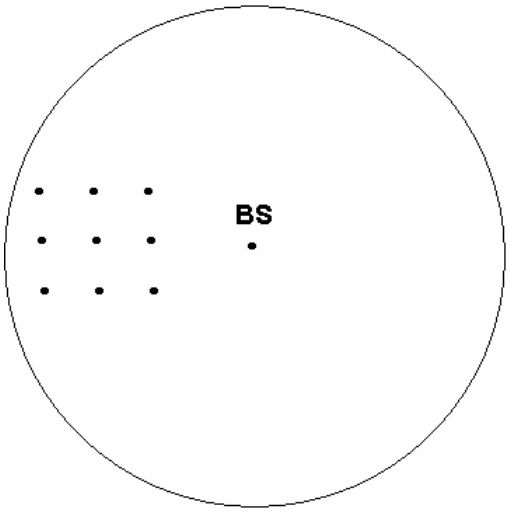

Figure 5.6 – The region in the railway station scenario.

The station scenario uses the parameters shown in Table 5.8. The region contains 6 clusters.

Table 5.8 – Parameters of the station scenario.

Radius of the circle [m]:	50
Cluster density [1/m^2]:	$8 \cdot 10^{-4}$
Average number of scatterers	20
Cluster radius [m]:	1
Carrier frequency [GHz]:	1.9525
Power of the MTs [W]:	0.125
Power of the BS [W]:	0.125
Type of antennas (the MT and the BS):	Omni-directional
Noise level of the Rx [W]:	10^{-12} (-120 dB)
Orthogonality factor:	0.06

The railway station scenario is different from these described earlier. Here, users are very close to each other, thus, only one region exists, inside which scatterers are common for all links. Every link between the BS and MTs uses the same scatterers, which are in the same positions and have the same reflection coefficients. The signal detected at the Rx from particular Txs is different, because terminals are in different places, thus, signals go through different distances. One can find here some analogy to the MIMO system, which is based on the same rules.

Deployments described different positions of scatterers and different distances between the particular terminals, all having 9 active users. The overview of the deployments in the railway station scenario is presented in Table 5.9.

The downlink in the railway station scenario is considered as in the previous deployments. In the system only one receiver, an MT, exist, the rest of the MTs being transmitters. There is only one desired link between the BS and the MT. The sources of the interferences are the other MTs, which are inside the pico-cell. The downlink in the railway station is considered for the same parameters as the uplink. In the cell there are 9 active users, thus, there are 8 links, which disturb the transmission from the BS to the desired MT.

As in the uplink, all users are inside only one circular region, all scatterers share the same circle with terminals, and the radius of this area is 50 m. In this case, the positions of all terminals are kept the same.

Table 5.9 – Overview of the deployments in the railway station scenario.

No.	Figure (from Annex E)	Description
1	Figure E.18	In this case users are deployed uniformly inside a large square region. The side of the square is 10 m. This situation is suitable to make simulations of the waiting room in the railway station. Users are distributed uniformly on the square grid, and the distance between consecutive terminals is about 5 m. The centre of this region is located at the distance of 25 m from the BS.
2	Figure E.19	This deployment is very similar to the previous one. Users are located uniformly in the square grid, in the square region. The only difference is the separation between terminals, which is equal to 1 m here.
3	Figure E.20	This case describes the situation where users are divided into two groups. The first group consists of 6 users, which are deployed in the same grid like in deployment 1, the second group has 3 users, which are closer to each other. The distance between them is about 1 m in the latter, while in the former it is 5 m. The distance between the centre of the first group and the BS is about 22 m, and for second group it is 25 m.
4	Figure E.21	This case describes a situation very similar to the first deployment. The only difference is that the middle user (MT5) is moved from the centre of the group to the other side of the BS. However, the distance between the MT5 and the BS remains the same.
5	Figure E.22	This case is also a variation of one of the previous deployments. In this case, the middle user from deployment 2 (MT5) is also moved to the other side of the BS, however, the distance between the MT5 and the BS is kept the same.
6	Figure E.23	This case is quite different. The location of the MTs within the region was generated by using a random number generator. The only restriction was that all users must be inside the circle.

The terminal working as Rx in the particular deployments is shown in Table 5.10.

Table 5.10 – Desired MTs in downlink deployments for the railway station scenario.

Deployment	1	2	3	4	5	6
Desired MT user	1	1	1	1 and 5	1 and 5	1

In Annex F, example results obtained from this scenario are presented.

5.2 The results

5.2.1 Influence of the number of simulations

The number of simulations is a very important parameter, which decides about the quality of the obtained results. It was necessary to make an investigation on the influence of this number on the results, which was done for all modes of the simulator being helpful to decide in which mode the final simulations would be made.

Only one scenario was chosen, because the same tendency was obtained for the city street, the highway and the railway station scenarios. The comparison was made for SINRs for MT2 in deployment 1 in the city street scenario. The tests were made for 2, 10, 20, 50, 100, 200, 300 and 500 iterations of the simulator for each mode (0, 1 and 3), Figure 5.7 and Figure 5.8.

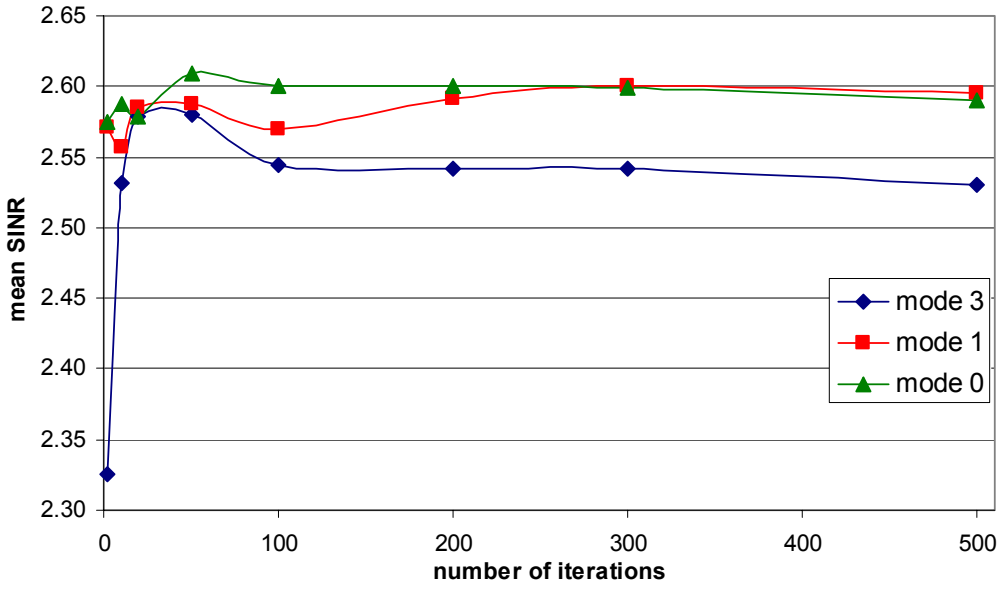

Figure 5.7 – Mean SINR for a different number of iterations.

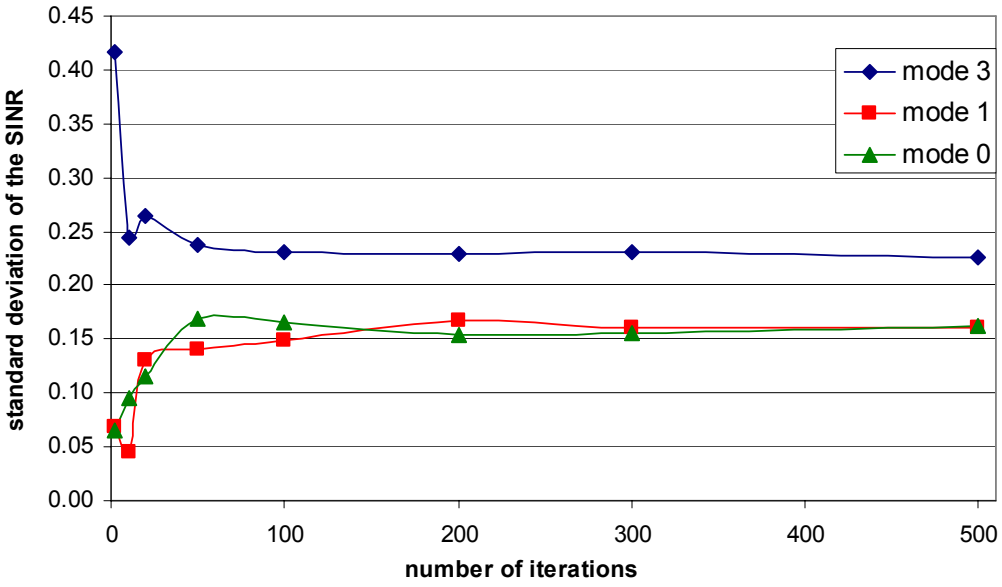

Figure 5.8 – Standard deviation for a different number of iterations.

One can see that there are differences in the results from the different modes of the simulator. The mean SINRs from mode 0 and mode 1 have similar values, and the curves become very similar when the number of iterations increases, as was expected. In these modes, the positions of the clusters are always the same, so the average delays of the multipath components are similar, therefore, the CIRs from these modes are high correlated to each other. The correlation is higher, when the number of simulations increases. However, these modes have an unacceptable behaviour: by analysing Figure 5.8, one can notice that for an increasing number of simulations, the standard deviation does not drop, the lowest value obtained for the lowest number of iterations. When the number of iterations increases, curves also increase, and after about 50 iterations, they saturated. This tendency comes from the fact the that positions of the clusters are the same, hence there are not many possibilities of changing the parameters.

Mode 3 shows the best properties since in consecutive iterations, the positions of the clusters are different, the standard deviation has to be higher than in the previous modes, because all the parameters describing scatterers and clusters are different. But in this case, when the number of simulations increases, the standard deviation decreases. When the number of simulations increases beyond a certain value, the curves become saturated. One can notice that when the number of simulations increases beyond 100, the standard deviation and the mean value are already in the saturated region, hence, increasing the number of simulations over 100 does not make sense: it increases the simulation time, but results have the same errors. In conclusion, simulations were made in mode 3 for 100 iterations.

In Figure 5.9 and Figure 5.10, results are presented for CIRs processed with a 2 ns resolution.

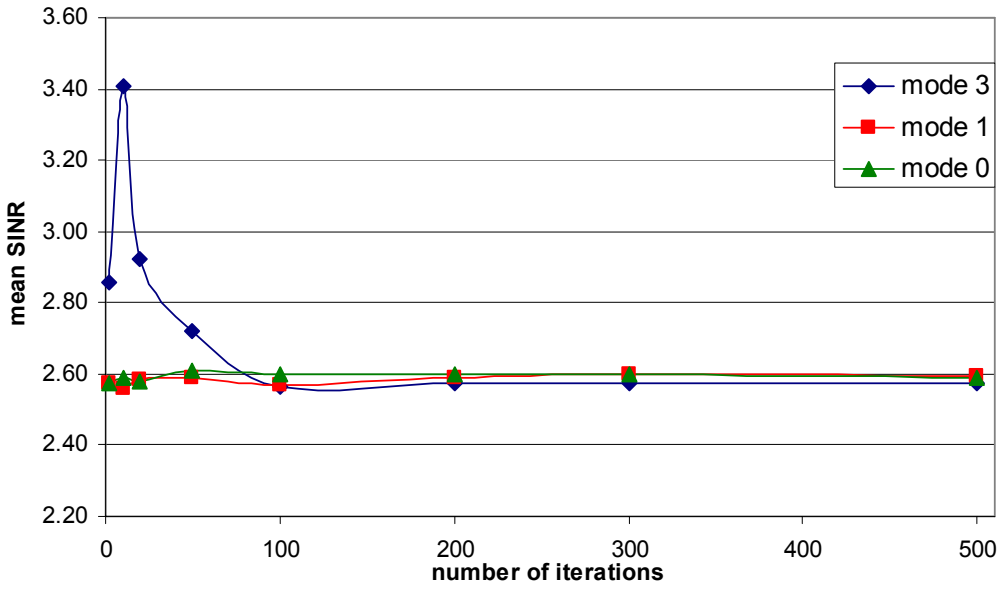

Figure 5.9 – Mean SINR for a different number of iterations, for CIR with 2 ns resolution.

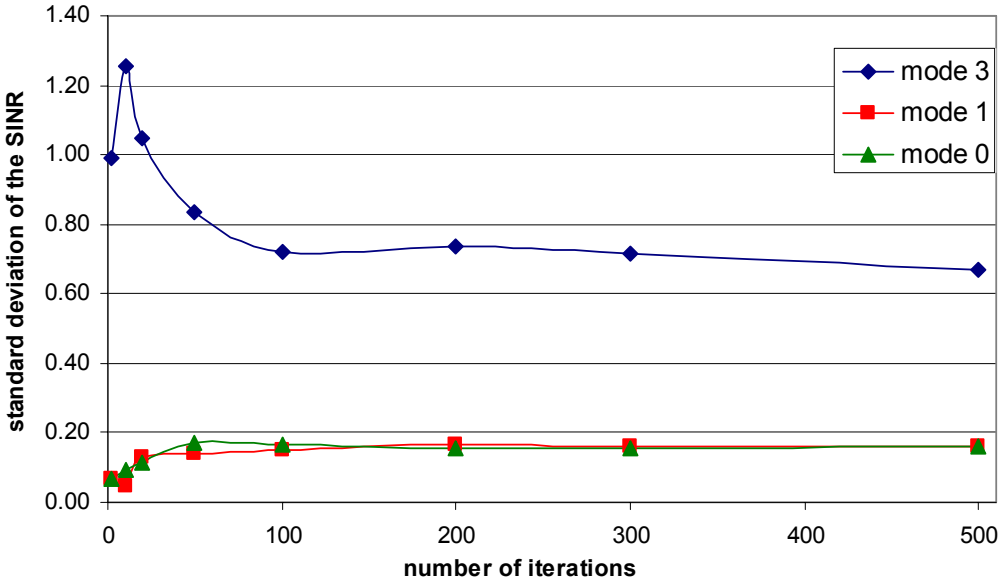

Figure 5.10 – Standard deviation for a different number of iterations, for CIR with 2 ns resolution.

The results presented earlier in Figure 5.7 and Figure 5.8 were the CIRs taken without any processing, i.e., unfiltered CIR. Figure 5.9 and Figure 5.10 show that the CIRs after the processing lead to the same conclusions on the influence of the number and mode of simulations.

5.2.2 Influence of the time resolution

In order to compare the influence of the time resolution, two methods of calculating the SINR are considered. In the first one, the whole CIR of the particular links is taken, being divided into bins with the period determined by the time resolution. All multipath components inside the same bin are summed together. This kind of calculating the SINR is called $SINR_{bin}$.

The other method of calculating the SINR is based on the CIR processed in the same way as before, but, the calculation of power considers only the first 4 bins. This kind of calculation is called $SINR_{4s}$.

Figure 5.11 presents $SINR_{bin}$ for deployment 4 in the city street scenario, for the different time resolutions: unfiltered (0 ns), 0.2 ns, 2 ns and 20 ns. In Annex G (from Figure G.1 to Figure G.4), CIRs for different time resolutions for the MT1-BS link are presented. In Figure 5.12 and in Table 5.11 and Table 5.12, one presents differences between the results using different time resolutions and without processing.

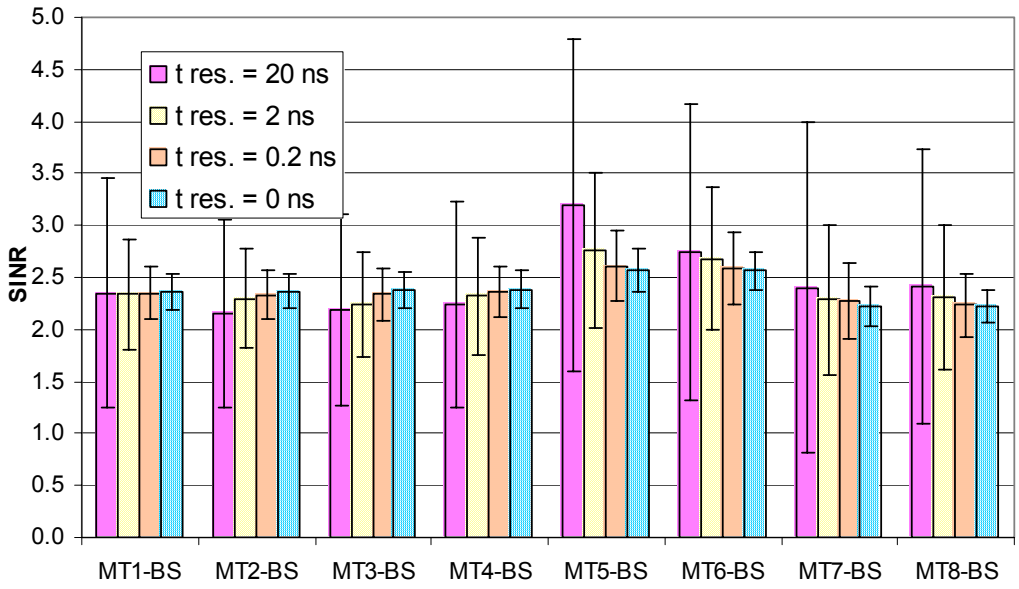

Figure 5.11 – Comparison between different times resolution for $SINR_{bin}$ (deployment 4 in the city street scenario).

Unfiltered CIR are considered as a reference. One can assume that the results from this case have the best accuracy. When the time filtering period increases, results become less accurate: more multipath components are summed together, thus, more information, which is carrying by

them is lost. This situation is visible in Figure 5.11 for the standard deviations, since they with the increase of the time resolutions, also the level of the mean values becomes more different.

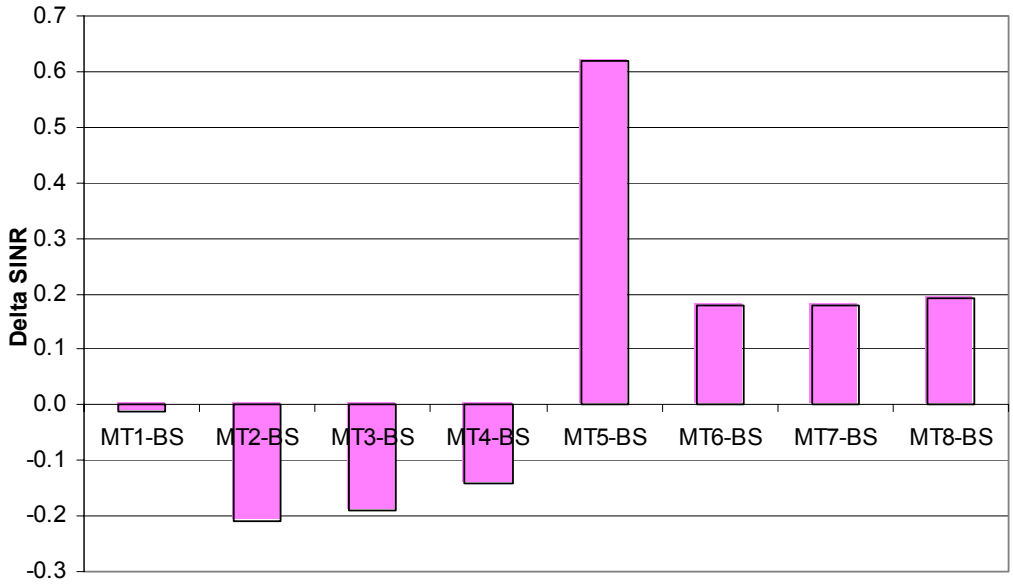

Figure 5.12 – Differences between $SINR_{bin}$ with a time resolution of 20 ns and unfiltered (deployment 4 in the city street scenario).

Table 5.13 contains averages of the SINR differences calculated for different time resolutions. The largest differences occur for 20 ns. As expected, the CIRs with 0.2 ns time resolution are more similar to the unfiltered ones.

Table 5.11 – Differences between $SINR_{bin}$ with a time resolution of 2 ns and unfiltered.

Deployment 4 in the city street scenario, t_{res} = 2 ns vs. unfiltered								
MTx-BS link	1	2	3	4	5	6	7	8
$\Delta SINR \cdot 10^{-3}$	-27.26	-67.67	-137.91	-63.64	187.39	115.58	59.14	85.03

Table 5.12 – Differences between $SINR_{bin}$ with a time resolution of 0.2 ns and unfiltered.

Deployment 4 in the city street scenario, t_{res} = 0.2 ns vs. unfiltered								
MTx-BS link	1	2	3	4	5	6	7	8
$\Delta SINR \cdot 10^{-3}$	-12.56	-28.57	-36.95	-24.84	42.85	24.06	48.24	10.19

The situation is the opposite for case of the $SINR_{4s}$, Figure 5.14 to Figure 5.16. The best accuracy is obtained for the CIRs processed with longer time slots, because when the time bin is longer, the more multipath components are summed together within this bin. As always the first

4 samples are considered, the longer time resolution means that more multipath components are taken into account, therefore, more energy of the signal is considered.

Table 5.13 – Comparison between differences of SINR and time resolution.

Time resolution [ns]	Average of $\Delta SINR_{bin}$		Average of $\Delta SINR_{4s}$	
	μ_{bin}	σ_{bin}	μ_{4s}	Σ_{4s}
0.2	0.0028	0.0333	0.3196	0.3640
2	0.0188	0.1100	0.3178	0.4003
20	0.0769	0.2768	0.1556	0.2978

The differences between the SINRs obtained for the different time resolutions in Table 5.13 show now that the most accurate results, relative to the results from the unfiltered CIR, are obtained for the case of 20 ns.

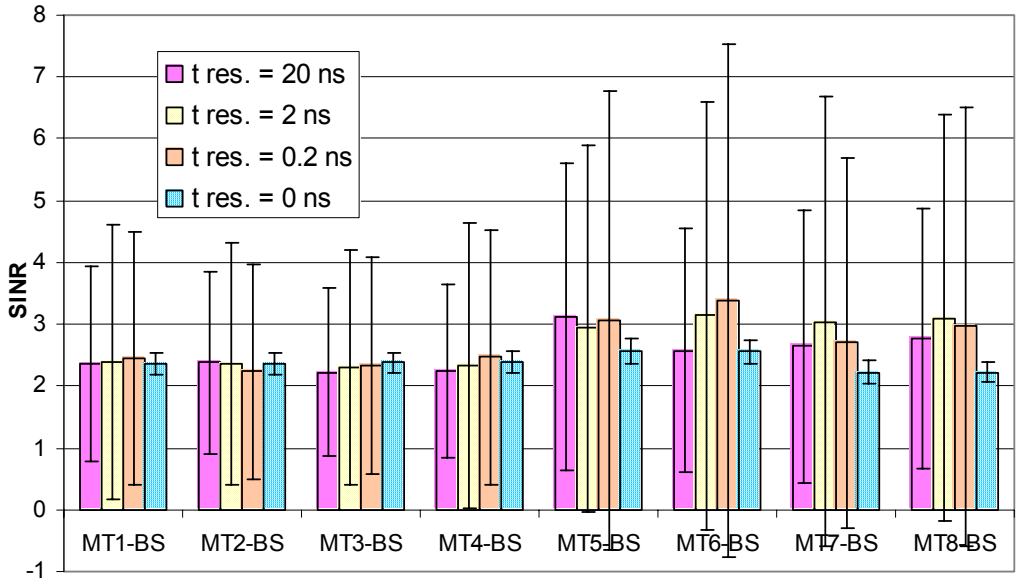

Figure 5.13 – Comparison between different time resolutions for $SINR_{4s}$ (deployment 4 in the city street scenario).

In this case of $SINR_{4s}$ one should address the accuracy of results. One can notice that SINRs have a standard deviation higher than the mean value, which is not acceptable; only for the case of 20 ns, the values of the standard deviations are lower, but still very high compared to the case of $SINR_{bin}$.

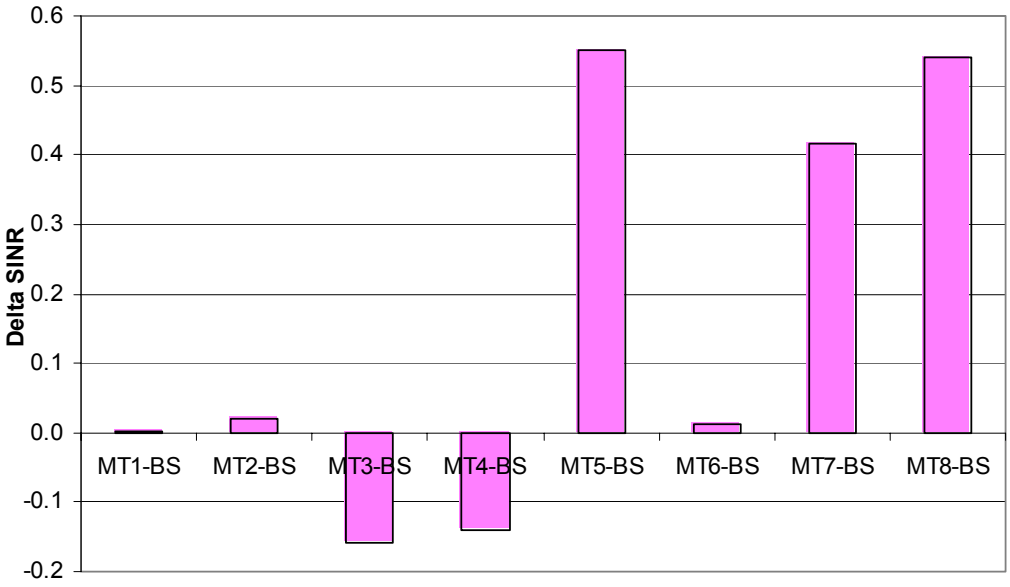

Figure 5.14 – Differences between $SINR_{4s}$ with a time resolution of 20 ns and unfiltered (deployment 4 in the city street scenario).

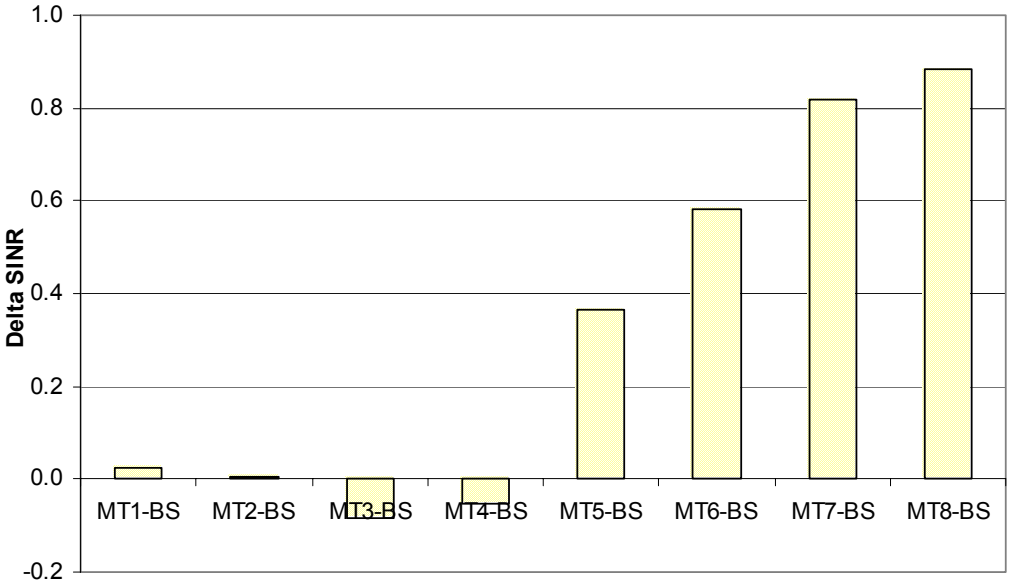

Figure 5.15 – Differences between $SINR_{4s}$ with a time resolution of 2 ns and unfiltered (deployment 4 in the city street scenario).

Simulations for the different scenarios use unfiltered CIRs, corresponding to highest possible accuracy.

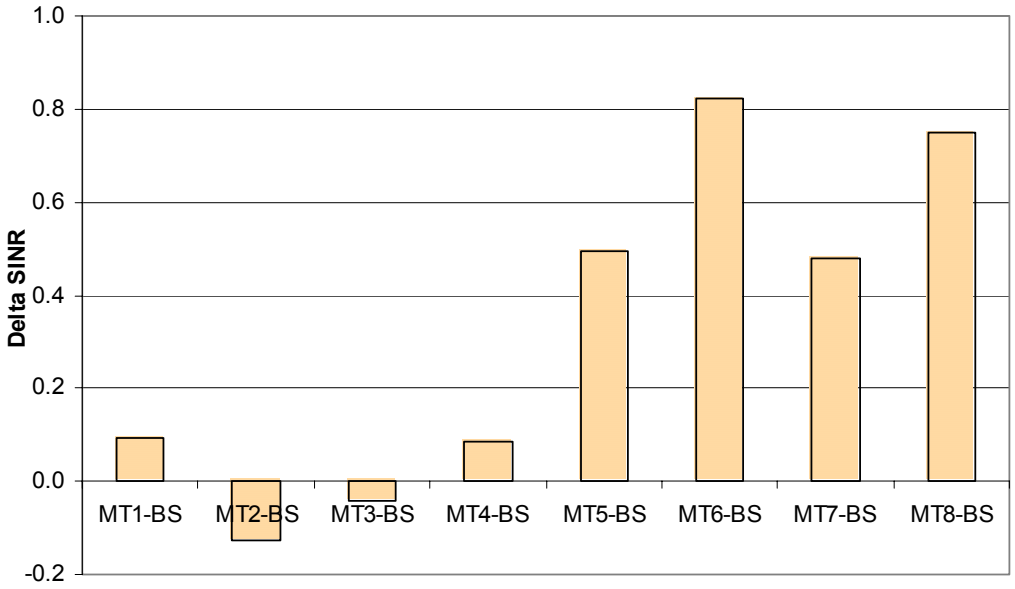

Figure 5.16 – Differences between $SINR_{4s}$ with a time resolution of 0.2 ns and unfiltered (deployment 4 in the city street scenario).

5.2.3 Influence of the deployment of terminals for synchronised Rxs

Simulations were done by using the scenarios presented in the previous section. This kind of scenarios can take place in real environments when the FDD mode is used. The CDMA system is used to distinguish users, and the Rx detects signals from the Txs at the same time.

The calculations of SINR are made based on (2.2), where desired and interference powers are obtained from the CIRs,

$$P = \sum_{i=1}^{N_{fft}} \left| H_i(f) \right|^2 \tag{5.1}$$

where:

- $H(f)$ is the Fourier transform of the CIR
- N_{fft}: number of the samples the spectrum (from the FFT algorithm)

In the case of the uplink in the city street scenario, the SINR is strongly correlated with the distance between the Tx (MT) and the Rx (BS). Only the signal from one MT is considered as desired, the rest from the other MTs being sources of interference. When the MT is closer to the BS, the Rx detects a stronger signal, which can be observed in Table 5.14 and Table 5.15. The

MTs from deployments 1-9 have almost the same average distance to the BS, hence, the average SINRs have almost the same level, with only slight fluctuations. In deployment 10, the average of the distances is significantly different from the previous cases, thus, the average SINR also shows a different level. This is a consequence of users being spread all over the region.

Table 5.14 – Average distances between MTs and the BS in the city street scenario.

deployment	1	2	3	4	5	6	7	8	9	10
average distance [m]	210.24	210.00	209.87	210.37	210.18	210.25	210.12	209.99	209.93	125.46

It is interesting that in the uplink in CDMA, when the MTs transmit the same power, the SINR is related only with distance. The shape of the groups, the number of users within the group, and the distance between terminals, do not play an important role in the uplink. To have a good quality of the signal and a good throughput (which depends on the quality of the signal), the MT should be located closer to the BS. This explains why power control of Txs is used; the quality of all users is expected to be the same, thus, users located in farther away from the BS have to transmit signals with higher levels.

Table 5.15 – Average SINRs of users in the city street scenario.

scenario	1	2	3	4	5	6	7	8	9	10
average SINR	2.385	2.383	2.384	2.383	2.383	2.382	2.384	2.384	2.384	2.490

Figure 5.17 shows the comparison between the SINRs, for deployments 7 and 10 in the city street scenario. In the case of deployment 7, the SINRs have almost the same level - values fluctuate slightly; the differences within consecutive distances between the MTs and the BS are about 10 m. The best SINR is obtained for MT3, MT5 and MT6, which are located at comparable distances to the BS, being the closest ones. The 10 m spacing between users has a slightly impact on the quality of the link, and fluctuations of the levels of the SINR may come from the randomness of the simulations. However, when deployment 10 is considered, one can observe that the differences in the location of the MTs, have quite an impact on SINRs; the

differences in the distances are equal to 50 m. Table 5.16 shows the differences in the distances and in the SINR, between consecutive MTs in deployment 10 in the city street scenario.

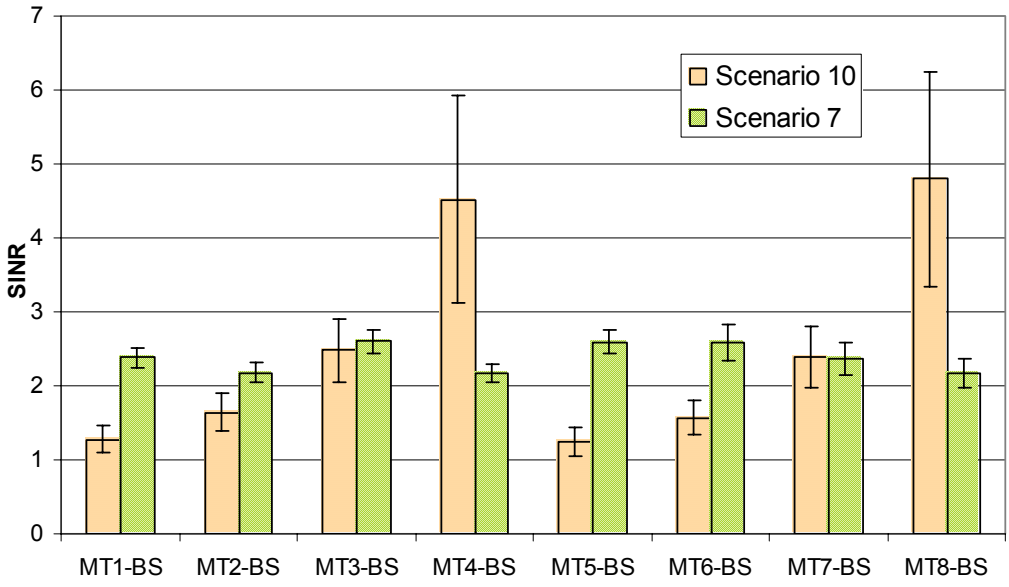

Figure 5.17 – SINR for the deployment 7 and 10 in the city scenario.

Table 5.16 means that between each pair the difference in the distance is the same; however, the differences between the SINRs are not equal. The difference between the farthest pairs (MT1-MT2 and MT5-MT6) is only 1 dB, Figure 5.18.

Table 5.16 – Overview of differences in deployment 10 in the city scenario.

Pair of the MTs	MT1 - MT2	MT2 - MT3	MT3 - MT4	MT5 - MT6	MT6 - MT7	MT7 - MT8
Difference in distance [m]	49.67	49.83	49.51	49.67	49.83	49.51
Difference in SINR [dB]	1.10	1.79	2.62	1.00	1.83	3.02

When the pair of MTs is closer to the BS, like the MT3-MT4 and MT7-MT8, the differences in SINR are greater. In Figure 5.18, the *x*-axis represents the average distances of the MTs from each pair, relative to the BS. When the distance to the BS is shorter, the difference between the SINRs increases. This tendency has an exponential behaviour, being related to exponential distribution of power.

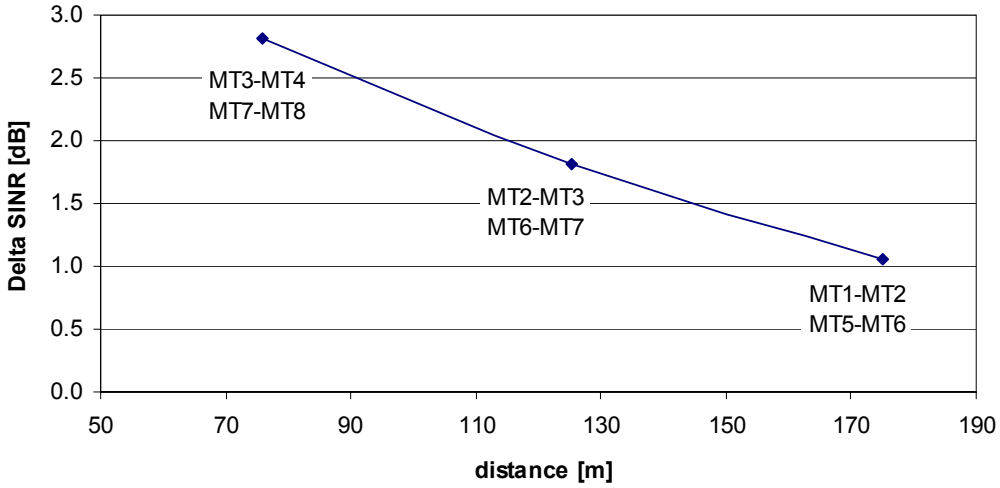

Figure 5.18 – Relation between the differences of the SINR and the distance of the pair.

In the uplink, for the highway scenario, a strong relationship between the distance of MTs and the BS, and the SINRs is present as well. For this case the relative differences between the averages distances are lower than in the city street scenario, therefore, the relative differences between the SINR are lower. The difference between the maximum and the minimum distance is about 6.5 % for the former and 40 % for the latter. In Table 5.17, one presents the average distances between the MTs and the BS, and in Figure 5.19 the average SINRs.

Table 5.17 – Average distances between the MTs and the BS in the highway scenario.

deployment	1	2	3	4	5	6
average distance [m]	3110.88	3056.21	3271.97	3219.59	3263.98	3227.50

The highest average SINR is obtained for deployment 3. In this case, users are divided into two groups, and the spacing between consecutive users within each group is the same, equal to 30 m. Users from the second group (from MT6 to MT9) are the farthest from all deployments. The SINRs of users from the first group are significantly higher compared to other deployments, which causes the average SINR to be higher.

In the city street scenario, the higher value of the average SINR is obtained for MTs very close to the BS. In the highway scenario, the distances between the closest MTs to the BS in the deployments are the same; thus, only terminals, located far away from the BS influence the overall value of the average SINR. The lowest average of the SINR is obtained for deployment

2, where all terminals are collected in one group, the spacing between the consecutive users being the lowest 15 m. The BS detects signals from the different users almost with the same level, therefore, the level of interference is the highest. In Figure 5.20, the comparison between SINRs for deployments 2 and 3 is presented.

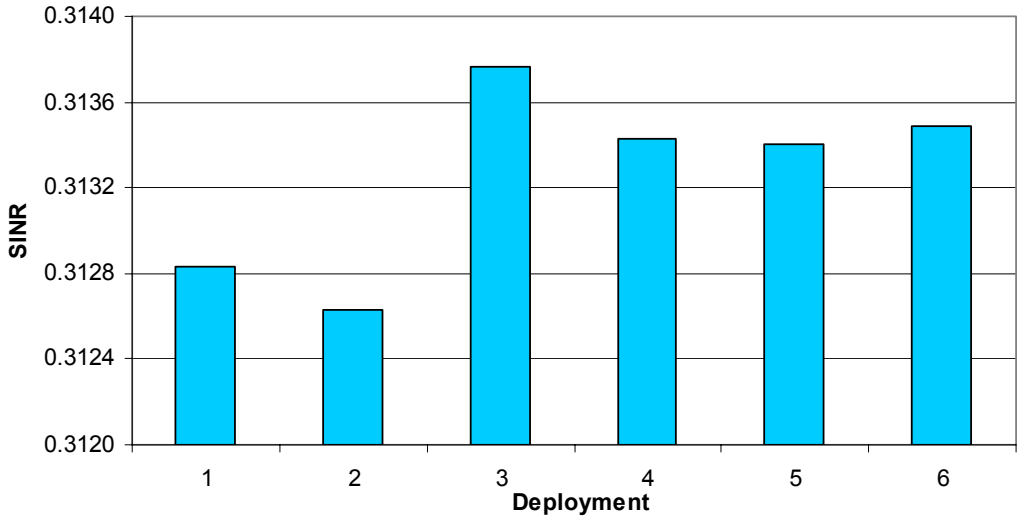

Figure 5.19 – Average SINR in the highway scenario.

To show that SINR depends mainly on the distance, it is interesting to deployments 4 and 6, which have similar average distances but different deployment of users. In one group, the spacing between terminals is twice shorter, but the results are almost the same.

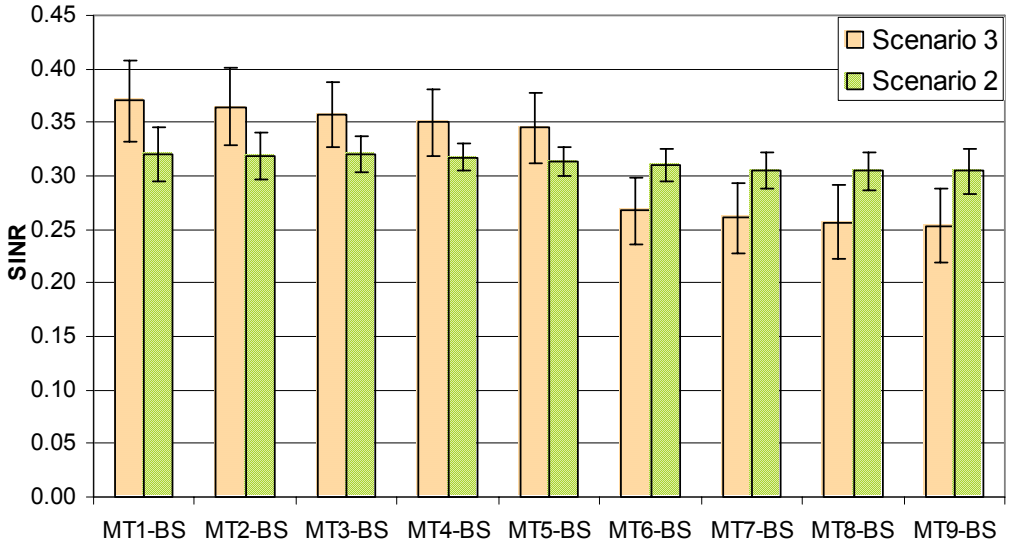

Figure 5.20 – SINR for deployments 2 and 3 in the highway scenario.

For the railway station scenario, Table 5.18 and Table 5.19 show average distances between the MTs and the BS, and average values of the SINRs. Only deployment 6 has a different average distance, rendering a different value of SINR; the first 5 deployments consist of different distributions of terminals, but the average distance to the BS is the same.

Table 5.18 – Average distances between MTs and BS in the railway station scenario.

deployment	1	2	3	4	5	6
average distance [m]	25.34	25.01	23.58	25.34	25.01	30.86

Figure 5.21 shows the SINRs in deployments 6 and 2. In deployment 6, the distribution of MTs comes from a random number generator, MTs being uniformly distributed within the whole region. There are some users very close to the BS (MT7 and MT1), while others are far away (MT3, MT4 and MT5). The SINR obtained from the closest MTs is significantly higher compared to the highest SINR in other deployments, thus, the average for this deployment is higher.

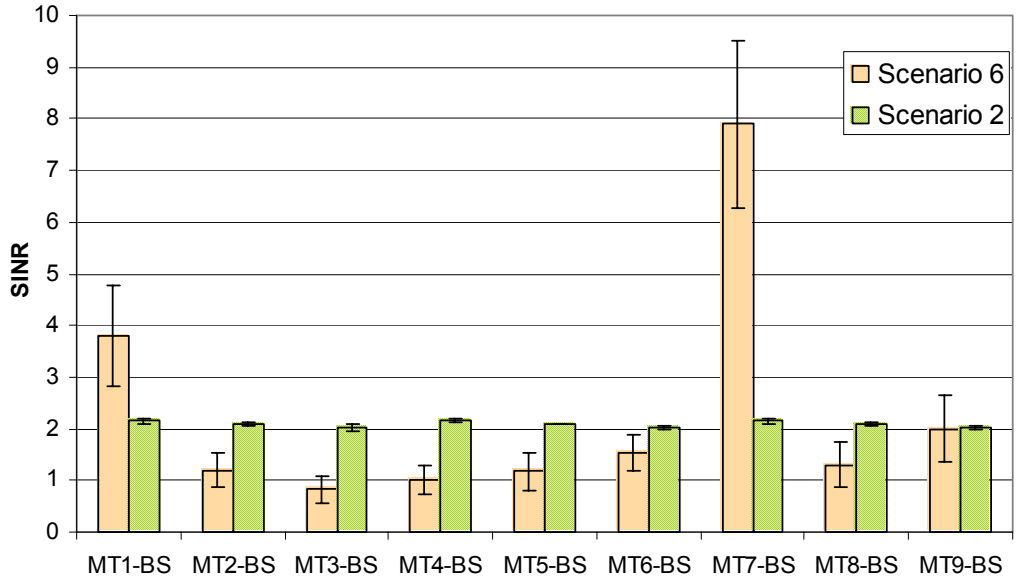

Figure 5.21 – SINR for the deployment 2 and 6 in the railway station scenario.

In the case of deployment 2, the SINRs from all MTs have the same level, being located at a close distance from each other, therefore, the distance between each of them and the BS is the same.

Table 5.19 – Average SINRs of users in the railway station scenario.

deployment	1	2	3	4	5	6
average SINR	2.090	2.084	2.098	2.096	2.090	2.303

Simulations were also done for the downlink in the street city, highway and railway station scenarios. In these cases, only one link between the BS and the MT for every deployment is considered as desired. One of the MTs is the Rx, and the BS and all other MTs are Txs. This kind of interference can take place when the others terminals communicate with the other BSs, being an example of the inter-cell interference.

This kind of interference can occur in the mode TDD. Neighbouring cells can use different frame layouts, interference coming from the different amount of time-slotes for the up- and downlinks. The MT to MT interference, which is not only typical of UMTS, but exists also for DECT.

For the city street scenario, SINRs are presented in Figure 5.22, while Figure 5.23 contains the average distances between the desired user and the other terminals within the deployment.

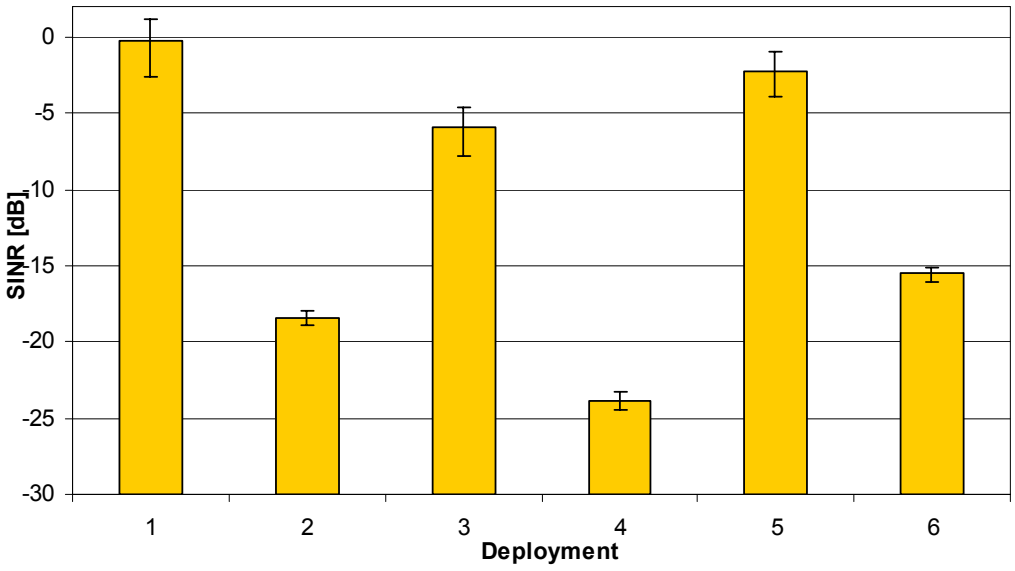

Figure 5.22 – The downlink in the city street scenario.

The distance between the BS and the desired MT was not taken into account during making this figure. In this case, the relationship between the average distances and the SINRs is not so clear like before. For the downlink, it is important if interfering users are spread or grouped around the desired user. It is worthwhile to make a comparison between deployments 1 and 2, where the desired MT1 detects signal from the BS, Table 5.20. The power detected in both cases has almost the same level, the difference between them being about 8 %, but SINRs are different, 98 %. The desired user from deployment 1 is located at the farthest distance from the BS, but the SINR has the highest level. The reason is that the average distances from other terminals is 22.6 m, while for deployment 2 it is equal to 1.75 m. For deployment 2, users are grouped around the desired user, which causes the SINR to drop very rapidly. The same conclusion is obtained for deployments 3-4, and 5-6.

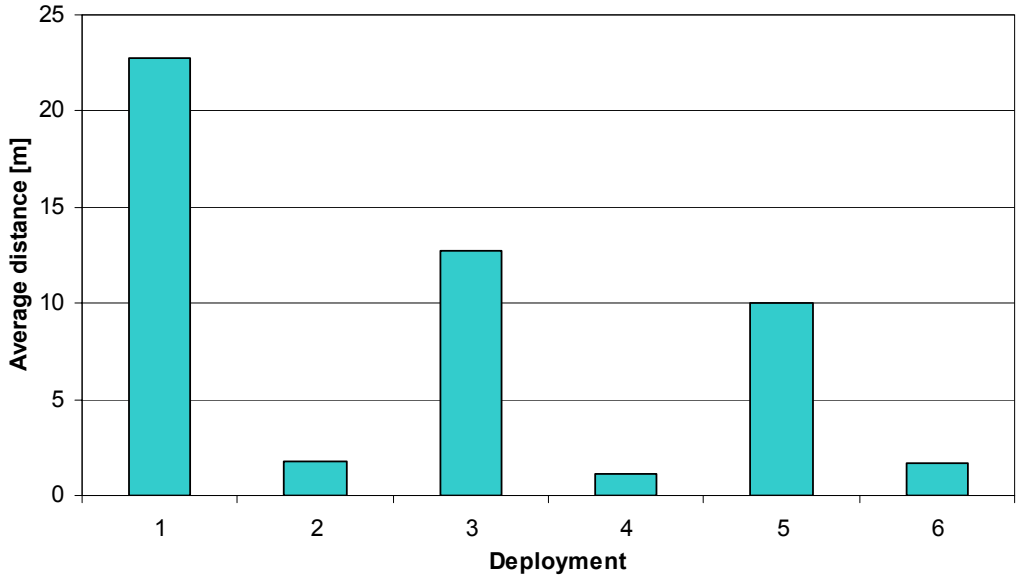

Figure 5.23 – Average distances in the city street scenario for the downlink.

Table 5.20 – Average power from the BS in the city street scenario.

deployment	Average power [mW]	Standard deviation [mW]	Distance between the MT1 and BS [m]
1	4.44	$1.75 \cdot 10^{-4}$	220.23
2	4.81	$1.76 \cdot 10^{-4}$	211.00

SINR is strongly dependent on the number of users. In the considered downlink deployments in the city street scenario, some characterise the different number of users, deployments 2, 4 and 6, Table 5.21.

Table 5.21 – Comparison between deployments 2, 4 and 6 in the city street scenario.

Deployment	Number of users	Average distance between users [m]	Distance from the desired MT to the BS [m]	SINR [dB]
6	3	1.71	210	-15.5
2	4	1.75	211	-18.4
4	7	1.14	210	-23.8

In these 3 cases, the distance between the desired user and the BS is the same, and the average distance to the interfering terminals is similar. The only difference exists in the number of MTs around the desired user. More users cause a lower SINR. In order, to check how much every additional user affects the SINR, simulations were done in exactly the same environment, but with a different number of users.

Additional deployments were defined. In the first one, users are located uniformly on the shape of the circle, Figure 5.24 (N_{ter} describes number of MTs; n_{ter} can change from 1 to N_{ter}).

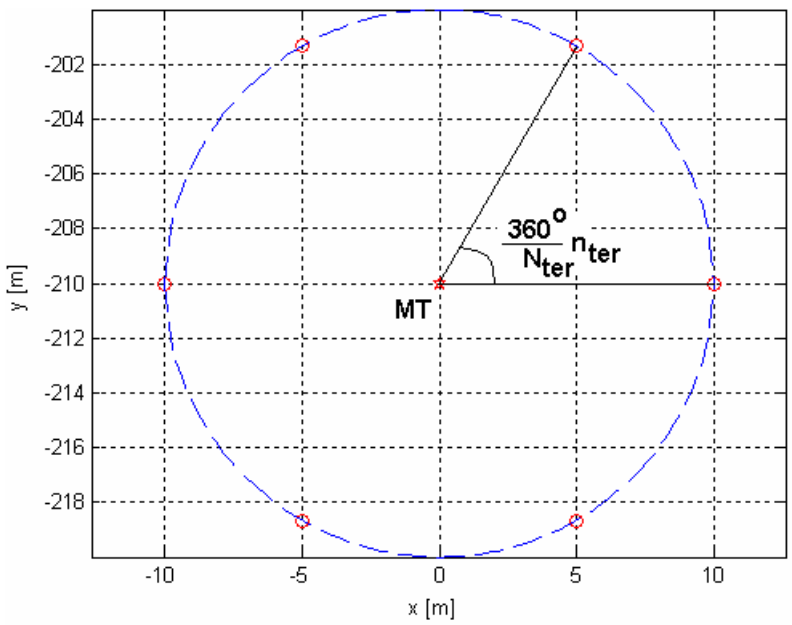

Figure 5.24 – Distribution of terminals on a circle.

In this case all distances between the desired MT to other MTs are always the same, as well as distances between consecutive MTs. The simulations were made for a number of additional users varying from 1 to 10. The positions of the desired MT and the BS and parameters of the environment were taken from deployment 6 in the city street scenario.

Results are depicted in Figure 5.25. When the number of MTs increases, SINR decreases. Consecutive results are correlated with each other, which means that one can assume that when MTs have a regular deployment in the cell, it is possible to calculate the possible SINR with good accuracy in the case of the downlink, hence, it is possible to predict the level of the interference, and it is easier to plan of the deployment of the BSs.

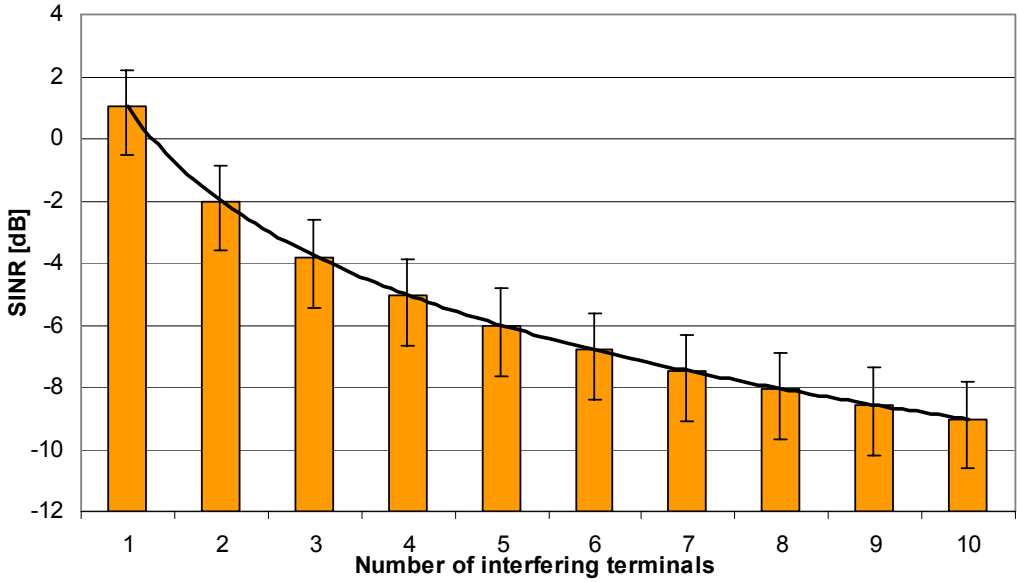

Figure 5.25 – SINRs for a different number of users distributed uniformly on the circle around the desired MT for the case of the city street scenario.

Based on Figure 5.25 one can observe the influence of the adding the next user to the system. The highest drop of the quality of the connection (the drop of the SINR) is obtained when there are a few terminals; by adding successive users, the level of interference increases.

Fluctuations in the number of users, when there are a lot of terminals in the area around the desired user do not have a huge impact on the quality of the link. It means that the cell is more predictable and stable; however, of course, the quality of the link is low. The same results were obtained when, instead of the uniform distribution of terminals, the random deployment was used.

The random distribution of 10 users in Figure 5.26 is depicted.

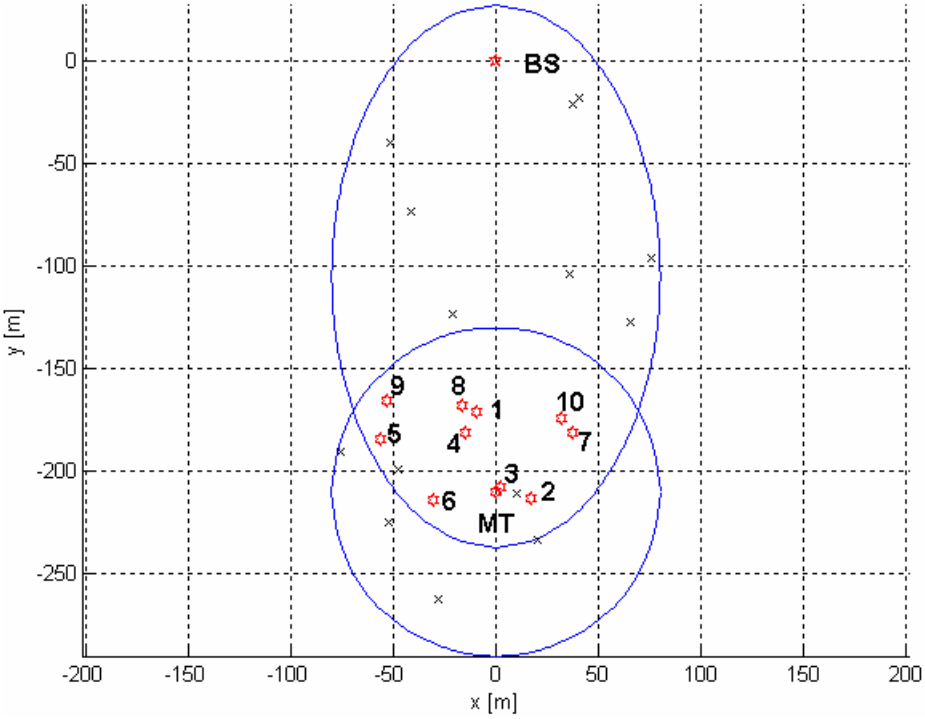

Figure 5.26 – Random position of terminals.

Users are located in the common area of the ellipse, that was constructed between the BS and the desired MT, and the circle that describes the pico-cell around the desired MT. The environment is kept the same as for users distributed on the circle. The SINRs obtained during these simulations are in Figure 5.27.

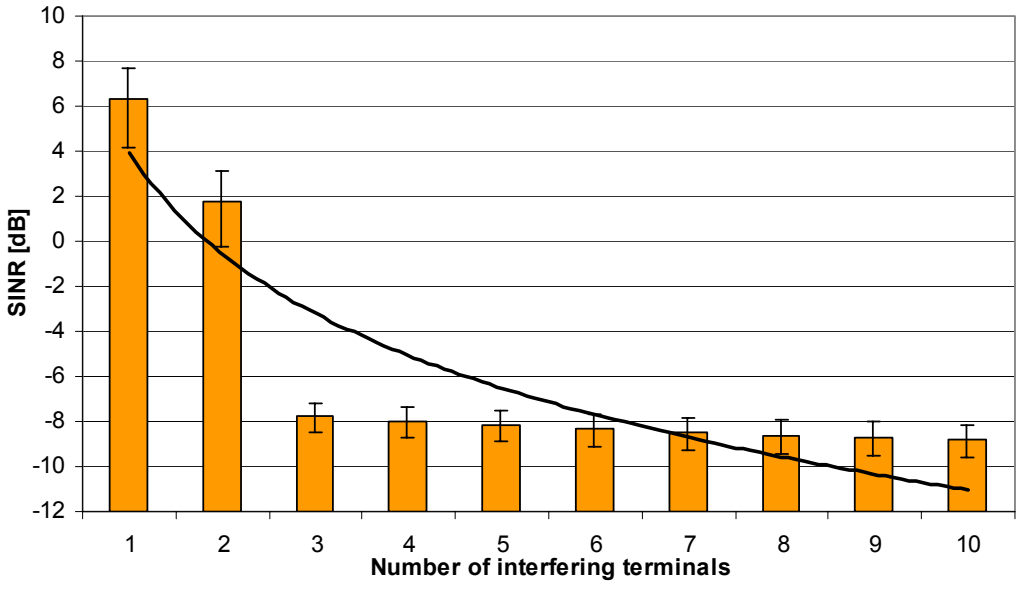

Figure 5.27 – SINRs for the different number of users distributed in random positions around the desired MT for the case of the city street scenario.

The distribution of the users is not regular, thus, the trend of consecutive SINRs is not as regular as well. When the number of the users increases the SINR drops, the highest drop being after the user 3, which is explained by the position of this user very close to the desired MT; this terminal causes the greatest grow the interference.

But the trend, that the differences between SINRs from users are more stable when in the area around the desired user there is a larger number of terminals is kept.

The results for the downlink in the highway scenario, lead to the same conclusions as in the city street scenario. The average SINRs for the deployments in this scenario are in Figure 5.28.

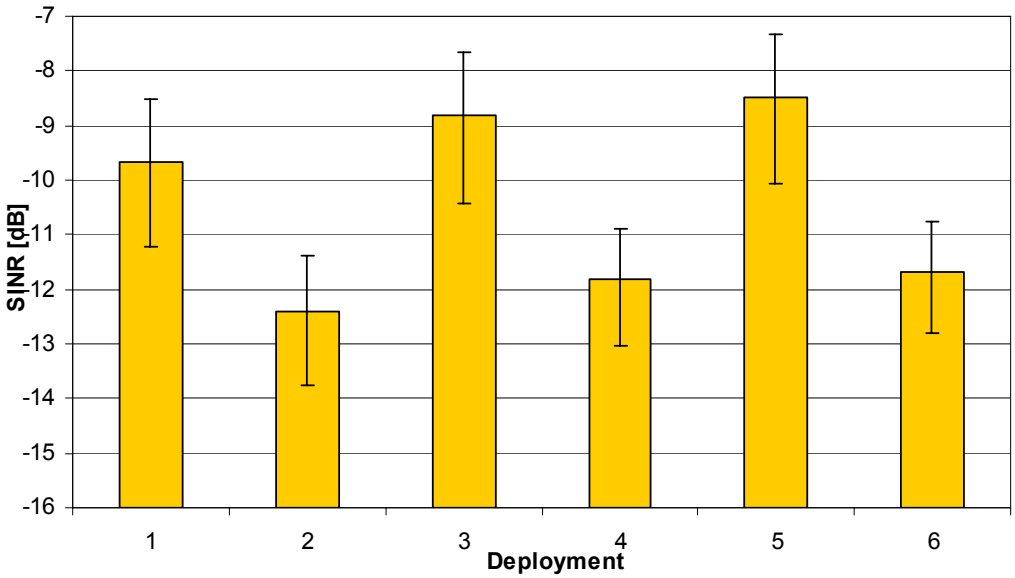

Figure 5.28 – The downlink in the highway scenario.

In Figure 5.29 one presents the average distances between the interfering terminals and the desired MT.

In deployment 2, users are very close to each other, the average distance in this case being 67 m, thus, the SINR for this deployment is the lowest. On the other hand, results from deployments 3 and 5 give the best SINR, because disturbing terminals are spread. In these cases, users are divided in two groups, and the spacing between these groups is 500 m. The desired users (MT1 in both cases) exist in the first group, where terminals are at the largest possible spacing between each other (30 m); users from the second group are located with a different spacing between each other, 15 m in one case and 30 m in the other. The conclusion is

that users that are positioned far away from the desired MT do not have great impact on the quality of the link.

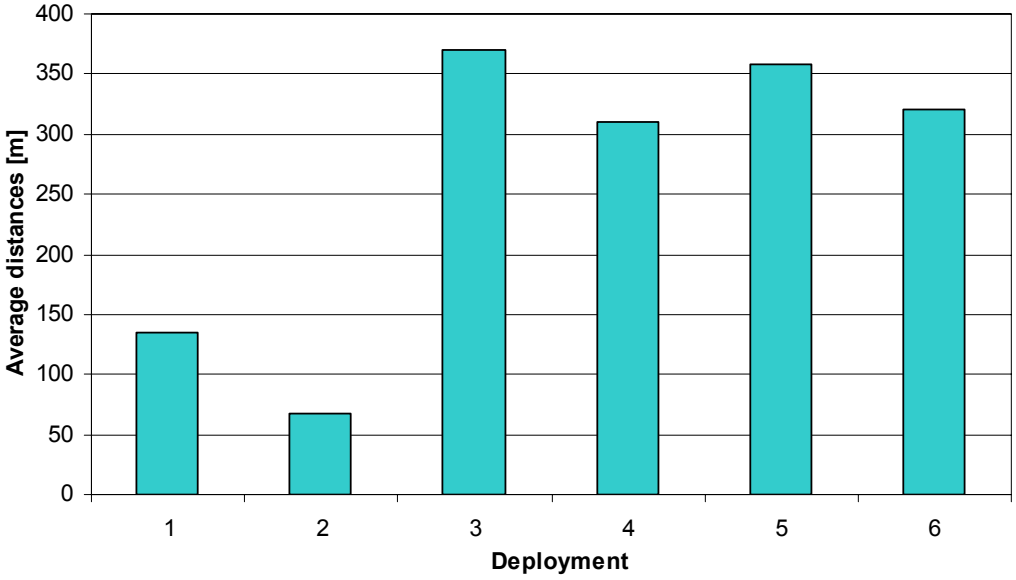

Figure 5.29 – Average distances in the highway scenario for the downlink.

The figures from Table 5.22 can summarise these conclusions. The best SINR is obtained when users positioned around the desired MT are spread. The second group does not play a very important role. For the cases when the spacing changes from 15 m to 30 m the impact on the SINR is low.

Table 5.22 – Comparison between SINRs from different groups in the highway scenario.

Spacing between the consecutive terminals [m]		SINR [dB]
Group I	Group II	
30	15	-8.49
30	30	-8.82
15	15	-11.82
15	30	-11.67

In the case of the railway station scenario, one can observe a strong relationship between the average distances between the other terminals and the desired MT, Figure 5.31, and the SINR, Figure 5.30. The highest SINR occurred in the case of the random deployment of terminals.

This result is obvious, because users are spread within the whole region, and most of the terminals are far away from the desired MT1, thus, the level of the interference is low.

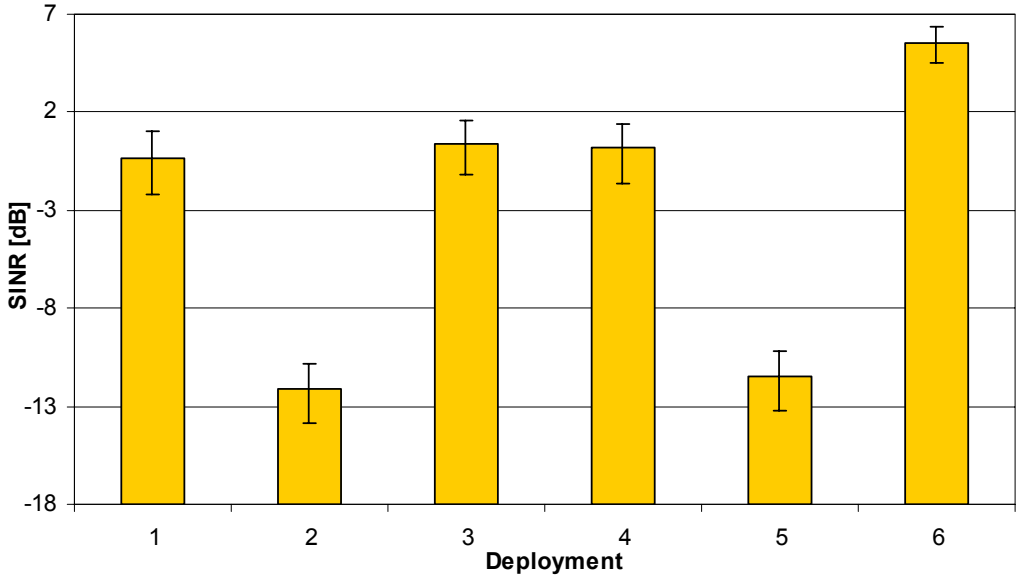

Figure 5.30 – The downlink in the railway station scenario.

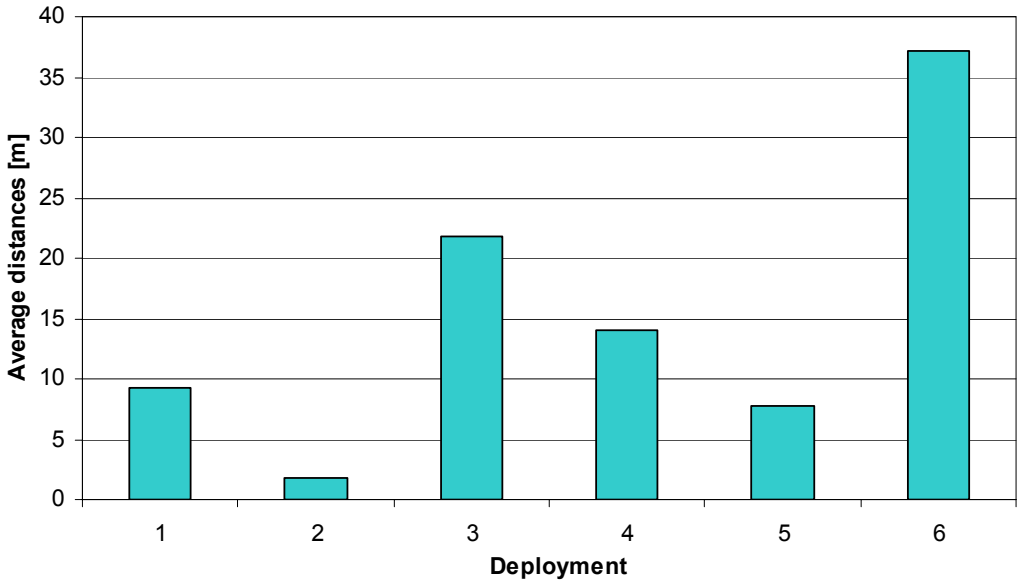

Figure 5.31 – Average distances in the railway station scenario for the downlink.

It is worthwhile to make a comparison between deployments 1 and 4, and 2 and 5, Table 5.23, where the number of desired user is the same. Deployments 4 and 5 are different from 1 and 2, because one user was moved to another place. The influence of changing the location is low for the mean value, and it is unnoticeable for the standard deviations. Analysing deployments 4 and 5, where the desired user is MT5, and interfering users are located in the group in the other side of the BS, one notices that in deployment 4 the spacing between disturbing terminals is twice

larger than in deployment 5; nevertheless the results are almost the same. When the disturbing users are located far away from the desired terminal, the situation is similar to uplink, where the distribution of terminals does not play an important role in the overall SINR.

Table 5.23 – SINR for different deployments and MTs in the railway station scenario.

SINR [dB]					
Desired MT1		Desired MT1		Desired MT5	
Deploym. 1	Deploym. 4	Deploym. 2	Deploym. 5	Deploym. 4	Deploym. 5
-0.31	0.16	-12.08	-11.43	3.53	3.53

5.2.4 Influence of the deployment of terminals for synchronised Txs

In the previous section, interference is taken into account when the Rx detected signals from the different Txs, when they are synchronised and arrive to the antenna at the Rx at the same time. Signals from different terminals are always detected at exactly the same time, no matter how far the Txs are located from the Rx. When the Rxs are not synchronised, they can be synchronised in a different way, i.e., every terminal transmits at the same time. The Rx will detect signals with different delays: the farther the terminal is located, the lower the level and the larger the delay the signal arrives to the Rx.

So far, SINR is calculated by taken into account the whole period of the CIRs, but here, some modifications are made. The CIR from the desired link is taken entirely, but CIRs that are considered as interferers are taken only in fragments. To calculate the power of interference, only the interference that overlies with the period of the desired link is taken. This concept is presented in Figure 5.32.

The SINRs obtained by using this way of calculation have higher levels, because only a part of the CIR of the disturbing link is considered in the interference power, hence, the sum of all interfering powers is lower. This can lead to different conclusions. In the previous section terminals located nearest to the BS have the best SINR, because their signal is the strongest. In this section, users that are the farthest away from the BS have the best SINR.

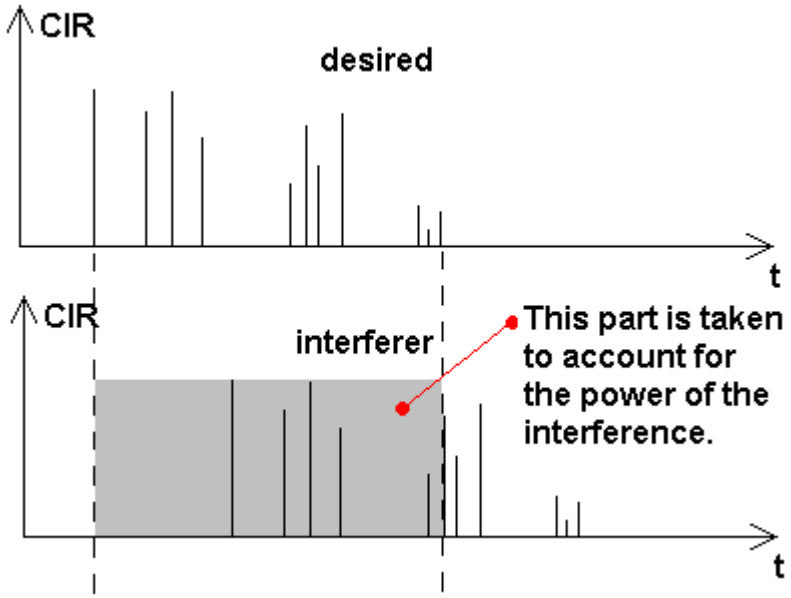

Figure 5.32 – Calculation of the SINR.

A comparison is made between the same deployments but with different types of synchronisation for the city street scenario. Figure 5.33 and Figure 5.35 show the results for deployments 7 and 10.

Figure 5.34 shows the average differences between the mean time delays of the MT-BS links for deployment 7, calculated as an arithmetic average of the difference between the mean delay of the considered MT-BS link and mean delay of other the users' links.

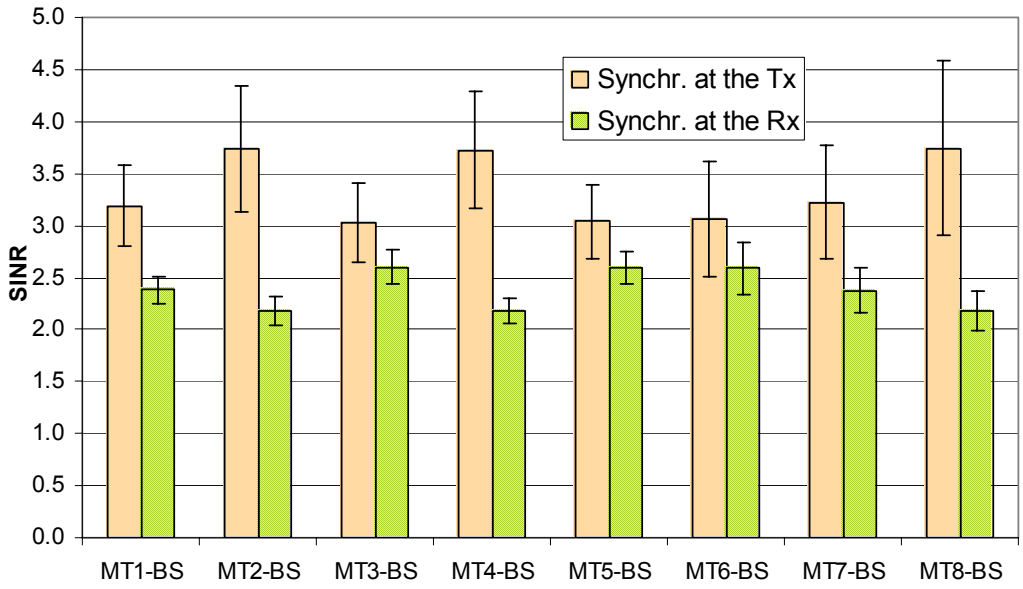

Figure 5.33 – Comparison between the two types of synchronisation for deployment 7 in the city street scenario.

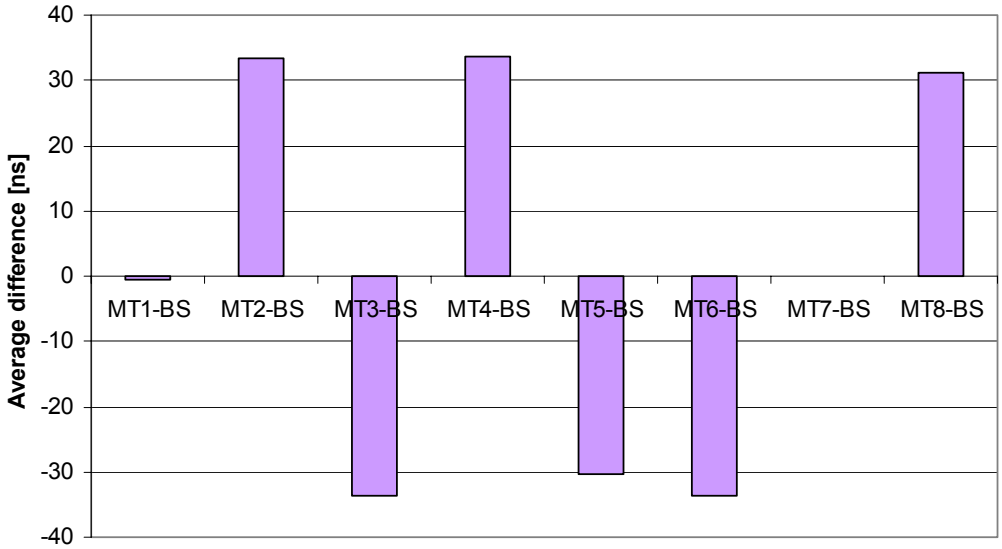

Figure 5.34 – Average differences for the mean time delays for deployment 7 in the city street scenario.

When this average difference has a positive value, it means that the CIR connected to the desired MT is delayed relative to the majority of the other users, therefore, the level of the power of interferences is low.

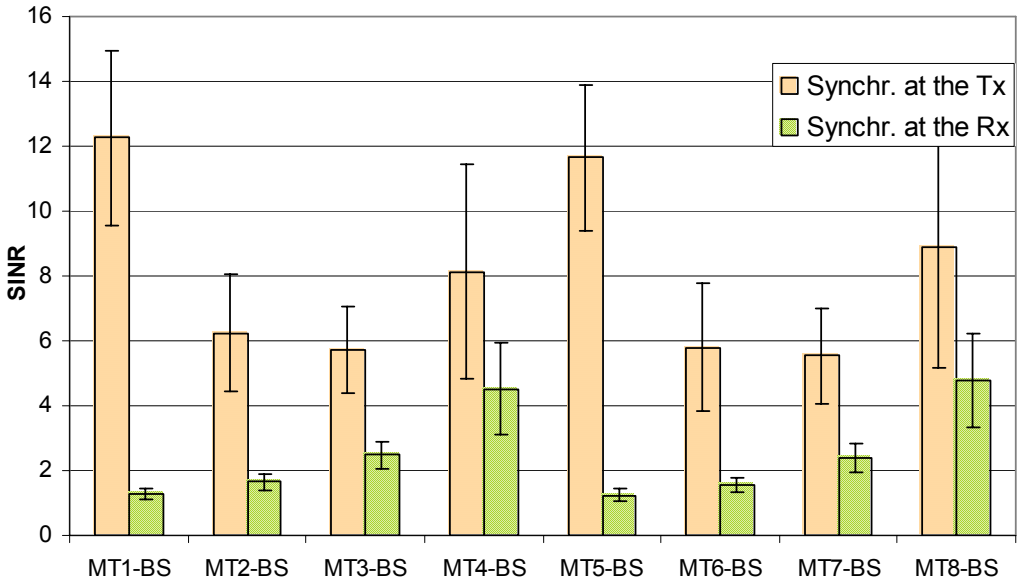

Figure 5.35 – Two types of synchronisation for the deployment 10 in the city street scenario.

In deployment 10, users 1 and 5 are at the largest distance from the BS, hence, signals from them arrive to the BS with the lowest level. The SINR should also be the lowest, signals are synchronised at the Rx, but for synchronised Txs, the signal from the farthest users cover the largest distance, being detected with the greatest delay. Figure G.5 to Figure G.12 show examples of CIR for the different delays. When the signal from user 1 or user 5 is arriving to the

BS, at the same time the signals from the nearer terminals are detected, but with a low power now, thus, the interference caused by them is not as high as before.

Figure 5.36 shows the comparison between the average SINRs for the two types of synchronisation. When Txs transmit the signal at the same time, the higher SINR is obtained for deployment 10, the same tendency being observed in the second type of the synchronisation, in a more visible way.

In the case of deployment 10, where users are spread within the whole area, the average SINR is the highest, because there is a disproportion between the distances from the terminals.

In Figure 5.36 to Figure 5.38, differences between average SINRs for the two types of synchronisation for the city street, highway and railway station scenarios are presented.

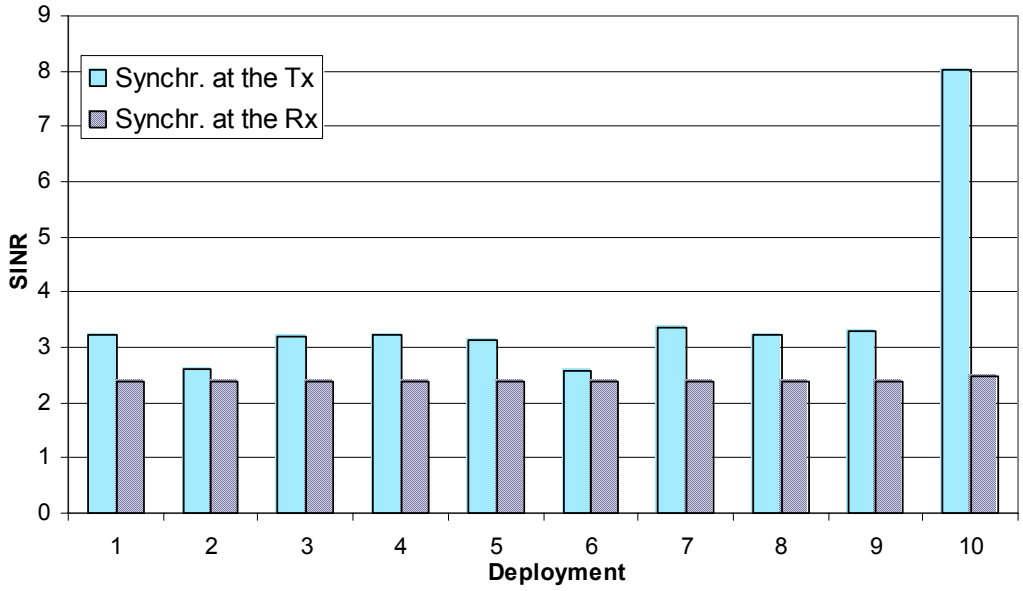

Figure 5.36 – Average SINR for the two types of synchronisation for the city street scenario.

One can notice that the tendency is the same. In the case of the highway scenario, the differences between the results from the two kinds of synchronisation are greater, because distances between terminals are larger. In most cases, the delay is long compared to the duration of the CIR, therefore, some interfering signals are taken into account only in small fragments during the calculating of the interference.

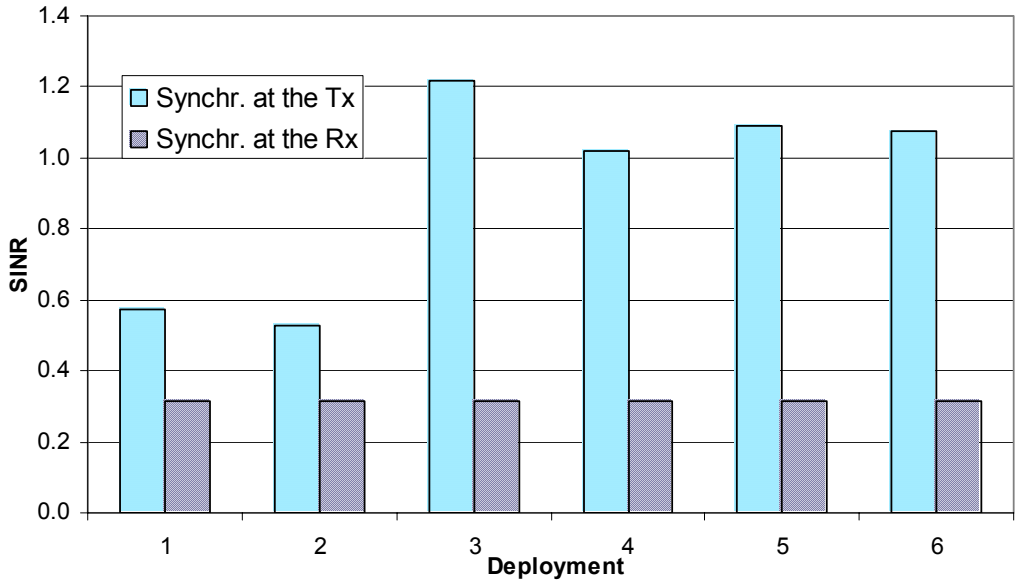

Figure 5.37 – Average SINR for the two types of synchronisation for the highway scenario.

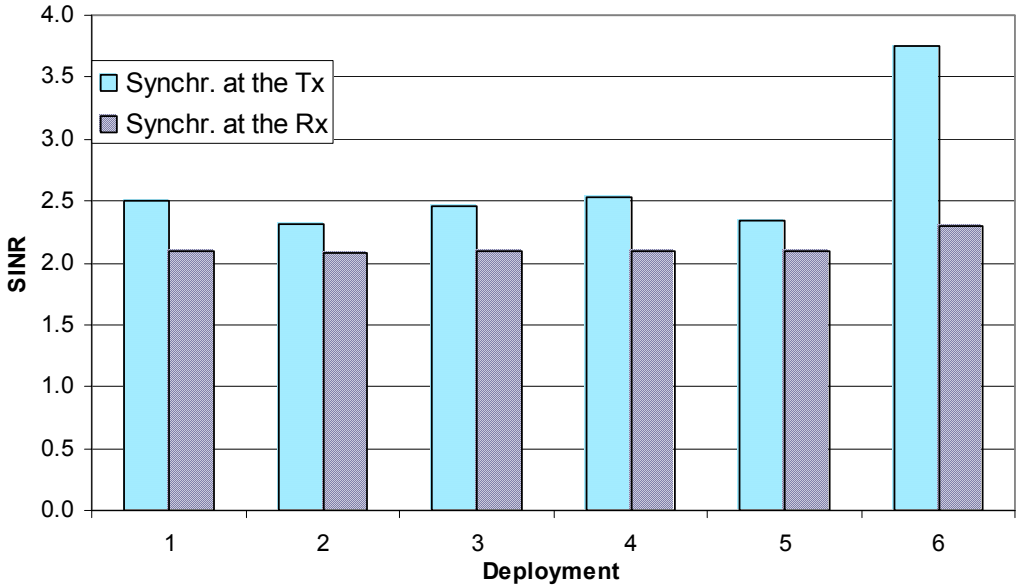

Figure 5.38 – Average SINR for the two types of synchronisation for the railway station scenario.

Figure 5.39 shows normalised average differences of propagation time between MTs and the BS.

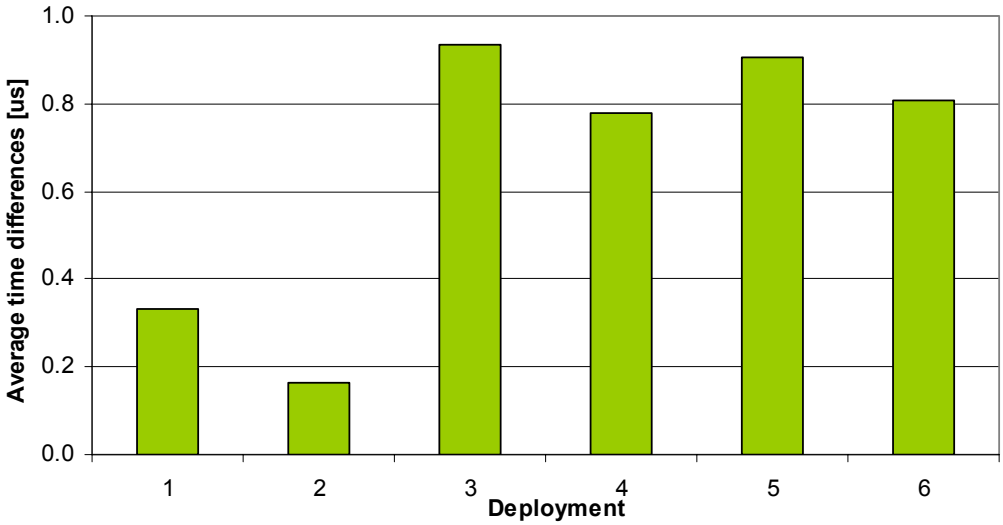

Figure 5.39 – Average differences between the propagation time of the MT-BS links in the highway scenario.

These propagation times were normalised relative to the LoS component of MT1. It is worthwhile to mention that the maximum duration of the CIR in the case of the highway scenario is determined by the double radius of the circle: 1.33 μs. In deployment 3, the average difference is 0.94 μs, 4 users (MT6, MT7, MT8 and MT9) having a difference in propagation time greater than 1.33 μs, thus, they are not taken into account to calculate interferences. The average SINR for this case is the largest.

The railway station scenario gives the same results as the city street one, Figure 5.40 and Figure 5.41.

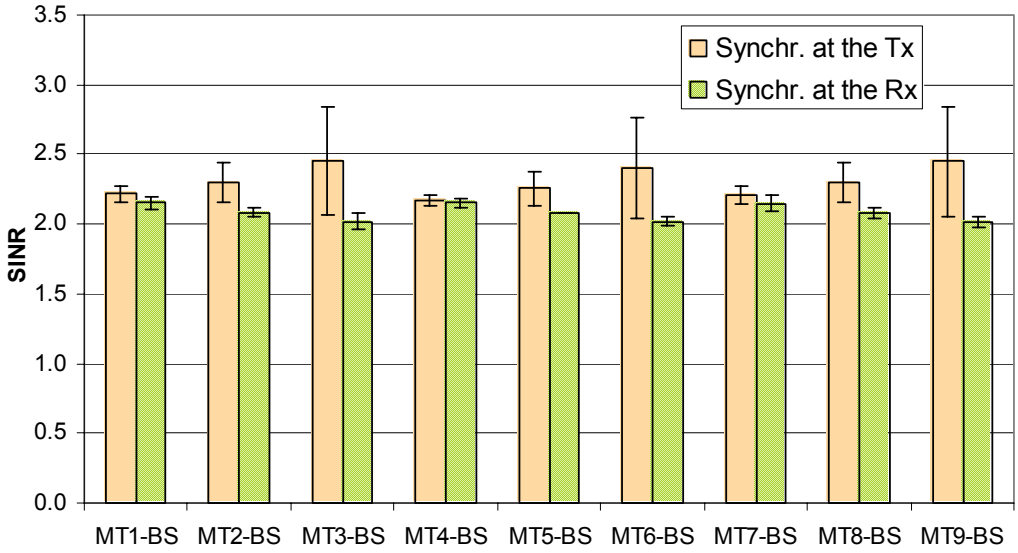

Figure 5.40 – Comparison between the two types of synchronisation for deployment 2 in the railway station scenario.

In the approach of synchronisation at the Tx, also downlink can be taken into account, but not in every link. For the case of the city street and highway scenarios, the time delay between the desired BS-MT links is larger or similar to the duration of the interfering signal. In these cases, the delay can be evaluated by the propagation time of the LoS component between the BS and the desired MT. For the city street scenario, this delay is about 0.70 μs, and the maximum propagation time of the disturbing signal is 0.80 μs. There is short time period during which interference can appear, but this period is connected with the low energy fragment of interfering CIRs and does not play an important role in interference. For the highway scenario, the situation is clearer; the LoS component of the BS-MT1 link has a delay about 10 μs. When the farthest MT from all deployments is taken into account, the distance between it and the MT1 is 740 m, and the maximum time duration of the CIR is 2.81 μs, interference does not exist. Table 5.24 shows a summary of the results, and Figure 5.42 presents results for the down- and uplinks for the same type of synchronisation in the railway station scenario. In both cases, MT1 is the desired user.

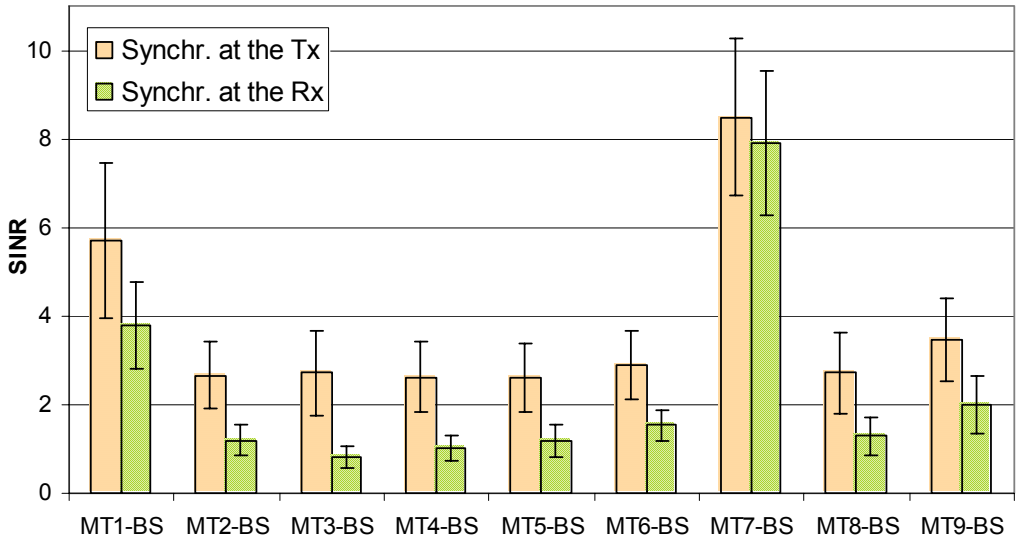

Figure 5.41 – Comparison between the two types of synchronisation for deployment 6 in the railway station scenario.

In all deployments, terminals are grouped into regular clusters. In the uplink, when users are grouped, the differences in propagation time between the MT-BS links are not very different, and a large part of the disturbing CIR is taken into account. However, in the downlink, the situation is different. There only one desired link between the BS and the MT, hence, there is a disproportion between the delay of the desired link, and the period of the interfering signals from MTs close to the desired one. In this case, only fragments of the disturbing link are taken into consideration, therefore, interference is lower and SINR is higher. In the interesting of

deployment 6, where users are spread uniformly, there is no difference between the up- and downlinks.

Table 5.24 – Comparison of statistical time parameters for CIRs.

	Highway scenario, 3, MT1-BS		Highway scenario, 3, MT1-MT9	
	μ [μs]	σ [ns]	μ [ns]	σ [ns]
$\bar{\tau}$	10.46	149.60	249.71	37.72
σ_τ	0.31	93.75	98.22	20.66

	City street scenario, 1, MT1-BS		City street scenario, 1, MT1-MT4	
	μ [ns]	σ [ns]	μ [ns]	σ [ns]
$\bar{\tau}$	796.88	17.27	197.74	42.52
σ_τ	48.27	9.28	137.20	35.31

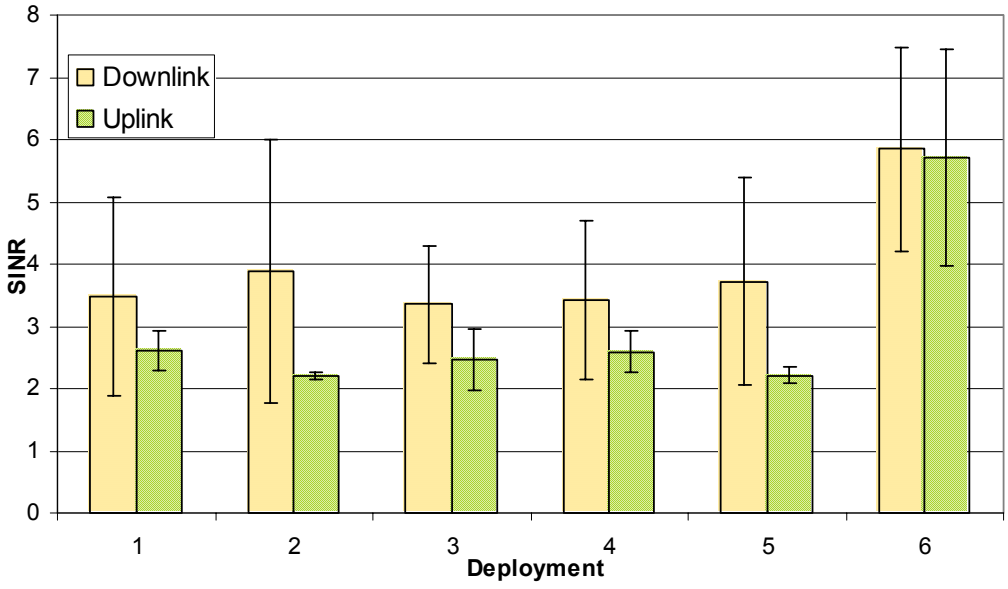

Figure 5.42 – Comparison between the SINR in up- and downlinks for MT1 as a desired user in the railway station scenario.

5.2.5 Example of interference in GSM and DECT

The SINR for GSM was calculated in the same way as for UMTS, but instead of using the orthogonality factor, the isolation between channels was used. Channels in GSM are separated by 200 kHz, and a mask is defined for the transmitters, Figure H.1. GSM was simulated in the uplink scenarios of UMTS. Given a desired MT, the other terminals transmit in different channels is assumed. Simulations were made for transmitter separated by 200, 400 and 800 kHz, which corresponds to an isolation of 30, 60 and 70 dB, respectively. As in UMTS, noise was $N_0=10^{-12}$ W (-120 dB).

Figure 5.43 to Figure 5.45 present SINRs for the city street, highway and railway station scenarios. Table 5.25 shows powers.

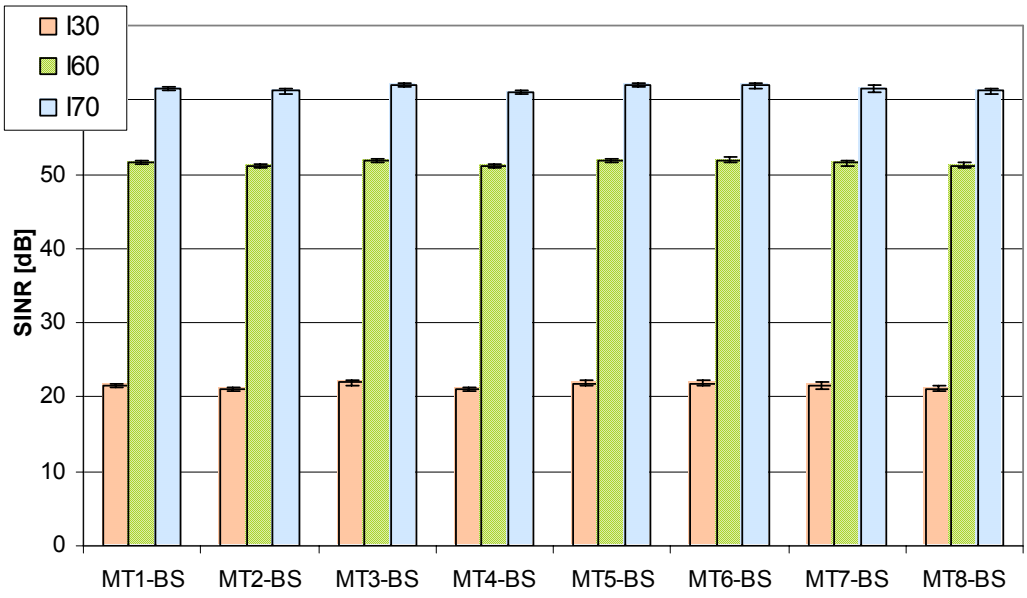

Figure 5.43 – SINRs for three types of transmitters' isolation in the city street scenario, deployment 7.

Table 5.25 – Comparison of the obtained powers in different scenarios.

	Mean $P_{MT1\text{-}BS}$ [dB]	Std. dev. $P_{MT1\text{-}BS}$ [dB]	Mean $P_{MTx\text{-}BS}$ [dB]
City street scenario, 7	-23.1	-66.5	-23.1
Highway scenario, 2	-48.9	-116.5	-48.9
Railway station scenario, 6	-9.5	-25.6	-11.8

One can see that for isolations of 60 and 70 dB the level of the interferences is very low, thus, the ratios are closer to the signal to noise ratio rather than to the signal to the interference one.

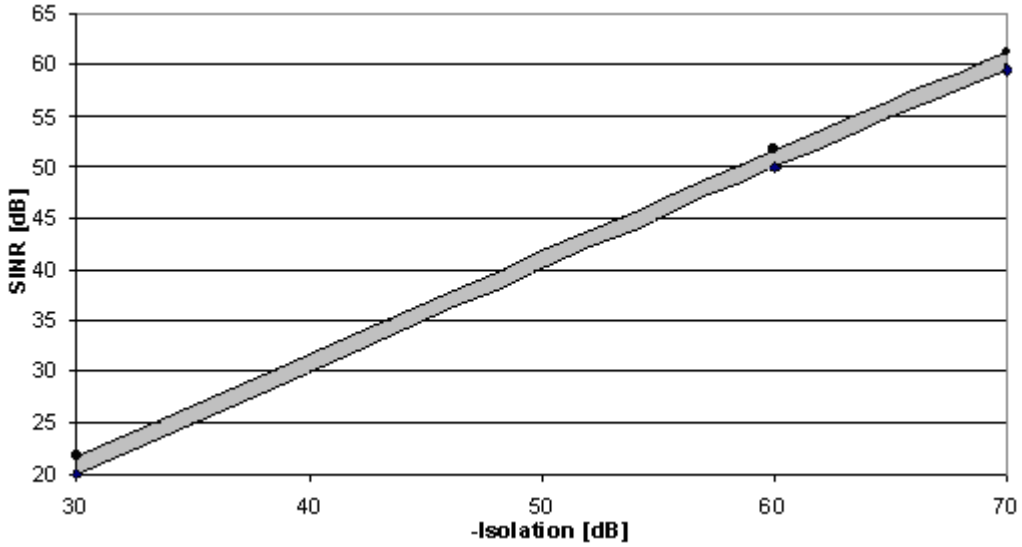

Figure 5.44 – SINRs for three types of transmitters' isolation in the highway scenario, deployment 3.

Some simulations were also made for DECT, which has 10 radio channels from 1881.792 MHz to 1897.344 MHz with a spacing of 1.728 MHz [Koła00]. DECT was simulated at 1881.792 MHz, frequency being only one parameter different from UMTS, therefore, the obtained results are not different.

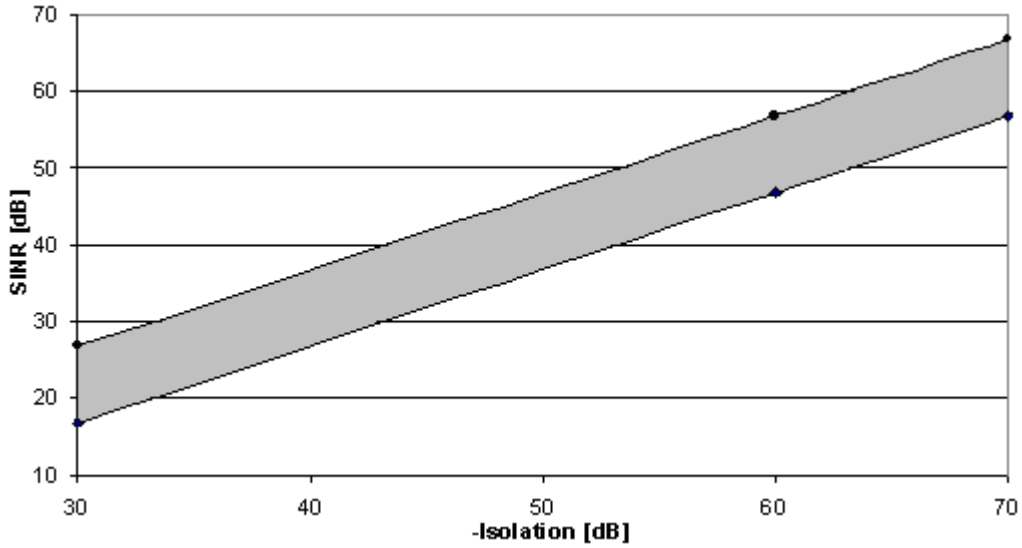

Figure 5.45 – SINRs for three types of transmitters' isolation in the railway station scenario, deployment 6.

5.3 General conclusions

The simulations have been made using three different types of the environments. A different shape describes every scenario, as well as different distances between the terminals are used. It is worthwhile to draw the general conclusions from the influence of propagation environments on the obtained results.

The railway station scenario represents the pico-cell. This environment groups all MTs and BS inside one circular region. This approach is convenient, because gives an opportunity to simulate relations between different terminals without making any modification of the scenario. Both the up- and downlinks can be calculated in exactly the same scenarios.

The pico-cell describes the propagation environment, which has small dimensions. As it was showed in the previous sections, in the SINR considerations the distance between the MTs and the BS plays very important role. The mean delays, as well as the powers of the particular links have comparable values. The results for synchronised Rxs and Txs are similar. One feature of this propagation environment should be highlighted. In the pico-cell, all combinations of the interference are possible. The interference takes place both in the down- and uplinks for synchronised Rxs and Txs. Only for this scenario this situation is possible.

The conclusions about micro-cell can be drawn basing on deployments in the city street scenario. In this approach, in the uplink, every link between the Tx and Rx is described by a separate ellipse. However, some problems occur when a downlink is taken into consideration. To describe link between the terminals located in the close distance from each other, an ellipse cannot be used anymore, rather than circle centred at the Rx position.

Despite this environment is described by the ellipse, the similar conclusions can be drawn as for the pico-cell, for the uplink approach. In deployments used for the simulations, the distances between terminals are few times longer than in the pico-cell. However, in the deployments, the terminals are positioned in similar distances from the BS, thus, the mean delays and powers of the particular links are the almost the same. Therefore, SINRs, obtained for the both types of the synchronisations are comparable. However, when the downlink is taken into consideration, the scenario becomes different. It occurs a disproportion in lengths of links related with the terminals and between the desired MT and BS. It causes that interference for synchronised Txs does not exist.

The highway scenario represents the macro-cell case, where distances between the MTs and BS are significantly larger than in the previous cases. In addition, the particular terminals are located more separated from each other. As the micro-cell, some problems occur when a downlink is taken into considerations. Instead of using the circles for particular links between the MTs, the ellipses are used.

The distances between the particular terminals comparing to the distance from the BS, are very small, thus, for the uplink the BS detects signals from different MTs with the similar powers. The statistical parameters of the links are also comparable. The obtained SINRs are lower. However, due to the fact, that all scatterers are located in nearby of the MT in an area that has radius small comparing to the distance to the BS, the CIR has short duration. The differences in the propagation times of the particular links are important, when the synchronised Txs case is taken into account the obtained SINRs are significantly higher. The same as for the micro-cell case, the interference for the downlink for synchronised Txs does not exist.

6 CONCLUSIONS

In Chapter 6, the final conclusions of the work are presented.

This work aimed at develops a radio channel model based on geometrical principles, to be used to simulate multiuser interference in a different deployment of the terminals in three different scenarios, i.e., micro-, macro- and pico-cells. First, an adequate radio channel model was chosen, after which it was implemented in a simulator.

Besides a review of the directional channel modelling state of the art, Chapter 2 includes the choice of the radio channel model, which considers single reflections from scatterers. The enhanced version of the model, proposed by the GROW, IST, where clusters of scatterers are used, describes very well the mechanisms of signal propagation. This model does not consider rough surface scattering, diffraction and multiple bounce of the multipath components. It is assumed that all scatterers, as well as the antennas of the Tx and the Rx, are located on the same plane. The consideration of a 3D space would cause an unnecessary increase of the processing time without an improvement on the results.

During the analysis of the simulations, one drawback of the model was noticed. When the number of the scatterers increases, so does the number of multipath components. The Rx detects more copies of the signal, which are delayed and shifted in different ways, hence more power is arriving to the Rx, and the situation where the power of the detected signal is greater than the power of the Tx is possible. The situation takes occurs, because CIRs are taken entirely in the calculation of power. This problem is resolved by considering CIRs after filtered with a certain time resolution, taking into account only a few first samples. As the parameter of interest is the ratio of powers, the absolute values of powers are not very important, and this drawback does not exist.

Chapter 3 contains the description of the multiuser interference theory considering the interference within the same cell and the interference between different cells. Using a linear combination of these two, it is possible to describe any interfering situation.

This work considers multiuser interference in the “low level” approach, which means that the estimations of the quality of the links is based on CIRs.

The chosen radio channel model was developed in C++. The implemented model is statistical in its nature. The separate aspects of the implementation were defined by different classes, in a flexible approach for possible future extensions.

The simulators developed by IST, consider only SU cases, where only single region is taken into account. The MU simulator considers more than one region, where every one describes the particular link between the Tx and Rx. Any number of the users can be placed in a propagation environment, and the mutual relations between the terminals can be analysed. The algorithm for the generation of regions is based on graph theory, because generation of clusters in the regions, which have common areas, needs to be processed in an order way.

The simulator considers the circular and elliptical regions, which can serve to describe the micro-, macro- and pico-cells. For the pico-cell, the position of the Rx is not fixed and can be located in any place within the circle. This approach gives an ability to simulate the real pico-cell scenarios e.g., room, where the BS can be positioned in an arbitrary place. Due to the small dimensions of the pico-cells, the accurate mapping of the terminal positions is needed. For the micro- and macro-cells, the positions of the terminals are fixed, and for case of the former are located in the foci of an ellipse, and for the latter, an MT is located in the centre of the circle and an BS in any place outside.

The work of the simulator is controlled by a config file. Parameters describing a propagation environment, i.e., the parameters of clusters and scatterers, as well as the parameters related with terminals, i.e., positions, antennas, etc., are defined by simple values, which gives an opportunity to make an investigation of the influence of these parameters on overall behaviour of the simulator and output results.

The great advantage of the simulator is a possibility of running of simulations with a determined propagation environment. The config file for this case contains fixed values of positions and reflection coefficients of particular scatterers. These data can be obtained from measurement campaigns. Results of the simulations generated in this way, can be helpful for the consecutives measurements, as well as for the investigations of the propagation conditions.

The simulator also gives an ability to make simulations of MIMO systems, both for MU, as well as for SU cases. Every terminal in the environment contains more than one antenna in MIMO array. These antennas can be placed both in linear or circular arrays. Aspects connected with MIMO for SU cases can be found in [Koko05].

The results obtained from the simulator need to be averaged over many of iterations. For each iteration, the simulator has to build a new scenario, which is changed with a reference to the

previous one. The simulator can be run in four modes, which define the way of changes of the environment.

A comparison has been made between the results from the different modes of the simulator, different number of iterations, different values of the times resolutions and different ways of calculating the SINRs. The main factor, which decides about the quality of the results, is the standard deviation. The highest value of the standard deviations was obtained for mode 3 but it decreases with the number of the iterations, therefore, it was chosen for simulations. The mean values and the standard deviations were calculated using the 100 iterations, which corresponds to the point, where curve become saturated.

Time resolution plays a very important role in the quality of the results. In fact, in real systems, Rxs do not detect the entirely multipath component. A comparison between the average results obtained for different time resolutions shows that the quality of the mean values decreases rapidly with the increase of the time resolution. This is the reason why CIRs were considered in unfiltered form.

Simulations were made for different types of deployments in the city street (micro-cell), highway (macro-cell) and railway station (pico-cell) scenarios. A different shape describes every scenario, as well as different distances between the terminals are used. It is worthwhile to draw the general conclusions from the influence of propagation environments on the obtained results. In all of these types of cells, the same conclusions about the nature of interference are obtained. However, it is very difficult to make a direct comparison between the results from the different types of the cells, given the different distances between terminals, and between the terminals and the BS. Additionally, a different level of powers at the Txs was used, SINRs are strongly related with the considered deployment, and general conclusions about the tendencies in the city street (micro-cell), highway (macro-cell) and railway station (pico-cell) scenarios cannot be drawn.

The railway station scenario groups all MTs and BS in one circular region. This approach is convenient, because gives an opportunity to simulate relations between different terminals, without making any modification of the scenario. Both the up- and downlinks can be simulated in exactly the same deployments.

In city street scenario for the uplink, every link between the Tx and Rx is described by a separate ellipse. However, some problems occur when a downlink is taken into consideration. To describe link between the terminals located in the close distance from each other, an ellipse can not be used anymore rather than circle centred at the Rx position.

The highway scenario is described by the circles centred at the MTs, however the distances between the MTs and BS are significantly larger than in the previous cases. Also, the particular terminals are more separated from each other. As the micro-cell, some problems occur when the downlink is taken into considerations. Instead of using the circles for particular links between the MTs, the ellipses are used.

Two methods of synchronisation are presented. In the first one, the Rx detects signals from all Txs at the same time (it is called Rx-synchronisation), and the second one considers the situation where all Txs transmit a signal at the same time, thus, signals are detected at the Rx with different delays (it is called Tx-synchronisation).

The results from all kinds of cells gave the same general conclusion. The level of the interference is greater in the Rx-synchronisation case, and since for Tx-synchronisation, CIRs of interfering signals are not taken entirely but only in the fragments, interference is lower.

Multiuser interference is also investigated for different ways of signal transmission. In the downlink, the desired MT can be disturbed by other MTs located in the surroundings. However, for UMTS, this kind of interference can only take place in the inter-cell interference scenarios.

The SINR in the uplink in the Rx-synchronisation is strongly correlated to distance. The higher level of SINR is obtained when the MT is located closer to the BS, the relation between distance and SINR being rather exponential. In the deployment where terminals are located at different distances from the BS, the average from all SINRs is greater than for the case when users are grouped. It should be mentioned that the same SINR is obtained for the cases when MTs are grouped when they are spread in the region, but the distance between each of them and the BS is the same. This is observed for all scenarios, which explains the need of using power control.

In the uplink for Tx-synchronisation, the results differ from the previous case. The distances between terminals and the BS also play a very important role, but the relation is different. In general, the best SINR is obtained for terminals located the farthest away from the BS.

The city street (micro-cell) and the railway station scenarios (pico-cell) have the same properties of behaviour of SINR. These types of scenarios are similar concerning propagation. Since the same level of Tx powers is used both in the MTs and in the BS, and distances between the MTs and the BS are comparable, the levels SINRs as well as their range of change are similar. In the pico-cell the mean delays, as well as the powers of the particular links have comparable values. The results, for synchronised Rxs and Txs are similar. In the micro-cell scenario, the distances between terminals are few times longer than in the pico-cell. However, in the deployments which are used, the terminals are positioned in similar distances from the BS, thus, the mean delays and powers of the particular links are the almost the same. Therefore, SINRs, obtained for the different types of the synchronisations are comparable.

In the highway scenario (macro-cell) the distance between the MT and the BS is greater than the distance between terminals, thus the paths between the BS and the MTs have lengths that are not so different, leading to lower levels of changes of SINR. The obtained SINRs are lower. The statistical parameters of the links are also comparable. However, due to the fact, that all scatterers are located in nearby of the MT, in area that has radius small in compare to the distance to the BS, the CIR has short duration. The differences in the propagation times of the particular links are important, when the synchronised Txs case is taken into account, where the obtained SINRs are significantly higher.

In the downlink, the link between the MT and the BS is obstructed by the other MTs, which are Txs, since they communicate with different BSs. The value of the SINR is related to the number of interfering terminals, but the relation is not linear. The addition of a user when the environment has a large number of terminals does not cause a significant decrease on the quality of the link. On the opposite situation the quality of the link decreases significantly. The lower values of the SINRs are obtained for deployments, where the disturbing terminals are grouped around the desired MT. The terminals positioned in the farther distances have not a great impact on the quality of the link.

Also for the downlink, the highway scenario (macro-cell) behaves differently from the street scenario (micro-cell) and the railway station (pico-cell). In the highway case, the influence of

the disturbing terminals is greater because the distances between terminals are small compared to the distance to the BS. SINRs have lower levels.

For Tx-synchronisation, in downlink the railway station scenario shows a very interesting property. For a random distribution of terminals, the way of the transmission does not have any influence on the SINR. Users are in the random positions, thus, path lengths are random.

Some investigations were made for DECT and GSM system. In GSM system, the power of interfering users is multiplied by the isolation of the transmitter, as a result, the power of interference has a very low level, and in fact the SINR ratio shows a signal rather than noise ratio. The only parameter that distinguishes DECT from UMTS in the simulator is the frequency; since the difference between the frequency carriers of these two systems is low, the results are more or less the same.

Many aspects of this work can be improved or enhanced. In this dissertation, only one BS is simulated in the system, which limits analyses like inter-cell interference (inter-cell interference was considered for the downlink). So, it is obvious that the future work should contain more advanced deployments with more than one BS. Also the multiuser considerations should be taken beyond of the CIR, i.e., modulation and multi access techniques should be taken into account. Another idea is that the influence of antennas (including the MIMO system) should be considered in the MU scenarios. Another step could be also the analysis of mitigations for interference from the different terminals, where an adaptive algorithm in the antenna steering control would be used.

Annex A Assessments of the channel simulator

In order to the simulator, the example presented in Figure A.1 was simulated. In this case, the environment has only one scatterer, the BS and the MT. In this example UL is considered, thus, the MT works as the Tx and the BS as the Rx.

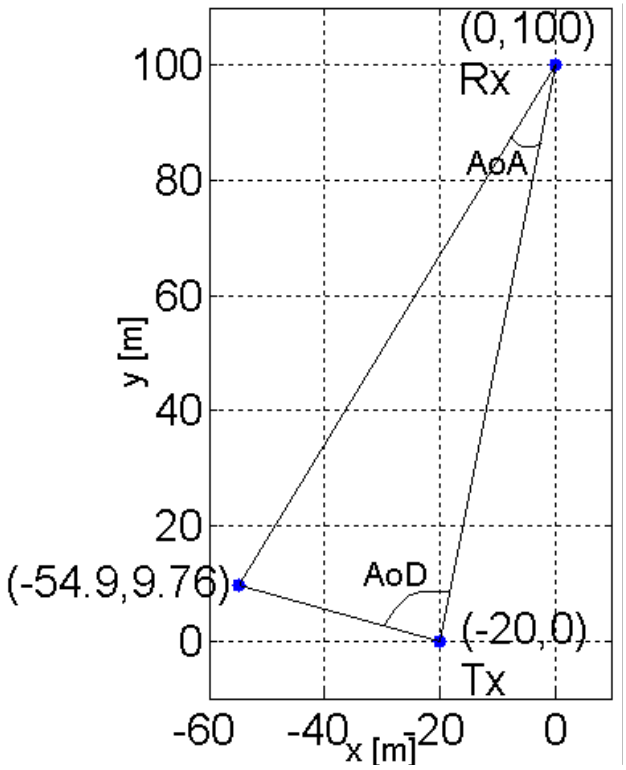

Figure A.1 – Example of calculations

The positions of the objects are depicted in Figure A.1. Other parameters of this example are:

- $|\Gamma| \cdot e^{j\Phi_{sc}} = 0.154 \cdot e^{j51.06}$: reflection coefficient of the scatterer
- $f = 1.87$ GHz: frequency

In Table A.1 two files are listed, which describe the positions and functions of the terminals, as well as the parameters of the scatterer.

The program returns the results that are listed in Table A.2. These parameters are obtained using the equations presented in Chapter 2. The AoA and AoD for the LoS component are obtained relative to the *x*-axis on the *x*-*y* plane. The entirely NLoS parameters are presented in a non normalised form.

Table A.1 – Files describing the environment of the test scenario.

File with the terminals:	p,1,1.87e+009 t,0,1 o,-20,0,0,10,MT1,0 a,0,1,180 m,1 n,a1,0,0 e o,0,100,0,0,BS1,1 a,0,1,180 m,1 n,a1,0,0 e
File with the scatterers:	c0,-54.9,9.76,1,0,1 s0,-54.9,9.76,0.154,51.06

After making the calculations, it was confirmed that the program works correctly.

Table A.2 – Output parameters.

	LoS	**NLoS**
Amplitude [mV/m]	169.84	18.80
Phase [deg]	42.42	278.88
Delay [ns]	340.17	133.04
AoA [deg]	258.69	20.01
AoD [deg]	78.69	85.68

The other tests involved the correct generation of the deployment of clusters within the region, and scatterers within clusters. The clusters within the region should be distributed uniformly, to check this aspect, a circular region with a radius of 100 m was generated and inside of it, 94 clusters were deployed. A mean value of coordinates of all clusters was calculated: $(\bar{x}, \bar{y})$ = (1.91534 m, 1.50414 m). Every coordinate can change in the range [-100, 100], thus, an ideal mean coordinates should be (0 m, 0 m). The results have an error (1.92 %, 1.5%) are acceptable to confirm that clusters are distributed uniformly.

Similar tests were made for the distribution of scatterers. A cluster with a radius of 5 m was generated. Within these clusters, 500 scatterers were generated using the Gaussian distribution, with the centre of the cluster being (0 m, 0 m) also for this case the mean value of the coordinates was calculated ($-12.222 \cdot 10^{-3}$ m, $-3.332 \cdot 10^{-3}$ m), which are acceptable.

Also other tests were made. The cluster was divided into symmetric parts, upper and lower sides, and right and left sides. Within all these quarters, the scatterers were counted, and the results are presented in Table A.3. The deployment of scatterers is not ideal symmetric and one can see some disproportion between the upper and lower sides, the amount of scatterers being different (4.8%). But one should not forget that the distribution of scatterers is generated by using a statistical distribution, and this level of disproportion for such a low number of samples is typical. The function generating the deployment of scatterers is affirmed to be correct.

Table A.3 – The scatterers within the cluster.

Side	No. of scatterers	Error [%]
Up	238	4.8
Down	262	
Right	256	2.4
Left	244	

Finally, the function generating the Channel Impulse Response was checked. This function divides time into bins, and sums coherently all components that are inside the bin. The delay of the ray after sum is determined as the middle of the bin. Some multipath components were generated, Table A.4.

Time was divided into 1 ns bins. The operation of summing can be considered on the complex plane. The results, which were confirmed by external calculations, are presented in Table A.5.

Some other tests connected with the CIR where done as well. Every scenario has a maximum time delay, due to the fact that locations of clusters are bounded by the region. For every scenario, one can use an equation that calculates the maximum time delay relative to the LoS component. For the pico- and the macro-cell scenarios (A.1) can be used, while for the micro-cell scenario (A.2) is used.

Table A.4 – Multipath components – example of calculations.

No.	Amplitude [V/m]	Phase [deg]	Delay [ns]
1	1	0	5.1
2	1	90	5.9
3	1	90	6.1
4	1	180	6.9
5	1	180	7.1
6	1	270	7.9
7	1	270	8.1
8	1	0	8.9

Table A.5 – The rays of the CIR.

No.	Amplitude [V/m]	Phase [deg]	Delay [ns]
1	1.41	45	5.5
2	1.41	135	6.5
3	1.41	225	7.5
4	1.41	315	8.5

$$\tau_{\max} = \frac{2R}{c} \tag{A.1}$$

$$\tau_{\max} = \frac{2\sqrt{b_{ell}{}^2 + f_{ell}{}^2} - 2f_{ell}}{c} \tag{A.2}$$

where:

- $f_{el[\mathrm{m}]}$: focal length of the ellipse
- $b_{ell[\mathrm{m}]}$: minor axis of the ellipse
- $R_{[\mathrm{m}]}$: radius of the circle

These three types of regions were generated, and every region was defined in the same way:

- Cluster density: 10^{-3} per 1 m^2
- Dimension:

  - 50 m – radius of the circle in the pico-cell scenario
  - 100 m – minor axis of the ellipse in the micro-cell scenario
  - 200 m – radius of the circle in the macro-cell scenario
- Cluster radius: 1 m – this is the standard deviation for the Gaussian distribution
- Average Number of the scatterers: 20 per cluster
- Positions of the BS and the MT:
  - (0, 0) and (10,10): pico-cell scenario
  - (0, 0) and (200,0): micro-cell scenario
  - (0, 1000) and (0,0): macro-cell scenario

The values of the maximum time delay (normalised to the delay of the LoS component) that are obtained from the simulation and that are calculated using (A.1) and (A.2), are presented in Table A.6.

Table A.6 – Maximum time delay [ns].

Cell	Values calculated	Values simulated
Pico-cell	333.3	341.5
Micro-cell	276.1	277.4
Macro-cell	1333.3	1297.1

One can see that the values obtained from simulations are larger than the calculated ones. This is caused by the assumption that only the centres of the clusters have to be inside of the region. When the cluster is located near the boundary of the region, it is very possible that some scatterers are placed outside, and these outside scatterers are the source of the increase of the maximum time delay.

One can then say that the simulator passed all the tests hence, it is considered to work properly.

Annex B Random numbers generators

Further tests were made to ensure that the simulator is working in the correct way. These tests involved checking the randomise functions. Histograms were prepared using 1 000 000 samples, which generated pseudo-random values in Gaussian, Poisson and Uniform distributions. Every histogram is similar to theoretical ones.

Figure B.1 concerns the Gaussian distribution.

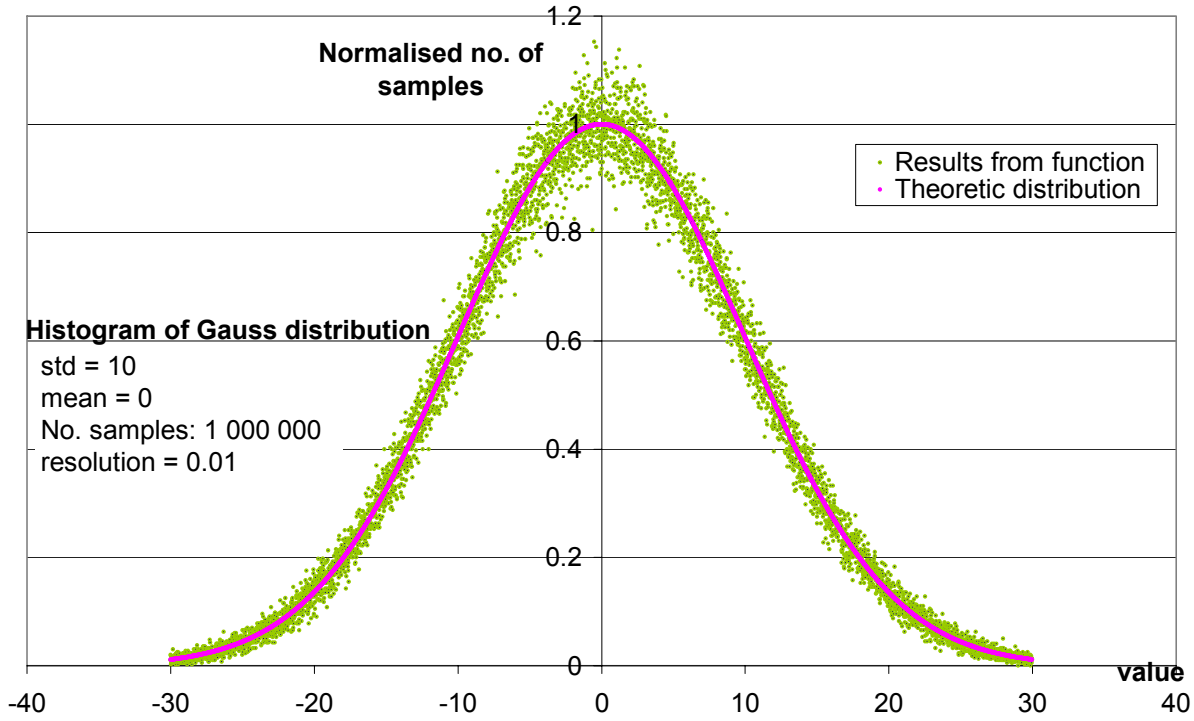

Figure B.1 – The histogram of Gaussian distribution.

The Gaussian distribution is described [Math05] by:

$$f(x) = \frac{\exp\left(-\frac{(x-\mu_G)^2}{2\sigma_G^2}\right)}{\sigma_G\sqrt{2\pi}} \tag{B.1}$$

where:

- μ_G: mean value
- σ_G: standard deviation

The histogram was obtained with the following parameters:

$\mu_G = 0$

$\sigma_G = 10$

Both the shape of the histogram and the shape of the theoretical curve are the same, so one can consider that the function works correctly.

Random numbers with a Poisson distribution are generated using a separate function, Figure B.2. The histogram is normalised to the number of times λ_P (parameter of Poisson distribution) occurs. The theoretical Poisson distribution, which is described [Math05] by:

$$f(x) = \exp(-\lambda_P)\left(\frac{\lambda_P^x}{x!}\right) \tag{B.2}$$

where:

- λ_P: parameter of Poisson distribution, in this example $\lambda_P = 10$

The results, which are obtained from this function and from the theoretical equation are the same.

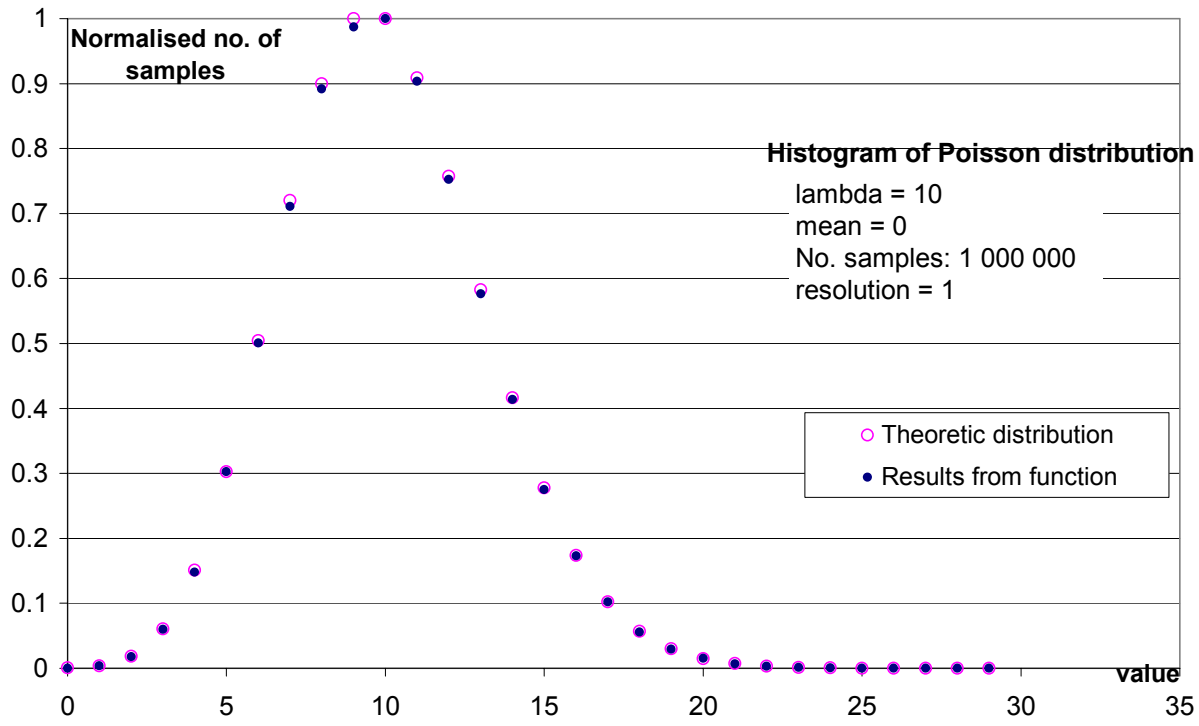

Figure B.2 – The histogram of Poisson distribution.

Figure B.3 contains the histogram associated to the uniform distribution, normalized to the average number of times all values occur. The shape of this histogram is uniform for all values, which shows that the function works correctly.

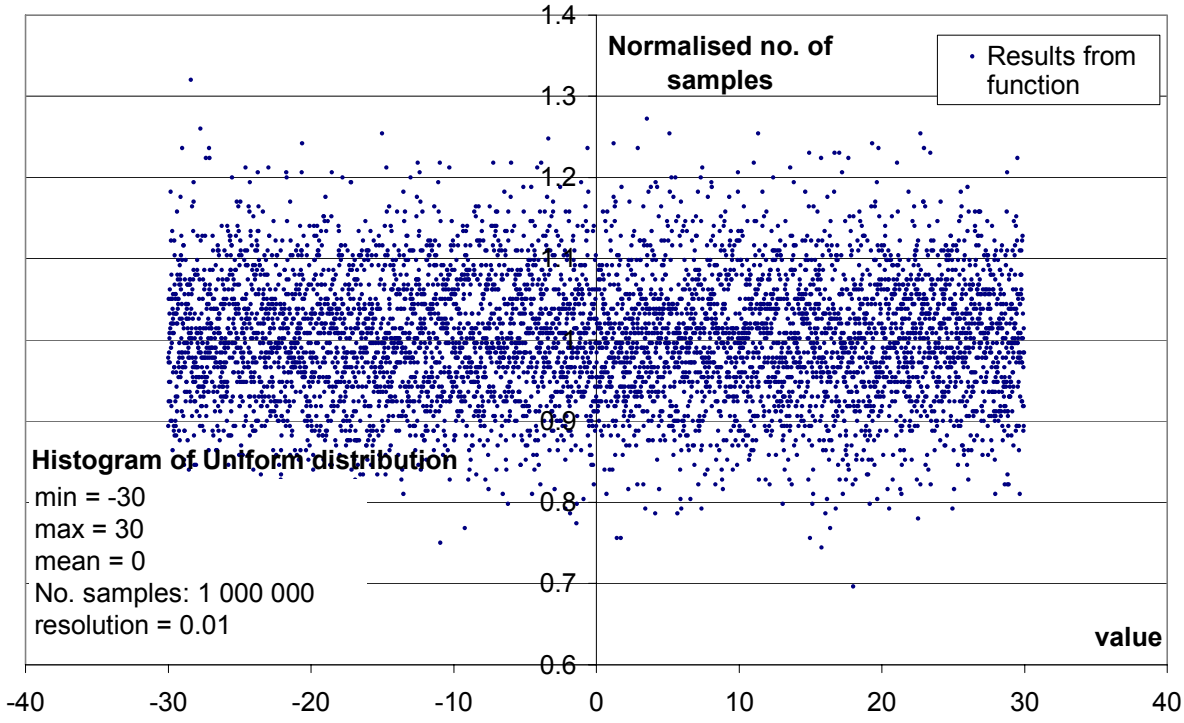

Figure B.3 – The histogram of uniform distribution.

Annex C Computational effort of the simulator

The influences of the different modes of the simulator and different number of the iterations, on the computation effort are presented in Table C.1, Table C.2 and Table C.3. These tests were made on a PC computer: PIII 1.2 GHz, 256 MRAM. In every mode of the simulator the same scenario (macro-cell) was used, which consisted of 10 clusters with the average number of the scatterers equal to 20.

As mentioned earlier, in mode 2, the simulator outputs the averages of all iterations. Therefore, no matter how many iterations were made, always the same number of the files is obtained. For different number of the iterations, the size of these files is similar. However, in other modes of the simulator, the greater amount of the iterations causes a larger number of output files, therefore the results occupy greater space on the computer disk.

Table C.1 – Comparison between the sizes of the files with the output results.

Size of the files [kB]		
No. of iterations	Mode	
	0/1/3	**2**
1	32.5	32.5
10	184.0	32.5
50	862.0	32.5
100	1660.0	32.5
500	8280.0	32.5

In mode 2, the simulator makes calculations of the averages values, which it is the reason that in this case more memory is used and simulations take longer time. In the other modes, almost the same value of the memory is used for different number of iterations. In mode 3 the usage of the memory is slightly higher compared to mode 0 and 1. In mode 3 in the every iteration, the simulator generates the whole environment from the beginning, thus the situation is more complicated than in modes 0 and 1.

Table C.2 – Comparison between the memory usages during the simulation.

Size of the memory [kB]			
No. of iterations	Mode		
	0/1	**2**	**3**
10	1296	1252	1292
50	1296	1296	1300
100	1296	2256	1300
500	1296	6348	1308

The relation between the number of iterations and the time of the simulation is linear for the different modes of the simulator. In every iteration, the simulator makes the same calculations, thus the same computation effort is used. Every iteration within the same mode takes the same time.

Table C.3 – Comparison between the times of the simulations.

Time of the simulations [s]				
No. of iterations	Mode			
	0	**1**	**2**	**3**
10	0.6	0.6	0.9	0.6
50	1.8	1.8	3.2	1.8
100	3.4	3.3	6.2	3.4
500	15.6	17.8	29.2	17.6

Annex D Assessments of the MUI simulator

The test of the multiuser interference simulator included the checking of the generation the deployment of the clusters within the regions. An environment, which consisted of many regions, which had common areas, was generated. This scenario included all the possible cells: the macro-, micro- and pico-cell. The generated environment is presented in Figure D.1.

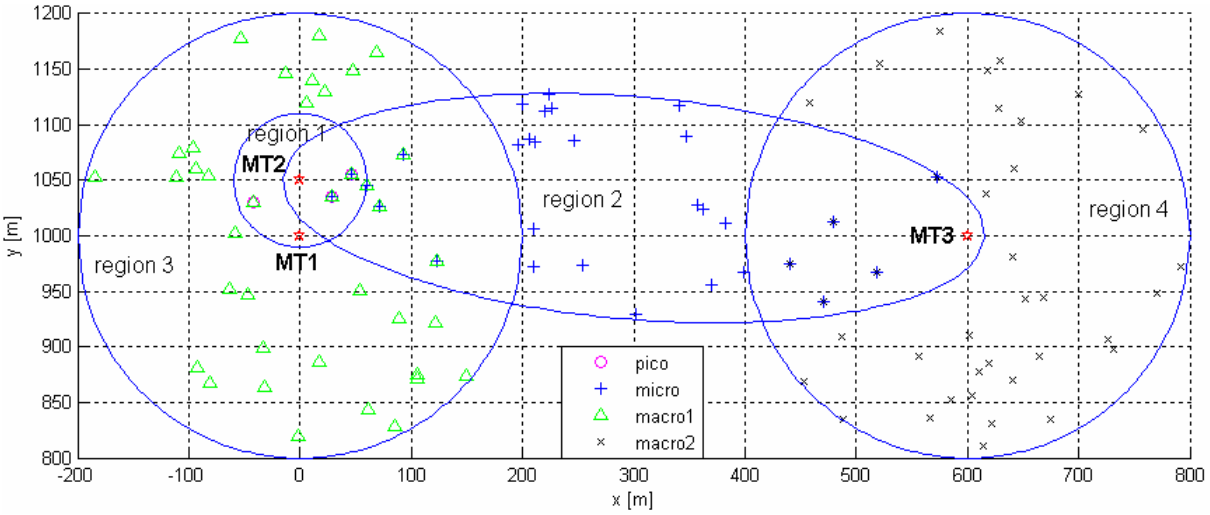

Figure D.1 – Environment for the test of the multiuser interference simulator.

This environment consists of the following terminals (see Table D.1):

Table D.1 – Positions (x,y) of the users in the test scenario (1).

	Position [m,m]
BS	0,0
MT1	0,1000
MT2	0,1050
MT3	600,1000

In Table D.2 are defined the particular links between the users. The dimension in Table D.2, in case of the micro-cell describes the length of the minor axis, and in case of the macro- and pico-cell, the radius of the circle.

The cluster density is common for all these regions and it is equal to $30 \cdot 10^{-5}$ per m^2. For every region, the expected number of the clusters was calculated and these results are shown in Table D.2. The implementation in the simulator fully agrees with the hand-made calculations.

Table D.2 – Description of the regions in the test environment.

Region no.	Type	Link	Dimension [m]	Number of the clusters calculated\obtained
1	Pico-cell	MT1-MT2	60	3\3
2	Micro-cell	MT2-MT3	100	30\30
3	Macro-cell	BS-MT1	200	38\38
4	Macro-cell	BS-MT3	200	38\38

In some cases, it is possible that the intended number of the cluster is not achieved. A scenario with this property is presented in Figure D.2. The following terminals are located in the environment (see Table D.3):

Table D.3 – Positions (x,y) of the users in the test scenario (2).

	Position [m,m]
BS	0,0
MT1	0,1000
MT2	200,1000
MT3	100,1000
MT4	80,1000

In Table D.4, the following links between the users are defined, which are the same as in the previous scenario, the cluster density is common for all these regions and it is equal to $30 \cdot 10^{-5}$ per m^2. For every region, the expected number of the clusters was calculated and these results are shown in Table D.4. One can notice that for the pico-cell the intended 6 clusters were not achieved.

To explain the reason for this situation, it is necessary to follow the way of generating the clusters for this case. The graph of the regions, which was described in Section 4.3.2, for this scenario is presented in Figure D.3. One can notice that all nodes have the same row, which is equal to 2. Thus, the sequence of generating the cluster in this example is determined by the sequence of the definition of the links in the configuration file.

Table D.4 – Description of the regions in the test environment.

Region no.	Type	Link	Dimension [m]	Number of the clusters
1	Macro-cell	BS-MT1	200	38\38
2	Macro-cell	BS-MT2	200	38\38
3	Pico-cell	MT3-MT4	80	6\3

For this example, the order was set to: *region 1*, *region 2* and *region 3*. The clusters within the *region 3* will be set in the end. In this case, *region 3* is located entirely inside common parts of *region 1* and *region 2*. The clusters in the other regions are already generated, and these regions are full. New ones clusters are not added, which makes it impossible to generate additional clusters to *region 3*. *Region 3* has only these clusters, which were generated for *region 1* and *region 2*.

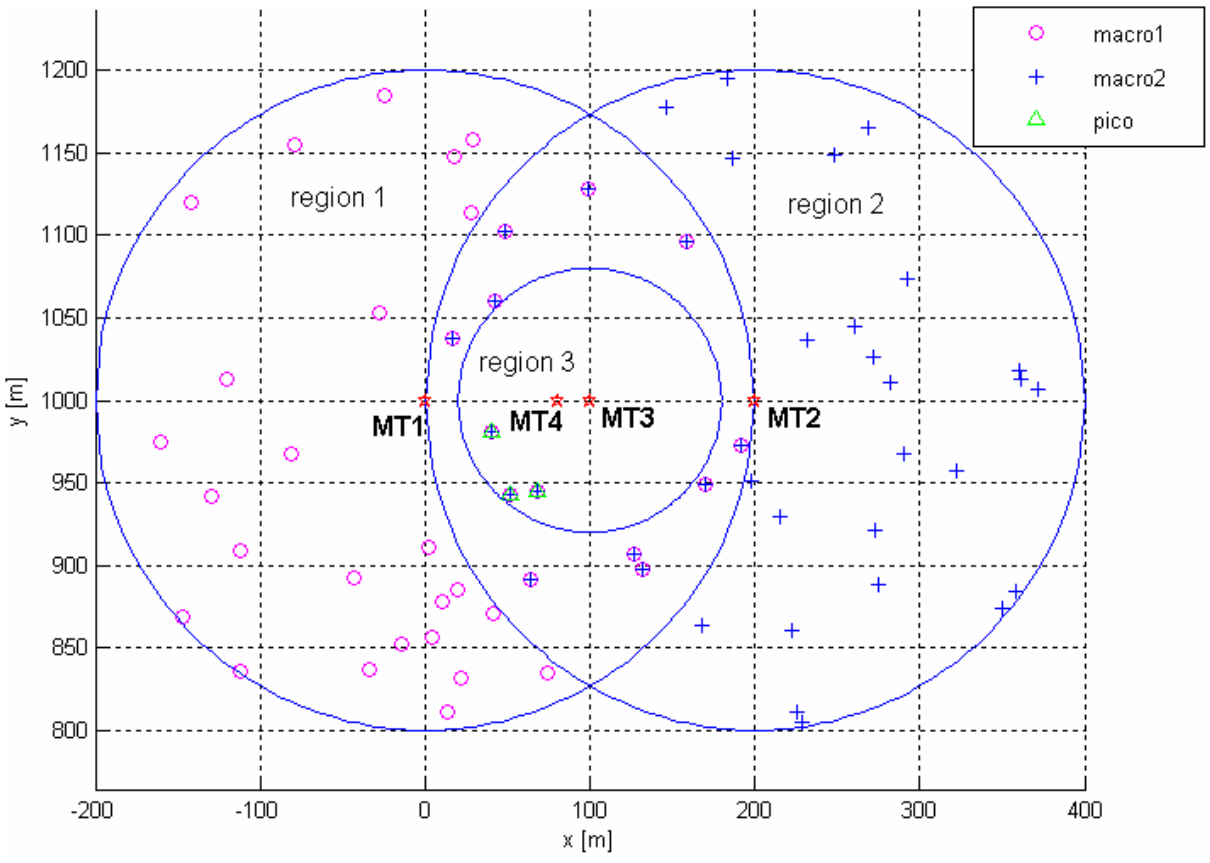

Figure D.2 – Example when the number of the clusters is not achieved.

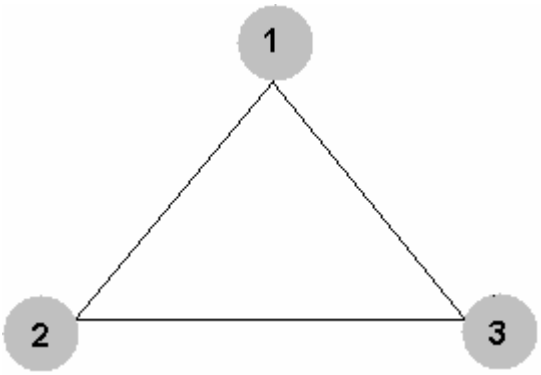

Figure D.3 – Graph of the regions for the test scenario.

But this problem can be easily solved. The general concept is that, the small regions, which are inside the greater ones, have to be defined first in the configuration file. When the definition of *region 3* will be on the first line, the clusters will be generated first. The environment for this case is in Figure D.4. For this case the number of the clusters is correct.

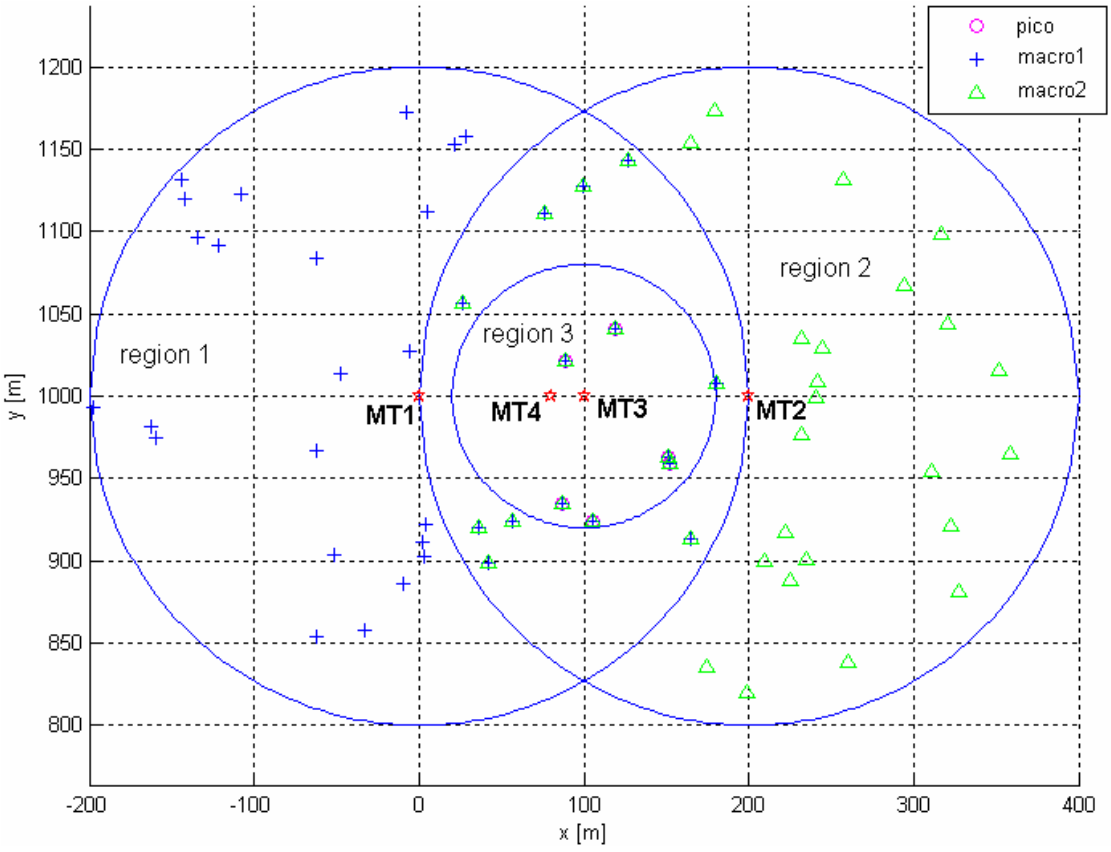

Figure D.4 – Example of the correct distribution of the clusters.

Annex E Deployments of terminals in the scenarios

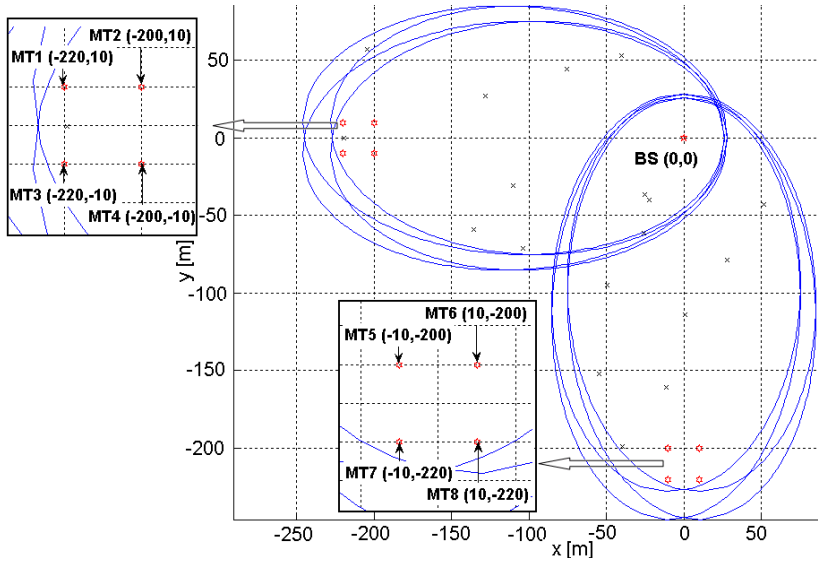

Figure E.1 – The uplink in the city street scenario, deployment no. 1.

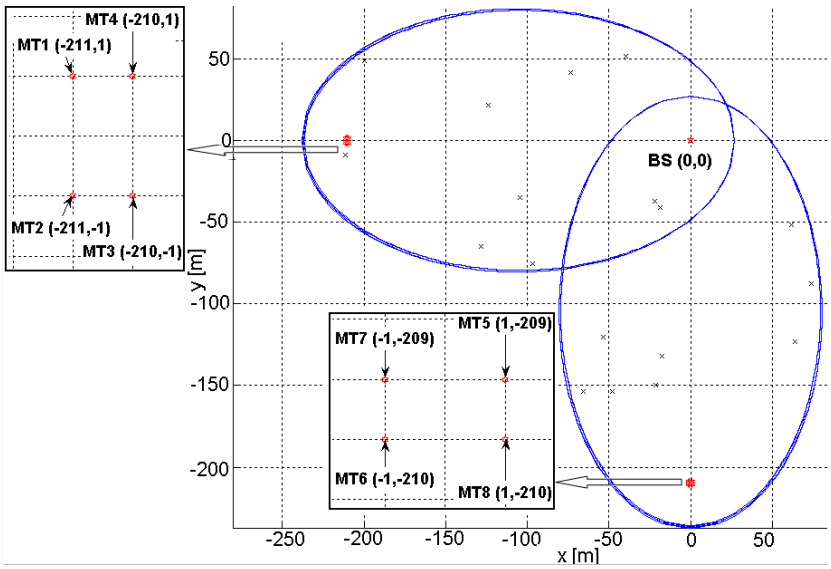

Figure E.2 – The uplink in the city street scenario, deployment no. 2.

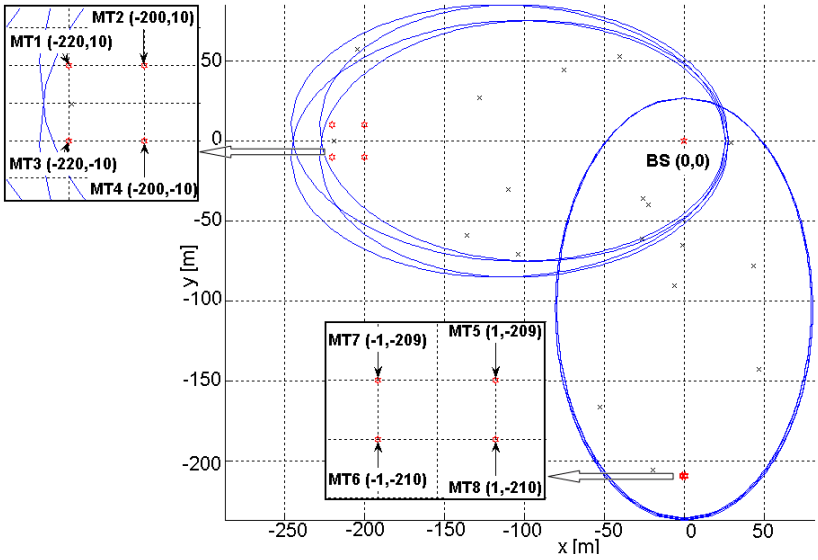

Figure E.3 – The uplink in the city street scenario, deployment no. 3.

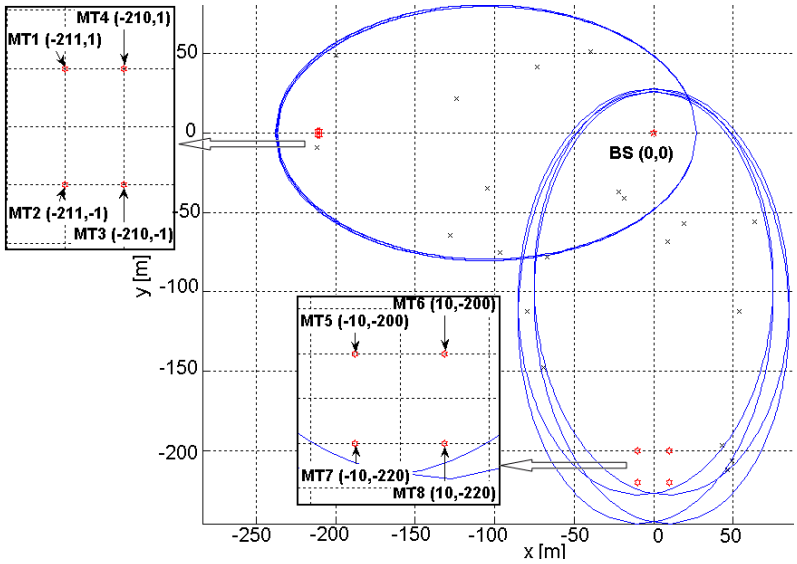

Figure E.4 – The uplink in the city street scenario, deployment no. 4.

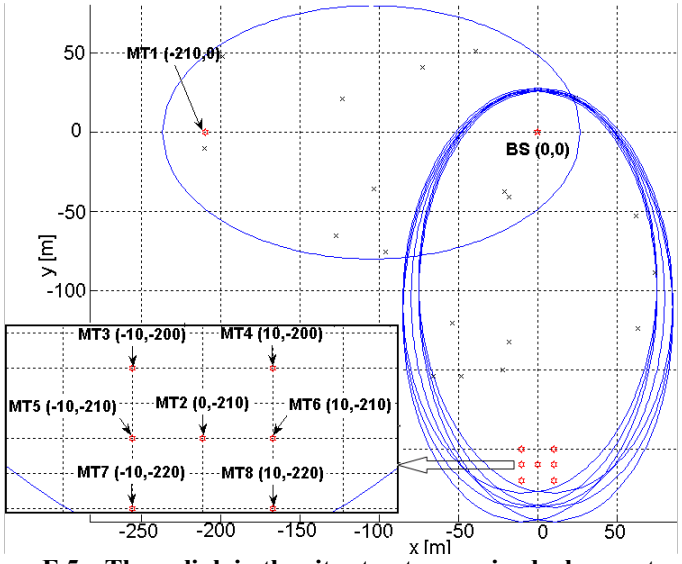

Figure E.5 – The uplink in the city street scenario, deployment no. 5.

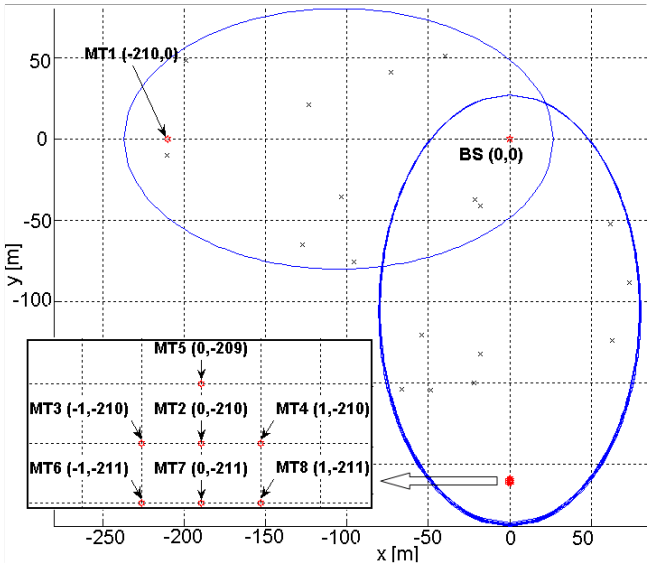

Figure E.6 – The uplink in the city street scenario, deployment no. 6.

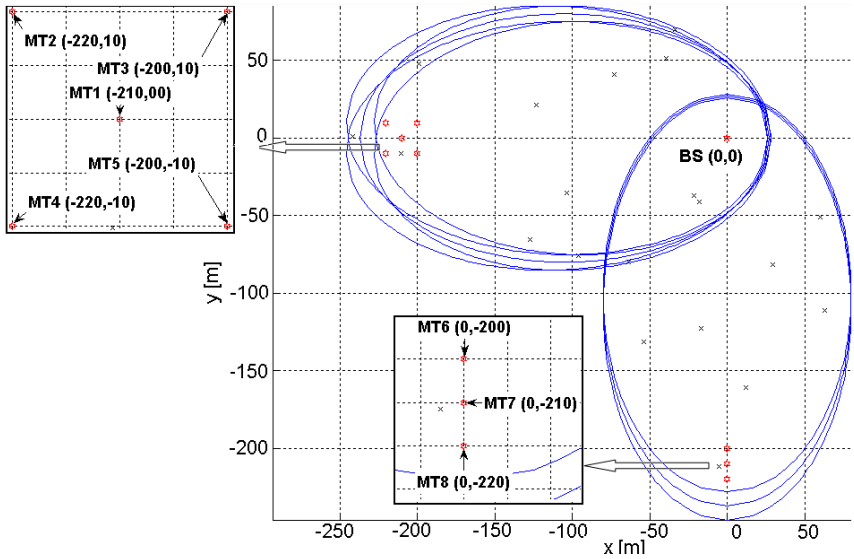

Figure E.7 – The uplink in the city street scenario, deployment no. 7.

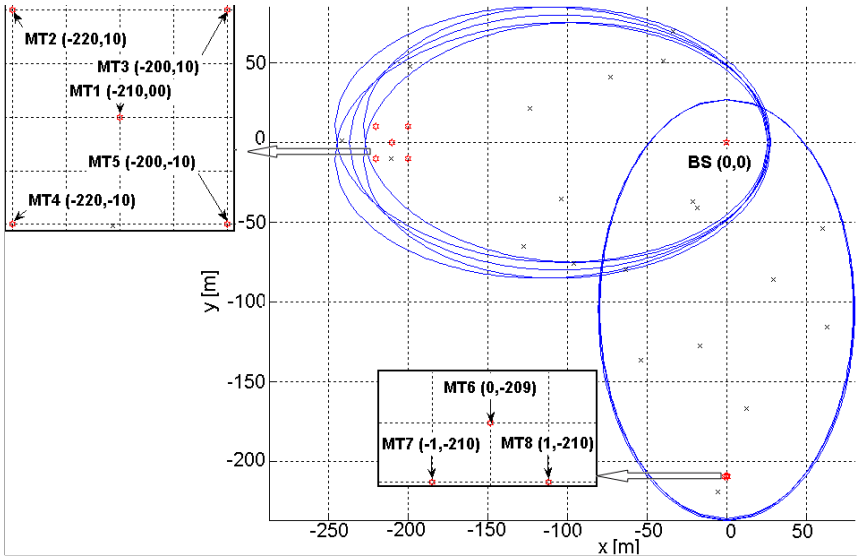

Figure E.8 – The uplink in the city street scenario, deployment no. 8.

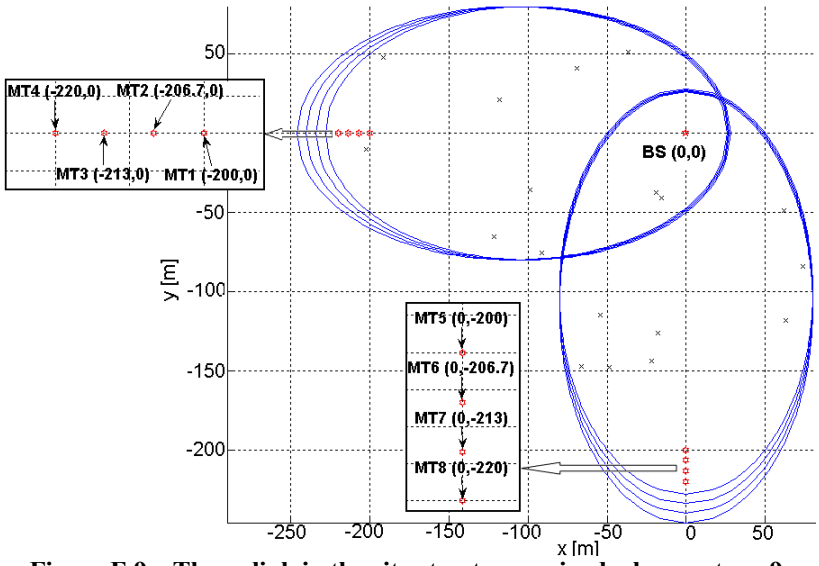

Figure E.9 – The uplink in the city street scenario, deployment no. 9.

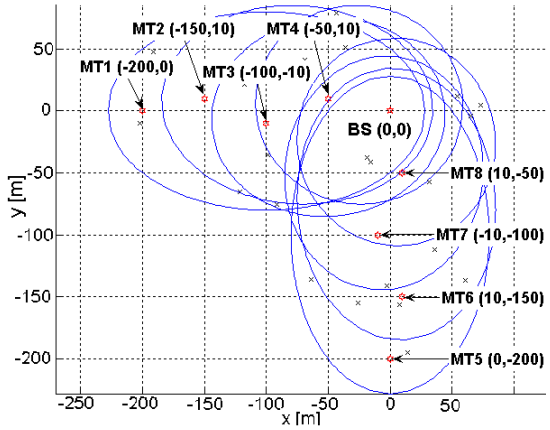

Figure E.10 – The uplink in the city street scenario, deployment no. 10.

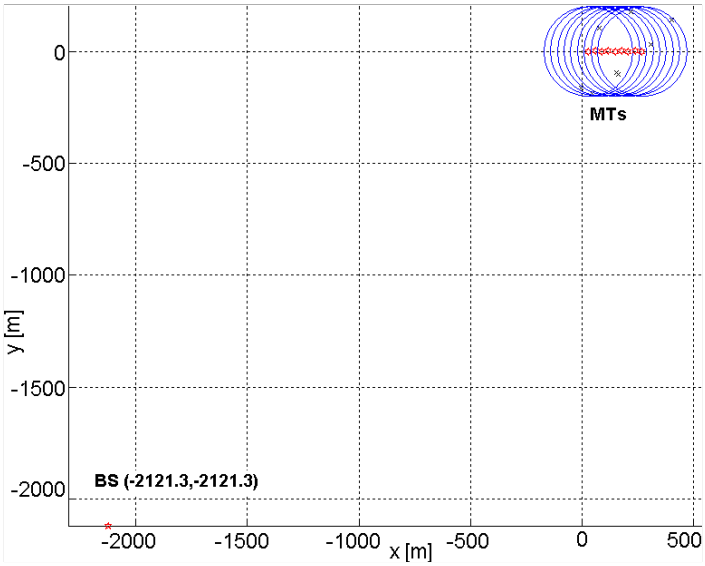

Figure E.11 – The position of the BS in the highway scenario.

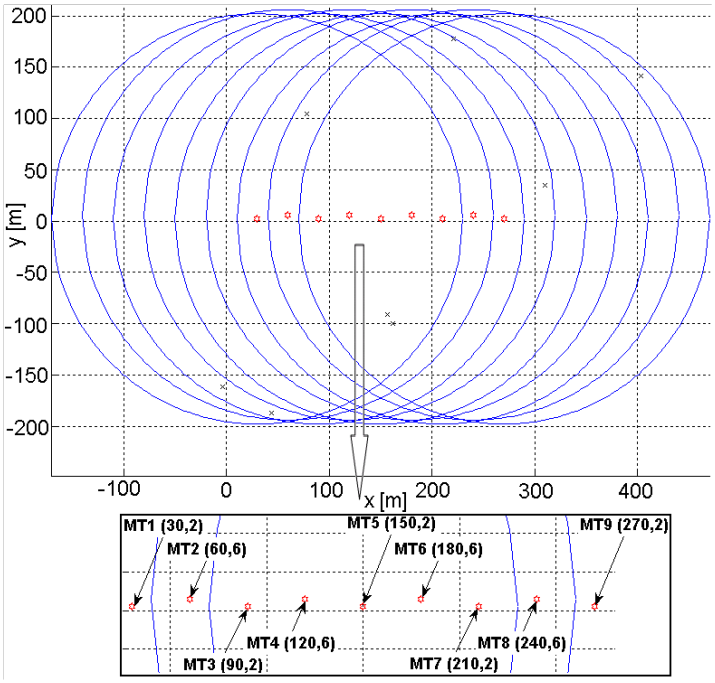

Figure E.12 – The uplink in the highway scenario, deployment no. 1.

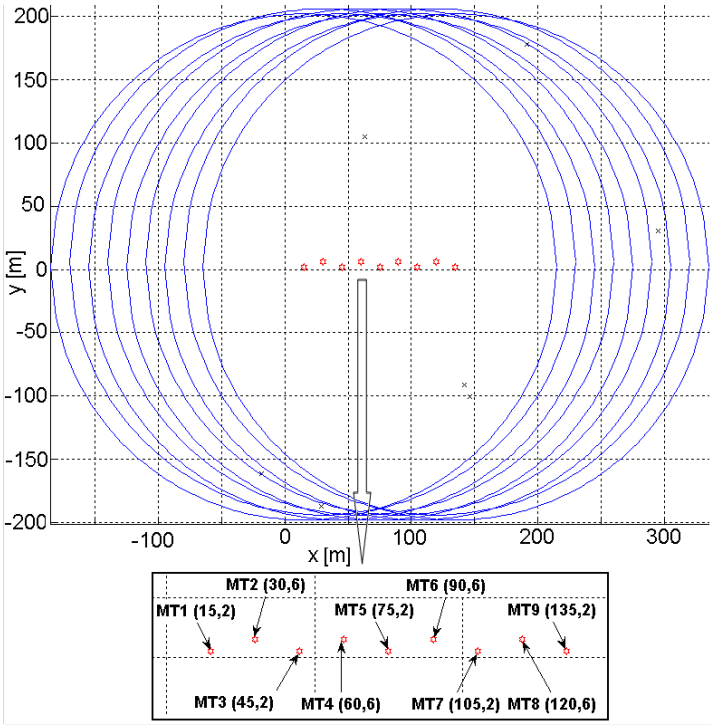

Figure E.13 – The uplink in the highway scenario, deployment no. 2.

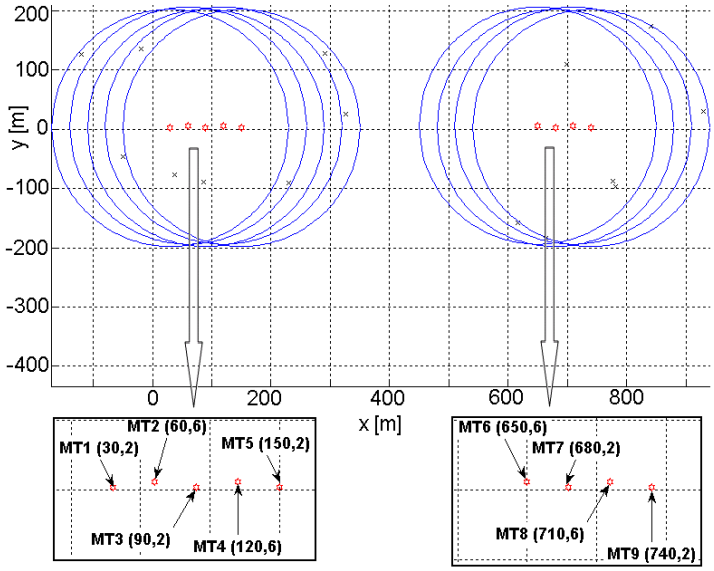

Figure E.14 – The uplink in the highway scenario, deployment no. 3.

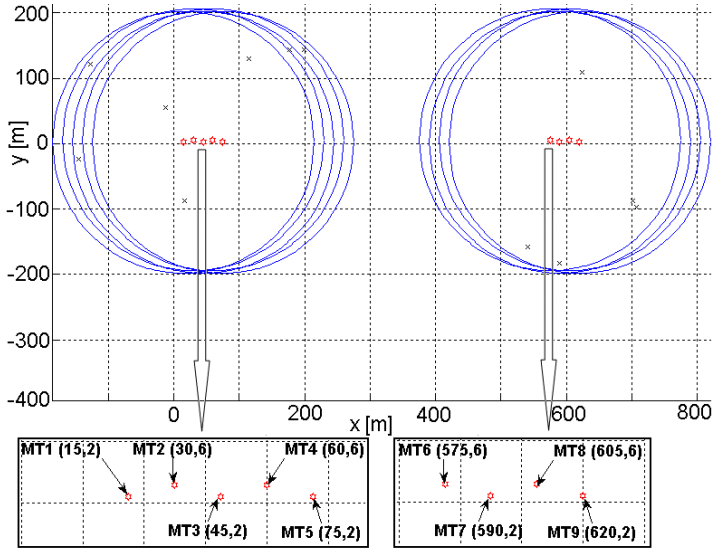

Figure E.15 – The uplink in the highway scenario, deployment no. 4.

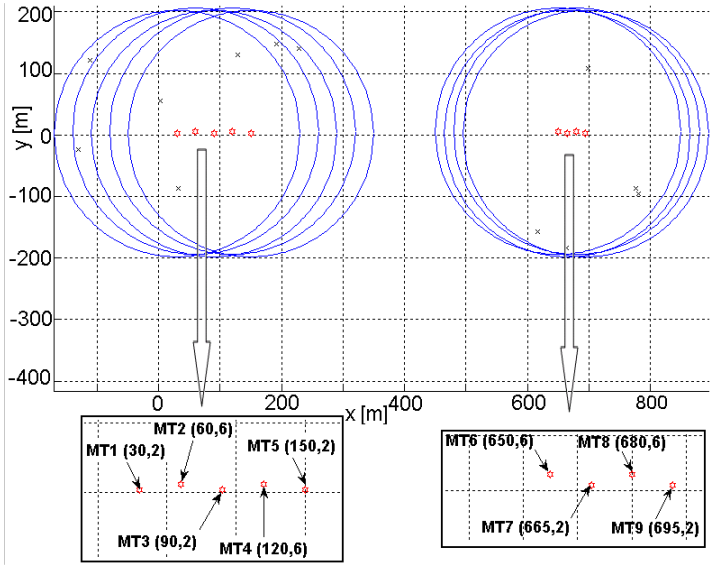

Figure E.16 – The uplink in the highway scenario, deployment no. 5.

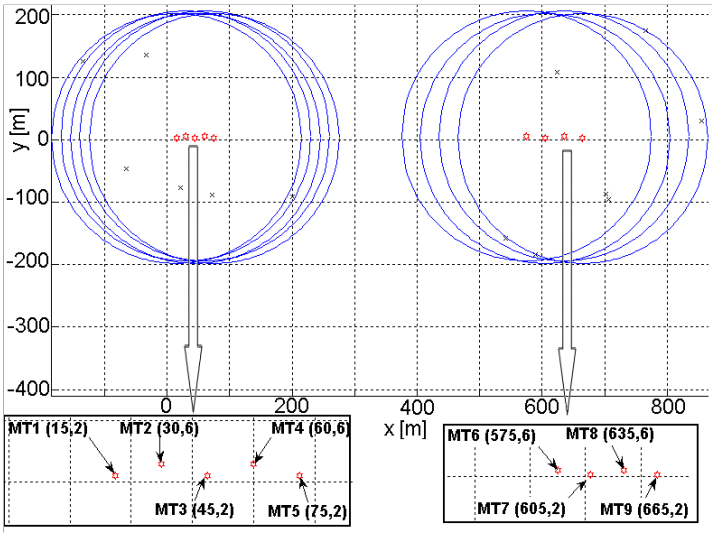

Figure E.17 – The uplink in the highway scenario, deployment no. 6.

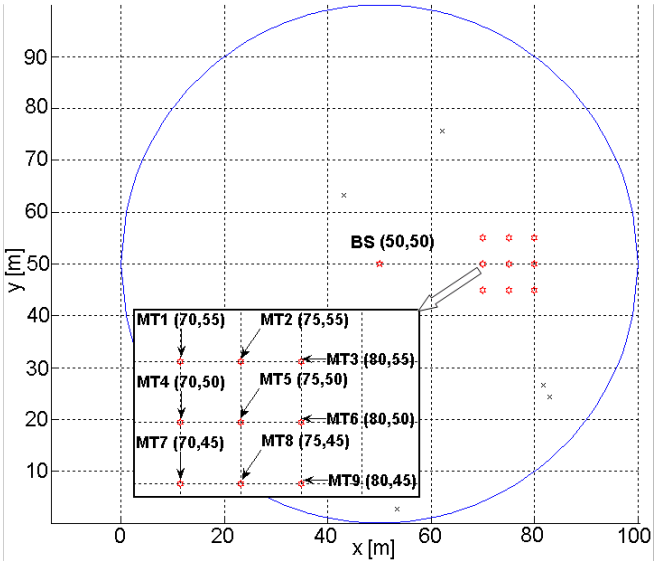

Figure E.18 – The uplink in the railway station scenario, deployment no. 1.

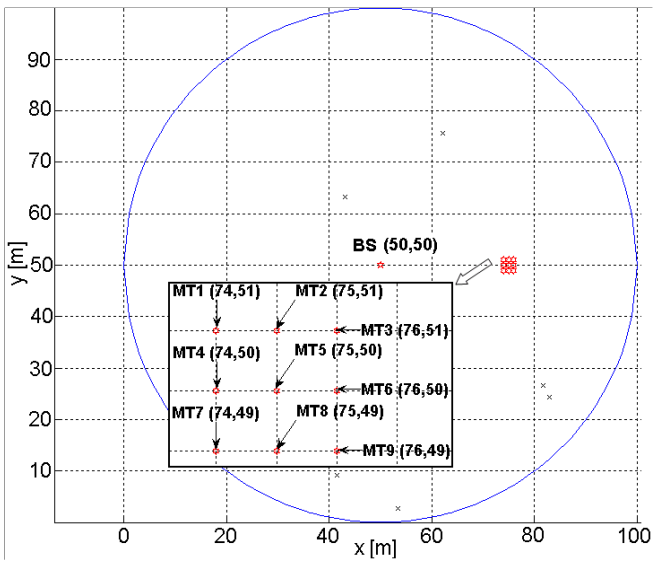

Figure E.19 – The uplink in the railway station scenario, deployment no. 2.

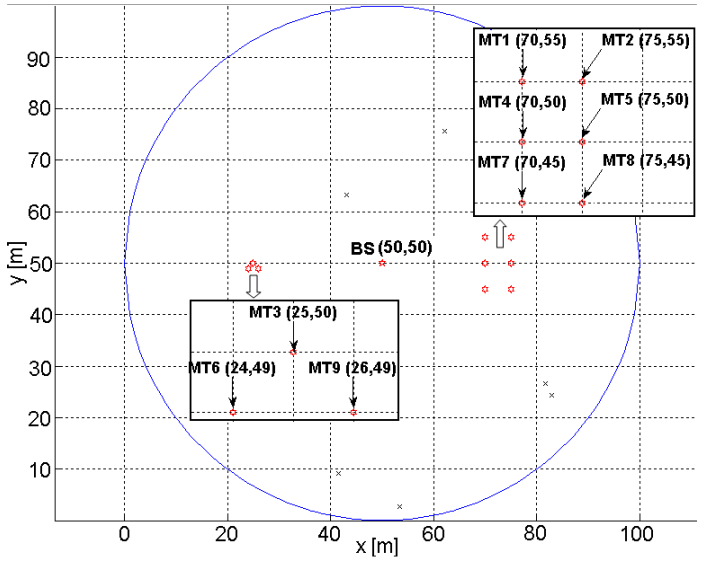

Figure E.20 – The uplink in the railway station scenario, deployment no. 3.

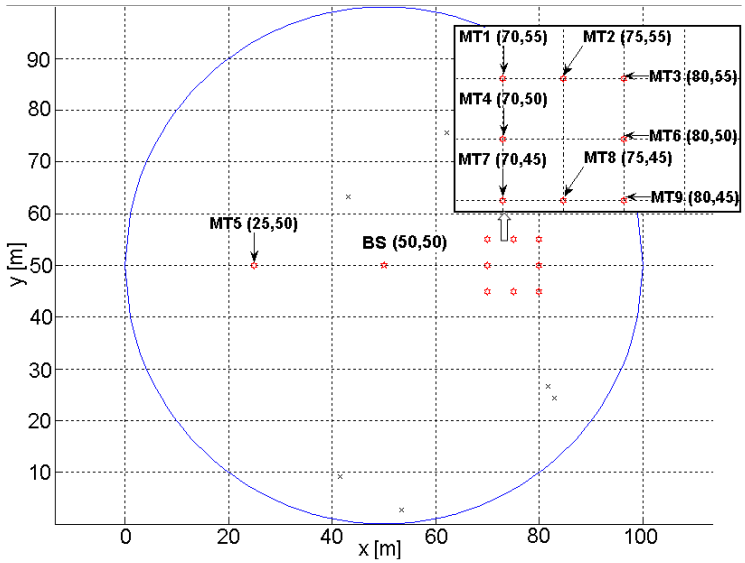

Figure E.21 – The uplink in the railway station scenario, deployment no. 4.

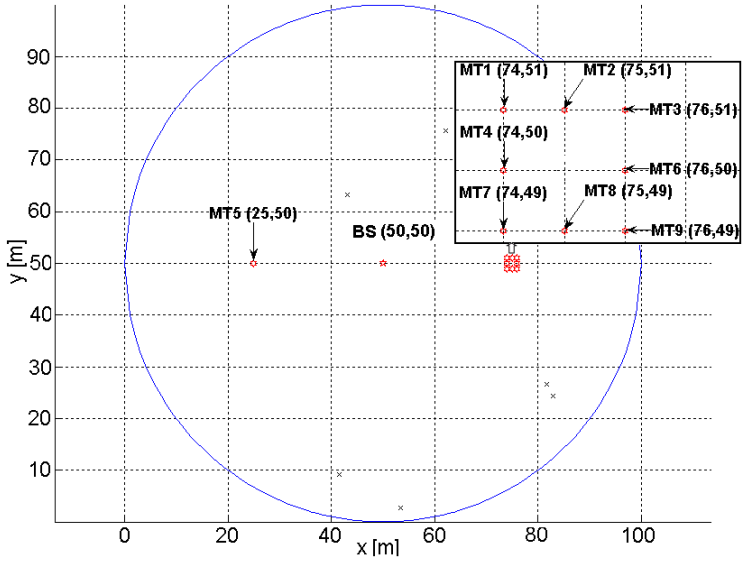

Figure E.22 – The uplink in the railway station scenario, deployment no. 5.

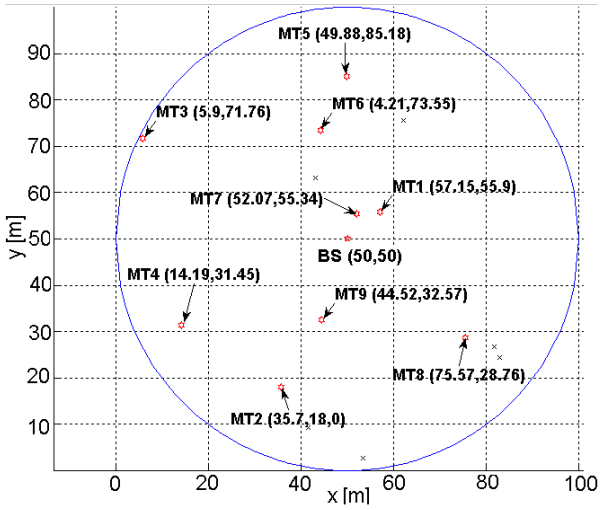

Figure E.23 – The uplink in the railway station scenario, deployment no. 6.

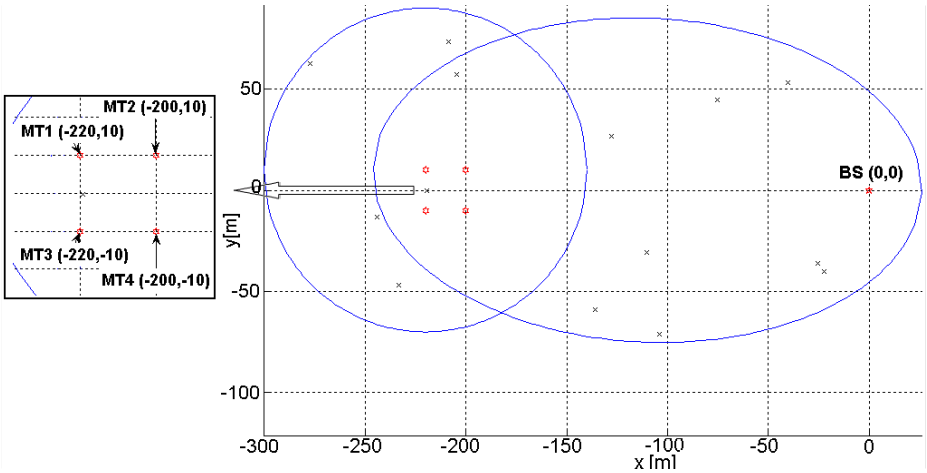

Figure E.24 – The downlink in the city street scenario, deployment no. 1.

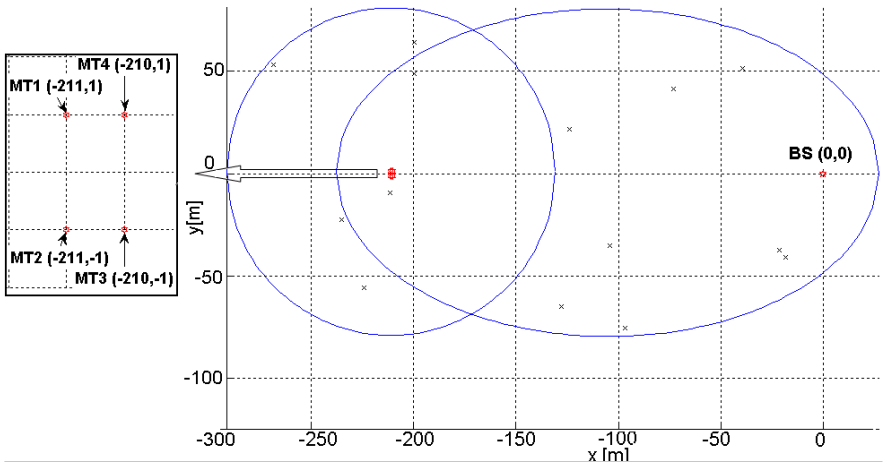

Figure E.25 – The downlink in the city street scenario, deployment no. 2.

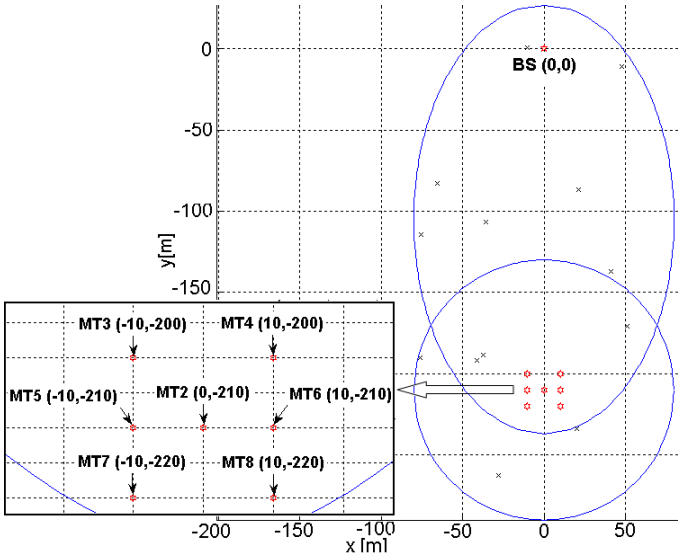

Figure E.26 – The downlink in the city street scenario, deployment no. 3.

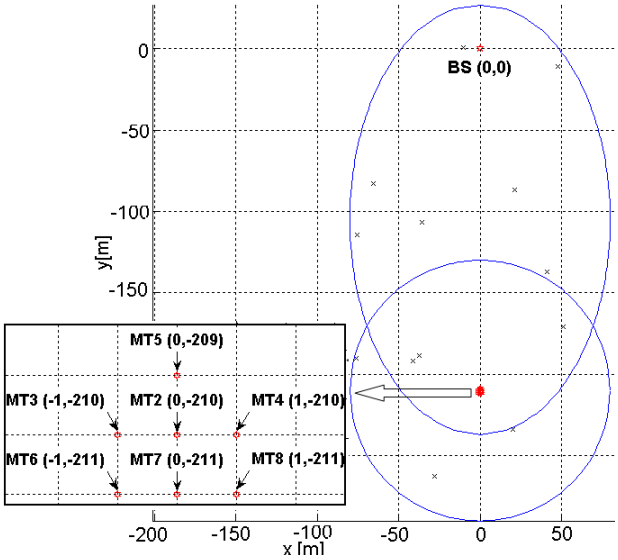

Figure E.27 – The downlink in the city street scenario, deployment no. 4.

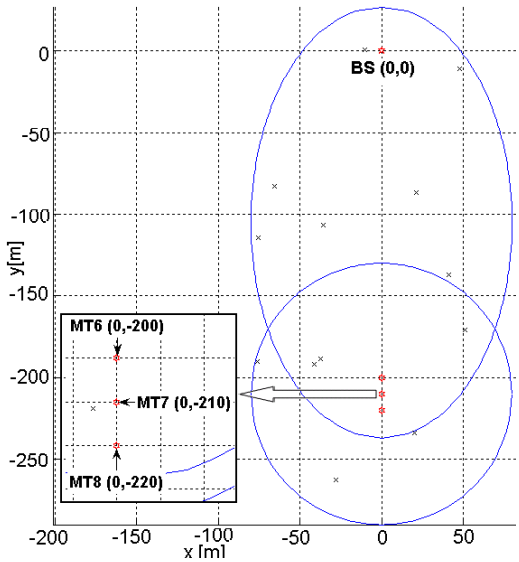

Figure E.28 – The downlink in the city street scenario, deployment no. 5.

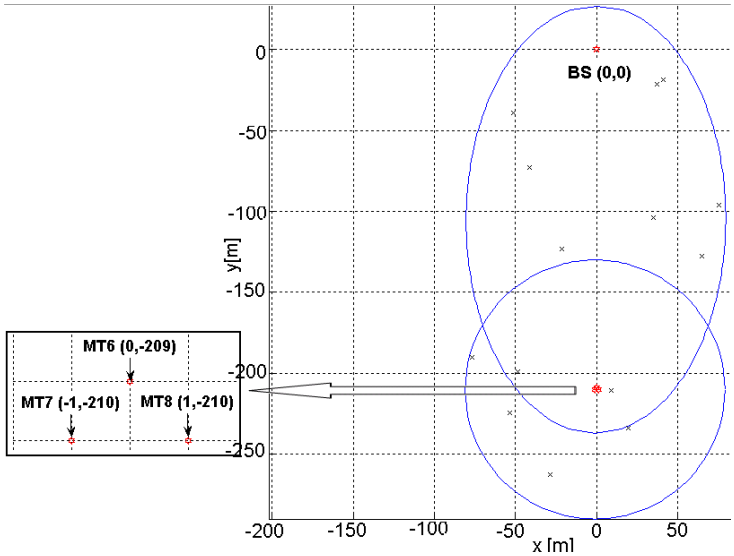

Figure E.29 – The downlink in the city street scenario, deployment no. 6.

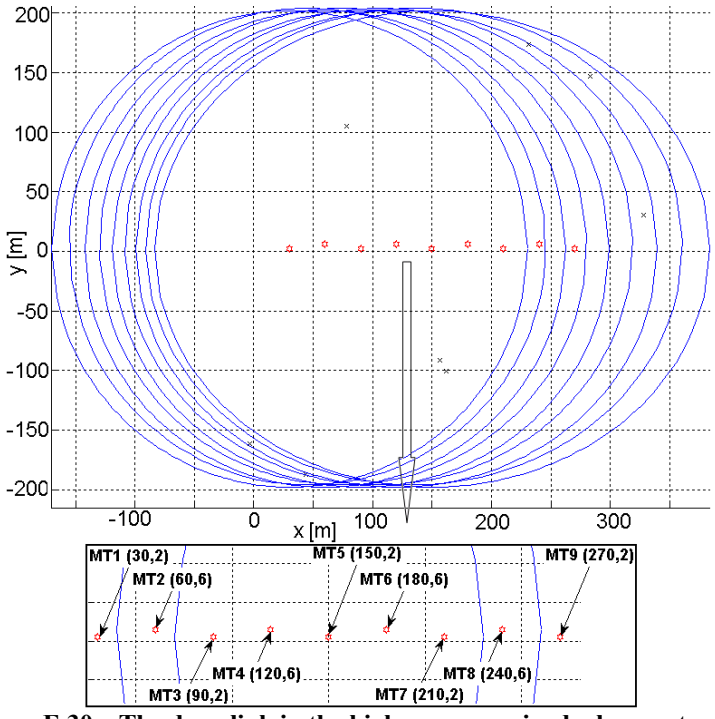

Figure E.30 – The downlink in the highway scenario, deployment no. 1.

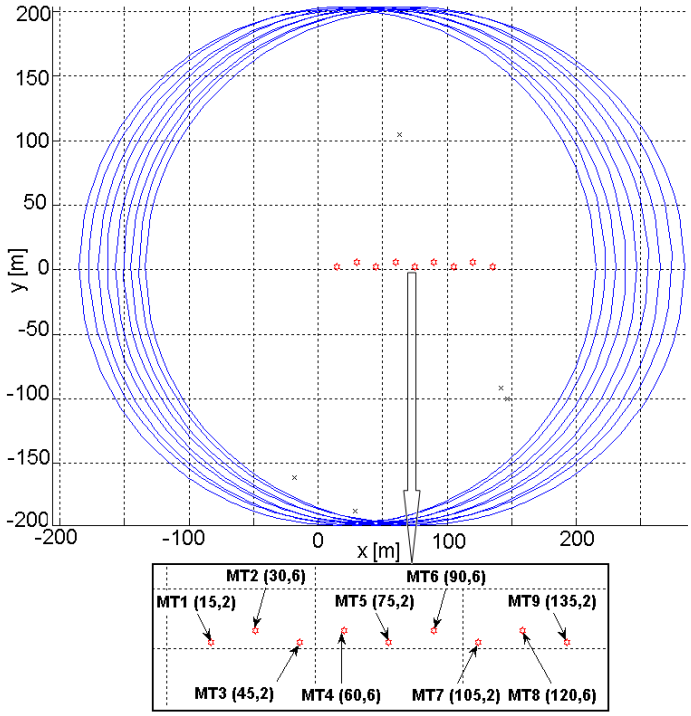

Figure E.31 – The downlink in the highway scenario, deployment no. 2.

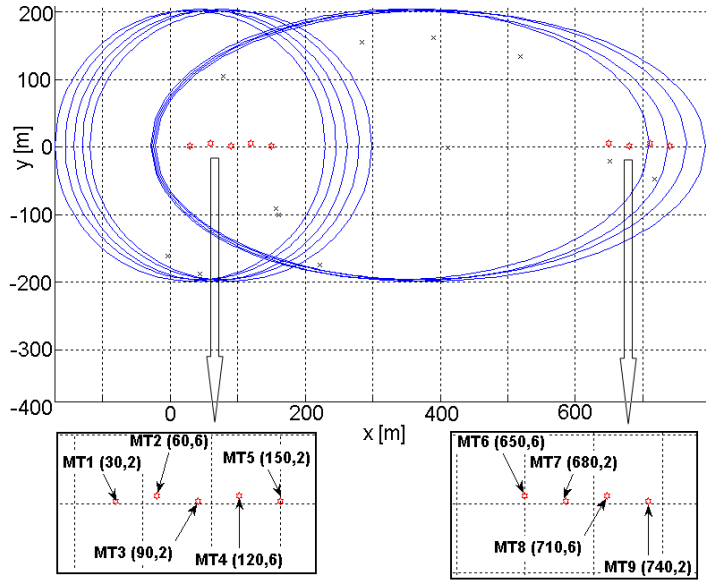

Figure E.32 – The downlink in the highway scenario, deployment no. 3.

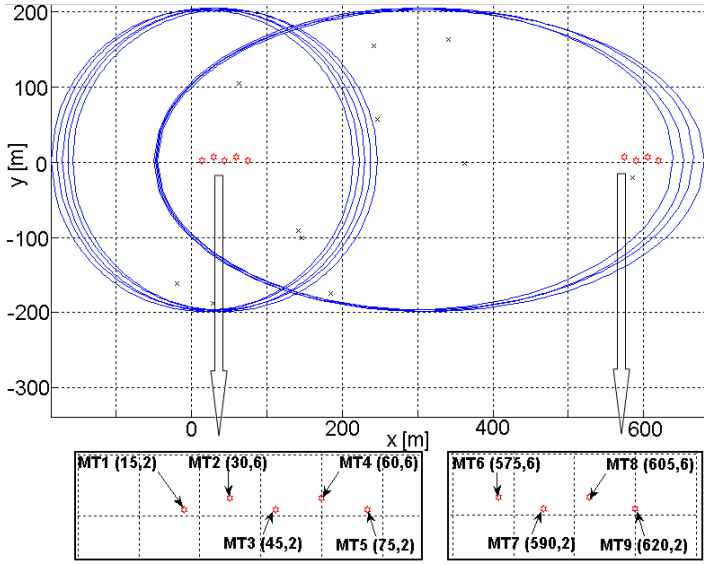

Figure E.33 – The downlink in the highway scenario, deployment no. 4.

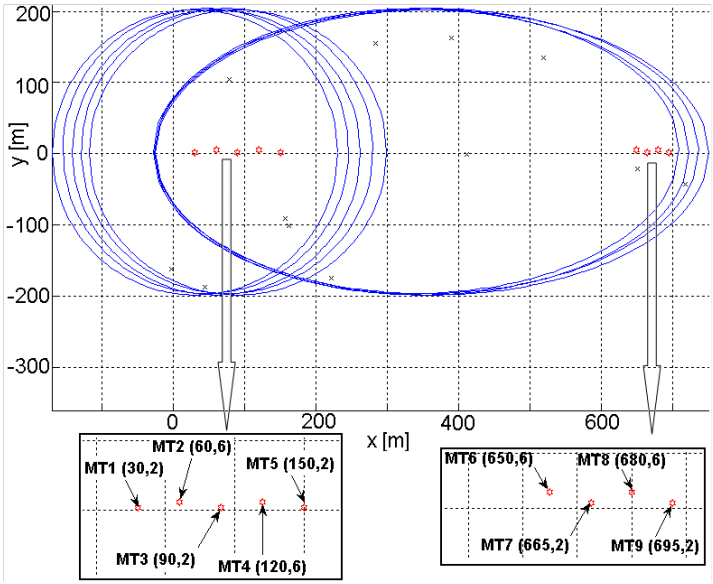

Figure E.34 – The downlink in the highway scenario, deployment no. 5.

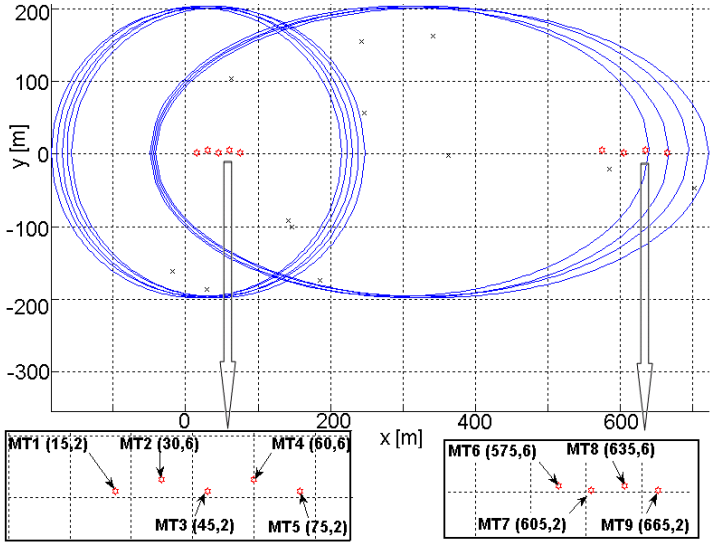

Figure E.35 – The downlink in the highway scenario, deployment no. 6.

Annex F Examples of the links

In this Annex examples of the realisations of the channel models are presented. Some uplinks between the BS and one of the MTs from the scenarios was chosen, which are described in Section 5.1. The channel model in the micro-cell is presented in deployment 1 in the city street scenario. The deployment of the all users is presented in Figure E.1. However, here are results obtained from the link between the BS and MT1. The position of the BS is (0,0) and of MT1 (-220,10), which makes the distance between these terminals 220.23 m. The parameters of the users and the environment are presented in Table 5.1.

The example realisation of the CIR is presented in Figure F.1. This CIR is without processing, in unfiltered form. This environment consists of 10 clusters and every cluster has 20 scatterers. One can notice that the samples of the CIR represent the multipath components, and every sample is related with a particular scatterer. This is the reason that, similar as the scatterers, the samples are grouped into clusters.

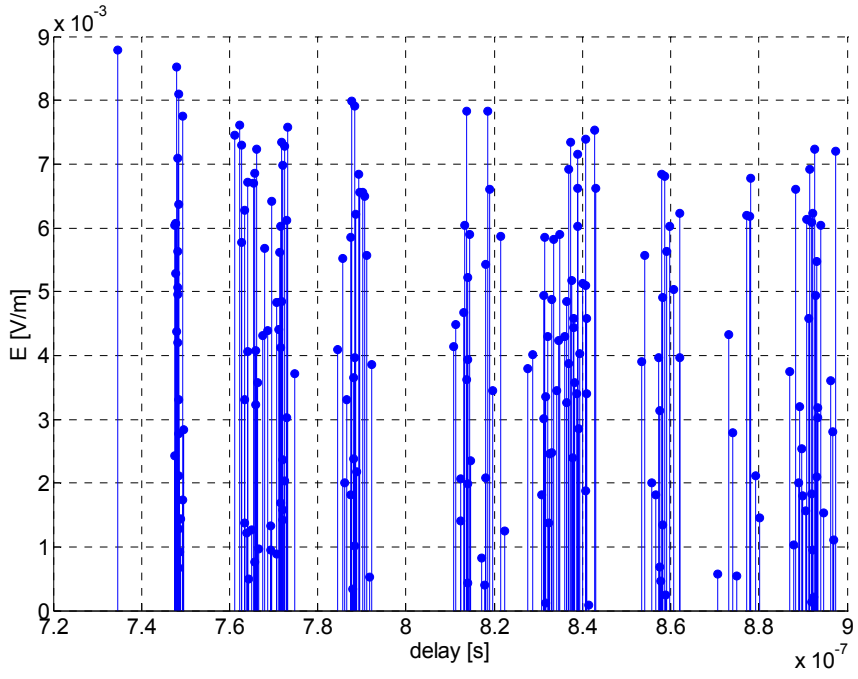

Figure F.1 – The example of the unfiltered CIR in the city street scenario.

CIR over which some normalisation was made is presented in Figure F.2. The time domain was divided into 2 ns bins, and all multipath components which were inside the same bin, were

summed. During the operation of the summation of the samples, the amplitude and the phase were taken into account.

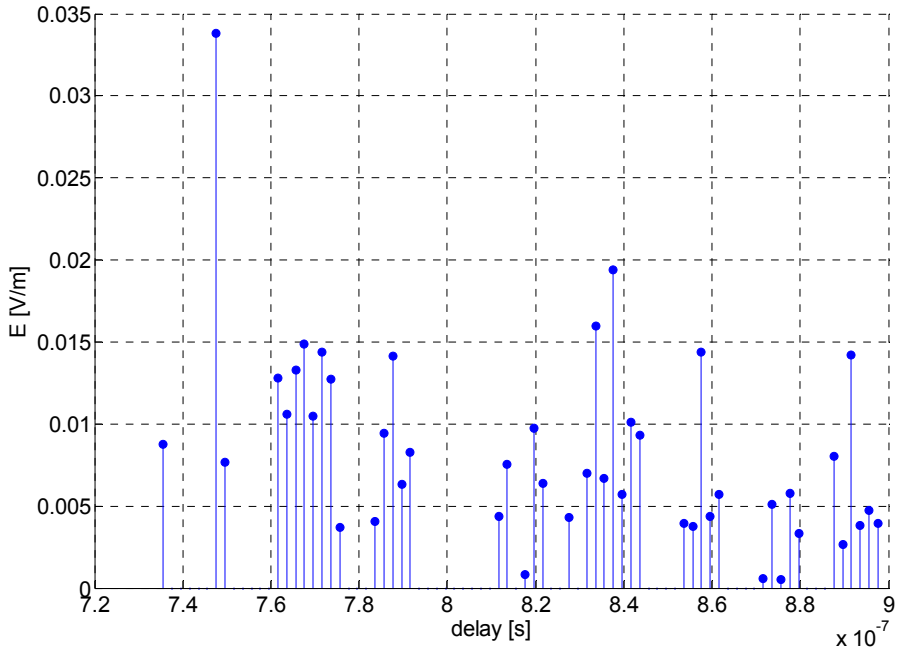

Figure F.2 – Example of the filtered CIR with 2 ns time resolution in the city street scenario.

In this case the samples of the CIR are distributed uniformly in the time domain, and the clusters which were visible in the previous case, do not exist now. The amplitudes of the CIRs (unfiltered and filtered) were not normalised.

In Figure F.3, the CIR in 2D space of the time and the angle is presented. The circle is divided into smaller ones, which correspond to the different time delays. Every circle is cut into pieces, which are connected with the different values of the AoA. The figure was prepared for the case, that the CIR is divided into 4 equal pieces in the time domain, and 36 pieces in the AoA domain. However, in this case the amplitude of the CIR was normalised to the maximum sample, as well as the delay and AoA, which were normalised relative to the LoS component.

The same CIR is presented in Figure F.4, but in this case instead of the AoA domain, the AoD domain was used. In these both cases one can notice, that all samples are grouped around the LoS component. The main energy of the signal is received and transmitted in a small range of angles.

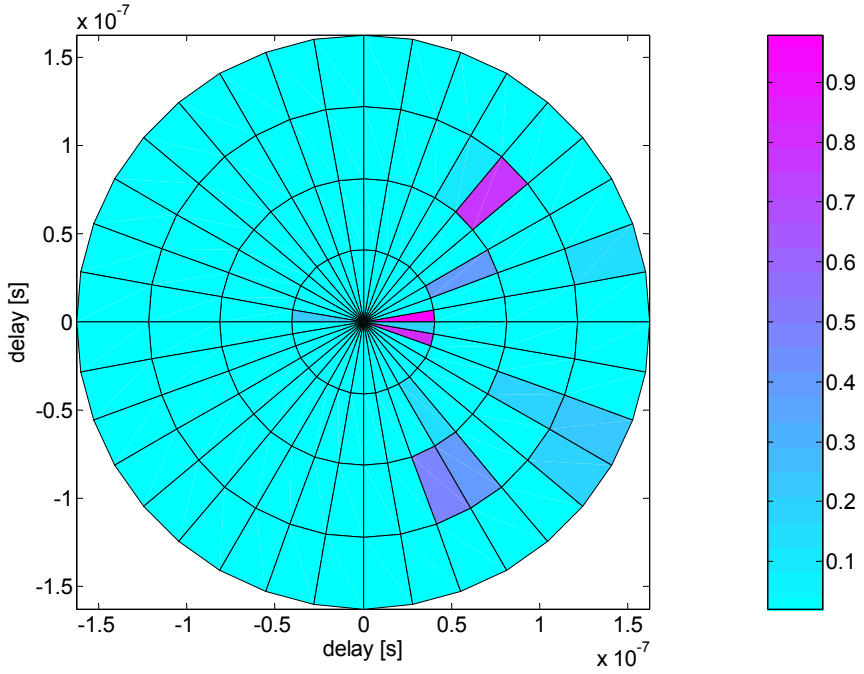

Figure F.3 – Example of the CIR in domain of the AoA and time delay for the city street scenario.

The presented CIR can be described by the statistical parameters (Table F.1):

Table F.1 – Statistical parameters of the example city street scenario link.

$\bar{\tau}$ [μs]	σ_τ [ns]	$\overline{AoA}$ [deg]	σ_{AoA} [deg]	$\overline{AoD}$ [deg]	σ_{AoD} [deg]
0.79	0.47	-3.72	42.35	-13.65	36.79

One can assume that the Tx transmits signal has the shape of a Dirac Delta pulse, with the amplitude equal to the square root of the power then it is possible to calculate power which is obtained in the Rx. The power is calculated using (5.1). For case of the unfiltered CIR the power is 4.62 mW, however when filtered CIR is taken into account the obtained power is equal to 4.73 mW.

The example of the CIR for the case of the highway scenario (macro-cell) is presented in the link between the BS and MT1 in the scenario 1 in the highway environment. Parameters of this link are taken from Table 5.5. In Figure F.5 the unfiltered CIR is presented, and Figure F.6 is the CIR with normalisation in the time domain with 2 ns resolution. This environment consists of 5 clusters with each 20 scatterers. The clusters are visible in both of the CIRs. The radius of the region is 200 m, and this causes that the duration of the CIR is much longer compared to the time resolution.

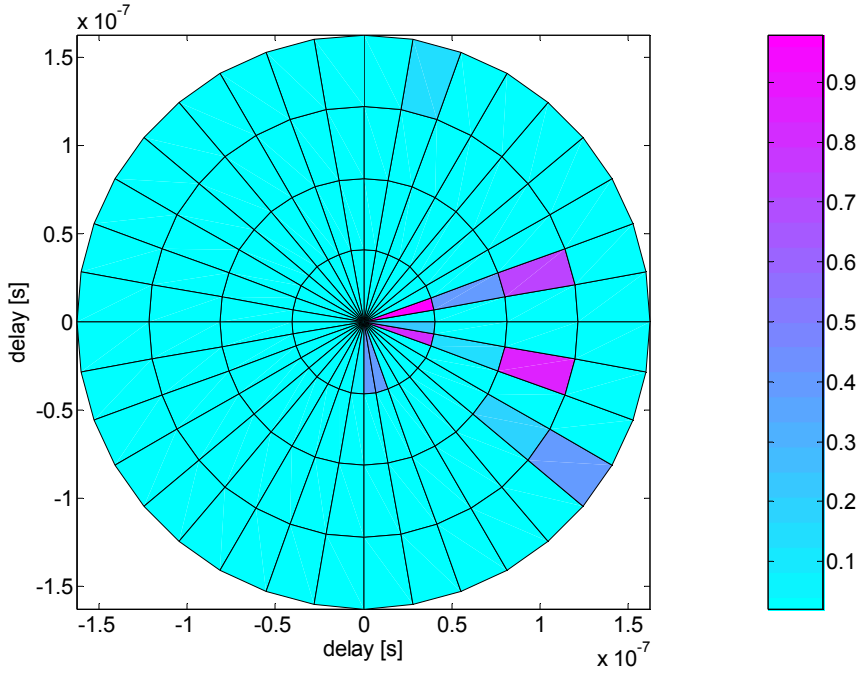

Figure F.4 – Example of the CIR in domain of the AoD and time delay for the city street scenario.

In Figure F.7 and Figure F.8 are presented the CIRs, which are normalised in the 2D space of delay and angles. In these pictures, it is visible that scatterers are located only around the MT. In the uplink (considered here), the BS is located far from the MT. This distance is also much longer than radius of the region of the scatterers. Thus, all samples of the CIR, which are received at the BS, are focused around the line which connects the Rx and the Tx. In Table F.2, the statistical parameters are presented. The standard deviation of the AoA is small, and the assumption can be made that all multipath rays are parallel to each other. In case of the CIR, which was normalised in the AoD domain, one can notice that all rays are spread around the Tx. The clusters are distributed around the MT in the circular area, thus the probability that the multipath component will be reflected is the same for all angles from 0 deg to 360 deg.

Table F.2 – Statistical parameters of the example highway scenario link.

$\bar{\tau}$ [µs]	σ_τ [ns]	$\overline{AoA}$ [deg]	σ_{AoA} [deg]	$\overline{AoD}$ [deg]	σ_{AoD} [deg]
10.40	0.25	-1.99	1.44	-20.18	94.51

Also in this case the powers were calculated. For the case of the unfiltered CIR the power is equal to 13.68 µW, and for case of the CIR normalised with the 2 ns time resolution the power is 11.14 µW.

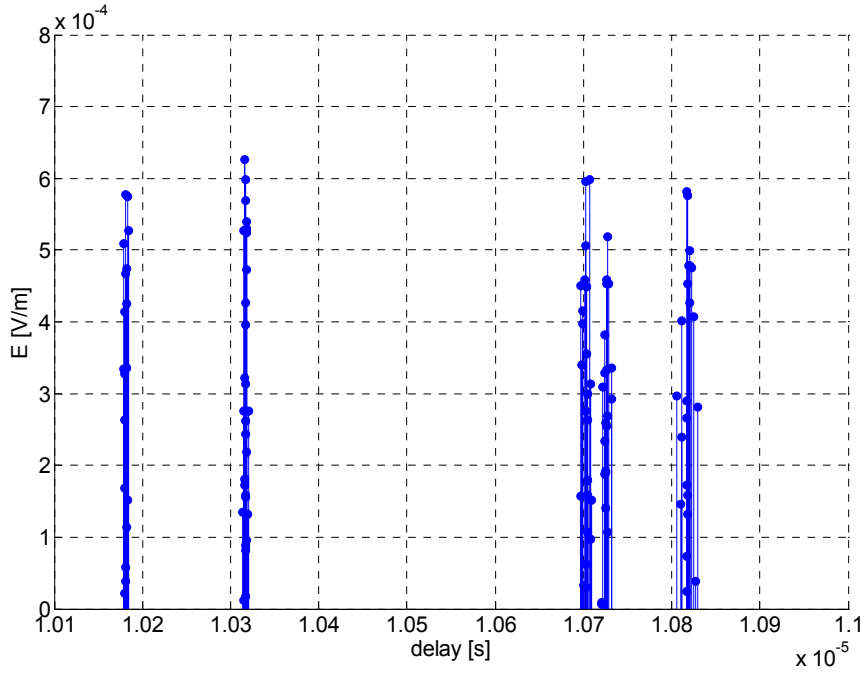

Figure F.5 – Example of the unfiltered CIR in the highway scenario.

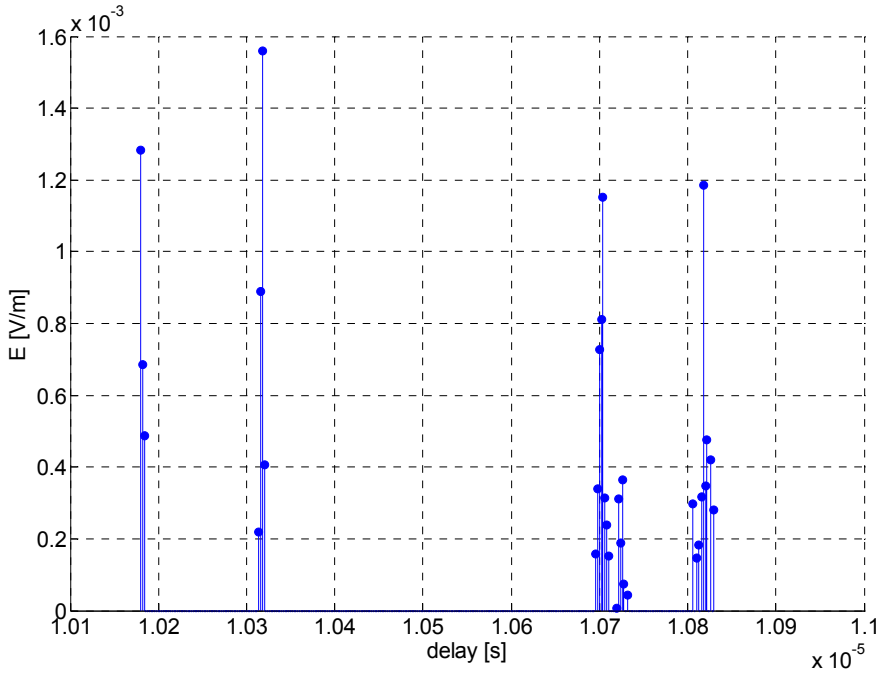

Figure F.6 – Example of the filtered CIR with 2 ns time resolution in the highway scenario.

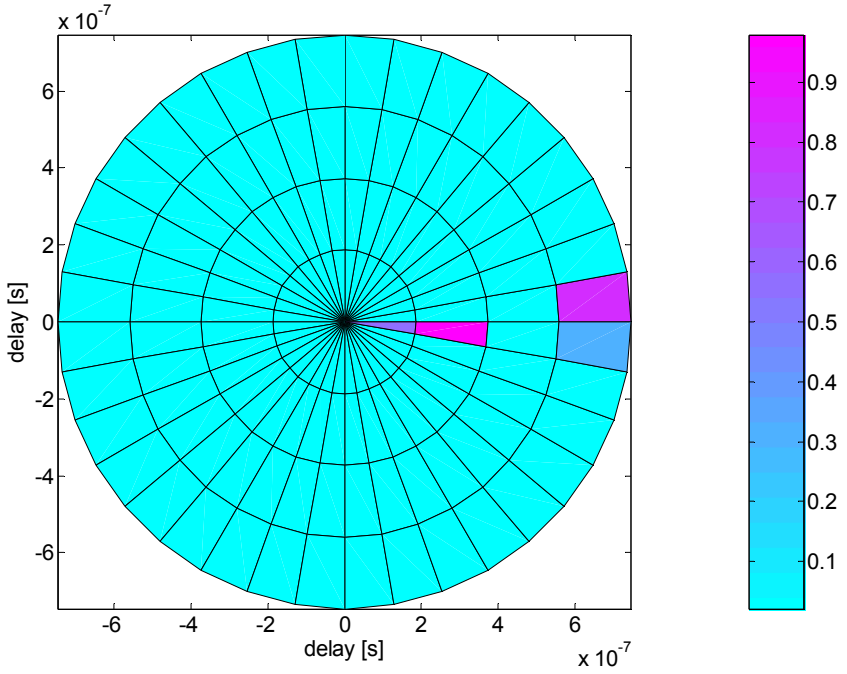

Figure F.7 – Example of the CIR in domain of the AoA and time delay for the highway scenario.

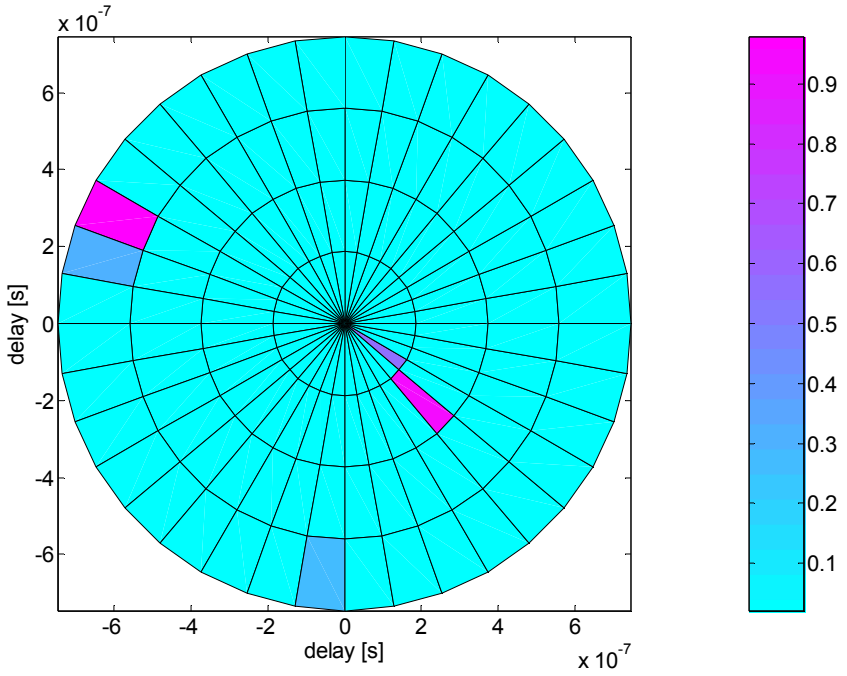

Figure F.8 – Example of the CIR in domain of the AoD and time delay for the highway scenario.

In case of the railway station scenario (pico-cell) the example uplink is taken between the BS and MT1 from scenario 1 in the railway station environment. The parameters of this link are presented in Table 5.8. The environment has 6 clusters. In Figure F.9 and Figure F.10 the unfiltered and filtered CIRs with 2 ns time resolution are presented. Also in this case, the

multipath components are grouped into clusters, the same like the scatterers. In Table F.3 the statistical parameters obtained from this link are presented, and in Figure F.11 and Figure F.12, are the CIRs in 2D domains. For the case of the railway station scenario, the multipath rays propagate over ways, which are spread over the whole circular region. Here, one can not notice, that rays are focused in any special direction.

Table F.3 – Statistical parameters of an example railway station scenario link.

$\bar{\tau}$ [µs]	σ_τ [ns]	$\overline{AoA}$ [deg]	σ_{AoA} [deg]	$\overline{AoD}$ [deg]	σ_{AoD} [deg]
0.18	74.93	23.34	71.51	-24.72	90.04

For this case also the powers were calculated. For the unfiltered CIR, the power is equal to 50.46 mW, and for the filtered with the 2 ns time resolution 50.19 mW. One can make a comparison between the powers obtained from the different scenario. In these three cases, the MTs work with the same Tx power level, therefore the highest level of the power is obtained for the pico- and city street scenario, where the distances are the shortest.

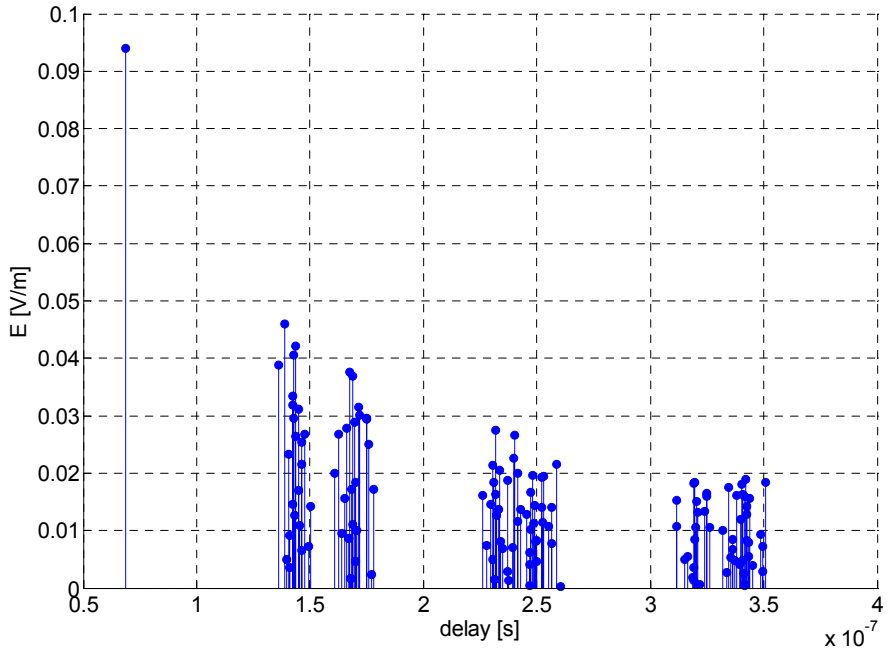

Figure F.9 – Example of the unfiltered CIR in the railway station scenario.

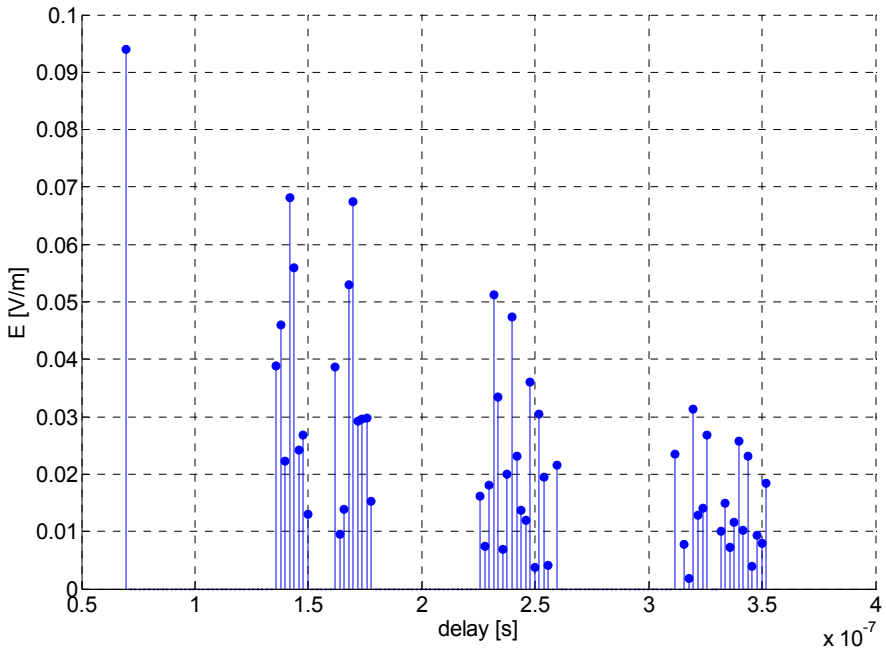

Figure F.10 – Example of the filtered CIR with 2 ns time resolution in the railway station scenario.

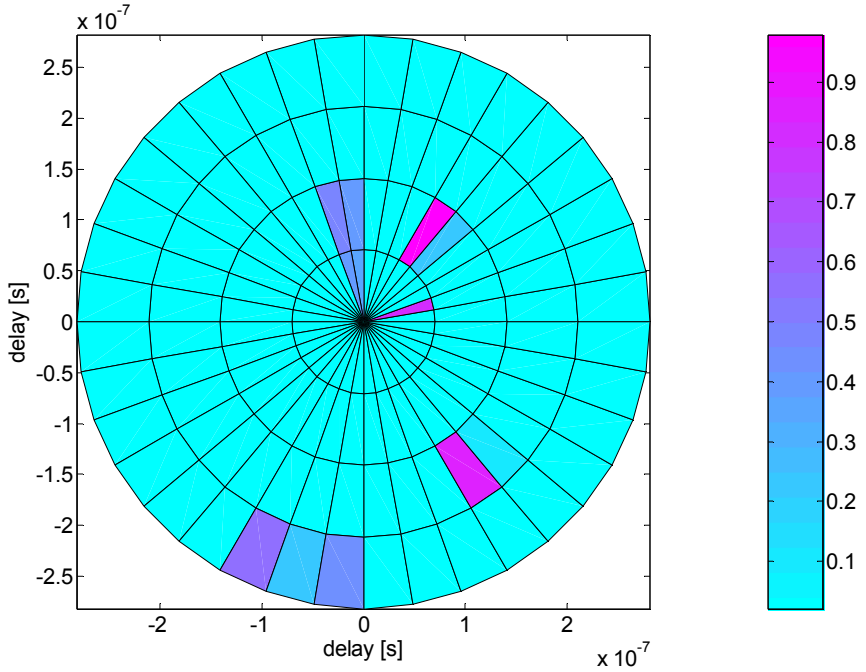

Figure F.11 – Example of the CIR in domain of the AoA and time delay for the railway station scenario.

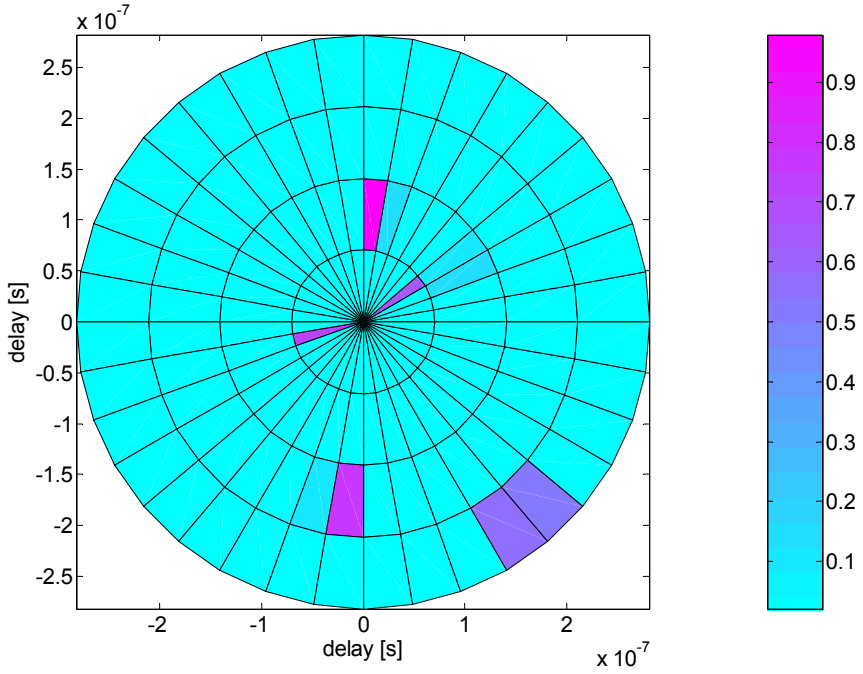

Figure F.12 – Example of the CIR in domain of the AoD and time delay for the railway station scenario.

For every scenario, the channel model is different, but one can find some similarities between the city street (micro-cell) and the railway station (pico-cell) scenarios. For these both cases, the samples of the CIRs in the time domain are distributed more uniformly than in the highway scenario. Also the CIRs in the domains of the time and the AoA and the AoD are not so different. In the highway scenario (macro-cell), the asymmetry between the CIRs in the domain of the AoA and the AoD appears which is caused by the scatterers located only around the MT.

Annex G Example of the CIRs

The CIRs presented in this annex are not filtered and not normalised. They were taken from one of the 100 iterations in mode 3 of the simulator.

The CIRs for deployment 4 in the city street scenario (MT1-BS link):

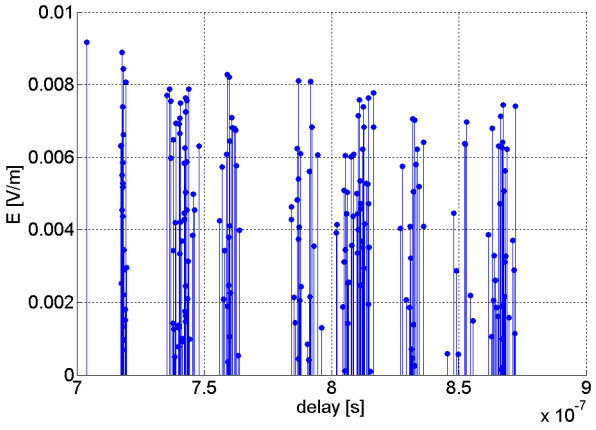

Figure G.1 – Unfiltered CIR.

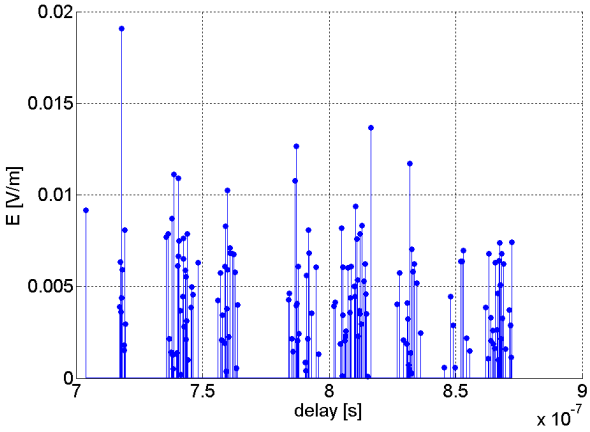

Figure G.2 – CIR with 0.2 ns time resolution.

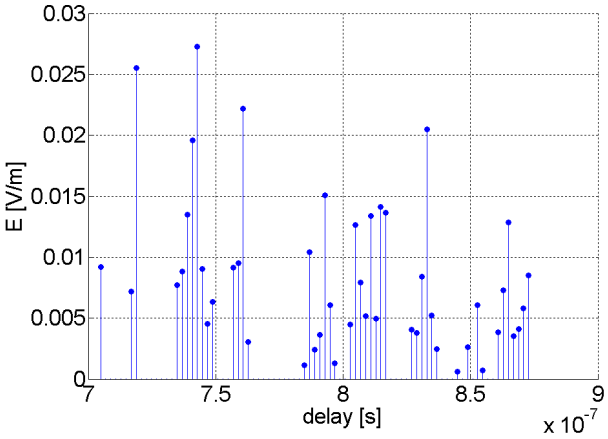

Figure G.3 – CIR with 2 ns time resolution.

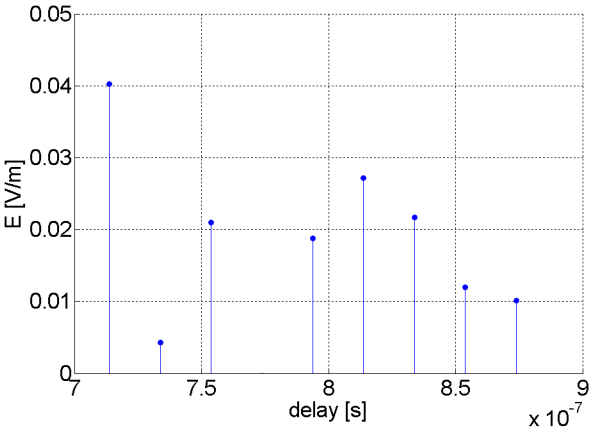

Figure G.4 – CIR with 20 ns time resolution.

The CIRs for deployment 10 in the city street scenario, for case of synchronisation at the Txs:

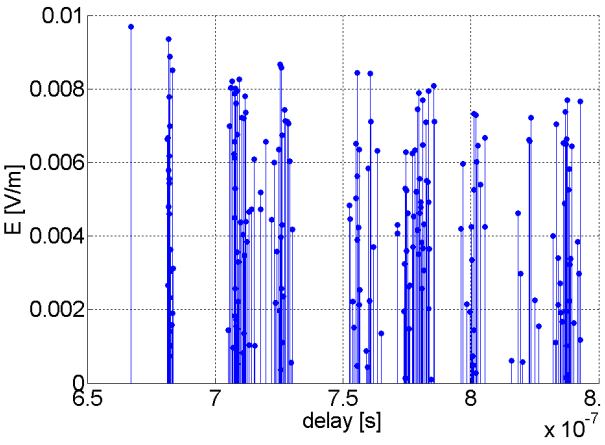

Figure G.5 – CIR of the MT1-BS link.

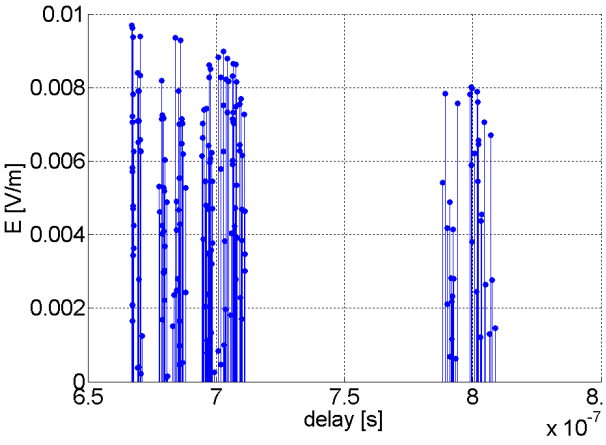

Figure G.6 – CIR of the MT5-BS link.

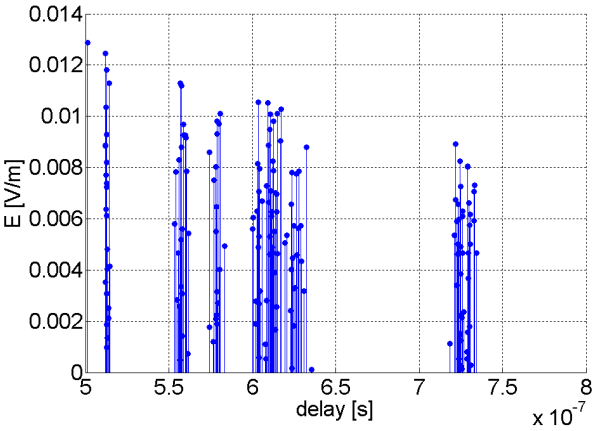

Figure G.7 – CIR of the MT2-BS link.

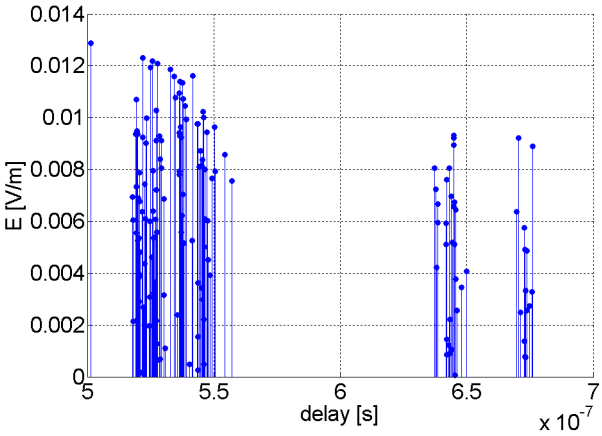

Figure G.8 – CIR of the MT6-BS link.

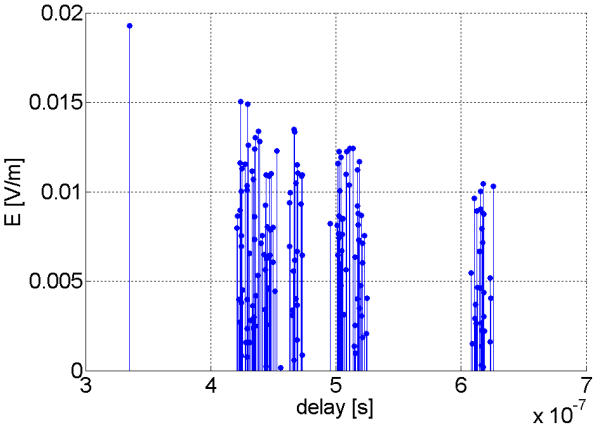

Figure G.9 – CIR of the MT3-BS link.

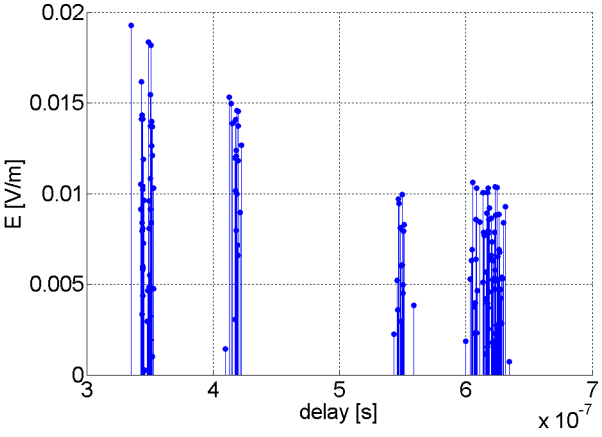

Figure G.10 – CIR of the MT7-BS link.

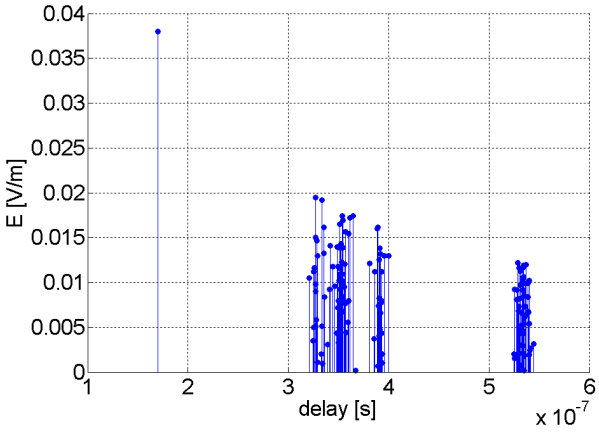

Figure G.11 – CIR of the MT4-BS link.

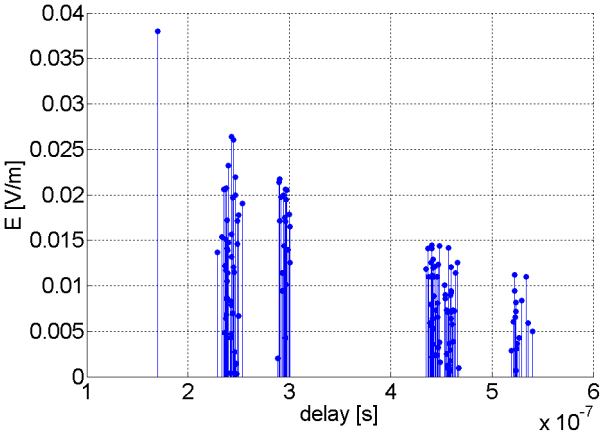

Figure G.12 – CIR of the MT8-BS link.

Annex H GSM mask

In Figure H.1 the GSM spectral mask is presented. Every transmitter in the GSM system has limited power in the neighbour frequencies by this mask. In the simulations, the situations were considered that the interfering Tx, works in frequencies which are located in distance of the 200, 400 and 800 kHz from the desired carrier. Using this mask, it is possible to determine the power of the interferers, and there were taken the following levels: 30 dB, 60 dB and 70 dB below the power at the desired frequencies

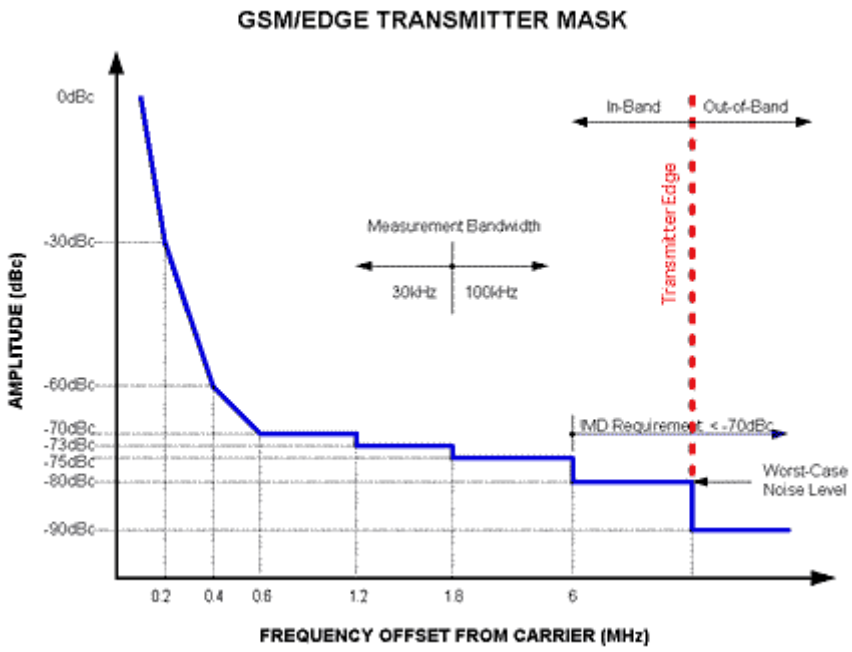

Figure H.1 – GSM mask [MADA03].

Annex I SINRs for the particular scenarios (Rx-synchronisation)

In this annex are presented the results from the particular scenarios: city street, highway and railway station. The numbers of the particular deployments are agreeable with the numbers of the deployments, which are described in Section 5.1. The horizontal axis of each figure presents the consecutive MT-BS links. The number of the link is taken from the number of the MT. The vertical axis shows the SINRs for these links. In the figures are presented the average values, which were obtained from 100 simulations in mode 3 of the simulator. The figures also show the standard deviation of each mean value. In this case the SINR was calculated as described in Section 5.2.3, using unfiltered CIRs.

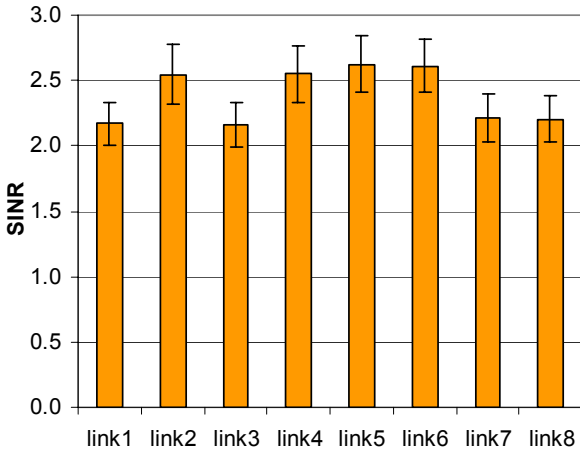

Figure I.1 – SINR for deployment 1 in the city street scenario.

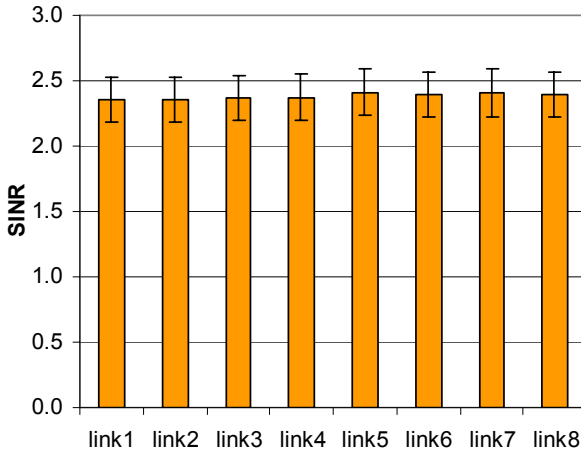

Figure I.2 – SINR for deployment 2 in the city street scenario.

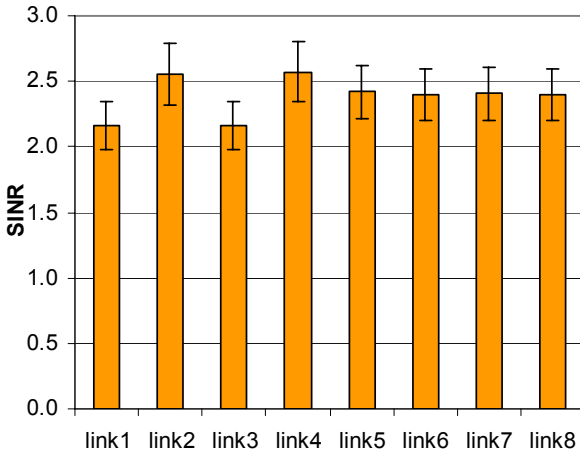

Figure I.3 – SINR for deployment 3 in the city street scenario.

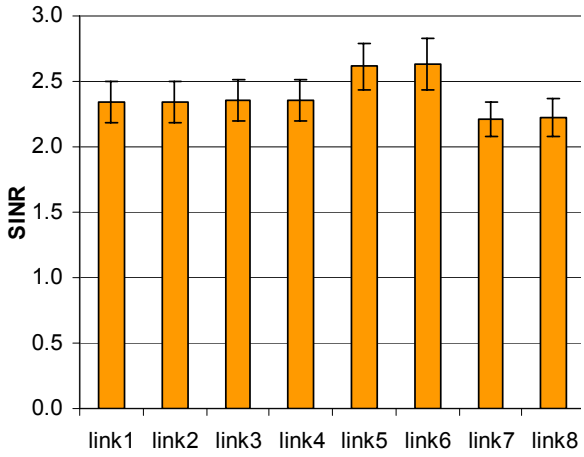

Figure I.4 – SINR for deployment 4 in the city street scenario.

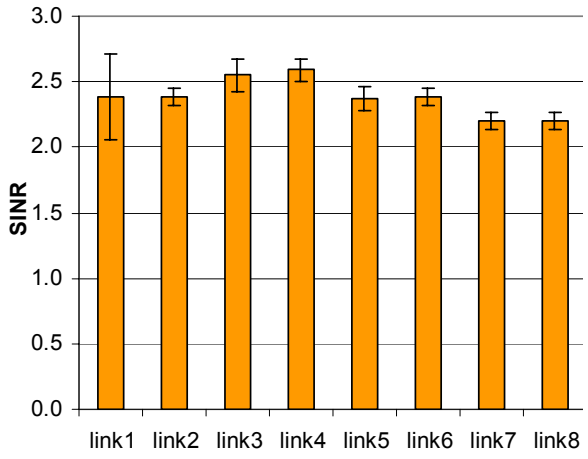

Figure I.5 – SINR for deployment 5 in the city street scenario.

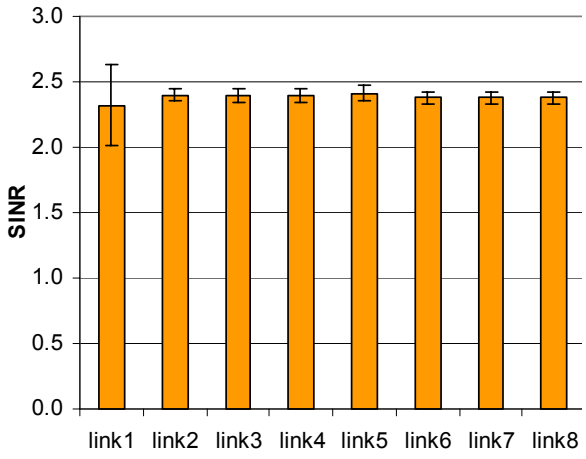

Figure I.6 – SINR for deployment 6 in the city street scenario.

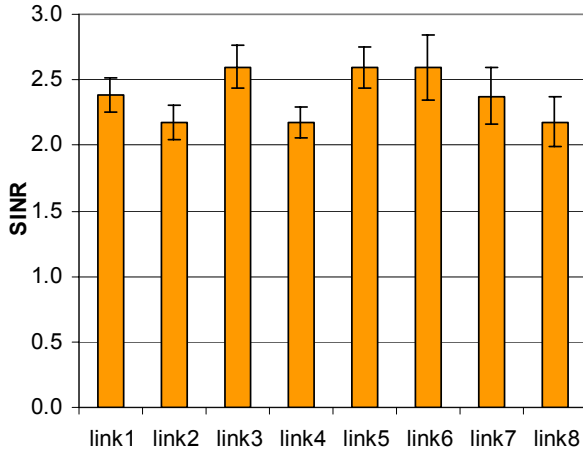

Figure I.7 – SINR for deployment 7 in the city street scenario.

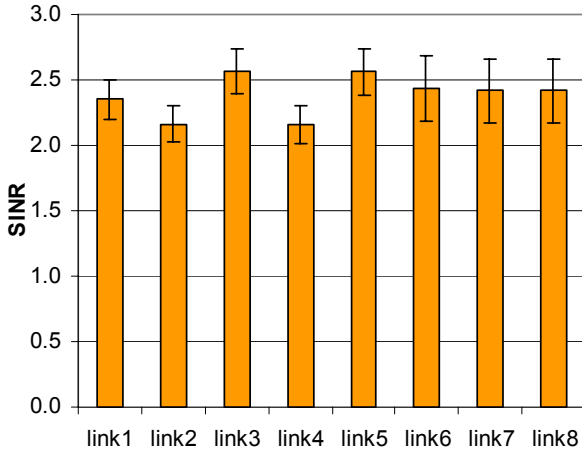

Figure I.8 – SINR for deployment 8 in the city street scenario.

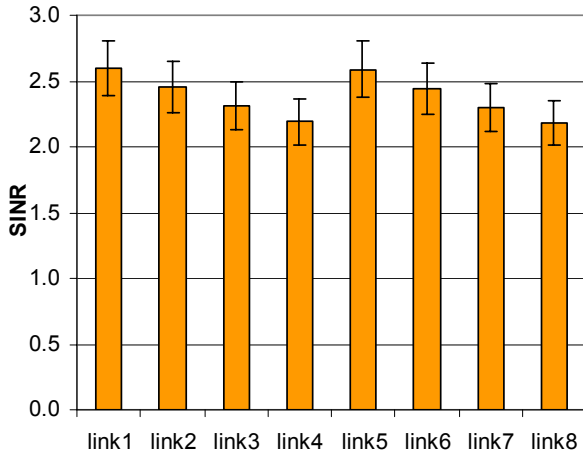

Figure I.9 – SINR for deployment 9 in the city street scenario.

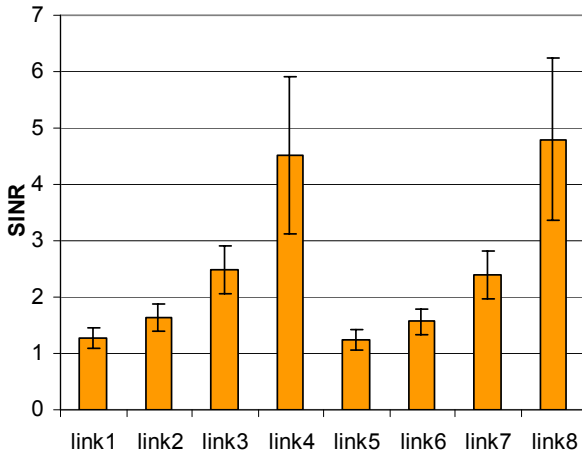

Figure I.10 – SINR for deployment 10 in the city street scenario.

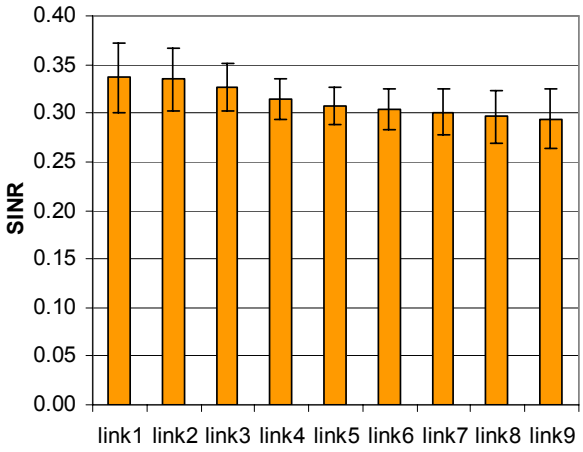

Figure I.11 – SINR for deployment 1 in the highway scenario.

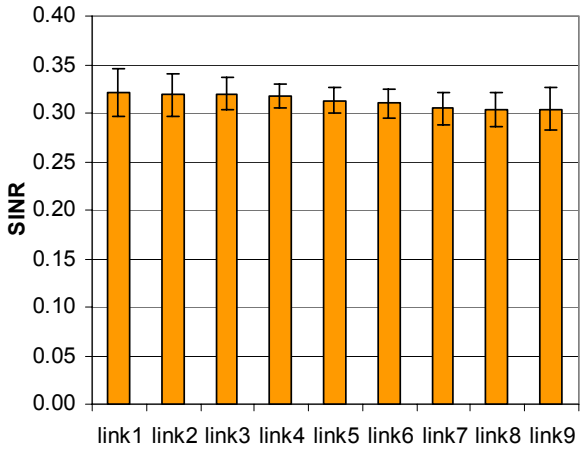

Figure I.12 – SINR for deployment 2 in the highway scenario.

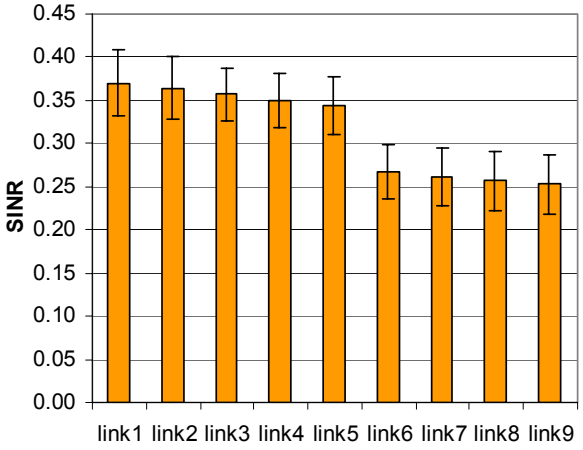

Figure I.13 – SINR for deployment 3 in the highway scenario.

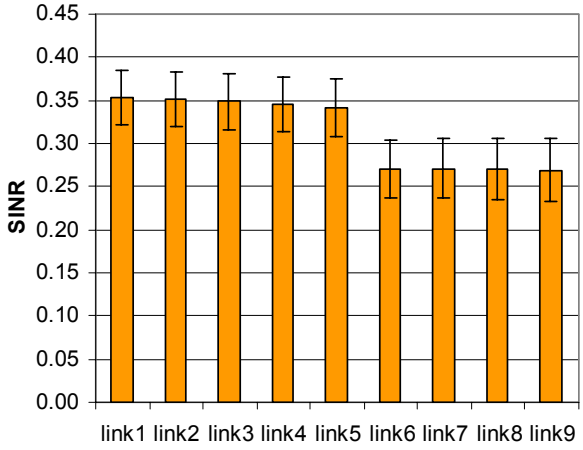

Figure I.14 – SINR for deployment 4 in the highway scenario.

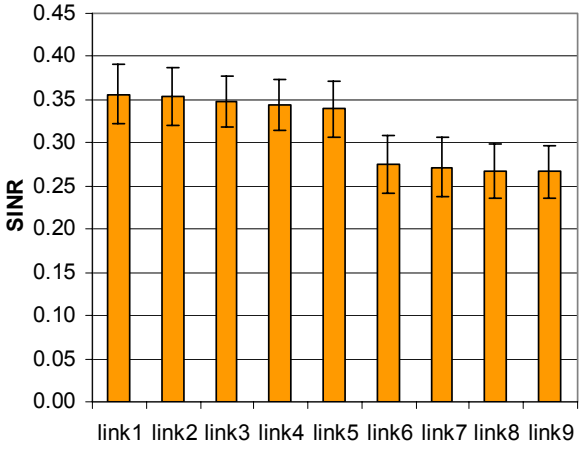

Figure I.15 – SINR for deployment 5 in the highway scenario.

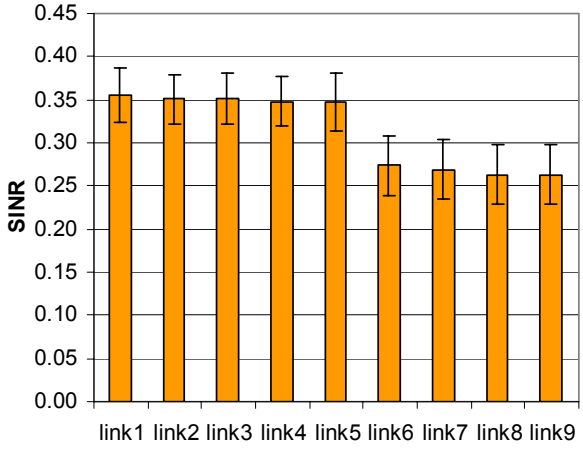

Figure I.16 – SINR for deployment 6 in the highway scenario.

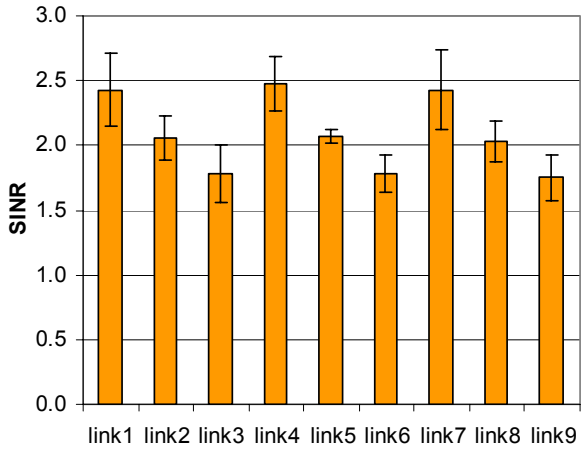

Figure I.17 – SINR for deployment 1 in the railway station scenario.

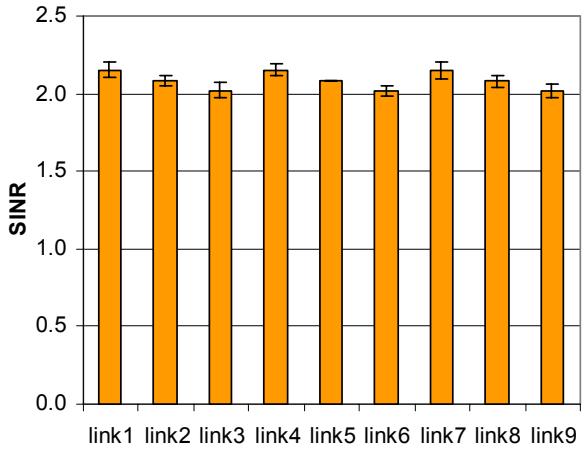

Figure I.18 – SINR for deployment 2 in the railway station scenario.

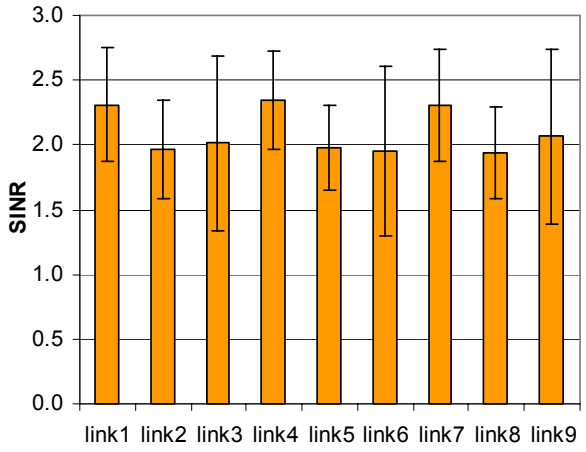

Figure I.19 – SINR for deployment 3 in the railway station scenario.

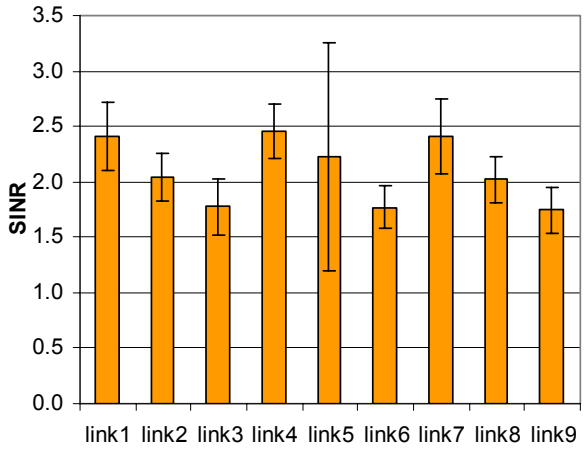

Figure I.20 – SINR for deployment 4 in the railway station scenario.

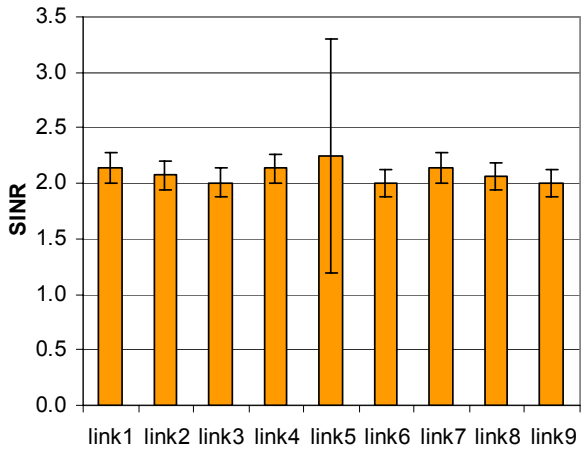

Figure I.21 – SINR for deployment 5 in the railway station scenario.

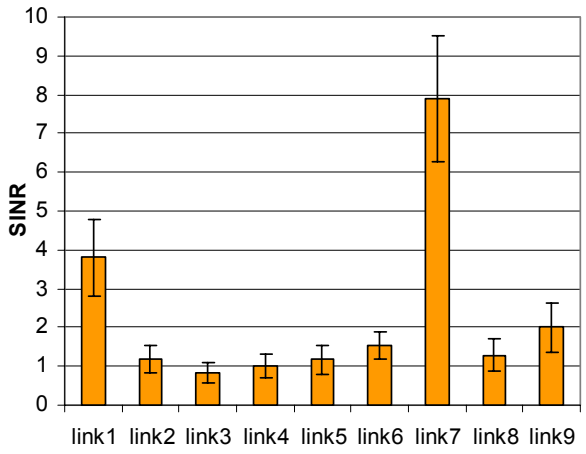

Figure I.22 – SINR for deployment 6 in the railway station scenario.

Annex J SINRs for the particular scenarios (Tx-synchronisation)

In this annex are presented the results from the particular scenarios: city street, highway and railway station. The numbers of the particular deployments are agreeable with the numbers of the deployments, which are described in Section 5.1. The horizontal axis of the each figure presents the MT-BS links. The number of the link is taken from the number of the MT. The vertical axis shows the SINRs for these links. In the figures the average values are presented, which were obtained from 100 simulations in mode 3 of the simulator. The figures also show the standard deviation of each mean value. In this case the SINR was calculated as described in Section 5.2.3, using unfiltered CIRs.

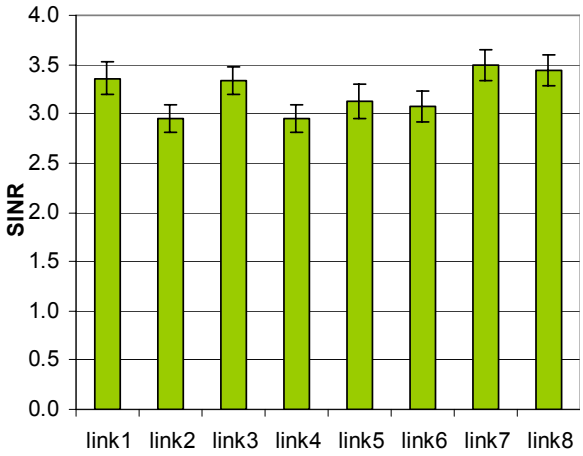

Figure J.1 – SINR for deployment 1 in the city street scenario.

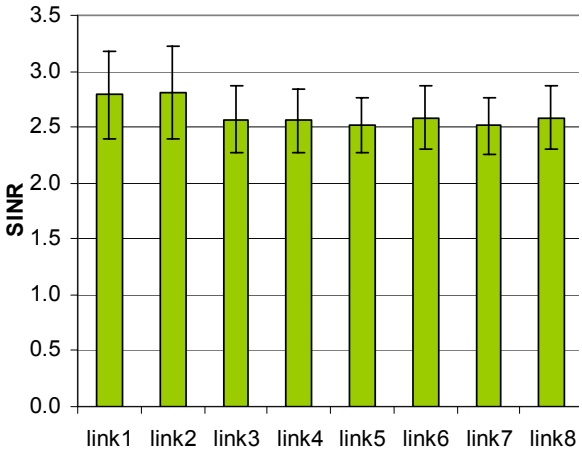

Figure J.2 – SINR for deployment 2 in the city street scenario.

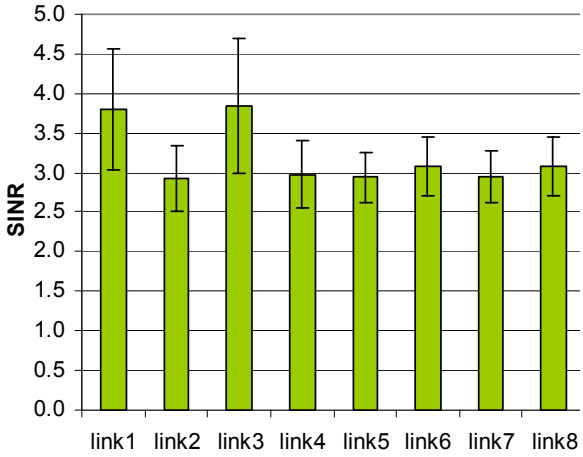

Figure J.3 – SINR for deployment 3 in the city street scenario.

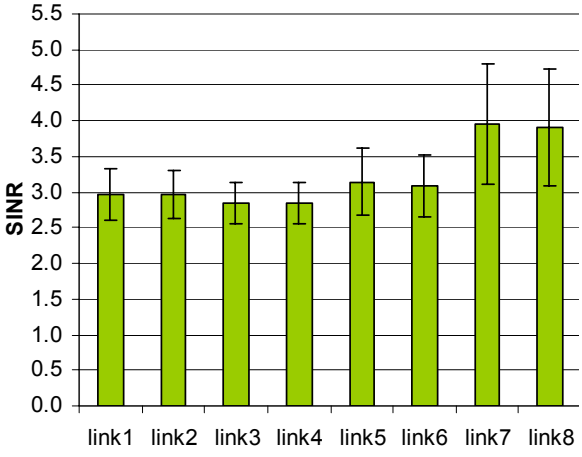

Figure J.4 – SINR for deployment 4 in the city street scenario.

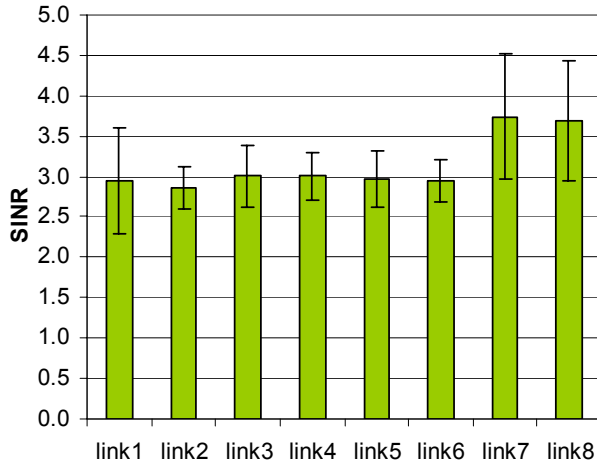

Figure J.5 – SINR for deployment 5 in the city street scenario.

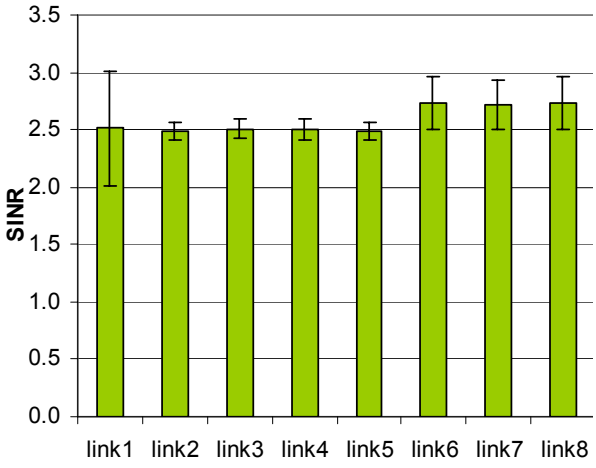

Figure J.6 – SINR for deployment 6 in the city street scenario.

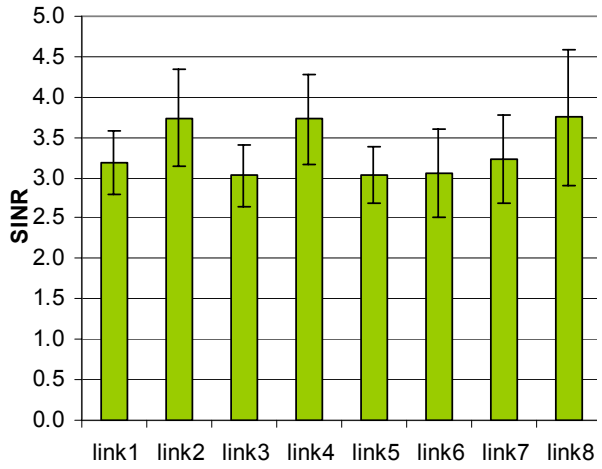

Figure J.7 – SINR for deployment 7 in the city street scenario.

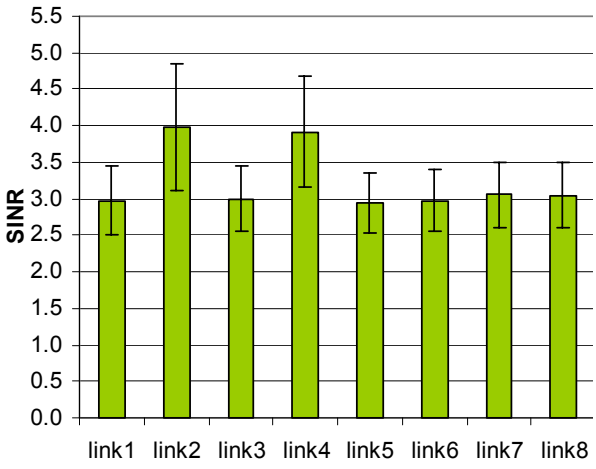

Figure J.8 – SINR for deployment 8 in the city street scenario.

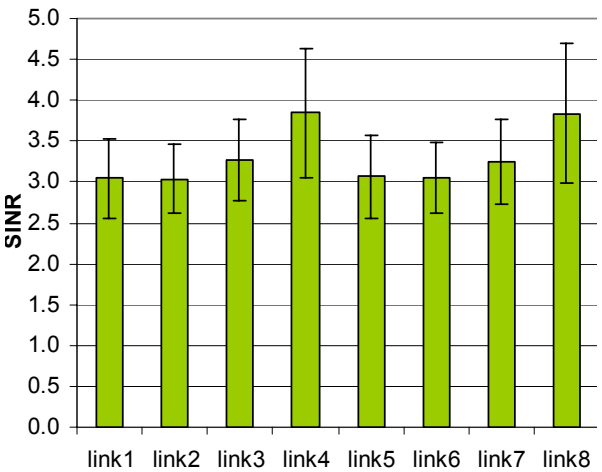

Figure J.9 – SINR for deployment 9 in the city street scenario.

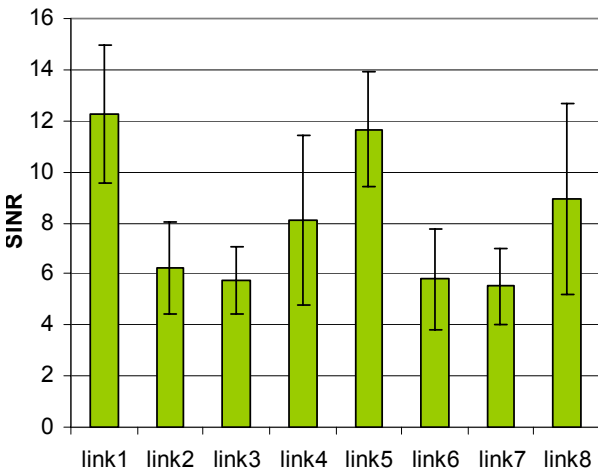

Figure J.10 – SINR for deployment 10 in the city street scenario.

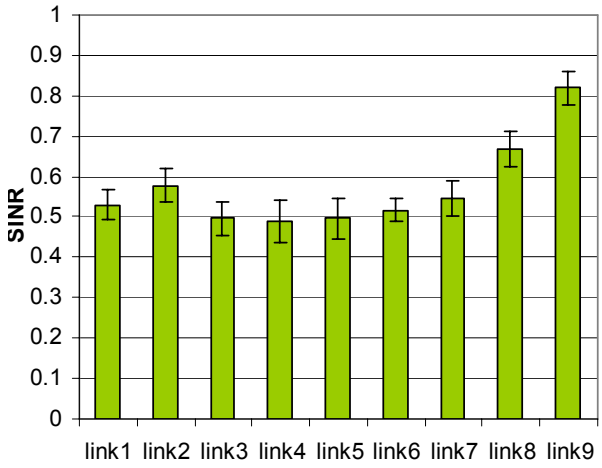

Figure J.11 – SINR for deployment 1 in the highway scenario.

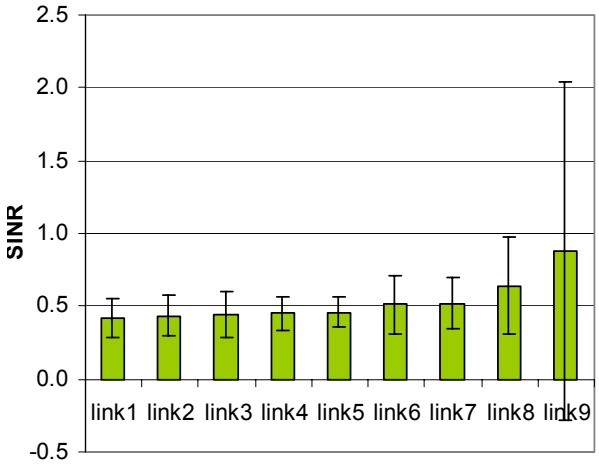

Figure J.12 – SINR for deployment 2 in the highway scenario.

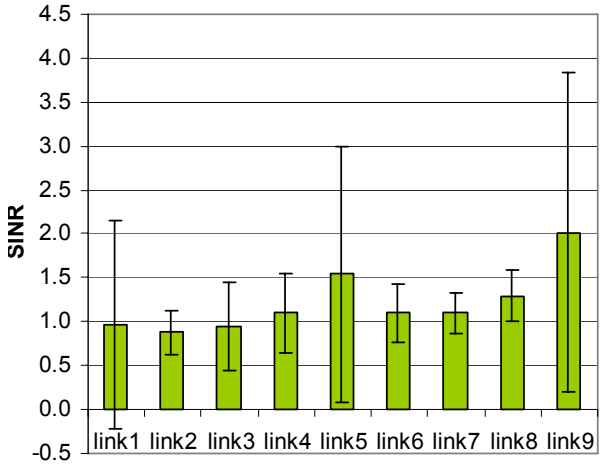

Figure J.13 – SINR for deployment 3 in the highway scenario.

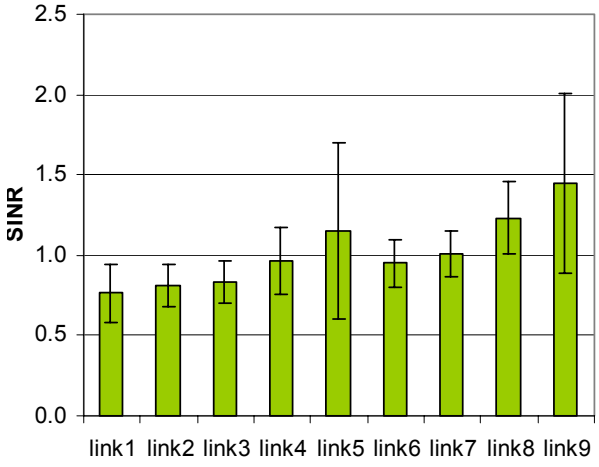

Figure J.14 – SINR for deployment 4 in the highway scenario.

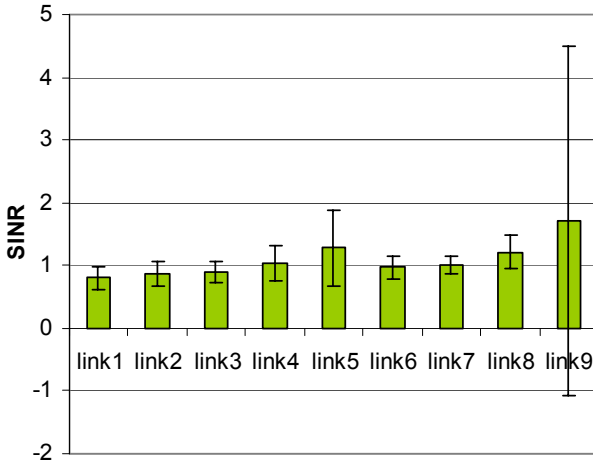

Figure J.15 – SINR for deployment 5 in the highway scenario.

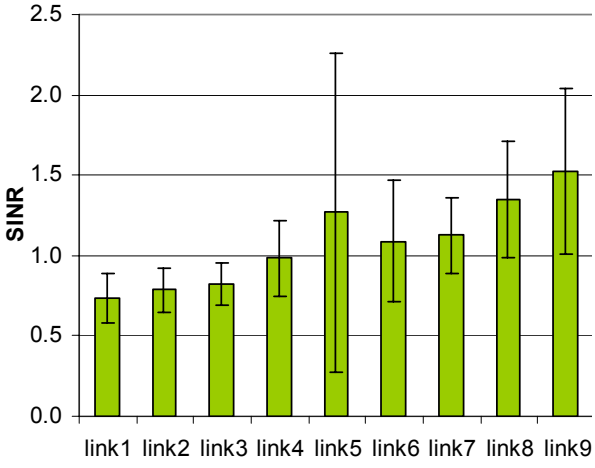

Figure J.16 – SINR for deployment 6 in the highway scenario.

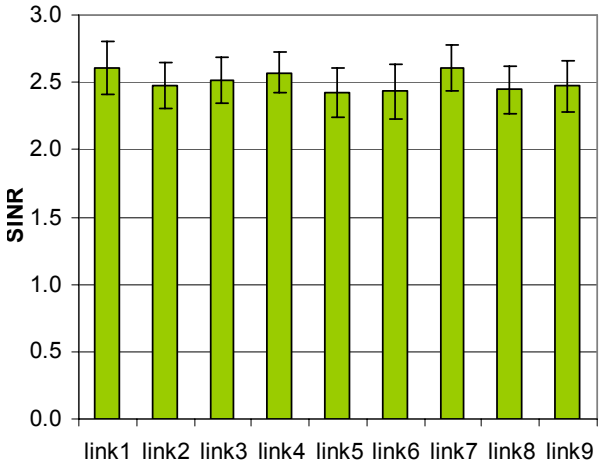

Figure J.17 – SINR for deployment 1 in the railway station scenario.

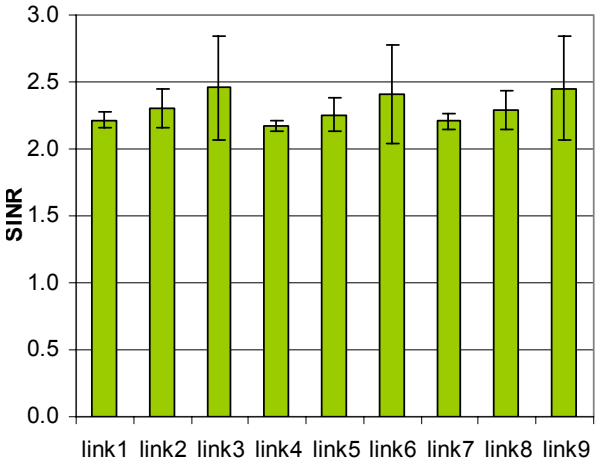

Figure J.18 – SINR for deployment 2 in the railway station scenario.

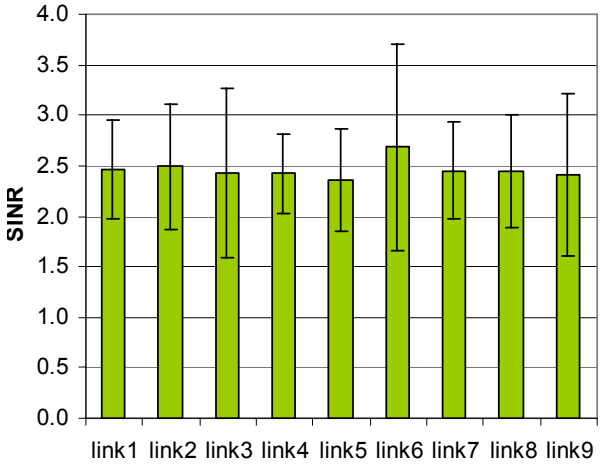

Figure J.19 – SINR for deployment 3 in the railway station scenario.

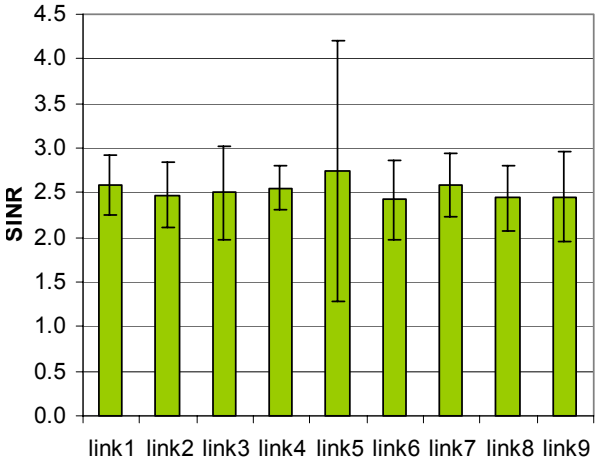

Figure J.20 – SINR for deployment 4 in the railway station scenario.

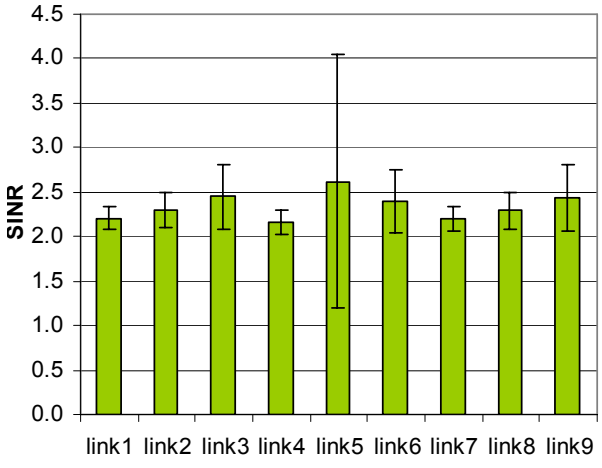

Figure J.21 – SINR for deployment 5 in the railway station scenario.

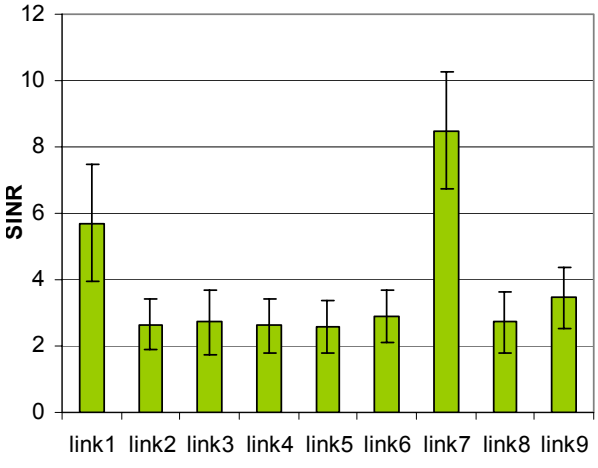

Figure J.22 – SINR for deployment 6 in the railway station scenario.

Annex K Statistical parameters of the links

This annex contains the statistical parameters, which were obtained from the simulations. All the simulations were made for 100 iterations and for mode 3 of the simulator. The results are presented in the tables. The tables are divided into sections, and every section corresponds to the particular deployments. The numbers of the deployments are agreeable with the numbers of the deployments, which were presented in Section 5.1. The columns of the tables present the particular links between the terminals (both the MT and the BS) in the environment. The statistical parameters are presented by the mean value and the standard deviation. The CIRs, which were taken to make calculations, were normalised relative to the delay of the LoS component, the amplitude is kept in not normalised and not filtered form.

- The uplink in the city street scenario:

Table K.1 – Statistical parameters of delays in the city street scenario in the uplink.

		MT1-BS	MT2-BS	MT3-BS	MT4-BS	MT5-BS	MT6-BS	MT7-BS	MT8-BS
Deployment 1									
$\bar{\tau}$	μ [ns]	65.59	78.01	65.30	74.55	69.76	68.07	57.45	60.84
	σ [ns]	20.36	25.97	20.31	21.70	21.69	21.48	18.62	18.23
σ_τ	μ [ns]	47.66	53.81	48.83	54.44	52.46	53.36	46.04	47.29
	σ [ns]	9.32	10.88	9.38	9.92	9.31	9.91	10.10	9.33
Deployment 2									
$\bar{\tau}$	μ [ns]	66.99	66.11	66.69	66.11	65.71	65.59	67.11	65.65
	σ [ns]	19.03	20.09	19.40	20.49	22.45	21.54	20.85	22.39
σ_τ	μ [ns]	50.40	50.02	50.61	50.26	49.43	49.33	50.15	48.78
	σ [ns]	8.84	9.58	9.02	8.88	9.61	9.22	9.30	9.07
Deployment 3									
$\bar{\tau}$	μ [ns]	65.40	76.86	64.96	75.24	64.26	63.46	63.20	64.08
	σ [ns]	19.84	24.40	18.11	24.15	22.53	20.86	21.32	22.93

Table K.1 (contd.) – Statistical parameters of delays in the city street scenario in the uplink.

σ_τ	μ [ns]	49.52	56.59	49.47	55.35	49.70	49.50	49.05	49.00
	σ [ns]	8.18	8.64	9.29	9.45	9.90	10.16	9.62	9.91
Deployment 4									
$\bar{\tau}$	μ [ns]	65.44	66.51	66.48	65.42	69.05	69.42	60.51	59.23
	σ [ns]	20.62	21.81	21.35	20.59	20.14	20.51	18.93	18.77
σ_τ	μ [ns]	49.54	49.53	49.95	49.99	52.06	52.33	45.42	46.35
	σ [ns]	10.72	10.86	10.56	10.76	9.54	9.56	9.99	9.81
Deployment 5									
$\bar{\tau}$	μ [ns]	67.73	71.46	73.36	76.26	66.73	70.29	61.72	64.03
	σ [ns]	19.77	24.25	24.73	25.01	23.67	23.36	22.90	23.53
σ_τ	μ [ns]	50.80	50.26	53.94	54.16	49.61	49.93	46.84	46.83
	σ [ns]	9.57	9.94	9.89	9.66	9.63	9.23	10.07	9.47
Deployment 6									
$\bar{\tau}$	μ [ns]	67.37	65.29	63.07	63.75	64.55	62.82	64.86	62.49
	σ [ns]	19.06	20.54	20.84	19.04	20.46	20.30	19.77	19.22
σ_τ	μ [ns]	51.09	50.61	49.89	50.99	51.18	49.96	50.82	50.52
	σ [ns]	9.29	9.71	9.37	10.09	9.95	9.45	9.75	9.87
Deployment 7									
$\bar{\tau}$	μ [ns]	61.60	57.29	65.33	57.45	68.25	66.17	62.10	56.16
	σ [ns]	19.27	19.29	23.91	21.25	25.46	21.83	20.04	20.60
σ_τ	μ [ns]	50.55	46.49	52.49	46.73	53.29	51.90	48.94	45.39
	σ [ns]	9.29	8.59	10.17	8.74	10.13	10.66	9.65	9.85
Deployment 8									
$\bar{\tau}$	μ [ns]	62.68	59.61	67.60	57.91	70.09	63.47	64.96	62.55
	σ [ns]	17.71	17.05	19.97	19.79	21.67	24.16	22.22	22.96
σ_τ	μ [ns]	50.56	46.89	52.99	47.12	54.52	49.67	50.21	48.99
	σ [ns]	10.06	10.13	10.10	9.70	10.69	10.92	11.07	10.79
Deployment 9									
$\bar{\tau}$	μ [ns]	68.13	65.82	63.81	59.57	68.69	64.46	64.61	60.62
	σ [ns]	20.38	19.92	20.30	19.70	22.11	19.91	20.90	19.08
σ_τ	μ [ns]	53.49	51.22	49.17	47.20	52.39	49.69	47.99	45.84
	σ [ns]	10.16	10.13	10.26	9.69	10.07	10.16	9.92	8.93

Table K.1 (contd.) – Statistical parameters of delays in the city street scenario in the uplink.

Deployment 10									
$\bar{\tau}$	μ [ns]	72.21	88.85	122.80	153.40	71.67	91.99	111.40	143.92
	σ [ns]	20.93	27.06	37.24	54.66	20.31	30.20	42.06	56.01
σ_τ	μ [ns]	53.89	63.81	81.42	107.60	53.40	65.25	80.96	105.60
	σ [ns]	9.28	12.01	15.88	18.14	9.28	11.91	16.32	19.57

Table K.2 – Statistical parameters of powers in the city street scenario in the uplink.

	MT1-BS	MT2-BS	MT3-BS	MT4-BS	MT5-BS	MT6-BS	MT7-BS	MT8-BS
Deployment 1								
μ_P [mW]	4.38	5.04	4.37	5.05	5.17	5.15	4.46	4.44
σ_P [μW]	0.22	0.36	0.22	0.36	0.29	0.26	0.21	0.19
Deployment 2								
μ_P [mW]	4.77	4.77	4.79	4.80	4.88	4.85	4.87	4.84
σ_P [μW]	0.21	0.21	0.22	0.22	0.28	0.27	0.29	0.28
Deployment 3								
μ_P [mW]	4.45	5.13	4.44	5.16	4.90	4.86	4.87	4.86
σ_P [μW]	0.22	0.32	0.24	0.34	0.23	0.22	0.23	0.22
Deployment 4								
μ_P [mW]	4.74	4.74	4.76	4.77	5.22	5.25	4.51	4.52
σ_P [μW]	0.18	0.18	0.19	0.18	0.24	0.24	0.17	0.17
Deployment 5								
μ_P [mW]	4.80	4.85	5.15	5.21	4.83	4.85	4.52	4.51
σ_P [μW]	0.22	0.31	0.45	0.35	0.34	0.30	0.25	0.24
Deployment 6								
μ_P [mW]	4.75	4.93	4.92	4.92	4.95	4.89	4.89	4.89
σ_P [μW]	0.24	0.23	0.24	0.23	0.24	0.22	0.22	0.22
Deployment 7								
μ_P [mW]	4.90	4.53	5.28	4.52	5.27	5.25	4.87	4.52
σ_P [μW]	0.23	0.20	0.29	0.18	0.28	0.26	0.21	0.17

Table K.2 (contd.) – Statistical parameters of powers in the city street scenario in the uplink.

Deployment 8								
μ_P [mW]	4.78	4.43	5.16	4.44	5.15	4.91	4.88	4.88
σ_P [μW]	0.28	0.24	0.31	0.24	0.33	0.26	0.25	0.26
Deployment 9								
μ_P [mW]	5.21	4.95	4.71	4.48	5.19	4.93	4.68	4.46
σ_P [μW]	0.29	0.26	0.23	0.20	0.28	0.25	0.22	0.19
Deployment 10								
μ_P [mW]	5.24	6.63	9.61	15.98	5.12	6.36	9.33	16.72
σ_P [μW]	0.30	0.72	2.83	29.41	0.24	0.66	2.95	29.95

- The uplink in the highway scenario:

Table K.3 – Statistical parameters of delays in the highway scenario in the uplink.

		MT1 -BS	MT2 -BS	MT3 -BS	MT4 -BS	MT5 -BS	MT6 -BS	MT7 -BS	MT8 -BS	MT9 -BS
Deployment 1										
$\bar{\tau}$	μ [μs]	0.35	0.33	0.36	0.36	0.37	0.36	0.35	0.36	0.37
	σ [μs]	0.14	0.14	0.15	0.14	0.15	0.15	0.15	0.16	0.13
σ_τ	μ [μs]	0.30	0.28	0.29	0.29	0.29	0.29	0.31	0.30	0.32
	σ [μs]	0.10	0.10	0.09	0.09	0.10	0.10	0.11	0.10	0.10
Deployment 2										
$\bar{\tau}$	μ [μs]	0.34	0.34	0.35	0.34	0.33	0.34	0.35	0.34	0.34
	σ [μs]	0.16	0.15	0.17	0.15	0.16	0.18	0.18	0.16	0.16
σ_τ	μ [μs]	0.28	0.27	0.27	0.28	0.28	0.29	0.29	0.29	0.29
	σ [μs]	0.10	0.11	0.11	0.11	0.11	0.11	0.11	0.11	0.10
Deployment 3										
$\bar{\tau}$	μ [μs]	0.36	0.35	0.34	0.35	0.35	0.39	0.39	0.36	0.35
	σ [μs]	0.15	0.14	0.14	0.16	0.14	0.17	0.17	0.15	0.17
σ_τ	μ [μs]	0.29	0.29	0.29	0.29	0.31	0.30	0.29	0.30	0.29
	σ [μs]	0.10	0.09	0.10	0.10	0.11	0.10	0.11	0.11	0.10

Table K.3 (contd.) – Statistical parameters of delays in the highway scenario in the uplink.

Deployment 4										
$\bar{\tau}$	μ [μs]	0.36	0.36	0.38	0.39	0.39	0.39	0.36	0.36	0.35
	σ [μs]	0.15	0.17	0.17	0.17	0.17	0.16	0.15	0.16	0.15
σ_τ	μ [μs]	0.31	0.31	0.32	0.32	0.31	0.30	0.30	0.30	0.29
	σ [μs]	0.10	0.11	0.10	0.10	0.10	0.10	0.11	0.11	0.10
Deployment 5										
$\bar{\tau}$	μ [μs]	0.37	0.37	0.35	0.37	0.37	0.37	0.36	0.37	0.36
	σ [μs]	0.16	0.15	0.15	0.16	0.16	0.16	0.16	0.16	0.15
σ_τ	μ [μs]	0.30	0.29	0.29	0.30	0.31	0.29	0.29	0.30	0.30
	σ [μs]	0.09	0.10	0.10	0.09	0.09	0.10	0.09	0.10	0.09
Deployment 6										
$\bar{\tau}$	μ [μs]	0.37	0.37	0.38	0.36	0.37	0.39	0.37	0.36	0.38
	σ [μs]	0.16	0.18	0.16	0.16	0.15	0.15	0.16	0.15	0.15
σ_τ	μ [μs]	0.30	0.30	0.32	0.31	0.31	0.31	0.29	0.27	0.30
	σ [μs]	0.11	0.10	0.10	0.10	0.10	0.10	0.10	0.09	0.09

Table K.4 – Statistical parameters of powers in the highway scenario in the uplink.

	MT1-BS	MT2-BS	MT3-BS	MT4-BS	MT5-BS	MT6-BS	MT7-BS	MT8-BS	MT9-BS
Deployment 1									
μ_P [μW]	12.85	12.80	12.53	12.14	11.93	11.78	11.66	11.49	11.38
σ_P [pW]	3.28	3.17	2.93	2.85	2.89	2.63	2.46	2.50	2.33
Deployment 2									
μ_P [μW]	12.88	12.82	12.85	12.78	12.62	12.52	12.34	12.31	12.31
σ_P [pW]	2.26	2.21	2.21	2.07	2.13	2.28	2.44	2.45	2.59
Deployment 3									
μ_P [μW]	12.80	12.64	12.40	12.19	12.03	9.56	9.35	9.22	9.10
σ_P [pW]	2.80	2.81	2.34	2.23	2.25	1.54	1.64	1.64	1.66
Deployment 4									
μ_P [μW]	12.45	12.40	12.34	12.22	12.12	9.83	9.83	9.79	9.75
σ_P [pW]	2.61	2.64	2.95	3.08	3.03	1.93	2.01	2.07	2.09

Table K.4 (contd.) – Statistical parameters of powers in the highway scenario in the uplink.

Deployment 5									
μ_P [μW]	12.44	12.36	12.20	12.06	11.90	9.85	9.76	9.65	9.60
σ_P [pW]	2.67	2.68	2.35	2.37	2.24	2.01	2.11	1.91	1.77
Deployment 6									
μ_P [μW]	12.53	12.43	12.45	12.35	12.34	9.95	9.80	9.60	9.57
σ_P [pW]	2.36	2.60	2.57	2.54	2.90	2.04	2.22	2.11	1.83

- The uplink in the railway station scenario:

Table K.5 – Statistical parameters of delays in the railway station scenario in the uplink.

		MT1-BS	MT2-BS	MT3-BS	MT4-BS	MT5-BS	MT6-BS	MT7-BS	MT8-BS	MT9-BS
Deployment 1										
$\bar{\tau}$	μ [ns]	91.33	87.65	90.12	92.69	92.53	92.13	93.27	94.10	90.84
	σ [ns]	32.91	34.68	36.12	32.74	34.72	33.43	34.04	34.97	35.42
σ_τ	μ [ns]	76.20	73.40	74.26	77.08	74.52	73.16	75.70	73.78	72.16
	σ [ns]	17.17	16.00	18.14	18.04	18.28	18.41	17.29	17.77	18.10
Deployment 2										
$\bar{\tau}$	μ [ns]	92.51	89.58	91.95	91.99	92.53	92.97	92.01	92.40	92.50
	σ [ns]	34.36	34.20	33.57	33.26	34.72	34.02	33.31	35.08	34.71
σ_τ	μ [ns]	74.99	74.12	74.39	74.92	74.52	74.19	74.81	74.38	75.30
	σ [ns]	17.17	17.92	18.03	17.12	18.28	18.56	17.05	17.75	17.71
Deployment 3										
$\bar{\tau}$	μ [ns]	91.33	87.65	94.53	92.69	92.53	94.14	93.27	94.10	95.56
	σ [ns]	32.91	34.68	34.49	32.74	34.72	33.75	34.04	34.97	32.72
σ_τ	μ [ns]	76.20	73.40	71.62	77.08	74.52	71.74	75.70	73.78	72.77
	σ [ns]	17.17	16.00	17.50	18.04	18.28	16.13	17.29	17.77	16.08
Deployment 4										
$\bar{\tau}$	μ [ns]	91.33	87.65	90.12	92.69	94.53	92.13	93.27	94.10	90.84
	σ [ns]	32.91	34.68	36.12	32.74	34.49	33.43	34.04	34.97	35.42

Table K.5 (contd.) – Statistical parameters of delays in the railway station scenario in the uplink.

σ_τ	μ [ns]	76.20	73.40	74.26	77.08	71.62	73.16	75.70	73.78	72.16
	σ [ns]	17.17	16.00	18.14	18.04	17.50	18.41	17.29	17.77	18.10
Deployment 5										
$\bar{\tau}$	μ [ns]	92.51	89.58	91.95	91.99	94.53	92.97	92.01	92.40	92.50
	σ [ns]	34.36	34.20	33.57	33.26	34.49	34.02	33.31	35.08	34.71
σ_τ	μ [ns]	74.99	74.12	74.39	74.92	71.62	74.19	74.81	74.38	75.30
	σ [ns]	17.17	17.92	18.03	17.12	17.50	18.56	17.05	17.75	17.71
Deployment 6										
$\bar{\tau}$	μ [ns]	67.74	87.86	84.41	89.36	92.13	98.54	42.24	88.15	94.66
	Σ [ns]	18.62	35.68	36.54	34.85	33.82	29.73	8.81	33.94	30.21
σ_τ	μ [ns]	83.50	69.43	70.11	69.63	71.39	74.28	74.62	70.84	77.37
	σ [ns]	18.89	18.13	17.27	15.71	16.07	15.21	14.45	17.90	17.14

Table K.6 – Statistical parameters of powers in the railway station scenario in the uplink.

	MT1-BS	MT2-BS	MT3-BS	MT4-BS	MT5-BS	MT6-BS	MT7-BS	MT8-BS	MT9-BS
Deployment 1									
μ_P [mW]	59.40	50.93	44.35	60.66	51.45	44.44	59.68	50.64	43.77
σ_P [mW]	0.56	0.34	0.23	0.60	0.36	0.23	0.62	0.37	0.23
Deployment 2									
μ_P [mW]	53.08	51.49	49.96	53.06	51.45	49.91	52.99	51.37	49.82
σ_P [mW]	0.39	0.36	0.33	0.40	0.36	0.33	0.40	0.36	0.33
Deployment 3									
μ_P [mW]	59.40	50.93	50.28	60.66	51.45	48.85	59.68	50.64	51.66
σ_P [mW]	0.56	0.34	0.37	0.60	0.36	0.34	0.62	0.37	0.40
Deployment 4									
μ_P [mW]	59.40	50.93	44.35	60.66	50.28	44.44	59.68	50.64	43.77
σ_P [mW]	0.56	0.34	0.23	0.60	0.37	0.23	0.62	0.37	0.23
Deployment 5									
μ_P [mW]	53.08	51.49	49.96	53.06	50.28	49.91	52.99	51.37	49.82
σ_P [mW]	0.39	0.36	0.33	0.40	0.37	0.33	0.40	0.36	0.33

Table K.6 (contd.) – Statistical parameters of powers in the railway station scenario in the uplink.

Deployment 6									
μ_P [mW]	112.88	38.99	26.63	32.98	37.52	49.59	190.91	41.53	63.66
σ_P [mW]	2.78	0.16	0.05	0.11	0.13	0.29	5.76	0.22	0.77

- The downlink in the city street scenario:

Table K.7 – Statistical parameters of delays in the city street scenario in the downlink (1).

		BS - MT1	MT2-MT1	MT3-MT1	MT4-MT1
Deployment 1					
$\bar{\tau}$	μ [ns]	62.29	131.03	132.70	149.48
	σ [ns]	17.27	42.52	42.31	52.69
σ_τ	μ [ns]	48.27	137.20	135.33	129.16
	σ [ns]	9.28	35.31	34.47	31.16
Deployment 2					
$\bar{\tau}$	μ [ns]	64.27	6.49	7.88	2.47
	σ [ns]	20.31	1.70	1.85	0.57
σ_τ	μ [ns]	48.37	39.74	44.37	20.54
	σ [ns]	10.10	4.46	4.88	2.10

Table K.8 – Statistical parameters of delays in the city street scenario in the downlink (2).

		BS - MT2	MT3-MT2	MT4-MT2	MT5-MT2	MT6-MT2	MT7-MT2	MT8-MT2
Deployment 3								
$\bar{\tau}$	μ [ns]	66.70	101.62	98.04	71.47	72.87	97.94	100.13
	σ [ns]	21.63	28.81	31.50	18.52	16.21	28.60	28.93
σ_τ	μ [ns]	49.60	128.03	125.08	118.28	118.46	126.63	127.50
	σ [ns]	10.00	30.04	34.07	26.90	25.40	30.09	31.00
Deployment 4								
$\bar{\tau}$	μ [ns]	66.70	2.60	2.60	2.59	4.12	2.64	4.21
	σ [ns]	21.63	0.66	0.62	0.58	1.04	0.65	1.15

Table K.8 (contd.) – Statistical parameters of delays in the city street scenario in the downlink (2).

σ_τ	μ [ns]	49.60	20.05	20.36	20.16	28.50	20.40	28.56
	σ [ns]	10.00	2.56	2.28	2.40	2.92	2.05	2.80

Table K.9 – Statistical parameters of delays in the city street scenario in the downlink (3).

		BS - MT7	MT6-MT7	MT8-MT6
Deployment 5				
$\bar{\tau}$	μ [ns]	66.70	71.39	72.39
	σ [ns]	21.63	18.67	18.63
σ_τ	μ [ns]	49.60	118.06	118.57
	σ [ns]	10.00	26.64	26.15
Deployment 6				
$\bar{\tau}$	μ [ns]	65.24	4.13	7.01
	σ [ns]	21.26	1.10	1.95
σ_τ	μ [ns]	48.55	28.71	39.50
	σ [ns]	8.84	2.98	4.07

Table K.10 – Statistical parameters of power in the city street scenario in the downlink (1).

	BS - MT1	MT2-MT1	MT3-MT1	MT4-MT1
Deployment 1				
μ_P [mW]	4.44	36.21	36.01	26.89
σ_P [μW]	0.18	628.12	638.34	237.82
Deployment 2				
μ_P [W]	$4.81 \cdot 10^{-3}$	0.99	0.80	3.79
σ_P [mW]	$0.18 \cdot 10^{-3}$	49.70	34.49	15.19

Table K.11 – Statistical parameters of power in the city street scenario in the downlink (2).

	BS-MT2	MT3-MT2	MT4-MT2	MT5-MT2	MT6-MT2	MT7-MT2	MT8-MT2
Deployment 3							
μ_P [mW]	4.75	52.47	54.81	79.36	74.39	54.09	51.09
σ_P [mW]	$0.22 \cdot 10^{-3}$	1.04	1.18	3.22	1.53	1.46	0.74
Deployment 4							
μ_P [W]	$4.75 \cdot 10^{-3}$	3.89	3.88	3.88	1.98	3.87	1.97
σ_P [W]	$0.22 \cdot 10^{-6}$	0.86	0.71	0.60	0.34	0.54	0.25

Table K.12 – Statistical parameters of delays in the city street scenario in the downlink (3).

	BS-MT7	MT6-MT7	MT8-MT6
Deployment 5			
μ_P [mW]	4.75	80.35	77.95
σ_P [mW]	$0.22 \cdot 10^{-3}$	3.22	2.55
Deployment 6			
μ_P [W]	$4.87 \cdot 10^{-3}$	1.92	0.98
σ_P [mW]	$0.26 \cdot 10^{-3}$	5.14	3.62

- The downlink in the highway scenario:

Table K.13 – Statistical parameters of delays in the highway scenario in the downlink.

		BS-MT1	MT2-MT1	MT3-MT1	MT4-MT1	MT5-MT1	MT6-MT1	MT7-MT1	MT8-MT1	MT9-MT1
Deployment 1										
$\bar{\tau}$	μ [μs]	0.36	0.21	0.32	0.35	0.34	0.32	0.34	0.31	0.28
	σ [μs]	0.15	0.05	0.11	0.15	0.14	0.14	0.12	0.11	0.11
σ_τ	μ [μs]	0.30	0.31	0.31	0.27	0.26	0.24	0.25	0.23	0.20
	σ [μs]	0.11	0.07	0.08	0.07	0.06	0.06	0.05	0.04	0.04

Table K.13 (contd.) – Statistical parameters of delays in the highway scenario in the downlink.

Deployment 2										
$\bar{\tau}$	μ [μs]	0.36	0.09	0.21	0.29	0.34	0.37	0.37	0.37	0.37
	σ [μs]	0.16	0.02	0.05	0.08	0.11	0.13	0.14	0.15	0.14
σ_τ	μ [μs]	0.29	0.24	0.32	0.34	0.33	0.31	0.29	0.27	0.27
	σ [μs]	0.11	0.04	0.07	0.09	0.08	0.07	0.07	0.06	0.06
Deployment 3										
$\bar{\tau}$	μ [μs]	0.36	0.20	0.31	0.33	0.32	0.14	0.15	0.13	0.12
	σ [μs]	0.14	0.05	0.10	0.14	0.14	0.05	0.05	0.04	0.04
σ_τ	μ [μs]	0.30	0.31	0.31	0.28	0.26	0.11	0.11	0.10	0.09
	σ [μs]	0.09	0.07	0.07	0.06	0.05	0.02	0.02	0.02	0.02
Deployment 4										
$\bar{\tau}$	μ [μs]	0.37	0.09	0.20	0.28	0.33	0.16	0.15	0.14	0.14
	σ [μs]	0.14	0.02	0.05	0.08	0.11	0.05	0.05	0.05	0.05
σ_τ	μ [μs]	0.30	0.23	0.31	0.33	0.32	0.12	0.12	0.11	0.11
	σ [μs]	0.10	0.04	0.07	0.09	0.09	0.03	0.02	0.02	0.02
Deployment 5										
$\bar{\tau}$	μ [μs]	0.36	0.20	0.33	0.36	0.36	0.14	0.14	0.15	0.14
	σ [μs]	0.16	0.05	0.11	0.14	0.13	0.04	0.04	0.04	0.04
σ_τ	μ [μs]	0.29	0.31	0.32	0.29	0.26	0.11	0.11	0.12	0.11
	σ [μs]	0.10	0.08	0.08	0.07	0.06	0.02	0.02	0.02	0.02
Deployment 6										
$\bar{\tau}$	μ [μs]	0.36	0.09	0.21	0.29	0.33	0.15	0.13	0.13	0.14
	σ [μs]	0.15	0.02	0.05	0.08	0.11	0.05	0.05	0.05	0.04
σ_τ	μ [μs]	0.29	0.23	0.31	0.33	0.32	0.11	0.11	0.10	0.11
	σ [μs]	0.10	0.03	0.07	0.08	0.07	0.03	0.03	0.03	0.02

Table K.14 – Statistical parameters of powers in the highway scenario in the downlink.

	BS-MT1	MT2-MT1	MT3-MT1	MT4-MT1	MT5-MT1	MT6-MT1	MT7-MT1	MT8-MT1	MT9-MT1
Deployment 1									
μ_P [mW]	1.01	8.34	4.45	3.26	2.60	2.12	1.91	1.65	1.45
σ_P [μW]	0.02	17.40	5.21	2.00	0.91	0.46	0.24	0.13	0.09
Deployment 2									
μ_P [mW]	1.02	19.95	7.83	5.18	4.10	3.43	3.02	2.66	2.39
σ_P [μW]	0.01	59.00	14.88	8.08	4.91	2.86	1.95	1.31	0.89
Deployment 3									
μ_P [mW]	0.99	8.70	4.55	3.33	2.60	0.52	0.52	0.48	0.45
σ_P [μW]	0.02	26.05	4.72	1.89	0.77	0.00	0.00	0.00	0.00
Deployment 4									
μ_P [mW]	1.00	20.09	8.44	5.67	4.50	0.62	0.60	0.57	0.55
σ_P [μW]	0.02	35.63	23.30	11.66	7.15	0.00	0.00	0.00	0.00
Deployment 5									
μ_P [mW]	1.01	8.52	4.32	3.09	2.45	0.51	0.49	0.52	0.50
σ_P [μW]	0.01	35.60	7.17	2.46	0.96	0.00	0.00	0.00	0.00
Deployment 6									
μ_P [mW]	1.02	19.53	8.12	5.46	4.29	0.63	0.57	0.53	0.53
σ_P [μW]	0.02	13.53	14.47	8.67	4.39	0.00	0.00	0.00	0.00

- The downlink in the railway station scenario:

Table K.15 – Statistical parameters of delays in the railway station scenario in the downlink.

		BS-MT1	MT2-MT1	MT3-MT1	MT4-MT1	MT5-MT1	MT6-MT1	MT7-MT1	MT8-MT1	MT9-MT1
Deployment 1										
$\bar{\tau}$	μ [ns]	91.33	32.57	64.71	33.53	49.06	70.53	68.87	74.31	82.56
	σ [ns]	32.91	7.24	22.56	7.55	12.28	23.28	17.33	22.52	28.83
σ_τ	μ [ns]	76.20	70.41	90.40	70.12	81.63	91.16	88.12	91.21	92.75
	σ [ns]	17.17	15.99	25.18	13.04	20.78	26.01	22.75	25.91	27.67

Table K.15 (contd.) – Statistical parameters of delays in the railway station scenario in the downlink.

Deployment 2										
$\bar{\tau}$	μ [ns]	92.51	3.23	8.87	3.22	5.22	10.31	9.04	10.93	15.29
	σ [ns]	34.36	0.83	2.32	0.88	1.43	2.95	2.40	2.90	3.76
σ_τ	μ [ns]	74.99	20.09	37.52	19.90	27.48	40.88	37.52	41.66	49.82
	σ [ns]	17.17	2.13	4.82	2.21	3.00	4.90	4.66	5.87	6.98
Deployment 3										
$\bar{\tau}$	μ [ns]	91.33	32.57	76.88	33.53	49.06	75.50	68.87	74.31	77.78
	σ [ns]	32.91	7.24	26.52	7.55	12.28	26.28	17.33	22.52	27.38
σ_τ	μ [ns]	76.20	70.41	53.74	70.12	81.63	51.95	88.12	91.21	53.62
	σ [ns]	17.17	15.99	11.31	13.04	20.78	11.45	22.75	25.91	10.99
Deployment 4										
$\bar{\tau}$	μ [ns]	91.33	32.57	64.71	33.53	76.88	70.53	68.87	74.31	82.56
	σ [ns]	32.91	7.24	22.56	7.55	26.52	23.28	17.33	22.52	28.83
σ_τ	μ [ns]	76.20	70.41	90.40	70.12	53.74	91.16	88.12	91.21	92.75
	σ [ns]	17.17	15.99	25.18	13.04	11.31	26.01	22.75	25.91	27.67
Deployment 5										
$\bar{\tau}$	μ [ns]	92.51	3.23	8.87	3.22	73.61	10.31	9.04	10.93	15.29
	σ [ns]	34.36	0.83	2.32	0.88	24.84	2.95	2.40	2.90	3.76
σ_τ	μ [ns]	74.99	20.09	37.52	19.90	50.31	40.88	37.52	41.66	49.82
	σ [ns]	17.17	2.13	4.82	2.21	11.18	4.90	4.66	5.87	6.98
Deployment 6										
$\bar{\tau}$	μ [ns]	67.74	79.41	78.69	79.38	92.48	93.26	35.98	88.90	92.30
	σ [ns]	18.62	31.22	32.15	30.60	38.45	33.52	8.03	38.64	34.14
σ_τ	μ [ns]	83.50	60.37	67.31	57.06	78.84	78.40	70.16	73.33	67.65
	σ [ns]	18.89	14.95	16.84	13.20	16.89	17.09	14.08	19.26	14.06

Table K.16 – Statistical parameters of powers in the railway station scenario in the downlink.

	BS-MT1	MT2-MT1	MT3-MT1	MT4-MT1	MT5-MT1	MT6-MT1	MT7-MT1	MT8-MT1	MT9-MT1
Deployment 1									
μ_P [mW]	59.40	244.46	116.12	241.49	158.47	99.19	107.05	96.55	78.19
σ_P [mW]	0.56	12.47	5.17	20.29	8.23	3.02	3.52	2.94	1.65
Deployment 2									
μ_P [mW]	53.08	3928.84	1079.95	3883.15	2011.04	871.66	1048.86	860.37	573.87
σ_P [mW]	0.39	400.63	154.44	111.97	138.79	77.60	45.14	46.01	36.09
Deployment 3									
μ_P [mW]	59.40	244.46	31.98	241.49	158.47	31.30	107.05	96.55	32.54
σ_P [mW]	0.56	12.47	0.05	20.29	8.23	0.05	3.52	2.94	0.06
Deployment 4									
μ_P [mW]	59.40	244.46	116.12	241.49	31.98	99.19	107.05	96.55	78.19
σ_P [mW]	0.56	12.47	5.17	20.29	0.05	3.02	3.52	2.94	1.65
Deployment 5									
μ_P [mW]	53.08	3928.84	1079.95	3883.15	29.82	871.66	1048.86	860.37	573.87
σ_P [mW]	0.39	400.63	154.44	111.97	0.04	77.60	45.14	46.01	36.09
Deployment 6									
μ_P [mW]	112.88	32.93	24.69	28.13	42.93	54.92	231.84	41.77	49.53
σ_P [mW]	2.78	0.08	0.04	0.05	0.25	0.47	12.71	0.23	0.30

References

[3GGP] 3GGP,Report No. 25.942 , 2000 (http://www.3gpp.org).

[AkPa04] Robert Akl,R., Parvez A., *Impact of Interference Model on Capacity in CDMA Cellular Networks*, Internal Report, University of North Texas, USA, 2004. (http://www.cs.unt.edu/~rakl/AP04a.pdf)

[AMSM02] Asplund, H. Molisch, A., F., Steinbauer, M., Mehta. N., *Clustering of scatterers in mobile radio channels*, Evaluation and modeling in the COST 259 Directional Channel Model. In Proc. ICC 2002 - IEEE Int. Conf. Commun., New York, NY, USA, April 2002.

[COST99] COST Action 231, *Digital Mobile Radio Towards Future Generation Systems* (Final Report), COST Telecom Secretariat, European Commission, Brussels, Belgium, 1999.

[ErCa98] Ertel,R., Cardieri,P., *Overview of Spatial Channel Models for Antenna Array Com munication Systems*, Internal Report, Virginia Polytechnic Institute, 1998 (http://www.comsoc.org/pci/private/1998/feb/pdf/Ertel.pdf) .

[HHLT00] Holma,H., Heikkinen,S., Lehtinen,O., Toskala,A., "Interference Considerations for the Time Division Duplex Mode of the UMTS Terrestrial Radio Access", *IEEE journal on selected areas in communications*, Vol. 18, No. 8, pp. 1386-1393, august 2000.

[HoSz98] Hołubowicz,H., Szwabe,M., *Radio systems with code spreading CDMA* (in Polish), Alcatel, Poznan, Poland, 1998.

[HoTo00] Holma,H., Toskala,A., *WCDMA for UMTS*, John Wiley & Sons, West Sussex,

UK, 2000.

[KoCi04] Kołakowski,J., Cichocki,J., *UMTS – Third generation of mobile telephony system* (in Polish), WKŁ, Warsaw, Poland, 2004.

[Koko05] Kokoszkiewicz,H., *MIMO Geometrically Based Channel Model*, Master Thesis, IST-TUL, Lisbon, Portugal, 2005

[Koła00] Kołakowski,J. *Generation and analysis of the TDMA signals* (in Polish), Internal Report, Warsaw University of Technology, Institute of Radioelectronics, Warsaw, Poland, 2000.

[Kosi04] Kosiło,T., *Mobile terrestrial radiocommunication* (in Polish), internal document, Warsaw University of Technology, Warsaw, Poland, 2003.

[Lee73] Lee,W.C.Y., "Effects on correlation between two mobile base-station antennas", IEEE Transactions on Communications, Vol. COM-21, No. 11, pp. 1214-1224, November 1973

[LiRa99] Liberti,J., Rappaport,T., *Smart Antennas for Wireless Communication: IS-95 and Third Generation CDMA Applications*. Prentice Hall, Upper Saddle River, NJ, USA, 1999.

[LKTB02] Laurila, J., Kalliola, K., Toeltsch, M., Bonek, E., *Wide-band 3-D Characterization of Mobile Radio Channels in Urban Environment*., IEEE Trans. Antennas Propagat., Vol. 50, No. 2, pp. 233–243, February 2002.

[MaCo04] Marques,M.,G., Correia,L.M.,*A Wideband Directional Channel Model for Mobile Communication Systems,* Springer-Verlag, Berlin, Germany, 2004.

[MADA03] MAXIM/DALLAS,Application note 1886, February 2003 (http://pdfserv.maxim-ic.com/en/an/AN1886.pdf)

[Math05] http://mathworld.wolfram.com/, August 2005

[MaHu03] Mahmoud,S., Hussain, Z., O'Sheay,P., *Space-Time Geometrical-Based Channel Models: A Comparative Study,* Internal Report, School of Electrical and Computer Engineering RMIT University, Melbourne, Australia, 2003.

[Marq01] Marques,M.,G., *A Wideband Directional Channel Model for Micro-Cells in UMTS*, Master Thesis, Instituto Superior Técnico, Lisbon, Portugal, 2001.

[MoBo99] Molisch, A., F., Bonek, E., *Efficient implementation of a geometry-based directional model for mobile radio channels.* In *Proc. VTC 1999 Fall - IEEE 50th Vehicular Technology Conf.*, Amsterdam, The Netherlands, September 1999.

[Orfa02] Orfanidis,J.S., *Electromagnetic Waves and Antennas*, Internal Report, Rutgers University, NJ, USA, 2002.
(http://www.ece.rutgers.edu/~orfanidi/ewa/)

[Pras98] Prasad,R., *Universal Wireless Personal Communications. Mobile Communication Series*, Artech House, London, UK, 1998.

[Reis04] Reis,C., *An analytical traffic model for the UMTS radio interface*, Master Thesis, IST-TUL, Lisbon, Portugal, 2004.

[Reza02] Rezaeian,J.,M., *The Information Capacity of Multiuser Channels*, 2002, Institute for Telecommunications Research, Ph.D. Thesis, The University of South Australia, Adelaide/Whyalla, South Australia, Australia, 2002.

[SaVa87] Saleh, A.,M., Valenzuela, R., A., A Statistical Model for Indoor Multipath Propagation. IEEE J. Select. Areas Commun., Vol. 5, No. 2, pp. 128–137, February 1987.

[VCGC03] Venes,J.,Cardoso,F.,Gil,J.,Correia,L.,M., *Antenna Arrays for Wideband Directional Channel Models,* Internal Document, IST/TUL, Lisbon, Portugal, 2003.